Physical Features of Sonochemical Degradation of Recalcitrant Organic Pollutants

A Thesis
Submitted in Partial
Fulfillment of the Requirements for the Degree of

DOCTOR OF PHILOSOPHY

By

T. Sivasankar

Department of Chemical Engineering
Indian Institute of Technology Guwahati
Guwahati – 781039, Assam, India

April 2008

Dedicated

to

My parents and my mentors

CERTIFICATE

It is certified that the work contained in the thesis entitled "**Physical Features of Sonochemical Degradation of Recalcitrant Organic Pollutants**", by **T. Sivasankar** (Roll No. 04610703), has been carried out under my supervision and that this work has not been submitted elsewhere for a degree.

Date:

Dr. V.S. Moholkar
Assistant Professor
Department of Chemical Engineering
Indian Institute of Technology Guwahati
Guwahati – 781 039
Assam

CONTENTS

LIST OF TABLES

भारतीय प्रौद्योगिकी संस्थान गुवाहाटी
Indian Institute of Technology Guwahati

LIST OF FIGURES

NOTATION

A	-	cross-sectional area perpendicular to propagation of acoustic wave
b	-	damping coefficient for bubble motion
c	-	velocity of sound
c_m	-	speed of sound in bubbly liquid or gas-liquid mixture
c_o	-	velocity of sound in the medium at reference state
C_p	-	specific molecular heat capacity (at constant pressure); concentration of pollutant molecules in the bubble.
C_{pR}	-	concentration of pollutant molecules at the bubble interface.
$C_{p,mix}$	-	specific heat capacity at constant pressure of a mixture of species.
C_V	-	heat capacity at constant volume
$C_{v,mix}$	-	specific heat capacity at constant volume of a mixture of species.
C_w	-	concentration of water molecules in the bubble.
C_{wo}	-	initial concentration of water molecules in the bubble.
C_{wR}	-	concentration of water molecules at bubble interface.
D	-	diffusion coefficient (subscripts explained in respective chapters).
E	-	energy content of the bubble.
f	-	frequency of the acoustic wave
f	-	internal degrees of freedom for a species.
H	-	free enthalpy at the bubble surface
h	-	van der Waal's hard core radius
h_w	-	specific molecular enthalpy of water.
I	-	acoustic energy density in the medium

k	-	Boltzmann constant
K	-	polytropic constant of the bubble contents
$\mathbf{k}$	-	wave number
l_{diff}	-	mass diffusion length.
l_{th}	-	thermal diffusion length in the bubble ($l_{th\text{-}L}$: thermal diffusion length in liquid)
m	-	molecular mass of a species.
n	-	concentration of a species (in molecule/m^3) at bubble interface; constant in Tait equation of state.
N_{Ar}	-	number of argon molecules in the bubble.
n_b	-	number density of the bubbles in the medium
N_{N2}	-	number of nitrogen molecules in the bubble.
N_{O2}	-	number of oxygen molecules in the bubble.
N_{tot}	-	total number of molecules in the bubble.
N_w	-	number of water molecules in the bubble.
N_p	-	number of pollutant molecules in the bubble.
P	-	pressure in the liquid medium
P_∞	-	pressure in the liquid medium far from bubble
P_A	-	pressure amplitude of the acoustic wave
P_g	-	partial pressure of gas in the bubble
P_i	-	pressure inside the bubble (gas and vapor pressure)
P_L	-	pressure in the liquid at the bubble interface
P_o	-	ambient pressure in the liquid medium
P_t	-	time variant pressure in the bulk medium driving bubble motion.
P_V	-	vapor pressure of the liquid medium
P_W	-	partial pressure of water molecules at the bubble bulk interface

P_P - partial pressure of pollutant at the bubble-bulk interface.

Q - heat transferred across bubble wall.

r - radial coordinate

R - radius of the bubble at any time

R_o - initial or equilibrium bubble radius

$\dot{R}$ - time derivative of bubble radius (dR/dt, bubble wall velocity)

$\ddot{R}$ - time derivative of bubble wall velocity (d^2R/dt^2, acceleration of bubble wall)

$\dot{r}$ - time derivative of radial coordinate (representative of liquid velocity away from bubble)

S - entropy of the liquid medium

T - temperature in the bubble.

t - time

t_{cond} - time scale of vapor condensation at bubble interface

t_{dif} - time scale of vapor diffusion in the bubble

T_o - ambient temperature in the liquid medium.

t_{osc} - time scale of oscillation of the bubble (or radial motion of the bubble)

U_w - specific internal energy of water molecules.

V - volume of the bubble.

W - work done by the bubble.

x - distance coordinate

x - mole fractions of different components in the bubble (subscripts explained in respective chapters).

x_{pR} - mole fraction of pollutant molecules in the liquid medium at bubble interface

x_{pW} - mole fraction of water molecules in the liquid medium at bubble interface

Z - acoustic impedance of the liquid medium

Greek letters

ω	-	angular frequency of the acoustic wave
λ	-	wavelength of the acoustic wave; constant in equation 2.29; coefficient of thermal conductivity of a species (subscripts explained in respective chapters).
γ	-	ratio of specific heats
κ	-	thermal diffusivity (subscripts explained in respective chapters)
μ	-	viscosity of the liquid medium
α_s	-	frictional loss coefficient for the acoustic wave
ω_o	-	natural oscillation frequency of the bubble
σ	-	surface tension of the liquid medium; molecular diameters of different species (subscripts explained in respective chapters).
σ_a	-	accommodation coefficient at the bubble surface
ρ, ρ_L	-	density of the bulk liquid medium
ρ_o	-	density of the liquid medium at reference state
ν	-	particle velocity, kinematic viscosity of the medium
ε	-	particle displacement; mole fraction of various components at the bubble wall (subscripts explained in respective chapters)
$\dot{\varepsilon}$	-	time derivative of particle displacement
ϕ	-	velocity potential
η	-	coefficient of viscosity of a species.
ν	-	kinematic viscosity of the liquid medium.
κ	-	thermal diffusivity.
ρ_i	-	molecular density of a species.
ρ_{mix}	-	molecular density of the mixture of species.

SUMMARY OF THE THESIS

The toxic organic pollutants contributed by industrial wastewater and agricultural run-offs are complex refractory molecules which are not easily degraded by conventional biological techniques. Therefore, search for more efficient technologies is necessary for effective degradation of such compounds. Developments of novel treatment methods encompasses investigations in advanced oxidation processes (AOP's), which are characterized by production of hydroxyl (OH) radical as primary oxidant. More recently, sonochemical oxidation (or sonolysis) has been investigated as a viable AOP for the destruction of aromatic pollutants. In this technique the free radicals are generated through transient collapse of cavitation bubble driven by an ultrasound wave. Thus, the radial motion of the cavitation bubble (or bubble dynamics) is the basic physical phenomenon underlying sonolytic degradation of pollutants. The sonochemical degradation of organic pollutants can occur in three distinct chemical pathways or mechanisms. The primary mechanism is the hydroxylation (or reaction with OH radicals) generated by the cavitation bubbles. The second mechanism is pyrolytic decomposition of the pollutant molecules evaporated and entrapped in the cavitation bubble at the extreme conditions reached during transient collapse. The third possible mechanism is the formation of supercritical water in a small thin shell around the bubble. Some pollutant molecules may undergo thermal decomposition in this supercritical zone. Significant research has been done in past one and half decade on sonochemical degradation of large variety of organic pollutants. However, approach in these studies was mainly experimental and no confirmation of the degradation mechanism was made on the basis of a model for radial motion of cavitation bubbles.

The principal aim of this thesis is to provide a physical insight into the sonochemical degradation of organic pollutants, which would decipher the primary physical mechanism of the degradation phenomena. Any attempt to elucidate the physical mechanism of the process would basically mean establishing relationship between the sonochemical degradation and the cavitation bubble dynamics. Thus thesis attempts to correlate the extent of degradation of the pollutants under similar conditions to the physical properties of the pollutants and the radial motion of the cavitation bubbles along with associated heat and mass transfer. Five most common acoustic aromatic pollutants have been chosen for the study, viz. phenol, p-nitrophenol, 2,4-dichlorophenol, chlorobenzene and nitrobenzene. The thesis comprises of 8 chapters. The content of various chapters is summarized below:

- Chapter 1 gives the general introduction for the thesis along with an overview of different advanced oxidation processes such as Fenton's process (and its derivatives), photocalalysis (and its derivatives), ozone-water systems, wet air oxidation. Next, an introduction to the sonochemical oxidation or sonolysis presented followed by review of literature in the area of sonochemical degradation of five pollutants considered in this thesis.

- Chapter 2 presents the basic principles of ultrasound wave phenomena and cavitation bubble dynamics. Different physical phenomena related to ultrasound waves such as acoustic intensity and impedance, attenuation, relation between acoustic pressure and velocity etc have been described. This is followed by discussion on cavitation inception, models for the radial motion of cavitation bubbles (with and without liquid compressibility effects), transport phenomena in the bubble, stable and transient cavitation etc. The principal aim of this chapter is to create necessary background on acoustics and bubble dynamics for the readers.

- Chapter 3 tries to illuminate the complex interrelation between physics and chemistry of a sonochemical reaction system using the well known model reaction of potassium iodide

oxidation. The results of this study reveal that the extent of vapor entrapment in the bubble and the intensity of the transient cavitation bubble collapse are the principal physical phenomena affecting the yield of any sonochemical reaction. A mechanism for the sonochemical yield has been worked out using the results of the study.

- Chapter 4 deals with sonochemical degradation of phenol, the most ubiquitous aromatic pollutant. Using different experimental techniques such as sparging of various monoatomic and diatomic gases through the medium and using different scavenging species, we try to elucidate the relative influence of radical production and radical scavenging (or conservation) on the sonochemical degradation of phenol. The results of the study reveal that sonochemical degradation of phenol is governed by extent of radical scavenging or conservation (and not radical production) in the medium. This outcome is attributed to hydrophillic nature of phenol as a result of which it stays mostly away from bubble-bulk interface. The importance of the probability of interaction between radical and pollutant in the sonochemical degradation process is also highlighted.

- Mechanistic features of the sonochemical degradation of volatile (chlorobenzene) and non-volatile (phenol) organic pollutants have been compared in chapter 5. By coupling experimental results to a bubble dynamics model we try to establish the relative contribution of the two principal pathways, viz. hydroxylation and pyrolysis, to the degradation of two kinds of pollutants. It is revealed that degradation of two volatile pollutants occurs primarily by thermal pyrolysis while hydroxylation is the predominant mechanism for degradation of nonvolatile pollutants. Reaction parameters such as initial pollutant concentration and salt addition to the medium influence both of the above pathways for degradation. However, extent of this influence on hydroxylation and pyrolysis pathway is different. This is attributed to dissimilarity of partitioning behavior and solubility of the two pollutants.

- Chapter 6 treats the sonochemical degradation of nitroaromatic pollutants (viz. nitrobenzene and p-nitrophenol). Different experimental techniques have been applied which reveal influence of several physical parameters related to cavitation phenomena such as extent of radical production from the bubble, thickness of liquid shell surrounding the bubble that gets heated up during transient collapse, concentration of pollutant in the interfacial region and extent of radical scavenging in the medium. Overall degradation of the pollutant achieved for a given combination of experimental conditions is a function of competing (and sometimes conflicting) effect of these parameters.

- Chapter 7 presents the study in sonochemical degradation of 2,4-dichlorophenol. Under similar experimental conditions, as adopted in earlier chapters, the sonochemical degradation of 2,4-dichlorophenol reveals interesting features. The degradation of 2,4-dichlorophenol primarily occurs in the interfacial region between bubble and bulk medium. Secondly, the extent of degradation is found to be controlled by production of the radicals by cavitation bubbles as well as scavenging (or conservation) of the radicals in the interfacial region. Dissolved oxygen in the medium is revealed to be an effective scavenger.

- Chapter 8 gives the overall conclusions of the studies in sonochemical degradation of five pollutants. These pollutants have widely different physical properties, as a result of which their response to the sonochemical phenomena in the liquid medium differs. This chapter tries to establish a general framework to discern the physical mechanism of sonochemical degradation of various pollutants as a function of several parameters: (1) extent of radical production, (2) extent of radical scavenging (or conservation), (3) location of degradation, (4) chemical pathway or mechanism of degradation and (5) physical properties of the pollutant. Such a framework would help predict the physical mechanism of any other pollutant. Moreover, several recommendations have been given for the future work in this area.

CHAPTER 1

GENERAL INTRODUCTION AND LITERATURE REVIEW

1.1 INTRODUCTION

The principal origins of water pollution in recent years are city sewage and industrial water discharge. The latter source, although small in volume (~ 25%), contributes more than half of total pollution load; with major contributions from small and medium scale industries. The main cause leading to this effect is rapid growth of the chemical and process industries in India that did not go hand-in-hand with the advances in water (or effluent) treatment technologies – both in terms of efficiency and economy. Several large and medium scale industries do not have adequate effluent treatment facilities, as they cannot afford enormous investment in pollution control due to slender profit margins. It is estimated that only about 10% of wastewater generated undergoes any treatment before being discharged into water bodies. Agricultural runoffs or water from fields that drains into rivers is another major pollutant as it contains fertilizers and pesticides. Intensive crop cultivation results in seepage of chemicals from fertilizers and pesticides into ground water causing heavy contamination. For example, high nitrate content in ground water is mainly from irrigation runoffs from agricultural fields, where chemical fertilizers have been used indiscriminately.

Industrial wastewater discharge and agricultural runoffs often contain complex organic pollutants that are not easily degraded by conventional biological processes such as aerobic processes, anoxic processes, anaerobic processes (sludge blankets) and combination of these. The application of these biological processes is mainly for the carbonaceous BOD removal, denitrification, pathogen killing and phosphorus removal. As far as treatment of the

complex aromatic compounds is concerned, search for more efficient technologies is necessary. Technologies such as phase separation (adsorption or stripping) or chemical oxidation/reduction do not offer a complete solution in this regard as the final disposal of the organic matter poses problems. Development of novel treatment methods encompasses investigations in advanced oxidation processes (AOPs), which are characterized by production of OH (hydroxyl) radical as primary oxidant. The OH radicals are extremely reactive species and a powerful oxidizing agent with an oxidation potential of 2.33V. The typical rate constants for the reaction of OH radicals with organic compounds ranges between 10^6-10^9 mol^{-1} s^{-1}. We outline below the basic chemistry of different AOPs practiced by researchers in past few decades (Andreozzi *et al.*, 1999). For greater details on each of the processes described below along with a state-of-the-art review of the literature employing these processes is given by Gogate and Pandit (2004, 2004a).

1.2 FENTON PROCESS

The Fenton process is more than a century old (Fenton, 1894); however, the interest in this process is renewed due to its ability to degrade toxic pollutants such as phenol and its derivatives. In this process, production of OH radicals occurs due to addition of H_2O_2 to Fe^{2+} salts (Haber and Weiss, 1934):

$$Fe^{2+} + H_2O_2 \longrightarrow Fe^{3+} + OH^- + OH^{\bullet}$$
$$Fe^{3+} + H_2O_2 \longrightarrow Fe^{2+} + HO_2^{\bullet} + H^+$$
$$Fe^{3+} + HO_2^{\bullet} \longrightarrow Fe^{2+} + O_2 + H^+$$

This is one of the simplest techniques for producing OH radicals, without use of any expensive and special chemical. Moreover, disposal of water treated with Fenton process is not problematic as Fe is an abundant and non-toxic element, while H_2O_2 is environmentally safe and easy to handle. Over the years, several modifications of the basic Fenton process described above have been developed. The prominent among them is the photoassisted

Fenton process in which Fe^{2+}/H_2O_2 system is exposed to simultaneous UV light resulting in strong acceleration of the rate of degradation (Kiwi *et al.*, 1993; Pulgarin & Kiwi, 1996). This is attributed to the photoreduction of hydroxylated Fe^{3+} ions to Fe^{2+} ions in the pH range 2 – 5, for the continuous supply of OH radicals as follows:

$$FeOH^{2+} + h\nu \longrightarrow Fe^{2+} + OH^{\bullet}$$

A recent modification of the Fenton process is the UV/Fe^{3+} oxalate/H_2O_2 process (Safarzadehet-Amiri *et al.*, 1996, 1997). The oxalic acid complexes with Fe^{3+} ions present in the media at pH 2 – 4. The ferric carboxylate complexes behave as photochemically active compounds in the UV-Vis range of 250-480 nm and undergo a series of photochemical reactions through Ligand to Metal Charge Transfer reaction (LMCT) as follows:

$$\left[Fe^{3+}\left(C_2O_4\right)_3\right]^{3-} + h\nu \longrightarrow \left[Fe^{2+}\left(C_2O_4\right)_2\right]^{2-} + C_2O_4^{\bullet-}$$

$$C_2O_4^{\bullet-} + \left[Fe^{3+}\left(C_2O_4\right)\right]^{3-} \longrightarrow \left[Fe^{2+}\left(C_2O_4\right)_2\right]^{2-} + C_2O_4^{2-} + 2CO_2$$

$$C_2O_4^{\bullet-} + O_2 \longrightarrow O_2^{\bullet-} + 2CO_2$$

These charge transfers increase the production of Fe^{2+} ions and OH radicals with high quantum yield (1.11-1.26). High efficiency of this process is attributed to higher absorption of ferric oxalate over broad range wavelength (200-400 nm) utilizing the UV-Vis radiation efficiently.

1.3 PHOTOCATALYSIS

These processes employ a semiconductor metal oxide as catalyst along with O_2 as oxidizing agent (Ollis and Al-Ekabi, 1993; Zhang *et al.*, 1994; Rajeshwar, 1995). Among several catalysts assessed, TiO_2 in anatase form has the desired properties such as high stability, efficient performance and low cost. The photocatalytic action begins with formation of electron – hole pairs at due to absorption of the radiation by TiO_2:

$$TiO_2 \longrightarrow h^+ + e^-$$

The electrons thus formed reduce some metal and dissolved oxygen to form superoxide radical ion $O_2^{\bullet -}$, while holes react with the water molecules adsorbed on the metal oxide surface to generate OH radicals:

$$TiO_2\left(h^+\right) + H_2O_{ad} \longrightarrow TiO_2 + HO_{ad}^{\bullet} + H^+$$
$$TiO_2\left(h^+\right) + HO_{ad}^- \longrightarrow TiO_2 + HO_{ad}^{\bullet}$$

As the concentration of adsorbed water is high, the above two reactions generate large number of OH radicals. In addition, the pollutant molecules adsorbed on the surface also get oxidized due to electron transfer:

$$TiO_2\left(h^+\right) + RX_{ad} \longrightarrow TiO_2 + RX_{ad}^{\bullet -}$$

A potential drawback of the photocatalytic process is recombination of holes and electrons which contributes to loss of oxidation potential. An alternative to make the photocatalytic process economically attractive would be to use the solar radiations instead of UV light. However, overlap between absorption spectrum of TiO_2 and the spectrum of solar radiation (at ground level) is quite small, which puts a limitation on this methodology. Significant research has therefore been devoted to broadening of the absorption spectrum of TiO_2 that result in higher quantum yield.

1.4 OZONE-WATER SYSTEM

Ozone-water systems have also emerged as a popular AOP for destruction of a number of organic pollutants. The chemistry of ozone in alkaline solutions is given as follows (Hoigne, 1998; Andreozzi *et al.*, 1999):

$$HO^- + O_3 \longrightarrow O_2 + HO_2^-$$
$$HO_2^- + O_3 \longrightarrow HO_2^{\bullet} + O_3^{\bullet -}$$

$$HO_2^{\bullet} \rightleftharpoons H^+ + O_2^{\bullet -}$$
$$O_3 + O_2^{\bullet -} \rightleftharpoons O_2 + O_3^{\bullet -}$$

$$O_3^{\bullet -} + H^+ \longrightarrow HO_3^{\bullet}$$
$$HO_3^{\bullet} \longrightarrow HO^{\bullet} + O_2$$

$$HO^{\bullet} + O_3 \longrightarrow HO_2^{\bullet} + O_2$$

The above mechanism suggests that addition of H_2O_2 to the aqueous solutions of ozone can enhance ozone decomposition. In addition, pH of the solution is also an important parameter since the concentration of HO_2^- (i.e. the conjugate base in O_3 decomposition) depends on it. Increase in the pH of the O_3 solution gives greater OH^- concentration which results in higher rate of $OH^{\bullet}$ formation (Glaze and Kang, 1989). Several derivatives of this process have also been developed as follows:

1.4.1 *Mn^{2+}/oxalic acid system*

Ozone decomposition can be enhanced for the generation of OH radicals using Mn^{2+}/ oxalic acid system. Mn^{2+} catalyzed ozonation of oxalic acid proceeds according to a radical mechanism at pH > 4, at which Mn(II) dioxalate and Mn(III) trioxalate forms. The oxidation process proceeds through following reaction (Andreozzi *et al.*, 1992, 1995):

$$Mn(III)(AO^{2-})_n + O_3 + H^+ \longrightarrow Mn(II) + (n-1)(AO^{2-}) + 2CO_2 + O_2 + OH^{\bullet}$$

1.4.2 *UV/H_2O_2 system*

OH radicals can be generated from homolytic cleavage of H_2O_2 by UV irradiation with wavelength < 280 nm (Baxendale and Wilson, 1957).

$$H_2O_2 \xrightarrow{h\nu} 2OH^{\bullet}$$

The quantum yield of this process reduces due to the cage effect of water molecules that causes recombination of radicals. However, the OH radicals attack H_2O_2 molecules generating $HO_2^{\bullet}$ radicals (which is a kind of autocatalytic effect):

$$2\left(H_2O_2 + OH^{\bullet}\right) \longrightarrow H_2O + HO_2^{\bullet}$$
$$2HO_2^{\bullet} \longrightarrow 2HO_2^{\bullet}$$

A limitation of this process is the small molar extinction coefficient of H_2O_2 (18.6 M^{-1} cm^{-1} at 254 nm), as a result of which the efficiency of utilization of incident light is small. Another factor that affects the process is the pH of the solution. The rate of photolysis is higher for more alkaline solutions.

1.4.3 *O_3/UV processes*

These processes have been effectively utilized for oxidation/ destruction of several toxic and refractory organics in water (Peyton and Glaze, 1988; Prado *et al.*, 1994). The process involves saturation of the aqueous system with ozone and irradiation with UV light at 254 nm. For this wavelength the extinction coefficient of ozone is 3600 M^{-1} cm^{-1} (two orders of magnitude higher than that of H_2O_2). This results in very high absorption of UV irradiation, resulting in better utilization of UV energy.

The chemistry of the process is, however, debated. Several reactions occur, either in parallel or series, resulting in production of OH radicals. A general representation of various reactions is given as follows:

$$O_3 \xrightarrow{h\nu} O^1(D) + O_2$$
$$O^1(D) + H_2O \longrightarrow H_2O_2$$
$$H_2O_2 \xrightarrow{h\nu} OH^\bullet + OH^\bullet$$

The above equations indicate significant presence of H_2O_2 in the solution, which also gets exposed to UV light. Therefore, the system as a whole has characteristics of both O_3/H_2O_2 and H_2O_2/UV systems.

1.5 WET AIR OXIDATION

This is also a popular technique for treatment of various industrial toxic and refractory wastes (Mishra *et al.*, 1995). Wet air oxidation essentially involves subcritical oxidation of organic matter in aqueous phase with oxygen (either in pure form or as air) at elevated temperatures of about 100-350^oC and at pressures ranging from 0.5-20 MPa. However, this process has the

limitation of slow oxidation kinetics. In addition, many organic pollutants (such as 2-ethyl hexane-1-ol or pthalic acid) are refractory to this technique. Requirement of severe conditions of temperature and pressure also raise the capital cost of equipment affecting overall economy of the process.

1.6 SONOCHEMICAL WASTEWATER TREATMENT

Sonochemical oxidation (or sonolysis) has emerged as a new technique for the degradation of biorefractory organic pollutants. Sizeable amount of literature (> 200 papers) have been published in last one and half decade that deal with sonochemical degradation of a variety of organic pollutants (for example Hua and Hoffmann, 1996; Colussi *et al.*, 1999; Petrier and Francony, 1997; Hung and Hoffmann, 1999; Lin and Ma, 1999; Peller *et al.*, 2001; Bhatnagar and Cheung, 1994; Barbier and Petrier, 1996; Beckett and Hua, 2000; Kotronarou *et al.*, 1991, 1992; Okouchi *et al.*, 1992; Kang *et al.*, 1999; Weavers *et al.*, 1998, 2000; Vinodgopal and Peller, 2003; Joseph *et al.*, 2000). State-of-the-art reviews of the literature in this area has been given by Gogate and Pandit (2004, 2004a), Adewuyi (2001) and Hoffmann *et al.* (1996). This technique is based on OH and other oxidizing radicals (such O and $HO_2^{\bullet}$) through cavitation bubbles. Cavitation can be defined as the nucleation, growth and collapse of gas or vapor bubbles in liquid medium driven by variation in the bulk pressure due to passage of an ultrasound wave. As a result of the transient cavitation bubble implosion, extremes of temperature and pressure (~ 5000 K and 500 bar) are generated inside the bubble. These extreme conditions are short lived (~ 10 ns or so) but have shown to result in the generation of highly reactive species such as hydroxyl ($OH^{\bullet}$), hydrogen ($H^{\bullet}$) and hydroperoxyl ($HO_2^{\bullet}$) radicals and hydrogen peroxide (Hart and Henglein, 1985, 1987). The cavitation bubble may undergo fragmentation during collapse due to surface and/or flow instabilities (Apfel, 1981). In this situation, the radicals in the bubble get mixed with bulk

liquid, where they can initiate and promote hydroxylation reaction leading to degradation of the pollutants (Colussi *et al.*, 1998; Brenner *et al.*, 2002). These radicals are extremely reactive species, and hence, they do not diffuse much from the point of bubble collapse in the medium. The reaction zone of the radicals generated from cavitation bubbles is, thus, restricted to a small area at the location of the bubble collapse.

Another possible mechanism for the degradation of pollutants is the thermal pyrolysis in the cavitation bubble. During the expansion phase of the radial bubble motion, evaporation of the dissolved pollutant molecules occurs at the bubble wall with subsequent diffusion of these molecules towards the center of the bubble. In the subsequent compression phase, pollutant molecules diffuse outward, i.e. towards the bubble wall. During the final moments of the compression phase, the bubble motion becomes extremely rapid and not all of the pollutant molecules that have entered the bubble can condense. The entrapped molecules are subjected to extreme conditions generated at the transient bubble collapse and undergo thermal pyrolysis (Weavers and Hoffmann, 1998; Storey and Szeri, 2000; Lesko, 2004). A third mechanism for the sonochemical hydrolysis of the organic pollutant is the formation of transient supercritical water pockets in the close vicinity of the cavitation bubble, as proposed by Hua *et al.* (1995). Some pollutants present in the close vicinity of the bubble (or at the bubble-bulk interfacial region) may undergo thermal decomposition at these conditions. Alternatively, formation of supercritical zones results in increased solubility of organic compounds. Higher amount of pollutant present in the bulk medium, thus, diffuses towards bubble interface and get exposed to the OH radicals. A consequence of this is greater degradation through hydroxylation route. Figure 1 depicts the different sites and mechanisms for the sonochemical degradation of the organic pollutants.

Out of these three pathways, dominant pathway for the degradation is decided by the nature and properties of the organic pollutant. An analysis of the degradation products of the

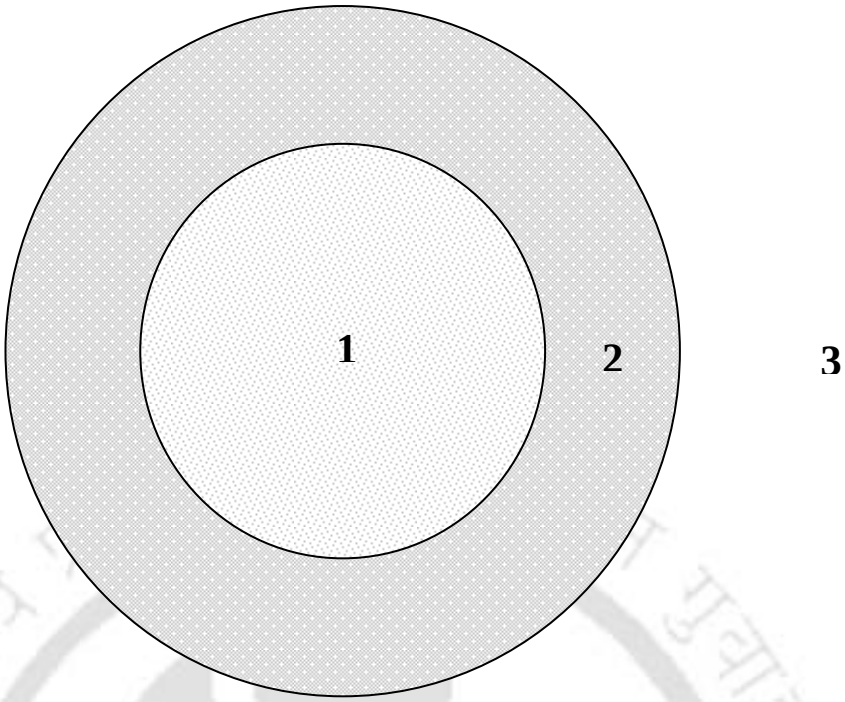

Figure 1.1. Possible sites and mechanisms for the sonochemical degradation of the pollutant. 1. Inside the cavitation bubble (by thermal pyrolysis); 2. In the bubble-bulk interfacial region (either by thermal pyrolysis or by hydroxylation or by both); 3. In the bulk liquid (by hydroxylation).

pollutant provides a preliminary insight into the dominant chemical mechanism for degradation. It can, however, be perceived that radial motion of cavitation bubble driven by the ultrasound wave is the physical basis for the degradation of pollutants with sonolysis.

1.7 AIM AND SCOPE OF THE PRESENT THESIS

As stated earlier, significant research has been done in past one decade on sonochemical degradation of large variety of organic pollutants such as aromatic compounds (benzene, phenol and their nitro-, halo- and other derivatives, polycyclic aromatic hydrocarbons), chlorinated aliphatic hydrocarbons, herbicides and pesticides, organic (azo) dyes, oxygenates such as Methyl tert-butyl ether (MTBE) and various surfactants. However, the approach in these studies was mainly experimental and no confirmation of the

degradation mechanism was made on the basis of a model for the radial motion of cavitation bubbles.

The principal aim of this thesis is to provide a physical insight into the sonochemical degradation of the organic pollutants, which will decipher its primary physical mechanism. As noted earlier, the principal physical phenomenon underlying the sonochemical degradation of the pollutants is radial motion of cavitation bubbles (or cavitation bubble dynamics). Therefore, any attempt to elucidate the physical mechanism of the process should basically mean establishing relationship between the sonochemical degradation through three pathways (viz. pyrolysis, hydroxylation and supercritical oxidation) and the cavitation bubble dynamics. This thesis attempts to correlate the extent of degradation of the two pollutants under similar experimental conditions to the physical properties of the pollutants and the fundamental phenomena of transport of vapor of water and organic pollutant across cavitation bubble using a bubble dynamics model that takes into account essential physics and chemistry of cavitation bubbles. For our investigations, we choose five most common aromatic contaminants observed in industrial wastewater, viz. phenol, p-nitrophenol, 2,4-dichlorophenol, chlorobenzene and nitrobenzene. The physical and chemical properties of these pollutants have been given in table 1. It can be seen that these pollutants differ widely in their properties such as solubility, vapor pressure and melting & boiling points. The discharge limits for these pollutants also varies significantly on the basis of the toxicity. In the next section, we present a review of the literature published in the area of sonochemical degradation of these pollutants.

1.8 LITERATURE REVIEW

Phenol is a constituent of coal tar and is formed during natural decomposition of organic materials. It is the basic feedstock from which a number of commercially important materials

are made including phenolic resins, bisphenol A, caprolactum, alkyl phenols and chlorophenols such as pentachlorophenol. Most commonly used production method for phenol is from cumene. It is also produced from chlorobenzene and toluene. p-Nitrophenol is an intermediate in the synthesis of azodyes and a number of pesticides, mainly insecticides such as parathion, parathion-methyl, and to a lesser extent, herbicides such as nitrofen and bifenox. Chlorophenols have been used as mothproofing agents, miticides, germicides, algicides, fungicides, and wood preservatives and to manufacture of other chemicals. All the chlorophenols have been used as biocides. Chlorophenols with at least two chlorines either have been used directly as pesticides or have been converted into pesticides. 2,4,6-Trichlorophenol was previously used as an antiseptic, a pesticide for wood, leather, and glue preservation and as an anti-mildew treatment. 2,4-Dichlorophenol is a chemical intermediate used principally in the manufacture of the herbicide 2,4-dichlorophenoxyacetic acid. Chlorobenzenes are used mainly as intermediates in the synthesis of pesticides and other chemicals. Nitrobenzene is a synthetic compound, which is used in production of aniline, which is a major intermediate in chemical industry for polyurethane production. It is also used as a solvent for cellulose ethers and acetates.

1.8.1 Sonochemical degradation of phenol

The intermediates and products of sonochemical oxidation of phenol usually include hydroquinone, catechol, p- and o-benzoquinone, muconic, maleic, succinic, formic, propanoic, oxalic and acetic acid, and CO_2. Early investigations into phenol degradation include that of Lure' *et al.* (1962) and Chen *et al.* (1971). Over a pH range of 3 – 9 Lure' *et al.* (1962) found the decomposition of phenol to be independent of pH. Chen *et al.* (1971) found that the conversion was first order only at very low concentrations (< 100 ppm). At high concentrations the conversion (typically > 300 ppm) was zero order. The rate of

degradation was negligible at low frequency (25 and 55 kHz) and the oxidation proceeded to completion only at high frequency (800 kHz). Berlan *et al.* (1994) observed that the primary degradation products such as dihydroxybenzenes and quinones get further degraded into low molecular weight carboxylic acids due to local extreme conditions resulting from cavitation. Petrier *et al.* (1994) found that rate of sonochemical phenol degradation to proceed more rapidly at higher (487 kHz) than low (20 kHz) frequency – due to better release of $OH^{\bullet}$ radicals in the solution at high frequency. Okouchi *et al.* (1992) observed degradation of phenol to occur in less than 100 min and with a pseudo first order rate. Addition of catalysts such as Fe^{2+} or MnO_2 increased the rate of degradation. Serpone *et al.* (1992) noticed that the disappearance of phenol at initial concentrations in the range 30-70 μM to follow zero order kinetics. The rate constant decreased with increasing pH. The intermediates formed in the degradation were also a function of pH: at pH of 3, catechol, hydroquinone and p-benzoquinone were the major intermediates while at pH of 5.4 only catechol and hydroquinone formed. No intermediate was seen at pH of 12. Moreover, rate of loss of phenol as a function of sonication time was found to be linearly related to sonication power P. Trabelsi *et al.* (1996) investigated oxidation of phenol in a screened reactor with ultrasound alone at 20 kHz, and secondly, with ultrasound associated with electrolysis. It was found that electrochemical oxidation of phenol in NaCl media combined with sonication at 20 kHz resulted in 75% conversion of initial phenol within 10 min, with formation of a toxic intermediate p-quinone. At a higher frequency of 500 kHz a conversion of 95% was observed within same treatment time with acetic and chlorocrylic acids as final products of degradation. Sonoelectro-oxidation at high frequency allowed total degradation in 20 min with no toxic aromatic intermediate. Takizawa *et al.* (1996) studied sonication of phenol and other phenolic compounds such as 4-methoxyphenol, 4-hydroxyanisol, 2-naphthol, resorcinol in aqueous media (water and water-ethanol) at 25^{o}C for 12-18h using 200 kHz in presence of

oxygen. They also identified catechol and hydroquinone as the oxidation products of phenol. They have also proposed mechanism for the production of hydroquinone from phenol due to attack of sonochemically produced hydroxyl radical on the phenolic benzene ring. Petrier and Francony (1997, 1997a) have studied degradation of phenol at various frequencies. The degradation was found to proceed faster at 200 kHz and initial degradation rate reaches maximum at 200 kHz. Primary degradation products were hydroquinone and catechol. 200 kHz was the optimum frequency for phenol degradation. Addition of 1-butanol, a hydroxyl radical scavenger, totally inhibits the reaction. Effect of frequency on the degradation of phenol was also studied by Jiang *et al*. (1999). The degradation of phenol showed a maxima with frequency. Compared to 20, 500 and 800 kHz frequencies, 200 kHz frequency resulted in greater degradation of phenol (indicating higher production of OH radicals). Zheng *et al.* (2005) found that sonochemical degradation of phenol was enhanced in presence of volatile hydrogen atom scavengers such as CCl_4 and perfluorohexane. Additives such as KIO_3 did not affect the degradation rate substantially. Again, hydroquinone was observed to be the major reaction product. Kubo *et al.* (2005) have examined the effects of amount of TiO_2 and combination of TiO_2 addition with gas (air or oxygen) supply on the degradation kinetics of phenol. The degradation rate increased with amount of TiO_2 and dissolved oxygen concentration. Kubo *et al* have tried to explain their results on the basis of a kinetic model that takes into account formation of hydroxyl radical by different mechanisms. Kubo *et al.* (2005a) have also examined the effect of amount of composite particles of TiO_2 and activated carbon (AC) and the AC/TiO_2 ratio on the ultrasonic degradation of phenol. The extent of degradation was proportional to the amount of composite particles added to the medium, while AC/TiO_2 ratio in the composite particles showed an inverse relationship with the degradation of phenol. The addition of coal ash to the medium (Nakui *et al.*, 2007) having

porous and uneven surface (as a result of which the nucleating sites for cavitation in the medium increase) accelerated the degradation of phenol.

Entezari and Petrier (2003, 2004) have studied effect of sonolysis, enzyme treatment, and a combination of the two processes for the degradation of phenol and its derivatives. The results showed mixed behavior: phenol and its halogenated derivatives (chloro-, bromo-, iodo-phenol) degraded faster with combined treatment of sonolysis and enzyme than with individual treatments. The enzyme used was Horseradish peroxidase. However, in case of p-methoxyphenol and p-cresol combined method gave same results as that of enzyme treatment and in case of p-nitrophenol enzyme had no additive effect. In another study, Entezari and Petrier (2005) compared effects of sonodegradation and sono-enzyme degradation on mixtures of phenol and its derivatives. The behavior of mixtures subjected to sonolysis alone and sonolysis with enzyme treatment was different. Sonodegradation of substituted phenol was easier than phenol in a mixture; with exception of phenol & p-nitrophenol mixture where phenol degradation was faster. This anomaly persisted in case of sono-enzyme degradation, although with higher rate. Moreover, for mixture of phenol and p-cresol it was found that sonodegradation of phenol was more difficult, as compared to phenol alone, while sonodegradation of p-cresol was easier than p-cresol alone. In sono-enzyme degradation, p-cresol as a more reactive compound facilitated removal of phenol in the mixture. In another study, Entezari *et al.* (2003) have compared performance of classical equipment (operating at 20 and 500 kHz) with that of a new cylindrical reactor (operating at 35 kHz) for phenol degradation. For same power inputs, the rate of phenol degradation was higher at 500 kHz than at 35 or 20 kHz. Addition of H_2O_2 and copper sulphate to medium provides a different oxidation system that proceeds more efficiently at 35 kHz and the time of destruction was about 1/3rd the time needed at 500 kHz. It was also observed that intermediates are eliminated much faster at 35 kHz in comparison with other frequencies. Wu *et al.* (2001) have reported

synergistic action of ultrasound and UV light on the decomposition of phenol in aqueous solution. Lower pH and higher concentration of dissolved oxygen were found to be favorable parameters for the degradation. Presence of Fe^{2+} enhanced phenol removal further. Gogate *et al.* (2004) have studied phenol destruction in a novel triple frequency flow cell with maximum capacity of 7.5 liters. In comparison with a conventional batch reactor and a single frequency flow reactor, the multiple frequency reactor was found to give order of magnitude higher sonochemical yield and about 140 times larger scale of operation. In this work an attempt has also been made to establish effect of surface cavitation on the degradation rate provided by TiO_2 particles. Papadaki *et al.* (2004) have studied effect of low frequency irradiation on removal of phenol and its derivatives in presence of several heterogeneous catalysts (noble metals and metal oxides). Especially, the presence of Fe^{2+} ions was found to have marked effect on rate of phenol degradation. Jiang and Waite (2003) have also reported enhancement in phenol degradation rate in presence of Fe^{2+} ions. The rate was also found to be a function of solution pH and initial reactant concentration. Synergistic effect of UV coupled with ultrasound in presence of TiO_2 suspension for the degradation of phenol and chlorophenols has also been reported by Chen & Smirniotis (2002) and Davydov *et al.* (2001).

Seymour and Gupta (1997) have reported drastic enhancement in the oxidation of aqueous pollutants by addition of a salt such as NaCl. The enhancement was 6-fold for chlorobenzene, 7-fold for p-ethyl phenol and 3 fold for phenol. Seymour and Gupta have explained their results in terms of increase in ionic strength due to salt addition that drives organic pollutants to the bubble-bulk interface, where maximum oxidation reactions occur. Using this methodology, Mahamuni and Pandit (2006) have studied the degradation of phenol using different additives such as NaCl and CCl_4 Phenol degradation increased by 1.13 times for 2% NaCl addition and 1.5 times for 8% NaCl addition using an ultrasound horn.

This was explained by the fact that higher amount of NaCl would create more salting out effect, and thus, would increase the concentration of phenol in the bubble-bulk interfacial region that raises the possibility of hydroxyl radical attack on phenol molecules. Addition of CCl_4 showed enhanced degradation in the case of solutions with higher phenol concentration. For low concentration of phenol, the chloride radicals produced out of dissociation of CCl_4 inside the bubble combine with H radicals (produced out of dissociation of water vapor inside the bubble) to form HCl at the cavity interface instead of reacting with phenol molecules, which is loss of oxidation potential.

Ultrasonic degradation of phenol in combination with ozonation has been studied by many researchers (Zhao and Zhao, 2003; Lesko, 2004; Kidak and Ince, 2007). Variation in the degradation of phenol with different operating parameters like pH, irradiation time, ozone flux and sound intensity was investigated by Zhao and Zhao (2003). Phenol degradation was seen to be highest at pH 11 and it increased proportionately with sound intensity, ozone flux and irradiation time. Lesko (2004) has reported degradation of phenol under sonication, ozonation and the combination of two. Although effect of coupling of these oxidation processes was only additive, the synergistic effect of sonolytic ozonation was observed for reduction of total organic carbon. The rate of TOC decomposition was found proportional to aqueous steady-state ozone concentration and ultrasonic power density. Quantitatively, at 358 kHz sonication combined with ozonation enhanced TOC loss rates by 43%. Kidak and Ince (2007) have shown that combining ultrasound with ozonation, UV photolysis and ozonation/UV photolysis results in effective degradation of phenol at alkaline pH. This synergistic effect is due to enhanced ozone mass transfer (upon hydrodynamic shear forces created by ultrasonic bubbles) and excess hydroxyl radical formation (upon thermal decomposition of ozone in the gaseous cavity bubbles). Nikolopoulos *et al.* (2006) have shown that kinetics of catalytic wet peroxide oxidation enhances 6 to 11 times in presence of

ultrasound. This effect is attributed to reduction of the diffusion resistance within the catalyst pores, due to which the performance of catalyst increases.

1.8.2 Sonochemical degradation of chlorobenzene

Drijvers *et al.* (1998) have reported several intermediates following degradation of chlorobenzene (CB) in air-saturated solution: methane, acetylene, butenyne, butadiyne, benzene, chlorophenols, phenylacetylene and other chlorinated or non-chlorinated monocyclic and dicyclic hydrocarbons. For argon saturated solutions, same products were formed except chlorophenols. Presence of chlorophenol in case of air saturation demonstrated interactions between radicals formed and O_2, and no direct degradation by $OH^{\bullet}$ radicals. No pH effect was seen and saturation with argon accelerated the reaction. Addition of radical scavenger such as benzoate demonstrated that no significant degradation took place in the bulk medium. Price *et al.* (1994) obtained a first order rate constant of 0.055 min^{-1} and 0.08 min^{-1} for sonication of CB and 1,4-dichlorobenzene (1,4-DCB) at an intensity of 39 W cm^{-2}. For a given intensity of 20.9 W cm^{-2} the reaction rate of 1,4-DCB was faster than CB. Drijvers *et al.* (2000) compared sonolysis of four monohalogenated benzenes (viz. fluoro-, chloro-, iodo-, and bromobenzene) at 520 kHz and at different initial concentrations. Based on the analogy of intermediate products, the degradation mechanism for all four compounds was found to be same and sonolysis rates depended on the initial concentrations. In another study, Drijvers *et al.* (1999) have studied effect of presence of trichloroethylene (TCE) in different concentrations on the degradation rate of CB. The sonolysis rate of CB did not alter by addition of TCE. They have explained their result on the basis of compensation for the lowering of overall polytropic constant by addition of TCE by an increased indirect degradation of CB by radicals formed out of TCE. A study by Dewulf *et al.* (2001) demonstrates that the pseudo-first order rate constant of CB increases by a factor of 14.3 if

initial concentration drops from 3440 μM to 1 μM. This finding contradicts the mechanism proposed earlier, i.e. pyrolysis. Dewulf *et al.* have proposed a new model to explain their result incorporating gas phase $OH^{\bullet}$ radical induced degradation, next to pyrolysis. Simulations showed that in the concentration range of 1 – 5 μM, the $OH^{\bullet}$ radical mechanism contributed to 48.5% of total degradation. Jiang *et al.* (2002) and Petrier *et al.* (1998) have studied ultrasonic degradation of chlorinated aromatics in aqueous solutions. The disappearance of CB is almost instantaneously accompanied by the release of chloride ions due to rapid cleavage of C-Cl bond with concomitant release of CO, C_2H_2, CH_4 and CO_2. Based on this, they have suggested thermal degradation inside cavitation bubble as a preferred pathway for decomposition of CB. The degradation products of chlorobenzene were methane, acetylene, butadiyne and chlorinated, and non-chlorinated mono- and dicyclic hydrocarbons with chlorophenol as the minor byproduct (Ondruschka and Hofmann, 1999). With these byproducts, Ondruschka and Hofmann (1999) speculate that the degradation of chlorobenzene would occur by thermal pyrolysis. Stavarache *et al.* (2002, 2004) have investigated effect of Fe_2SO_4, $PdSO_4$, $PdCl_2$ and Pd(0) on degradation of CB in aqueous solution at 200 kHz. They propose possibility of a complex formation between $PdCl_2$ and CB. Sekiguchi and Saita (2001) have reported enhancement in the CB degradation due to presence of alumina particles at 20 kHz frequency. The possible mechanism for enhancement was the increase in number of cavitation bubbles, and hence, increase in the decomposition rate. Rong *et al.* (2001) have studied degradation of chlorobenzene in a recycle ultrasonic reactor. The extent of degradation is found to increase with increasing volumetric flow rate, reactor volume and frequency with electric power kept constant. Rong *et al.* (2001) have shown that the sonochemical effects can be interpreted in terms of the ultrasonic intensity or the ultrasonic energy consumed in the reactor. Studies of Okuno *et al.* (2000) and Petrier *et al.* (1999) with chlorobenzene and other chloro-aromatics subjected to ultrasound showed an

interesting trend in degradation. Compounds having higher vapor pressure showed efficient and faster degradation rates. Recently, Petrier *et al.* (2007) studied the oxygen induced concurrent ultrasonic degradation of chlorobenzene and 4-chlorophenol. The cavitation induced degradation rates of organic compounds in water are mainly linked to their vapor pressure and solubility. For argon saturated medium, more volatile chlorobenzene enters the cavitation bubble and undergoes pyrolytic destruction. The degradation of 4-chlorophenol occurs subsequently only when the chlorobenzene has been destroyed completely. But the degradation of the two compounds occurs simultaneously for an oxygen saturated medium. This has been explained by two mechanisms: first, the oxygen present in the shell (where supercritical conditions exist at the moment of collapse) increases the production of OH radicals, and secondly, additional production of OH radicals from the dissociation of chlorobenzene within the cavitation bubble.

1.8.3 Sonochemical degradation of nitrobenzene

The principal intermediates for nitrobenzene reduction are 4-nitrocatechol and benzoquinone. Weavers *et al.* (1998) have studied effect of sonolysis, ozonolysis and combination of two on the degradation of nitrobenzene (NB), 4-chlorophenol and 4-nitrophenol. The degradation rate enhanced at 20 kHz due to sonolytic ozonation, while at 500 kHz an apparent retardation was seen. The total degradation rate was characterized by three first order rate constants, k_{US}, k_{O3} and $k_{US/O3}$, due to individual and combined mechanisms. The retardation at 500 kHz was correlated with increasing k_{O3}. This is consistent with pathway involving thermolytic destruction of O_3 to form atomic oxygen, which then reacts with water vapor in cavitation bubbles, yielding gas phase hydroxyl radical. The principal degradation products for sonochemical degradation of nitrobenzene at low frequency (20 kHz) are 4-nitrophenol, 3-nitrophenol and 4-nitrocatechol (Weavers *et al.*, 1998). These products hint at hydroxylation

(or reaction with OH radicals generated from cavitation bubbles) as the major chemical pathway for degradation. Cropek and Kemme (1998) have reported formation of phenol, 4-methyl-3-pentenal, 4-methyl-4-hydroxy-2-pentanone, phenol, nitrophenol, butylated hydroxytoluene and benzoquinone as degradation products of nitrobenzene. Hung *et al.* (2000) found rate of reduction of NB by Fe^o enhanced by presence of ultrasound. The first order rate constant for ultrasonic degradation of NB in absence of Fe^o was found to be 1.8×10^{-3} min^{-1} compared to 7.8×10^{-3} min^{-1} in presence of 70 g L^{-1} Fe^o. The total degradation rate of Fe^o was given by a linear combination of the three mechanisms: ultrasound, Fe^o and combination of two; each characterized by a first order rate constant. The faster degradation rates in presence of ultrasound and Fe^o are attributed to several causes: continuous ultrasonic cleaning and activation of Fe^o surface, accelerated mass transport due to turbulence created by cavitation bubbles and acidity produced by H^+ released from HNO_3, a product of sonolysis of nitrobenzene and water. Zhao and Zhao (2001) and Zhao and Lu (2003) have studied sonochemical degradation of nitrobenzene along with Fenton's reagent and ozone. Effects of process parameters like pH, sonication time, nitrobenzene concentration, ferrous ion concentration, H_2O_2 concentration, ozone flux and ultrasound intensity were studied. The efficiency of nitrobenzene degradation was higher under acidic conditions for Fenton's reagent and ozone. The removal efficiency of nitrobenzene was improved by increasing the sound intensity, ozone flux and reaction time. The extent of nitrobenzene degradation showed an optimum concentration for ferrous ion and H_2O_2. Other techniques employed for degradation of nitrobenzene include reaction with Fenton reagent (Rodriguez *et al.*, 2003), hybrid reactor with trickling filter and activated sludge (Majumder and Gupta, 2003), ozonation catalyzed by Mn-oxide (Ma *et al*., 2005), photocatalytic degradation (Bhatkhande *et al*., 2003) and ozonation/UV process (Latifoglu and Gurol, 2003).

1.8.4 Sonochemical degradation of p-nitrophenol

The main sonooxidation products of p-nitrophenol (p-NP) are nitrites (NO_2^-) and nitrates (NO_3^-), short chain carboxylic acids, formic acid (or formate), acetic acid (or acetate) and oxalic acid (or oxalate) with intermediates such as 4-nitrocatechol, hydroquinone and benzoquinone. Kotronarou *et al.* (1991) and Hoffmann *et al.* (1996) found two independent mechanisms for degradation of p-nitrophenol: (a) via gas phase reaction that takes place in pure water; (b) the direct decay (pyrolysis) of the p-NP molecules. Out of the two species generated, viz. NO_2^- and NO_3^-, NO_3^- did not interfere with sonochemical reactions of p-NP; however NO_2^- appeared to affect decay of p-NP and formation of 4-nitrocatechol. Presence of 100 μM $NaNO_2$ in a solution of 100μM p-NP was found to reduce the rate constant for disappearance of p-NP from 3.67×10^{-4} s^{-1} to 2.0×10^{-4} s^{-1}. The degradation of p-NP involved high temperature reactions of p-NP in the interfacial region of cavitation bubbles and the main pathway was C-N bond cleavage with hydroxyl radical reaction. Degradation of p-NP in a high power ultrasonic system (NEARFIELD acoustic processor) in presence of argon and oxygen has been investigated by Hua *et al.* (1995). The highest degradation rate was in presence of Ar/O_2 mixture (4:1 v/v) with a pseudo-first order rate constant of 1.2×10^{-3} s^{-1}, at an intensity of 1.4 W cm^{-2}. Cost *et al.* (1993) also studied sonochemical reactions of p-NP in solutions containing phosphate and bicarbonate ions and humic acid. The pesudo first order rate constant (3.4 to 3.2×10^{-4} s^{-1}) was slightly lower than that for deionized water (4.4×10^{-4} s^{-1}). Cost *et al.* have also studied the degradation rate of phenol in natural water. Other chemicals in natural water did not affect the degradation rate. Barbier and Petrier (1996) investigated the ultrasonic degradation and mineralisation of 4-nitrophenol (4-NP) at two frequencies (20 and 500 kHz) and in water saturated with O_2/O_3 mixture. Coupling ultrasound with ozone increased the potential of ozonation to mineralise 4-NP degradation products. At low pH of 2, 4-NP mineralisation at 500 kHz was 1.8 times faster than at 20 kHz

for same O_3 consumption. Tauber *et al.* (2000) distinguished between the two mechanisms of p-NP degradation in argon saturated at different pH: at pH 10 the decomposition was solely due to $OH^{\bullet}$ induced reactions, while at pH 4 oxidative pyrolytic degradation dominated. Effect of pH on p-NP degradation has also been investigated by Jiang *et al.* (2002), who found the rate to fall with increasing pH. They have explained their result in terms of easier diffusion and accumulation of neutral species at the hydrophobic gas/liquid interface of bubbles in comparison to their ionic form. Hua and Hoffmann (1996) have reported acceleration in the sonochemical degradation of p-NP in presence of CCl_4. This effect is attributed to presence of HOCl species, resulting from CCl_4 sonolysis. Sivakumar *et al.* (2002) have studied effect of dual frequency (25 and 40 kHz) on p-NP degradation. For three frequency modes, 25 kHz, 40 kHz and 25 & 40 kHz together, the effects of parameters such as initial solution pH and bulk temperature were studied. The dual frequency mode was found to be much better than the single frequency mode. The results have been explained on the basis of simulation of radial bubble dynamics under influence of single frequency and dual frequency. Entezari and Petrier (2003, 2005) studied the degradation of substituted phenols, either individual or in the form of mixtures, by sonolysis, enzyme treatment and the combination of these. The extent of degradation of p-nitrophenol in individual solution and in the solution of mixture was same.

Apart from sonolysis, several other techniques have also been applied for the degradation of p-nitrophenol. These include activated sludge process (Bhatti *et al.*, 2002), hydrodynamic cavitation jets (Kalumuck and Chahine, 2000), adsorption on activated carbon (Kumar *et al.*, 2007), electro-Fenton method (Zhang *et al.*, 2007), photo-Fenton method (Kavitha and Palanivelu, 2005), photocatalysis (Essam *et al.*, 2007), UV/Fe^{3+} process combined with electrocatalysis (Zhou and Lei, 2006) and UV/H_2O_2 process (Daneshvar *et al.*, 2007).

1.8.5 Sonochemical degradation of 2,4 Dichlorophenol (2,4 DCP)

In comparison to phenol and chlorobenzene, the number of studies dealing with sonochemical degradation of 2,4 dichlorophenol (2,4 DCP) are limited. The intermediates and products (i.e. 2-chlorophenol, 4-chlorophenol and phenol) of sonochemical degradation of 2,4 DCP reported by Goskonda *et al.* (2002), Yasman *et al.* (2004) and Wu *et al.* (2007) hint at hydroxylation as the dominant chemical mechanism. Goskonda *et al.* (2002) have examined ultrasonic mineralization of 2,4 DCP. Effect of parameters such as initial concentration, bulk temperature, pH and presence of co-solutes such as detergents and humic acid were also investigated. Ultrasonic degradation of 2,4 DCP was enhanced by coupling with other treatment processes like photoelectrochemical (Compton *et al.*, 1997), sonoelectrochemical (Yasman *et al.*, 2004) and electro-catalysis (Yasman *et al.*, 2006). Compton *et al.* (1997) used an oxide coated titanium tip placed in a conventional three electrochemical cell which allows light from a monochromated source to be focused onto the electrode surface. Low intensity ultrasound (1 to 3 W/m^2) was used in order to avoid attenuation of light due cloud formation which occurs at high intensity. Ultrasound shifts the observed photocurrent responses to more negative potentials and thereby enhances the degradation processes. Yasman *et al.* (2004) developed a new method for the degradation of 2,4 DCP using combination of ultrasound waves, electrochemistry and Fenton's reagent. Yasman *et al.* (2004) attribute high degradation power of this method to large production of OH radicals and high mass transfer due to sonication. In another study, Yasman *et al.* (2006) have optimized the reaction system for Fe^{2+} ions (2 mM) required for this process. Sonoelectrochemical treatment with finely divided (black) Pd and Pd–Fe powder allows far more effective destruction of 2,4 DCP. The bimetallic catalyst (Pd–Fe) appears to be

energetically and economically superior to the Pd. In both cases, the reaction times were considerably shortened in comparison with traditional electro-catalytic processes.

Zhou *et al.* (2008) investigated the effect of ultrasound enhancement on the degradation of 2,4 DCP using a new Fenton like (Fe/EDTA) system. With simultaneous application of ultrasound, the degradation rate of 2,4 DCP showed marked rise than the degradation with Fe/EDTA and sonication alone. Increasing the dosage of iron form 5 g/l to 25 g/l increased the degradation rate of 2,4 DCP. However, the degradation rate decreased slightly when the dosage of iron was increased from 25 g/l to 50 g/l. In addition, degradation rate showed proportional variation with EDTA concentration and inverse variation with initial concentration of 2,4 DCP. Variation of the power input (from 110W to 550W) showed an increasing degradation rate. The optimum power was found to be 385 W.

Degradation of 2,4 DCP using other techniques such as biological treatment, adsorption and photobiodegradation has also been studied. Ziagova and Kyriakides (2007) have compared ability of *pseudomonas sp*. to degrade 2,4 DCP in presence of glucose as a conventional carbon source. Wu and Yu (2008) have studied continuous flow adsorption of 2,4 DCP from aqueous solutions by immobilized Phanerochaete Chrysosporium biomass in a fixed bed column. Influence of microbial variations and operating conditions on removal of 2,4 DCP, using upflow anaerobic sludge blanket (USAB) reactor, has been studied by Sponza and Cigal (2008). Wang *et al.* (2007) have investigated adsorption of 2,4 DCP by activated carbon fiber activated by static air. Wang *et al.* (2007a) developed aerobic granules (with addition of glucose as co-substrate) for the biological degradation of 2,4 DCP in a sequencing batch reactor. Wu *et al.* (2007) have reported efficient phobiodegradation of 2,4 DCP in aqueous solution catalyzed by PDVB-ZnPc.

Table 1.1. Physico-chemical properties of the pollutants

Sl.No.	Properties	Phenol	Chlorobenzene	p-nitrophenol	Nitrobenzene	2,4-dichlorophenol
1	**CAS Registry No.**	108-95-2	108-90-7	100-02-7	98-95-3	120-83-2
2	**Chemical formula**	C_6H_6O	C_6H_5Cl	$C_6H_5NO_3$	$C_6H_5NO_2$	$C_6H_4Cl_2O$
3	**Molecular weight**	94.11	112.56	139.11	123.11	163
4	**Color**	Colorless to light pink.	Colorless.	Colorless to slightly yellow crystals.	Yellow.	Colorless crystals, white or pale yellow solid.
5	**Physical state**	Crystalline solid.	Liquid.	Yellow to brown crystals.	Liquid	Yellow crystals
6	**Melting point ºC**	43	-45.6	113 - 114	5.7	45
7	**Boiling point ºC**	181.8	132	279	210.8	210
8	**Density at 20 ºC**	1.0545 @ 45 ºC /4 ºC	1.1058	1.27	1.2037	1.383
9	**Odor**	Distinct aromatic, somewhat sickening, sweet and acrid odor.	Aromatic, almond like.	Odorless.	Bitter almonds and shoe polish.	-
10	**Odor threshold:**					
	Water (ppm)	7.9	0.05	-	0.11	0.21
	Air	1 ppm (w/v)	1 - 8 mg/m^3	-	0.092 mg/m^3	0.21
11	**Solubility:**					
	Water at 25 ºC (ppm)	83000	500	16000	1900	4500
	Organic solvents	Very soluble in alcohol, chloroform, ether, benzene, acetone and water.	Soluble in ether, alcohol and benzene.	-	Soluble in ether, alcohol and acetone.	Soluble in carbon tetrachloride, alcohol, benzene and ethyl ether, soluble in aqueous alkali.
12	**Partition coefficients:**					
	Log K_{ow}	1.46	2.84	1.91	1.86	3.06
	Log K_{oc}	1.21 - 1.96	2.52	-	1.56	-
13	**Vapor pressure at 25 ºC**	46 Pa	1598 Pa	0.0032 Pa	33.69 Pa	25.84 Pa
14	**Henry's law constant**	4.0 x 10^{-7} m^3/mol	3.58 x 10^{-3} atm-m^3/mol	-	1.31 x 10^{-5} atm-m^3/mol	-
15	**Autoignition temperature ºC**	715	637	-	482	-
16	**Flash point, open cup ºC**	85	29.4	169	87.7	-
17	**Flash point, closed cup ºC**	79	-	-	-	-
18	**Flammability limits (in air, by % v)**	1.7 - 8.6	1.8 - 9.6	1	-	-
19	**Synonyms**	Benzenol, hydroxybenzene, monophenol, oxybenzene, phenyl alcohol, phenyl hydrate, phenyl hydroxide, phenylic acid and phenylic alcohol.	Monochlorobenzene, benzene chloride, phenylchloride, MCB and chlorobenzol.	4-hydroxynitrophenol, Paranitrophenol, 4-nitrophenol, PNP, Niphen and Mononitrophenol.	Nitrobenzol and oil of Mirbane.	4-Hydroxy-1,3-dichlorobenzene.
20	**Effluent Discharge limit (mg/l)**	1	100 µg/l (EPA)	60 µg/l (EPA)	1 mg/l (EPA)	20 µg/l (EPA)

CHAPTER 2

Basic Principles of Ultrasound Wave Phenomena and Cavitation Bubble Dynamics

Sonochemical degradation of a variety of organic pollutants has been investigated for the past two decades. Sonolysis is basically an advanced oxidation process in which the oxidizing OH radical is produced out of cavitation bubbles, whose radial motion and transient collapse is governed by the ultrasound wave. Thus, the basic or fundamental physical phenomena underlying the degradation of pollutant through sonolysis are propagation of ultrasound wave through the liquid medium and the radial motion of the cavitation bubbles. As noted earlier, the principal aim of this thesis is to discern the physical features of the sonochemical degradation of various aromatic pollutants. This would essential mean linking up the results of sonochemical degradation of pollutant to the radial motion of cavitation bubbles. This is basically the main approach adopted in the present thesis. It would be helpful if we familiarize ourselves with some basic principles of ultrasound wave phenomena and bubble dynamics before proceeding to the main components of the research work.

In this chapter, some basic principles of the ultrasound wave phenomena and cavitation bubble dynamics are described. Information presented in this chapter is largely derived from standard textbooks (Mason and Lorimer, 2002; Young, 1989; Leighton, 1994; Shah *et al.*, 1999; Suslick, 1988; Ensminger, 1988; Pierce, 1989) and popular reviews (Neppiras, 1980; Plesset and Prosperetti, 1977; Brenner *et al.*, 2002; Flynn, 1964) in the area of acoustics, cavitation and sonochemistry.

2.1 PHYSICS OF AN ACOUSTIC WAVE

Sound passes through a compressible medium, such as air or water, in the form of a longitudinal wave. The pressure as well as density of the medium undergoes periodic variation with passage of wave. The particles or molecules of the medium undergo an oscillatory motion around a mean position with passage of sound wave. In the general form, propagation of the acoustic wave is described by the wave equation (Pierce, 1989):

$$\nabla^2 P - \frac{1}{c^2}\frac{\partial^2 P}{\partial t^2} = 0, \text{ where } c^2 = \left(\frac{\partial P}{\partial \rho}\right)_{S = \text{constant}} \tag{2.1}$$

A simple solution to this equation is written as:

$$P(x,t) = P_A \cos(\omega t - \mathbf{k}x) \tag{2.2}$$

where ω is the angular frequency of the acoustic wave, written as $\omega = 2\pi f$. **k** is the wave number given as $2\pi/\lambda$, where λ is the wavelength of the wave and f is the frequency. A relation between particle velocity (ν) and acoustic pressure (P_A) can be derived as follows (Mason and Lorimer, 2002):

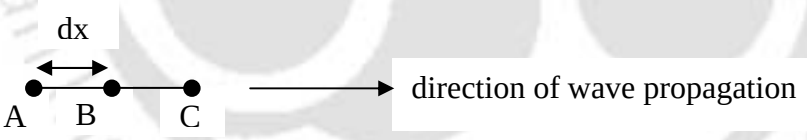

Figure 2.1. Motion of a fluid element under influence of acoustic wave

Consider an acoustic wave with amplitude P_A passing through the medium. Let the ambient pressure in the medium be P_0. The velocity of the wave is c. Any fluid element (Figure 2.1), initially located at point A (with zero velocity) moves to point B under the influence of the wave. If the distance between point A and B is dx, this displacement occurs in dx/c seconds. If the velocity of the fluid element at point B is v, then the acceleration of the element is:

$$\frac{\nu}{dx/c}.$$

If the density of the medium is ρ, the mass of the fluid element (for unit area perpendicular to the direction of the fluid propagation) is: ρdx. Using fundamental principle:

$$(\text{Mass} \times \text{Acceleration}) = \text{Force}$$

$$\text{we get: } \rho dx \times \frac{\nu c}{dx} = (\text{Pressure} \times \text{Area}) = P_A \times 1 = P_A$$

$$P_A = \rho \nu c$$

$$\text{or } \frac{P_A}{\rho c} = \nu$$

2.2 ACOUSTIC IMPEDANCE AND INTENSITY

On the basis of pressure amplitude of the acoustic wave passing through the medium and the velocity of the oscillatory motion of the fluid elements, one can define the quantity "acoustic impedance" which is an analogue of resistance. Correlating the case to Ohm's law, the applied pressure corresponds to voltage and the velocity of oscillatory motion corresponds to current. The acoustic impedance is, thus, written as:

$$Z = \frac{\text{Acoustic pressure}}{\text{Particle velocity}} = \frac{P_A}{\nu} = \rho c$$

The quantity ρc, which is proportionality between pressure and velocity of the acoustic wave is called characteristic impedance of the medium. For two common media, viz. air and water, the characteristic impedance can be calculated as follows:

Air: $\rho = 1.2\ \text{kg/m}^3$, $c = 341\ \text{m/s}$, $\rho c = 400\ \text{kg/m}^2\text{s}$
Water: $\rho = 1000\ \text{kg/m}^3$, $c = 1500\ \text{m/s}$, $\rho c = 1.5 \times 10^6\ \text{kg/m}^2\text{s}$

Acoustic intensity is basically the measure of rate at which energy in the wave crosses a unit area perpendicular to the direction of propagation. Leighton (1994) has shown that the total energy density in a plane progressive acoustic wave is: $\frac{1}{2}\rho\left|\dot{\varepsilon}\right|^2_{\max}$, where ε is the displacement of the particle and $\dot{\varepsilon}$ is its time derivative, indicating velocity. If the velocity of the acoustic

wave is c, then the total energy crossing a segment of area A in time Δt will be: total energy density $\times$ $Ac\Delta t$.

On this basis, we can identify that the energy crossing a unit area in unit time is:

$$I = \text{total energy density} \times c = \frac{1}{2}\rho\left|\dot{\varepsilon}\right|_{max}^{2} c \tag{2.3}$$

The velocity of the particles, $\left|\dot{\varepsilon}\right|_{max}$, can be written in terms of pressure amplitude and acoustic impedance as:

$$\left|\dot{\varepsilon}\right|_{max} = \frac{P_A}{Z} = \frac{P_A}{\rho c} \tag{2.4}$$

Thus, the intensity of acoustic wave is:

$$I = \frac{P_A^2}{2\rho c} \tag{2.5}$$

The intensity of the acoustic wave is proportional to the square of the pressure amplitude of the acoustic wave.

2.3 ATTENUATION

During propagation through a medium, the energy of the acoustic wave (and as a result, the pressure amplitude) reduces. The principal causes of this effect are: (1) frictional loss; (2) thermal loss and (3) damping due to bubbles.

2.3.1 Frictional loss

The frictional loss is mainly attributed to the viscosity of the medium. Some of the momentum of the wave is absorbed by the medium, as a result of which it is set into unidirectional motion. These fluid currents are termed as acoustic streaming. An expression given by Stokes (1849) describing this loss is:

$$\alpha_s = \frac{8\mu\pi^2 f^2}{3\rho c^3} \tag{2.6}$$

The above expression indicates that the attenuation faced by acoustic waves of higher frequency is larger.

2.3.2 Thermal loss

This effect is attributed to conduction of heat between adjacent regions of compression and rarefaction. The compression or high pressure region will be at a temperature higher than average temperature of medium while the rarefaction or low pressure region will be at a temperature lower than the average temperature. Conduction of heat between these regions will result in loss of the compression work, as not all of it would be returned while the ensuing expansion. Kirchoff (1868) has given an absorption coefficient accounting for this effect as:

$$\alpha_{th} = \frac{2\pi^2 k(\gamma-1)f^2}{\rho\gamma C_V c^3} \tag{2.7}$$

where, k is the polytropic constant, $\gamma = C_P / C_V$, and f is the frequency of acoustic wave.

2.3.3 Damping due to bubbles

The third cause of attenuation of an acoustic wave is absorption and scattering due to the bubbles present in the liquid medium. A rigorous analysis of this effect is given by Prosperetti and Commander (1989). We give herewith the final results of this analysis and refer the reader to original paper for greater details.

The ratio of velocity of sound in pure liquid (c) to that in a bubbly liquid (c_m) is:

$$\frac{c}{c_m^2} = 1 + \frac{4\pi c^2 n_b R_0}{\omega_0^2 - \omega^2 + 2ib\omega} \tag{2.8}$$

where n_b is the number density of bubbles and R_0 is the equilibrium radius. For small bubbles (with size smaller than corresponding to the resonant frequency), the natural oscillatory frequency (ω_0) and damping coefficient (b) is given as:

$$\omega_0^2 \simeq \frac{P_0}{\rho R_0^2}\left(3\gamma - \frac{2\sigma}{P_0 R_0}\right) \tag{2.9}$$

$$b = \frac{\gamma - 1}{10\gamma}\frac{P_0}{\rho\kappa} + \frac{2\mu}{\rho R_0^2} \tag{2.10}$$

2.4 CAVITATION BUBBLE DYNAMICS

Cavitation is generally known to be a fluid transportation problem. The first investigation in the cavitation phenomenon was made by Sir John Thornycraft and Sidney Barnaby in their attempt to the erosion of propeller blades. However, research in the past several decades has conclusively proven that controlled cavitation can be a useful tool in intensification of several physical and chemical processes. The principal cause behind cavitation, which can be defined as nucleation, growth, oscillation and collapse of small gas or vapor bubbles, is the pressure variation in the system. On the basis of this criterion, cavitation can be categorized as:

(1) **Acoustic Cavitation**, which results due to pressure variation generated due to passage of an acoustic wave.

(2) **Hydrodynamic Cavitation**, which results due to pressure variation in the liquid flow due to changing flow geometry.

Other two means of producing cavitation, which are largely restricted to fundamental studies of cavitation phenomenon, are:

(1) **Optic Cavitation**, which is a result of local evaporation of liquid due to an intense energy dissipation, such as laser.

(2) **Particle Cavitation**, which is produced by any elementary particle (such as proton) rupturing the liquid.

2.4.1 Inception of cavitation

Theoretically, cavitation phenomenon involves creation of voids in the liquid. With progression of sound wave in the medium, the molecules of the liquid oscillate about mean position. In the compression phase, the distance between the molecules decreases, while during rarefaction the molecules are pulled apart and the distance between them increases. If the amplitude of the acoustic wave is large enough, the distance between molecules may exceed the critical distance to hold the liquid intact (also known as van der Waal's distance), resulting in creation of voids. Typically, this pressure amplitude required for this phenomenon is $2\sigma/R$, where σ is the surface tension and R is the van der Waal's distance. For water, the values are σ = 0.072 N/m and R = 4×10^{-10} m. Thus, the theoretical pressure and amplitude required for creation of void is ~ 1500 atm.

However, actual cavitation phenomenon occurs at far lower pressure amplitude. This is attributed to the phenomenon of nucleation. Nucleation occurs due to presence of solid particles, or tiny free-floating bubbles present in the liquid that act as weak spots. Another source of nucleation is the gas pockets trapped in the crevices of the solid boundaries in the medium. These solid boundaries could be walls of the reactor or tip of the ultrasound horn. These gas pockets have a concave meniscus. The radius of curvature of the gas pocket, as seen from liquid, is negative. Therefore, the surface tension force (or Laplace pressure) acts in the liquid. The pressure inside the bubble is lesser than the ambient pressure. Due to this pressure difference, the dissolved gas in the medium diffuse into the gas pocket, thus stabilizing it. These gas pockets can grow in response to reduction in ambient pressure with passage of acoustic wave. A mathematical analysis of the crevice model for nucleation has been presented by Atchley and Properetti (1989).

Atchley and Properetti (1989) have proven that the rate of growth of these gas pocket depends on two physical quantities: First, the rate of fall of Laplace pressure (as the meniscus

of gas pocket recedes), and secondly, the rate of reduction in partial pressure of gas. If the rate of fall of Laplace pressure is slower than reduction in partial pressure of gas, the pocket growth is slow. On the other hand, if all of partial pressure of gas is slower, the growth of gas pocket is very rapid, due to which the gas pocket comes out of the crevice giving rise to nucleation in the medium.

The gas pockets present *in situ* in the medium comprise of air. However, nuclei of any other gas can also be supplied externally – by sparging the desired gas through porous media (such as a glass frit), which would offer sufficient pressure drop to disperse the gas uniformly in form of small bubbles (*as described in the subsequent chapters, this technique has been adopted widely in this thesis*). The phenomenon of nucleation broadens the definition of cavitation as growth, oscillation and collapse of gas bubbles already present in the medium or vapor bubbles generated out of passage of ultrasound wave.

2.4.2 Radial Motion of Cavitation Bubbles

Under the influence of the acoustic wave, which creates periodic pressure variation in the medium, the cavitation bubble undergoes volume oscillations. The amplitude of these volume oscillations depends on the amplitude of the acoustic wave. For relatively small pressure amplitudes, the volume oscillations of the bubbles are also small and essentially in phase with the acoustic pressure wave. However, for larger pressure amplitude, the volumetric oscillations become nonlinear comprising of an explosive initial growth followed by a transient collapse and a few afterbounces. The subject of radial motion of cavitation bubble has been extensively investigated in past 100 years. The first ever analysis of the collapse of an “empty” cavity under constant ambient pressure was given by Lord Rayleigh (1917). This analysis used the definition of cavity given by Besant (1889) as “a spherical portion of liquid suddenly annihilated”. We give herewith a sample derivation of the radial motion of cavitation bubbles (Leighton, 1994):

Consider a bubble of size few micrometers size located in an incompressible liquid. The initial radius of the bubble is R_0. At time $t > 0$, a time varying pressure field is applied in the liquid. This is essentially a pressure P(t) which is super-imposed on ambient pressure P_0. Thus, the pressure in the liquid at large distances from the bubble is $P_\infty = P_0 + P(t)$. As a result of this pressure variation, the bubble radius changes attaining a new value R(t). This motion imparts a kinetic energy to the liquid, written as:

$$\text{K.E.} = \frac{1}{2}\rho \int_R^\infty \dot{r}^2 4\pi r^2 dr \tag{2.11}$$

If the liquid is incompressible the mass balance of liquid between bubble wall and any shell concentric with the bubble of radius r gives:

$$\dot{r}\, r^2 = \dot{R}\, R^2 \tag{2.12}$$

Substituting above equation in expression for KE and integrating gives:

$$\text{K.E.} = 2\pi R^3 \dot{R}^2 \rho \tag{2.13}$$

However, this gain in the kinetic energy of liquid is equal to the work done remote from bubble by P_∞ and the work done by pressure P_L in the liquid just outside bubble wall. Using this energy balance, we get:

$$\int_{R_0}^{R} \left(P_L - P_\infty\right) 4\pi R^2 dR \tag{2.14}$$

Equating the equations 2.13 and 2.14 gives:

$$\int_{R_0}^{R} \left(P_L - P_\infty\right) 4\pi R^2 dR = 2\pi R^3 \dot{R}^2 \rho \tag{2.15}$$

Differentiating the above energy balance w.r.t R gives:

$$\left(P_L - P_\infty\right) 4\pi R^2 = 2\pi R^3 \rho \frac{\partial}{\partial R}\left(\dot{R}^2\right) + 2\pi\rho \dot{R}^2 3R^2 \tag{2.16}$$

Using chain rule:

$$\frac{\partial}{\partial R}\left(\dot{R}^2\right) = \frac{1}{\dot{R}}\frac{\partial\left(\dot{R}^2\right)}{\partial t} = \frac{2\dot{R}}{\dot{R}}\frac{\partial\dot{R}}{\partial t} = 2\frac{\partial^2 R}{\partial t^2} \tag{2.17}$$

Finally, we get:

$$\frac{\left(P_L - P_\infty\right)}{\rho} = \frac{3}{2}\dot{R}^2 + R\ddot{R} \tag{2.18}$$

P_L, the pressure in the liquid just outside bubble surface is determined as follows:

The bubble may initially comprise of either gas or mixture of gas and vapor. Thus, the pressure inside the bubble is $P_i = P_g + P_V$. Due to surface tension forces, the pressure inside the bubble is greater than pressure in liquid outside bubble surface by amount $2\sigma/R_0$. Thus:

$$P_i = P_L + \frac{2\sigma}{R_0} \tag{2.19}$$

If the bubble is initially in static equilibrium, then pressure throughout the liquid medium (including the region immediately outside the bubble surface) is P_0. Thus,

$$P_i = \left(P_0 + \frac{2\sigma}{R_0}\right) \tag{2.20}$$

Once set into the radial motion, the bubble radius changes from an initial value R_0 to any value R at time t. The pressure of gas in the liquid falls, however, vapor pressure stays the same. Assuming that gas present in the bubble obeys polytropic law, we can write:

$$P_i = \left(P_0 + \frac{2\sigma}{R_0} - P_V\right)\left(\frac{R_0}{R}\right)^{3K} + P_V \tag{2.21}$$

where k is the polytropic constant. Inserting expressions for P_i in equation 2.18, we get:

$$R\frac{d^2R}{dt^2} + \frac{3}{2}\left(\frac{dR}{dt}\right)^2 = \frac{1}{\rho}\left\{\left(P_0 + \frac{2\sigma}{R_0} - P_V\right)\left(\frac{R_0}{R}\right)^{3K} + P_V - \frac{2\sigma}{R} - \left(P_0 + P(t)\right)\right\} \tag{2.22}$$

The above expression ignores the effect of viscosity of the medium. Plesset (1949), Poritsky (1952), Noltingk and Neppiras (1950) later extended the above approach to include effect of

viscosity of the medium. We give herewith the final equation (popularly known as Rayleigh-Plesset equation) and refer the reader to original papers for detailed derivation.

$$R\frac{d^2R}{dt^2} + \frac{3}{2}\left(\frac{dR}{dt}\right)^2 = \frac{1}{\rho}\left\{\left(P_0 + \frac{2\sigma}{R_0} - P_V\right)\left(\frac{R_0}{R}\right)^{3K} + P_V - \frac{2\sigma}{R} - \frac{4\mu}{R}\frac{dR}{dt} - \left(P_0 + P(t)\right)\right\} \quad (2.23)$$

The above expression still did not account for the compressibility of liquid. During large amplitude volume oscillations, the velocity of bubble wall (dR/dt) reached or even exceeded the sonic velocity (1500 m/s for water as liquid medium). At this instance, the compressibility effect needs to be taken into account.

2.4.3 Equation Accounting for Liquid Compressibility

The Rayleigh-Plesset equation did not take into account liquid compressibility, and hence, cannot be applied for $dR/dt > c$. In past six decades several authors have attempted to incorporate liquid compressibility into mathematical formulation for radial bubble motion. The first attempt in this regard was done by Gilmore (1954) who used the Kirkwood-Bethe hypothesis (1942) as the basis. This hypothesis stated that for spherical waves with finite amplitude, the quantity $r\phi$ (r - radial coordinate, ϕ - velocity potential) propagates with velocity equal to sum of the liquid velocity and sound velocity. The local velocity of sound is expressed as a function of the free enthalpy on the surface of the bubble. The main components of the Gilmore model for radial bubble motion are:

1. *Radial motion*:

$$R\left(1-\frac{dR/dt}{c}\right)\frac{d^2R}{dt^2} + \frac{3}{2}\left(1-\frac{dR/dt}{3c}\right)\left(\frac{dR}{dt}\right)^2 = \left(1+\frac{dR/dt}{c}\right)H + \frac{dR/dt}{c}\left(1-\frac{dR/dt}{c}\right)R\frac{dH}{dR} \quad (2.24)$$

2. *Free enthalpy at bubble surface*:

$$H = \left(\frac{n}{n-1}\right)\frac{A^{1/n}}{\rho_0}\left\{\left[\left(P_0 + \frac{2\sigma}{R_0}\right)\left(\frac{R_0}{R}\right)^{3k} - \frac{2\sigma}{R} + B\right] - \left[P_0 - P_A \sin\omega t + B\right]^{n-1/n}\right\} \quad (2.25)$$

3. *Velocity of sound*: $c = \left[c_0^2 + (n-1)H\right]^{1/n}$, where $c_0 = \sqrt{\frac{An}{\rho_0}}$ (2.26)

4. *Tait equation of state*: $P = A\left(\frac{\rho}{\rho_0}\right)^n - B$ (2.27)

(For water the constants A, B and n are: A = 3001 atm, B = 3000 atm and n = 7)

In an alternate approach, Keller and coworkers proposed the following equation (Keller and Kolodner, 1956; Keller and Miksis, 1980; Prosperetti and Lezzi, 1986; Brennen, 1995):

$$\left(1-\frac{\dot{R}}{c}\right)R\rho\frac{d^2R}{dt^2}+\frac{3}{2}\left(\frac{dR}{dt}\right)^2\rho\left(1-\frac{\dot{R}}{3c}\right)=\left(1+\frac{\dot{R}}{c}\right)\left(P_g - P_0 - P(t)\right) + \frac{R}{c}\frac{dP_g}{dt}-4\mu\frac{dR/dt}{R}-\frac{2\sigma}{R} \tag{2.28}$$

Prosperetti and Lezzi (1986) presented a general form of the above equation as one-parameter family of equations:

$$\left[1-(\lambda+1)\frac{\dot{R}}{c}\right]\rho R\frac{d^2R}{dt^2}+\frac{3}{2}\left(\frac{dR}{dt}\right)^2\rho\left[1-(\lambda+1/3)\frac{\dot{R}}{c}\right]=\left(1+(1-\lambda)\frac{\dot{R}}{c}\right)\left(P_g - P_0 - P(t)\right) + \frac{R}{c}\frac{dP_g}{dt}-4\mu\frac{\dot{R}}{R}-\frac{2\sigma}{R} \tag{2.29}$$

However, all equation with different numerical values of λ resulted in similar results. Lofstedt *et al.* (1995) and Barber *et al.* (1997) came up with a solution to this problem by deleting prefactors in parenthesis containing $\dot{R}/c$. This gives the following equation for the radial motion of bubble, which has gained immense popularity in the sonoluminescence and sonochemistry community (for further details see the review by Brenner *et al.*, 2002):

$$\rho\left[R\frac{d^2R}{dt^2}+\frac{3}{2}\left(\frac{dR}{dt}\right)^2\right]=\left[P_g - P_0 - P(t)\right] - 4n\frac{\dot{R}}{R}-\frac{2\sigma}{R}+\frac{R}{c}\frac{dP_g}{dt} \tag{2.30}$$

For the modeling of radial bubble motion in this thesis, the above equation has been used.

2.4.4 Transport Phenomena in the Bubble

The change in the temperature and pressure of the bubble contents with radial motion shows peculiar features. The radial bubble motion comprises of a growth phase, which occurs relatively slowly; followed by a transient collapse which occurs in few tens of nanoseconds (Storey and Szeri, 2000). Due to this unusual feature of motion, the transport phenomena in the bubble (basically heat and mass transfer) shows some peculiar characteristics described below. The pressure inside the bubble is given by the following expression, which accounts for the finite volume of gas molecules:

$$P_g = \left(P_0 + \frac{2\sigma}{R_0} \right) \frac{\left(R_0^3 - h^3 \right)^{\gamma}}{\left(R^3(t) - h^3 \right)^{\gamma}} \tag{2.31}$$

R_0 is the initial or equilibrium radius and h is the van der Waal's hard core radius.

2.4.4.1 Heat Transfer

The thermal behavior of the bubble contents and the extent of heat transfer through the bubble is determined by the relative time scales of heat transfer and radial motion. If the heat transfer time scale is shorter than bubble dynamics time scales, the gas in the bubble remains at constant temperature (equal to the ambient temperature in liquid). This isothermal behavior allows value of γ in equation 2.31 to be set to 1. Conversely, if the time scale of bubble motion is smaller than that of heat transfer, the bubble contents would behave adiabatically. Thus, γ in equation 2.31 should be replaced with K (polytropic constant). The criteria for determining the first definition of the thermal Peclet number for cavitation bubble was given by Kamath *et al.* (1993) as:

$$Pe = \frac{R_0^2 \omega}{\kappa} \tag{2.32}$$

where ω is the angular frequency of the acoustic wave and κ is the thermal diffusivity. $\sqrt{\kappa/\omega}$ is the thermal diffusion length of the bubble contents. However, Hilgenfeldt *et al.*

(1996) argued that the radial motion of bubbles contains much smaller time scales. Therefore, the definition of Peclet number is altered as:

$$Pe = \frac{|\dot{R}|R}{\kappa} \tag{2.33}$$

The condition for which Pe >> 1, which essentially imply adiabatic behavior, last for very short duration (~ 10 ns). Therefore, Hilgenfeldt *et al.* (1996) suggest settling $\gamma = 1$ uniformly in time in bubble motion.

2.4.4.2 Gas and Vapor Transport in Bubble

During radial oscillations both gas and vapor diffuse across bubble. However, the extent of gas transport and vapor transport differs as a result of different time scales for diffusion of gas and evaporation/condensation of vapor. In this section, we describe the features (along with essential equations) of the gas and vapor transport in the bubble.

2.4.4.2.1Gas Diffusion

The time scale for the diffusion of gas estimated as R_0^2/D is in milliseconds. The time scale of bubble motion (which is almost same as the time scale of ultrasound wave) is much shorter. Therefore, net diffusion of gas across bubble wall is a period of few acoustic cycles is negligible. However, diffusion of gas for longer periods needs to be taken into account. The slow pumping of the dissolved gas in liquid in the bubble is called rectified diffusion. Over past 6 decades, several authors have investigated this phenomenon for small amplitude oscillations of cavitation bubbles (Hsieh and Plesset, 1961; Eller and Flynn, 1965; Safar, 1968; Crum, 1980), rectified diffusion is mainly attributed to two effects as follows:

Area Effect

Gas diffuses into the bubble during expansion, while leaves the bubble during compression. The surface area of the bubble (given as $4\pi R^2$) in the expanded and compressed form are not equal. Therefore, more gas enters the bubble during expansion then

leaves during compression. As a result, there is gradual accumulation of gas inside the bubble.

Shell Effect

The gas that diffuses into the bubble is mainly present in the thin liquid shell surrounding the bubble. The volume of this shell varies with radial oscillation of bubbles. When the bubble expands, this shell is compressed as a result of which the concentration of dissolved gas in the shell increases. This increases the concentration gradient for gas diffusion during expansion. Reverse happens during compression phase. Here, the bubble volume decreases with corresponding rise in the shell volume. This reduces the concentration of dissolved gas in the liquid in the shell, and thus, the driving force for outward diffusion of gas. Consequently, gas accumulates in the bubble due to unequal transfer of gas in the expansion and compression phases of the bubble motion.

More recently, Fyrillas and Szeri (1996) have presented a general formulation of the rectified diffusion applicable to large amplitude non-linear motion of cavitation bubbles. They put forth the idea of "separation of time scale" to account for the rectified diffusion. Fyrillas and Szeri (1996) proposed that the dissolved gas content in the liquid can be divided in two parts. First the oscillatory part (in close vicinity of bubble) that changes on a fast time scale (which is essentially the time scale of the acoustic wave), and secondly, the smooth part (at large distance from bubble wall) that changes on a time scale given by R_0^2/D. Fyrillas and Szeri (1996) solved the diffusion equation coupled to the equation for radial motion of cavitation bubble using singular perturbation analysis and found that the contribution by the oscillatory portion of dissolved gas to the overall mass transport was negligible. The smooth part, however, makes contribution to the change in gas content of the bubble.

2.4.4.2.2Vapor Transport

During the expansion phase, evaporation of liquid occurs at the bubble interface and the vapor molecules diffuse towards the bubble core. Several authors have attempted to model the vapor transport in the bubble and its influence on radial motion (for example, Prasad Naidu *et al.*, 1994; Flynn, 1964; Gong and Hart, 1998; Sochard *et al.*, 1997; Moss *et al.*, 1999). Yasui (1997, 1997a) has account nonequilibrium phase change and 25 chemical reactions in the bubble. Yasui assumed that the vapor transport was condensation limited and diffusion of vapor to the bubble wall was instantaneous. The principal result of Yasui's study was that some water vapor remained in the bubble at the amount of transient collapse. Endothermic dissociation of water vapor reduced the final temperature peak reached in the bubble.

Another physical factor that contributes the vapor transport is the accommodation coefficient (denoted as σ_a). The accommodation coefficient represents resistance to condensation at the bubble interface. Lower values of σ_a indicate greater resistance to condensation, and thus, non-equilibrium phase change at bubble interface. The most general treatment of the vapor transport in the cavitation bubble was given by Storey and Szeri (2000), who showed that vapor transport in the bubble is a two-step process: (1) diffusion of vapor molecules to the bubble wall, and (2) the condensation at bubble wall. Therefore, time scales of both of these steps (viz. t_{dif} and t_{cond}) and their relative magnitudes with time scale of bubble motion (t_{osc}), influence the vapor transport. In the initial phase of bubble collapse, time scales of both of the steps mentioned above are similar than the time scale of bubble oscillation (or t_{cond}, t_{dif} and t_{osc}). However, as the bubble accelerates during collapse, the above inequality reverses. The time scale of vapor diffusion becomes greater than the time scale of bubble dynamics ($t_{osc} >> t_{dif}$). Consequently, the vapor in the bubble has insufficient

time to diffuse towards bubble interface or bubble wall at which it can condense. This creates nearly fixed composition of bubble. Another mechanism that contributes parallely to the entrapment of water vapor is the inequality between time for condensation of vapor and time scale of bubble motion (i.e. $t_{cond} >> t_{dif}$). The extent of vapor entrapment by this mechanism is a function of the accommodation coefficient. Both of the mechanisms stated above can contribute to the entrapment of vapor. However, as shown by Storey and Szeri (2000) the condition $t_{diff} >> t_{osc}$ is reached in the bubble motion much earlier than $t_{cond} >> t_{osc}$. Therefore, Storey and Szeri (2000) concluded that the vapor transport was diffusion (and not condensation) limited.

Parallel studies in the Hoffmann group at Caltech (Colussi *et al.*, 1998; Colussi and Hoffmann, 1999) showed the influence of accommodation coefficient which affects the condensation time scale, t_{cond}. Initially, Hoffmann and Coworkers (Colussi *et al.*, 1998) used a value of $\sigma_a \sim 0.001$, which was unrealistically low. Due to this, the vapor transport as predicted by their model, was condensation limited. However, in the second paper Colussi and Hoffmann (1999) used a value of $\sigma_a = 0.3$. With this, the results of Colussi and Hoffmann (1999) are in line with those of Storey and Szeri (2000). On the basis of results of Storey and Szeri (2000, 2001), Toegel *et al.* (2000) developed a diffusion limited model using boundary layer approximation. The existence of boundary layer has been confirmed by several authors (Fujikawa and Akamatsu, 1980; Kamath *et al.*, 1993; Kwak and Na, 1996, 1997). The model of Toegel *et al.* (2000) has been used in our study for correlation the experimental results.

2.5 STABLE AND TRANSIENT CAVITATION

On the basis of the amplitude of the radial motion of cavitation bubble, the cavitation phenomenon is classified into two types: stable and transient. Stable cavitation refers to small

amplitude oscillatory radial motion around a mean for several acoustics cycles. Radial motion in transient cavitation comprises of an explosive growth (several times the initial radius) followed by an extremely rapid transient collapse. Depending on the non-condensable gas contained in the bubble, the bubble may undergo several afterbounces. Four of physical conditions are: (1) pressure amplitude of ultrasound wave (P_A), (2) Frequency of ultrasound wave (f), (3) initial bubble radius (R_0) and (4) ambient or static pressure in the liquid (P_0). Qualitatively speaking, for $P_A << P_0$, the bubble motion is oscillatory. However, as P_A increases the amplitude of the radial motion as well as the intensity of the collapse increases. Transient cavitation threshold (denoted as P_T) is defined as the minimum amplitude of the acoustic wave (for a given value of P_0) at which the bubble motion becomes transient.

In order to define P_T, one must have a suitable criterion for distinguishing transient bubble motion. We describe here some of the well-known criteria for defining the transient bubble motion.

(1) Flynn (1975) defined a critical expansion ratio for the bubble $\left(R_{max}/R_0\right)_c$, exceeding which the bubble collapse is dominated by the inertial forces and the spherical convergence of the liquid surrounding the bubble transfers ever increasing quantities of KE of the contracting bubble. Flynn calculated $\left(R_{max}/R_0\right)_c$ value for bubbles of size smaller than the resonant size corresponding to frequency of the acoustic wave (but not so small that surface tension becomes dominant) using simulations of radial motion of bubble. He observed that as the P_A approaches P_T, there is a sharp rise in the velocity of the collapsing bubble. with $\left(R_{max}/R_0\right) \sim 2$, the velocity of the bubble wall exceeded sonic velocity. On the basis of these results, two criteria were formulated for the defining transient bubble motion:

- An expansion of 2 times the original size (R_0).

- Bubble wall velocity during collapse should reach or exceed sound velocity ($dR/dt \geq C$).

(2) Akulichev (1967) and Rosenberg (1971) suggested use of a phase plane (a plot of dR/dt vs R calculated using simulations of bubble dynamics equation) to distinguish the transient bubble motion.

(3) Neppiras (1980) has given an analytical expression for the transient cavitation threshold using balance between the pressure just outside the bubble and the pressure in the bulk liquid at the instance of minimum bubble radius (or maximum compression) during radial motion as:

$$P_T > P_0 + \frac{4}{3}\sqrt{\frac{2\sigma^3}{3R_0^3\left(P_0 + 2\sigma/R_0\right)}} \tag{2.34}$$

Neppiras' expression can be simplified for two cases:

- Very small bubbles, where $2\sigma/R_0 >> P_0$

$$P_T \approx P_0 + \frac{4\sigma}{3\sqrt{3}R_0} \tag{2.35}$$

- Medium to large size bubbles (for which $P_0 >> 2\sigma/R_0$):

$$P_T \approx P_0 \tag{2.36}$$

(4) Apfel (1986) and Holland and Apfel (1989) defined a mechanical index, representative of the likelihood of occurrence of transient cavitation. This index was a ratio of max negative pressure in the bulk to the insonation frequency, and was proportional to the mechanical work that needs to be performed on the bubble during negative phase of acoustic cycle. With this analysis, Apfel corrected the critical expansion ratio for transient collapse as 2.3. Combining analysis of Apfel (1986) and Flynn (1975), we get a general expression for P_T as:

$$R_0 = \frac{0.82}{\omega}\frac{1}{\sqrt{P_T/P_0}}\left(P_T - P_0\right)\left[1 + \frac{2}{3}\frac{\left(P_T - P_0\right)}{P_0}\right]^{1/3} \tag{2.37}$$

The above expression relates three critical variables: P_T, R_0 and ω $(=2\pi f)$.

2.6 FACTORS AFFECTING RADIAL MOTION

Several factors related to the liquid medium, cavitation bubble and the ultrasound wave influence radial motion of cavitation bubble. We give herewith a qualitative description of the nature of influence of these factors. For more quantitative information we refer the reader to other sources (Mason and Lormer, 2002; Shah *et al.*, 1999; Leighton, 1994; Moholkar, 2002).

2.6.1 Cavitation Bubble Related Parameters

***Initial (or equilibrium) bubble radius (R_0)*:** For a given set of condition of acoustic pressure amplitude and frequency, the intensity of the cavitation bubble collapse decreases as R_0 increases. Larger bubbles undergo lesser expansion, and hence, a milder collapse. Presence of large amount of gas in the bubble cushions the collapse, which puts limit on the temperature and pressure peak attained at collapse.

***Nature of gas*:** The natures of the gas, whether monatomic or diatomic, have a major impact on the temperature and pressure peak attained during collapse. Bubbles of monatomic gases such as argon attain higher temperature during collapse (due to their smaller heat capacity) than diatomic gases such as nitrogen, oxygen and air.

2.6.2 Ultasound related parameters

***Frequency*:** With all other factors remaining the same, the intensity of the cavitation bubble collapse decreases with increasing frequency of ultrasound. The physics behind this phenomenon can be explained as follows: with rise in the frequency of the acoustic wave, the period of the acoustic wave (comprising of a rarefaction and a compression) decreases. With this, the bubble is exposed to reduced pressure for a smaller duration. The extent of expansion of the bubble decreases. The subsequent collapse is also less intense.

***Acoustic pressure amplitude*:** With ultrasound frequency, initial bubble radius and other factor remaining the same, the intensity of the cavitation bubble collapse increases with increasing acoustic pressure amplitude. With higher acoustic pressure amplitude the energy of the wave increases. As a result, the expansion of the bubble during rarefaction half period of the wave increases. The ensuing collapse of the bubble (in the compression half period) is also more intense.

2.6.3 Liquid medium related parameters (P_0, μ, σ, Pv)

***Viscosity of the medium*:** Viscosity of the medium is representative of the natural cohesive forces active in the liquid. It acts as a break on the radial motion of bubbles. Moreover, it is also responsible for the attenuation of the acoustic wave. Increase in liquid viscosity dampens the radial motion of the bubbles, thus limiting the maximum size attained during radial motion. The cavitation intensity, as indicated by the temperature and pressure peak attained during collapse, decreases with increasing viscosity of the liquid.

***Surface tension*:** Surface tension indicates the difficulty in creating cavitation in the liquid. An increase in surface tension of the liquid increases the cavitation threshold, i.e. the minimum acoustic pressure amplitude for creation of cavitation in liquid. The intensity of the cavitation bubble collapse increases with increasing surface tension of the medium.

***Vapor pressure*:** If the vapor pressure of the liquid is large, it results in large evaporation of the liquid vapor into the cavitation bubble. Some fractions of this vapor are entrapped in the bubble during transient collapse, as noted earlier. This vapor works towards increasing the heat capacity of the bubble contents-due to which the temperature peak attained during collapse reduces. Moreover, endothermic dissociation of the vapor also contributes to lowering of the temperature peak.

Rise in the bulk temperature of the liquid increases the vapor pressure of liquid. For the reasons mentioned above, the cavitation intensity reduces with increase in the bulk temperature of liquid.

***Static pressure*:** The expansion of the cavitation bubble and the intensity of the subsequent collapse depends on the extent of fall of pressure in bulk liquid below the ambient (or $P_0 - P_A$) during the rarefaction period of the acoustic wave. Increase in the ambient or static pressure of the liquid reduces this extent. As a result, the amplitude of the radial motion of bubble decreases. For sufficiently high ambient pressure, the transient motion of the cavitation bubble can be transformed into a stable oscillatory type. On a whole, the cavitation intensity in the medium reduces with rise in the static or bulk pressure of the medium.

CHAPTER 3

A Mechanistic Approach to Enhancement of the Yield of a Sonochemical Reaction

3.1 INTRODUCTION

Literature review presented in chapter 1 indicates that sonolysis or sonochemical oxidation is being widely practiced for the degradation of recalcitrant organic pollutants. This effect is attributed to the generation of highly reactive free radicals such as $O^{\bullet}$, $OH^{\bullet}$, $HO_2^{\bullet}$ due to the transient cavitation bubble collapse driven by the ultrasound wave. Before proceeding to the studies in sonochemical degradation of various organic pollutants, we need to understand the exact mechanism of a sonochemical process and the physical factors (and the interrelations between them) that affect the yield of such a process. In this chapter we make an attempt towards this using the popular model sonochemical reaction of potassium iodide oxidation.

As noted in chapter 2, ultrasound passes through the liquid medium in the form of a longitudinal wave comprising of alternate compression and rarefaction cycles, as a result of which the local pressure varies. This variation in local pressure brings about intense volume oscillations of existing cavitation nuclei (or free gas content) in the medium. The cavitation nuclei are tiny, free-floating bubbles in the liquid or gas pockets trapped in the crevices of the solid boundaries in the liquid medium. Evaporation occurs at the gas-liquid interface with diffusion of vapor into the cavitation bubble. During the subsequent compression phase, the liquid vapor tends to condense at the bubble wall. An interesting phenomenon occurs at this time. During the final moments of collapse, the bubble wall velocity reaches or even exceeds the velocity of sound in water, and not all the vapor that has entered the bubble can escape. This

vapor, thus, gets entrapped in the cavitation bubble. Extremes of temperature and pressure are reached in the bubble during instance of maximum compression (~ 5000 K and 500 bar), and the trapped vapor decomposes at these conditions into various radicals. These radicals get mixed with the bulk liquid with fragmentation of the bubble during collapse and induce chemical reaction or acceleration of the chemical reaction. The extent of radical formation in a single cavitation bubble is a function of two parameters: amount of water vapor trapped in the bubble and the temperature and pressure peak reached in the bubble during transient collapse.

The rate of a chemical reaction induced by ultrasound: $M + R^{\bullet} \rightarrow$ products, can be represented as: Rate = $k_R [M] [R^{\bullet}]$; where [M] is the concentration of the reactant, $[R^{\bullet}]$ is the concentration of the radicals resulting out of cavitation bubbles and k_R is the rate constant. The rate of the sonochemical reaction and the yield obtained during a specific reaction time can be enhanced by increasing either the initial reactant concentration or by increasing the radical production from the bubble. The aim of the present study is to assess the effect of a physical (lowering the dissolved gas content or degassing of the liquid medium) and chemical (increasing the initial reactant concentration) technique on the enhancement of the yield of a sonochemical reaction. In the context of the thesis subject, the sonochemical yield essentially means the extent of degradation of the pollutant obtained for given experimental conditions. The chemical technique that we adopt follows directly from the rate expression given above, while the physical technique of degassing the liquid medium is in spirit of earlier works (Moholkar and Warmoeskerken, 2003; Moholkar *et al.*, 2004) of one of the authors of the present paper. In these works, it was demonstrated that reduction in the dissolved gas content of the medium, while maintaining the free gas content (or cavitation nuclei population) fairly constant, significantly enhances efficiency of the sonochemical reactor. For our study we choose a well-known chemical reaction induced by ultrasound: oxidation of potassium iodide (KI) to liberate iodine. For explaining the physical phenomena, we use a bubble dynamics model, which takes into account the heat diffusion, and water vapor transport through the bubble during radial

motion driven by ultrasound.

Several authors have dealt with the matter of sonochemical yield using KI oxidation as a model reaction (Tuziuti *et al.*, 2004; Tuziuti *et al.*, 2005; Kirpalani and McQuinn, 2006; Seymour *et al.*, 1994; Entezari and Kruss, 1994, 1996; Shirgaonkar and Pandit, 1997; Gutierrez *et al.*, 1991; Henglein and Gutierrez, 1990) before. However, in these studies no attempt was made to explain the trends in iodine liberation using a bubble dynamics model. Few authors have tried to explain the variation in iodine liberation with different reaction conditions using a bubble dynamics model. Gogate *et al.* (2001, 2003) have correlated the iodine liberation rate to the extremes of temperature and pressure obtained at the transient collapse using a bubble dynamics model. However, the model used by Gogate *et al.* (2001, 2003) does not take into account the transport of water vapor and the entrapment of water vapor. Prasad Naidu *et al.* (1994) explained the trends in the rate of iodine formation with sonication of aqueous KI solutions of various concentrations and under different gas atmospheres, using Rayleigh-Plesset equation for the radial bubble motion coupled with Flynn's assumption (Flynn, 1964) that the bubble becomes a closed system during collapse phase when the partial pressure of gas becomes equal to the vapor pressure of water. Thus, the amount of water vapor in the bubble was kept same in all simulations, without modeling the continuous transport of water vapor during radial bubble motion. Moreover, the Rayleigh-Plesset equation does not take into account for compressibility of the medium, and hence, Prasad Naidu *et al.* (1994) terminated their simulations at the instance when the bubble wall velocity reaches the velocity of sound in water.

The present work addresses the matter of enhancement of sonochemical yield with a different and more rigorous perspective. We take mechanistic approach of correlating the sonochemical yield to the fundamental phenomena of water vapor entrapment in cavitation bubbles resulting in generation of radicals, which is at the very basis of sonochemical reaction. The bubble dynamics model used in this study relaxes several assumptions made by earlier authors, which gives a more detailed description of the physics and chemistry of cavitation

bubbles, and its correlation with the sonochemical phenomena observed in the bulk medium. Therefore, in addition to revelation of the efficacy of different techniques in enhancing the sonochemical yield, the results of the present study also provide an insight into the mechanism of the sonochemical phenomena and the complex nature of interactions between various physical parameters.

3.2 EXPERIMIENTAL

3.2.1 Experimental set-up

A schematic diagram of the experimental set-up used in the present study is shown in figure 3.1(A). The experiments were done in a jacketed glass reactor (dimensions: height – 120 mm, diameter – 50 mm, inner jacket diameter – 62 mm). For bubbling of air during sonication (purpose of which is discussed later in this section), a gas sparger (or aerator) made of glass was used, the schematic of which is shown in figure 3.1(B) along with relevant dimensions. In order to disperse the gas in the solution in the form of fine bubbles, the aerator had porous silica filter (pore size ~ 40 μm). During reactions, the aerator was so positioned that the porous silica filter exactly faces the bottom of the ultrasound tip. This ensured uniform distribution of the bubbles forming cavitation nuclei into the solution. The air flow rate through the sparger was controlled using a rotameter, and was set at 5 l/h. In order to maintain the bulk temperature constant during sonication, cooling water was circulated through the jacket of the reactor. For the sonication of KI solution, a microprocessor based and programmable ultrasound processor was used (Sonics & Materials Inc., Model VCX 500). This processor had a frequency of 20 kHz with maximum power output of 500W. The processor had variable power output control, which was set at 20% during experiments, resulting in net consumption of 100W power during sonication. In addition, the processor had facility of automatic frequency tuning and amplitude compensation, which ensures constant power delivery to ultrasound probe.

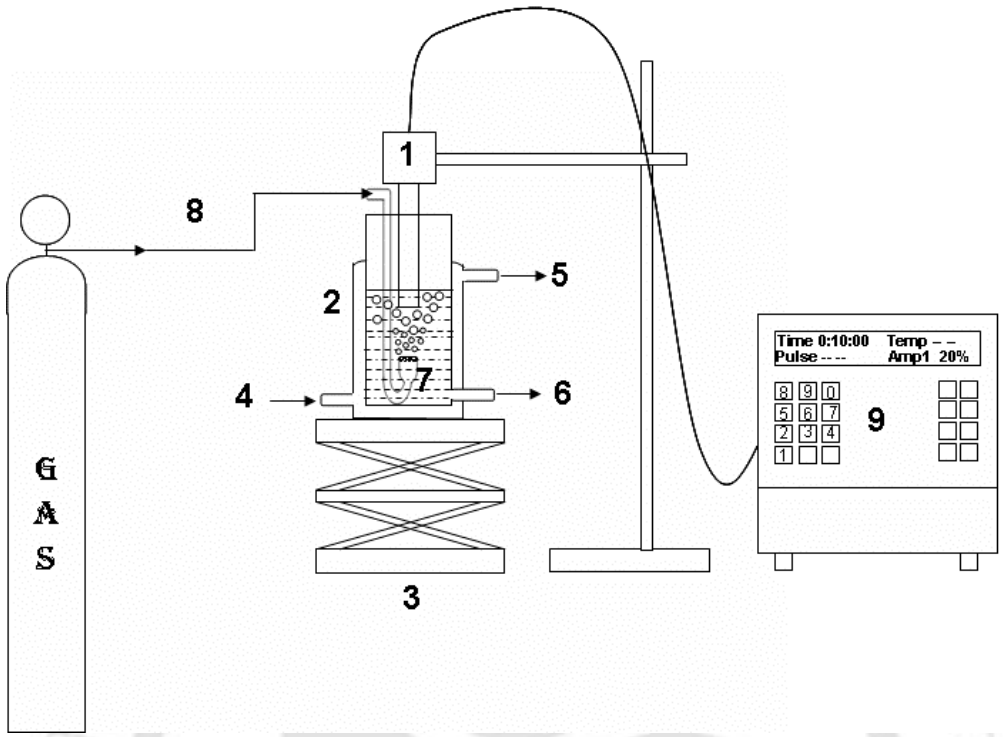

(A)

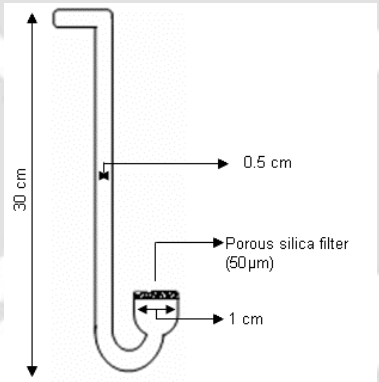

(B)

Figure 3.1. (A) Experimental set-up [Legends: 1. Ultrasound horn; 2. Jacketed reactor; 3. Laboratory jack; 4. Cooling water inlet; 5. Cooling water outlet; 6. Sample withdrawl port; 7. Aerator for bubbling of air in the reaction medium; 8. Aerator connection to gas storage vessel; 9. Control unit of the ultrasound processor]. (B) Schematic of the aerator along with

3.2.2 Experimental procedure

Potassium iodide (KI) was bought from Merck (Grade: Proanalysis) and was used without any pre-treatment. The KI solutions were prepared using water from Millipore (Model:

Elix 3). The experiments were carried out in two categories: (1) degassed medium and (2) saturated medium. In each category the initial concentration of KI was varied as 2%, 5% and 10% w/v. Thus, in total there were 6 sets of experiments. The reproducibility of the results in each set of experiments was assessed with 3 experimental runs. During experiments the reaction temperature was maintained at 28^{o}C with reaction volume being 150 ml. The sonication of the reaction medium was done for 10 minutes with a power input of 100 W to the ultrasound probe, as mentioned earlier. During sonication, the reaction temperature increased only slightly (~ 1-2^{o}C). For the experiments in first category, i.e. degassed reaction medium, the reaction solution was subjected to vacuum for 30 minutes with intense stirring to reduce the dissolved gas content. For this purpose, a vacuum pump (Riviera, Model: TID-25-S) producing a vacuum of 700 mm Hg (or 60 mm Hg pressure) in the solution was used. By this method, the dissolved oxygen content of the solution could be lowered to 2.7 ppm. This method, however, reduces the free-gas content of the medium as well – leaving the medium not only degassed but also de-nucleated. To compensate for this effect, air was introduced through the aerator during sonication of the degassed KI solutions, so as to provide cavitation nuclei in the medium. In the second category of experiments, where a saturated medium was used, the dissolved oxygen content of the solution was 7.9 ppm.

3.2.3 Method of analysis

The iodine liberated during sonication was analyzed using a UV-Visible spectrophotometer (Perkin Elmer, Model: Lambda 35). The iodine liberated in the solution forms a complex I_3^- with the iodide ions already present in the KI solution. The UV-Visible spectrum of this complex has a peak at 354 nm. Therefore, the iodine liberation was accounted by monitoring the absorbance values at 354 nm. In order to quantify the iodine liberation during sonication of KI solutions of various concentrations, calibration of the spectrophotometer was done using KI solutions with known iodine concentrations. For this purpose, the 0.01N iodine solution was prepared by dissolving the corresponding amount of iodine in a solution with the

particular concentration of KI for which the calibration had to be done. The concentration of iodine in this solution was determined by titrating against sodium thiosulphate, which was standardized against 0.1N potassium iodate solution. This standard iodine solution was used diluted with the same KI solution to obtain iodine solutions of different known concentrations. Absorbance values for these solutions were obtained by keeping the un-sonicated or original KI solution of respective concentration as the blank. The calibration curve produced from these values was used estimate the concentration of iodine liberated during various experiments.

3.3 MODELING OF THE SONOCHEMICAL PHENOMENA

It is well known that the species inducing *sonochemistry*, i.e. radicals such as $OH^{\bullet}$, $H^{\bullet}$, $O^{\bullet}$ and $HO_2^{\bullet}$, are generated during bubble collapse. However, to date, a direct quantification of this phenomenon is still not possible. One has to rely on numerical solutions of bubble dynamics equation to determine the temperature reached during bubble collapse, which is a crucial parameter influencing the extent of radical generation. The other parameter of paramount importance is the amount of water vapor entrapped in the bubble at the time of collapse. This parameter, too, needs to be determined from bubble dynamics simulations. Modeling of the radicals generation by cavitation bubbles is an active area of research for past 3 decades and various authors have addressed the matter with different approaches (Kamath *et al.*, 1993; Gong and Hart, 1998; Sochard *et al.*, 1997; Moss *et al.*, 1999; Yasui, 1997, 1997a; Storey and Szeri, 2000; Colussi *et al.*, 1998; Colussi and Hoffmann, 1999; Toegel *et al.*, 2000).

The most general treatment of the problem of water vapor transport in strongly forced bubble was presented by Storey and Szeri (2000) in a landmark paper published in 2000. The principal result of paper by Storey and Szeri (2000) was that water vapor transport in the bubble is a two-step process: diffusion to bubble wall and condensation. Thus, it is influenced by two time scales, viz. time scale of diffusion (t_{dif}) and time scale of condensation (t_{cond}), and their magnitudes relative to bubble dynamics (or oscillations) time scale, t_{osc}. In the earlier phases of

bubble collapse, $t_{osc} >> t_{dif}$, t_{cond}, which results in uniform bubble composition. As the bubble wall acceleration increases during collapse, the time scales for bubble dynamics and diffusion become equal. At this stage, rate of reduction of water vapor in the central region of bubble is lesser than at the bubble wall. With further acceleration of bubble wall, $t_{osc} << t_{dif}$, and the water vapor has insufficient time to diffuse to bubble wall, which results in nearly fixed distribution of water vapor in the bubble. Another mechanism, which traps water vapor in bubble during collapse, is the non-equilibrium phase change at bubble wall, as mentioned above. The time scale for the condensation varies inversely with the accommodation coefficient (σ_a). Qualitatively, when $t_{osc} >> t_{cond}$, the condensation is in equilibrium with respect to the bubble motion. On the other hand, when $t_{cond} >> t_{osc}$, no water vapor can escape bubble during collapse. Thus, the amount of water vapor trapped in the cavitation bubble during collapse is sensitive to the value of σ_a (Colussi *et al.*, 1998; Colussi and Hoffmann, 1999).

The exact mechanism that traps water vapor in the bubble is determined by the relative magnitudes of t_{osc}, t_{dif} and t_{cond}. When the bubble dynamics time scale is smaller than either the diffusion or condensation time scale, water vapor entrapment occurs. However, both mechanisms can contribute to the water vapor entrapment. Storey and Szeri (2000) showed that the condition $t_{osc} << t_{dif}$ is reached well before $t_{osc} << t_{cond}$. Thus, the phenomenon of water vapor trapping in the cavitation bubble is diffusion limited. In view of the results of Storey and Szeri (2000) with full numerical simulations, Toegel *et al.* (2000) developed a diffusion limited model using boundary layer approximation. For the validation of this model, Toegel *et al.* (2000) have compared their results with those of Storey and Szeri (2000) finding an excellent qualitative and quantitative agreement. For explanation of the sonochemical phenomena we use the model of Toegel *et al.* (2000), which has been described in paragraphs below.

3.3.1 Bubble dynamics

The radial bubble motion is described by the Keller-Miksis equation written as (Brennen, 1995 and Prosperetti and Lezzi, 1986):

$$\left(1-\frac{dR/dt}{c}\right)R\frac{d^2R}{dt^2}+\frac{3}{2}\left(1-\frac{dR/dt}{3c}\right)\left(\frac{dR}{dt}\right)^2=\frac{1}{\rho_L}\left(1+\frac{dR/dt}{c}\right)(P_i-P_t)+\frac{R}{\rho_L c}\frac{dP_i}{dt}-4\nu\frac{dR/dt}{R}-\frac{2\sigma}{\rho_L R} \qquad (3.1)$$

This is a modification of the Rayleigh-Plesset equation, which takes into account the liquid compressibility. ρ_L, σ and ν denote the physical properties of the liquid medium, viz. the density, surface tension and kinematic viscosity, respectively. c is the speed of sound in the medium. The pressure inside the bubble (P_i) is written using a van der Waals type equation of state as:

$$P_i = \frac{N_{tot}(t)\,kT}{\left[\frac{4\pi}{3}\left(R^3(t)-h^3\right)\right]} \qquad (3.2)$$

Here k is the Boltzmann constant, N_{tot} denotes the total number of molecules in the bubble, which vary according to condensation and evaporation of water vapor and T is the temperature of bubble contents. h is the van der Waals hard core radius of various species in the bubble, viz. nitrogen, oxygen and water vapor. Since the hard-core radii of these species differ very little (~ 5%), we take a common value, $h = R_o/8.86$, for all species, where R_o is the equilibrium radius of the bubble. A simple expression for P_t, the pressure in the bulk liquid driving bubble motion is written as:

$$P_t = P_o - P_A \sin 2\pi ft \qquad (3.3)$$

Here P_o is the ambient pressure and P_A and *f* denote the pressure amplitude and frequency of the acoustic wave. After substituting dR/dt = s, the above equation is transformed into two simultaneous equations:

$$\frac{dR}{dt}=s \qquad (3.4)$$

$$\frac{ds}{dt}=\frac{(1+s/c)}{R\rho_L(1-s/c)}(P_i-P_t)+\frac{1}{\rho_L c(1-s/c)}\frac{dP_i}{dt}-\frac{4\nu s}{R^2(1-s/c)}-\frac{2\sigma}{\rho_L R^2(1-s/c)}-\frac{3}{2}\frac{s^2(1-s/3c)}{R(1-s/c)} \qquad (3.5)$$

3.3.2 Mass transfer across bubble

During bubble oscillations, both gas and water vapor diffuse across the bubble wall. The

time scale for the diffusion of gas can be given as ~ R_o^2/D, where D is the diffusion coefficient. For representative value as R_o ~ 10 μm and D ~ 10^{-9} m^2/s, the time scale for gas diffusion is 0.1 ms – which is far higher than time scale of bubble dynamics (which is same as time scale of ultrasound wave, 50 μs for 20 kHz wave). Thus, transport of gas across bubble in one acoustic cycle can be ignored. However, gas transport across bubble over larger time duration needs to be accounted for. Depending on the amplitude of the ultrasound wave driving bubble motion and the extent of saturation of the liquid medium, the bubble may grow or shrink during oscillations due to transport of gas across the bubble. This process is called rectified diffusion, which has been investigated over past several decades for small amplitude oscillations of the bubble (Hsieh and Plesset, 1961; Eller and Flynn, 1965; Safar, 1968). More recently, a generalized formulation of rectified diffusion of rectified diffusion is given by Lofstedt *et al*.(1995) and Fyrillas & Szeri (1994), which can be applied to large amplitude nonlinear motion of bubbles driven by ultrasound waves of pressure amplitude greater than transient cavitation threshold (typically > 1 bar for bubbles of size 5 – 20 μm). The major conclusions of the study of Lofstedt *et al.* (1995) and Fyrillas & Szeri (1994) in the contest of current work is as follows: For acoustic pressure amplitudes > 1 atm, the bubble grows during oscillations if the liquid medium is relatively saturated (≥ 80% or so). On the other hand, if the medium is unsaturated (relative saturation ≤ 30% or so) the bubble shrinks during radial motion. While choosing parameters for simulation of radial bubble motion, we make use of these conclusions. For greater details on mathematical analysis of rectified diffusion, we refer the reader to original papers of Lofstedt *et al.* (1995) and Fyrillas & Szeri (1994).

Diffusion of the water vapor across the bubble wall shows interesting features, as already discussed earlier. During bubble oscillations the surface temperature of the bubble exceeds bulk water temperature only for a very brief moment during collapse. On this basis, the bubble can be divided into two parts: (i) a “cold” boundary layer in thermal equilibrium with liquid, and (ii) a

hot homogeneous core. Of course, this distinction assumes that the condensation of water molecules at the bubble wall is fast enough to maintain equilibrium. The instantaneous diffusive penetration depth, by dimensional analysis, is taken to be: $l_{diff} = \sqrt{Dt_{osc}}$, where t_{osc} is the time scale of bubble oscillations: $R/|dR/dt|$.

On the basis of the fact that the water vapor transport is always diffusion limited, the rate of change of water molecules in the bubble (N_W) is given by:

$$\frac{dN_W}{dt} = 4\pi R^2 D \left.\frac{\partial C_W}{\partial r}\right|_{r=R} \approx 4\pi R^2 D \left(\frac{C_{WR} - C_W}{l_{diff}}\right) \tag{3.6}$$

where C_{WR} is the equilibrium concentration of water molecules at the bubble wall, calculated using vapor pressure at the bulk temperature (T_o) and C_W is the actual concentration of water molecules in the bubble core.

Upper limit on diffusion length: The above analysis holds good for bubble in motion, where the bubble wall velocity, dR/dt, has a non-zero value. However, at the instances of maximum and minimum radius, the bubble wall velocity is zero, and we need an alternate expression for the diffusion length. For this purpose, we identify that for dR/dt = 0, the equation for vapor transport inside the bubble becomes a pure diffusion equation:

$$\frac{\partial C_W}{\partial t} = D\left(\frac{\partial^2 C_W}{\partial r^2} + \frac{2}{r}\frac{\partial C_W}{\partial r}\right) \tag{3.7}$$

with boundary conditions: (1) r = 0, $\partial C_W/\partial t = 0$ for $t \geq 0$; (ii) r = R, $C_W = C_{WR}$ for $t \geq 0$; (iii) $C_W = C_{W0} = 0$ for t = 0 and $0 \leq r \leq R$. The analytical solution to the above problem is given by Crank (1975):

$$\frac{C_W - C_{W0}}{C_{WR} - C_{W0}} = 1 + \frac{2R}{\pi r}\sum_{n=1}^{\infty}\frac{(-1)^n}{n}\sin\left(\frac{nr}{R/\pi}\right)\exp\left(-\frac{n^2 Dt}{(R/\pi)^2}\right) \tag{3.8}$$

From the inspection of the above solution, the characteristic length for the diffusion is R/π. We choose this as the upper limit for the diffusion length. Thus:

$$l_{diff} = \min\left(\sqrt{\frac{RD}{|dR/dt|}}, \frac{R}{\pi}\right) \tag{3.9}$$

Estimation of the diffusion coefficient for water vapor in the ternary system nitrogen-oxygen-water on the basis of Chapman-Enskog theory (Hirschfelder *et al.*, 1954) is explained later.

3.3.3 Heat transfer across bubble

With complete analogy with mass transfer, the heat transfer across bubble wall is:

$$\frac{dQ}{dt} = 4\pi R^2 \lambda \left(\frac{T_o - T}{l_{th}}\right) \tag{3.10}$$

where, λ is the thermal conductivity of the bubble contents and l_{th} is the thermal diffusion length: $\min\left(\frac{R}{\pi}, \sqrt{\frac{R\kappa}{|dR/dt|}}\right)$. Thermal diffusivity κ is calculated as: $\kappa = \frac{\lambda}{\rho_{mix} C_{p,mix}}$, where, $\rho_{mix} C_{p,mix} = \sum_{i=1}^{n} \rho_i C_{pi}$. The densities ρ_i of the various species present in the bubble are expressed in terms of molecules/m^3 and C_{pi} are the molecular specific heats. The C_p values for various species, viz. nitrogen, oxygen and water are listed in table 3.1. Calculation of the effective thermal conductivity of the mixture of these three species is explained later.

3.3.4 Overall energy balance

Treating bubble as an open system, the overall energy balance for the bubble contents is written as:

$$\frac{dE}{dt} = \frac{dQ}{dt} - \frac{dW}{dt} + h_W \frac{dN_W}{dt} \tag{3.11}$$

However, the total energy E is a function of the temperature and volume of the bubble, and the number of molecules of various species in it. Thus, the rate of change of E for air bubbles is written as:

$$\frac{dE}{dt}=\left(\frac{\partial E}{\partial N_W}\right)_{N_{N2},N_{O2},V,T}\frac{dN_W}{dt}+\left(\frac{\partial E}{\partial N_{N2}}\right)_{N_W,N_{O2}V,T}\frac{dN_{N2}}{dt}+\left(\frac{\partial E}{\partial N_{O2}}\right)_{N_W,N_{N2},V,T}\frac{dN_{O2}}{dt}+\left(\frac{\partial E}{\partial T}\right)_{N_W,N_{N2},N_{O2},V}\frac{dT}{dt}+\left(\frac{\partial E}{\partial V}\right)_{Nw,N_{N2},N_{O2},T}\frac{dV}{dt} \quad (3.12)$$

where, V is the volume of the bubble and N_{N2}, N_{O2} and N_W are the number of nitrogen, oxygen and water molecules in the bubble, respectively. Per the discussion for rectified diffusion given earlier, for a few acoustic cycles, we neglect the transport of gases during radial motion. Thus, $dN_{N2}/dt = dN_{O2}/dt = 0$. The enthalpy of the water molecule entering the bubble from "cold" interface is: $h_W = 4kT_o$. The specific energy of the water molecule in the bubble is the thermal energy U_W and is written as:

$$\left(\frac{\partial E}{\partial N_W}\right)=U_W=N_W kT\left(3+\sum\frac{\theta_i/T}{\exp(\theta_i/T)-1}\right) \quad (3.13)$$

Here θ_i are the characteristic vibrational temperatures, values of which for various species are listed in table 3.1. The rate of work done by the bubble (dW/dt) reduces to expansion work: P_i dV. Comparing equations 3.11 and 3.12, and identifying that $(\partial E/\partial T) = C_v$ and $(\partial E/\partial V) = 0$, as internal energy of an ideal gas is mainly a function of its composition and temperature, we can now write another equation for the change of the temperature of the bubble:

$$C_{v,mix}\frac{dT}{dt}=\frac{dQ}{dt}-P_i dV+(h_W-U_W)\frac{dN_W}{dt} \quad (3.14)$$

The specific heat of the mixture $C_{v,mix}$ is written in terms of molecular specific heats of individual components ($C_{v,i}$) and number of molecules of individual components (N_i) as:

$$C_{v,mix}=\sum_{i=1}^{N}C_{v,i}N_i \quad (3.15)$$

The C_v values for various species, viz. nitrogen, oxygen and water are listed in table 3.1.

3.3.5 Transport parameters for air – water vapor mixture

In case of air-water vapor mixture we encounter a ternary system: nitrogen – oxygen – water vapor. To determine the diffusion coefficient for water vapor in this system, we first

calculate the binary diffusion coefficients for N_2-H_2O and O_2-H_2O mixtures. Diffusion coefficient of species 1 in the mixture of two species 1-2, to a first approximation is written as (Condon and Odishaw, 1958):

$$D = \frac{3}{8} \frac{\sqrt{\pi kT/\mu_{12}}}{n_{12}\pi\sigma_{12}^2 \Omega_{12}^{(1,1)*}} \tag{3.16}$$

m_1 and m_2 are the molecular masses of species 1 and 2 respectively, and $\mu_{12} = 2m_1m_2/(m_1+m_2)$ is the reduced molecular mass of the two species. $n_{12} = n_1+n_2$ is the joint concentration of the two species. σ_{12} is a parameter in the potential function characteristic of 1-2 interaction. It is approximated as $(\sigma_1+\sigma_2)/2$ where σ_1 and σ_2 are the molecular diameters of water and argon. $\Omega_{12}^{(1,1)*}$ is a dimensionless correction of first order that describes the deviation of the collisional cross-section from the hard sphere cross-section. Values of this parameter are given by Hirschfelder *et al.* (1954) as a function of the reduced temperature of the two species: $T_{12}^* = \sqrt{\left[T/(\varepsilon/k)\right]_1\left[T/(\varepsilon/k)\right]_2}$. Values of the potential parameter (ε/k) for various species (in K) are available in various texts (Hirschfelder *et al.*, 1954; Reid *et al.*, 1987). The overall diffusion coefficient for water vapor in ternary mixture is calculated as (Hirschfelder *et al.*, 1954):

$$\frac{1}{D} = \frac{\varepsilon_{N2}}{(1-\varepsilon_{H2O})D_{N2\text{-}H2O}} + \frac{\varepsilon_{O2}}{(1-\varepsilon_{H2O})D_{O2\text{-}H2O}} \tag{3.17}$$

where ε represents mole fraction of the respective species at the bubble wall. For the determination of conductivity of the ternary mixture, the viscosity of various individual species is evaluated as (Hirschfelder *et al.*, 1954):

$$\eta = \frac{5}{16} \frac{\sqrt{\pi\, mkT}}{\pi\sigma^2\Omega^{(2,2)*}} \tag{3.18}$$

Thereafter, the conductivity of the species is related to its viscosity using the Eucken correction formula:

$$\lambda = \frac{15k}{m}\eta\left(\frac{4f_i}{30}+\frac{3}{5}\right) \tag{3.19}$$

Table 3.1: Thermodynamic properties of various species

Species	Degree of freedom (f_i)	Molecular specific heat (C_p)	Molecular specific heat (C_v)
N_2	5	$\frac{7}{2}k$	$k\left(\frac{5}{2}+\frac{\left(\theta_{N_2}/T\right)^2\exp\left(\theta_{N_2}/T\right)}{\left(\exp\left(\theta_{N_2}/T\right)-1\right)^2}\right)$
O_2	5	$\frac{7}{2}k$	$k\left(\frac{5}{2}+\frac{\left(\theta_{O_2}/T\right)^2\exp\left(\theta_{O_2}/T\right)}{\left(\exp\left(\theta_{O_2}/T\right)-1\right)^2}\right)$
H_2O	6	4k	$k\left(3+\sum_i^3\frac{\left(\theta_{i,H_2O}/T\right)^2\exp\left(\theta_{i,H_2O}/T\right)}{\left(\exp\left(\theta_{i,H_2O}/T\right)-1\right)^2}\right)$

Note: The vibrational temperatures of various species are as follows: θ_{N2} = 3350 K, θ_{O2} = 2273 K, $\theta_{1,H2O}$ = 2295 K, $\theta_{2,H2O}$ = 5255 K, $\theta_{3,H2O}$ = 5400 K.

where f_i is the number of degree of freedom for the species at the bubble wall. Values of f_i for various species are listed in table 3.1. The effective heat conductivity of the ternary mixture is then constructed from individual conductivities as (Condon and Odishaw, 1958):

$$\lambda_{mix} = \sum_i \frac{\varepsilon_i\lambda_i}{\sum_j \varepsilon_j\phi_{i,j}} \tag{3.20}$$

$$\phi_{i,j} = \frac{1}{\sqrt{8}}\left(1+\frac{m_i}{m_j}\right)^{-1/2}\left(1+\left(\frac{n_i}{n_j}\right)^{-1/2}\left(\frac{m_i}{m_j}\right)^{1/4}\right)^2 \tag{3.21}$$

where i,j = N_2, O_2, and H_2O.

3.3.6 Estimating the physical parameters for aqueous KI solutions

The liquid medium in the present case is aqueous solution of potassium iodide. The physical properties of water (such as vapor pressure and surface tension) change with addition of KI. To obtain the vapor pressure of water in KI solution, we are following the expression given

by Horvath (Horvath, 1985):

$$\phi = \frac{x-1}{x}\left[\ln(1-x) - 1.1517x + 0.0148\sqrt{x} + 3.204x^{3/2} - 11.44x^{2}\right] \quad (3.22)$$

where ϕ is the osmotic coefficient and x, the mole fraction of KI in the solution. In terms of concentration of KI (C_{KI}, in mol/lit), x is written as:

$$x = \frac{C_{KI}}{C_{KI} + 55.51} \quad (3.23)$$

The relation between ϕ, the vapor pressure pure water P_{H_2O} and the vapor pressure of water in KI solution P_v is given as:

$$\phi = \left[\frac{-1000}{36C_{KI}}\right]\ln\left(P_v / P_{H_2O}\right) \quad (3.24)$$

The vapor pressure of pure water (in mm Hg) at temperature T (in K) is calculated using Antoine's equation:

$$\ln P_{H_2O} = 18.3036 - \frac{3816.44}{T - 46.13} \quad (3.25)$$

A quick inspection of equations 3.22-3.25 reveals that vapor pressure of water is lowered with addition of KI. We refer to this result later in the paper. The surface tension of water increases with dissolution of KI. The surface tension of the aqueous KI solution has been correlated to KI concentration (C_{KI}, in mol/lit) as (Prasad Naidu *et al.*, 1994):

$$\sigma = \sigma_{H_2O} + \frac{142.3616}{100000}C_{KI} \quad (3.26)$$

σ_{H_2O} is the surface tension of pure water taken to be 0.07272 N/m.

3.3.7 Numerical solution

The equations 3.4, 3.5, 3.6 and 3.14 constitute the complete formulation for radial motion of bubble, which can be solved simultaneously using Runge-Kutta adaptive step size method (Press *et al.*, 1992). We would like to mention that the phenomenon of bubble collapse (or bubble fragmentation) depends on many factors such as the surface instability, local flow

conditions, and the bubble population in the vicinity of the bubble. For the conditions of maximum surface instability and flow instability, the bubble collapses (or fragments) at first compression after an initial expansion. Considering this, the condition for bubble collapse is taken as the first compression after an initial expansion. Three important parameters required for the simulation of bubble dynamics equation are frequency (*f*) and pressure amplitude (P_A) of ultrasound and the equilibrium bubble radius (R_o).

Frequency: The frequency of the ultrasound was taken as 20 kHz – same as the frequency of ultrasound processor used in the experiments.

Pressure amplitude: Based on the total power consumption of the processor and the cross-sectional area of the ultrasound probe tip, the amplitude of ultrasound wave emitted by the probe was calculated as 1.5 bar. The ultrasound wave undergoes attenuation as it propagates through the medium, and hence, the acoustic pressure amplitude actually experienced by the bubble is smaller than 1.5 bar. This attenuation varies directly with the size and population density of bubbles (number of bubbles per unit volume of liquid) (Prosperetti and Commander, 1989). In a non-degassed medium, the attenuation of ultrasound wave is higher due to larger size and larger population of bubbles. Therefore, for the simulation of radial bubble motion in a non-degassed medium, we use a value P_A = 1.25 bar, which accounts for the attenuation effect. For a degassed medium, the attenuation effect is negligible and a value P_A = 1.5 bar is used for simulations.

Equilibrium bubble radius: The equilibrium radius of the bubbles is difficult to estimate. Moreover, it keeps on changing due to phenomenon of rectified diffusion during oscillations. Typically for P_A > 1 bar, the bubble shrinks during oscillations in a highly unsaturated medium, while in a relatively saturated medium it grows due to process of rectified diffusion. Therefore, we have chosen two equilibrium sizes of bubbles for simulation: a smaller size of 10 μm representing bubbles in the degassed medium, while a larger size of 20 μm representing bubbles in the non-degassed medium.

While calculating the composition of the bubble at the time collapse, we assume that

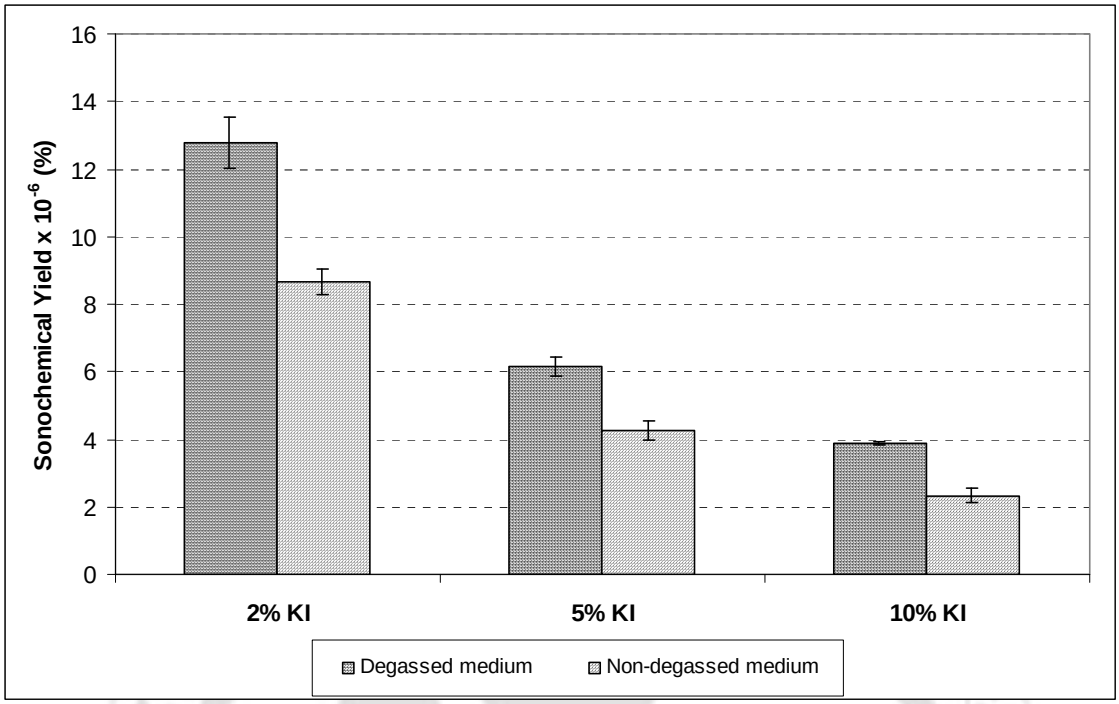

Figure 3.2. Experimental results on iodine liberation under various reaction conditions.

thermodynamic equilibrium is attained. This assumption is based on the relative magnitudes of bubble collapse time scale and time scale of various radical reactions. The time scale of bubble collapse is of the order of a few tens of nanoseconds (~ 10^{-8} s, Storey and Szeri[25]), while time scale of radical reactions is at least two orders of magnitude smaller (~ 10^{-10} s, Krishnan *et al*. 2006). Thus, thermodynamic equilibrium should prevail till the point of minimum radius during collapse. The equilibrium mole fraction of the various species in the bubble (i.e. H_2O, H_2, O_2, $H^{\bullet}$, $OH^{\bullet}$, $O^{\bullet}$, H_2O_2, $HO_2^{\bullet}$, O_3) at the conditions of temperature and pressure at first the compression of the bubble was calculated using software FACTSAGE, which uses the free-energy minimization algorithm proposed by Eriksson (1975).

3.4 RESULTS AND DISCUSSION

The iodine liberation during sonication depends on the amount of radical species

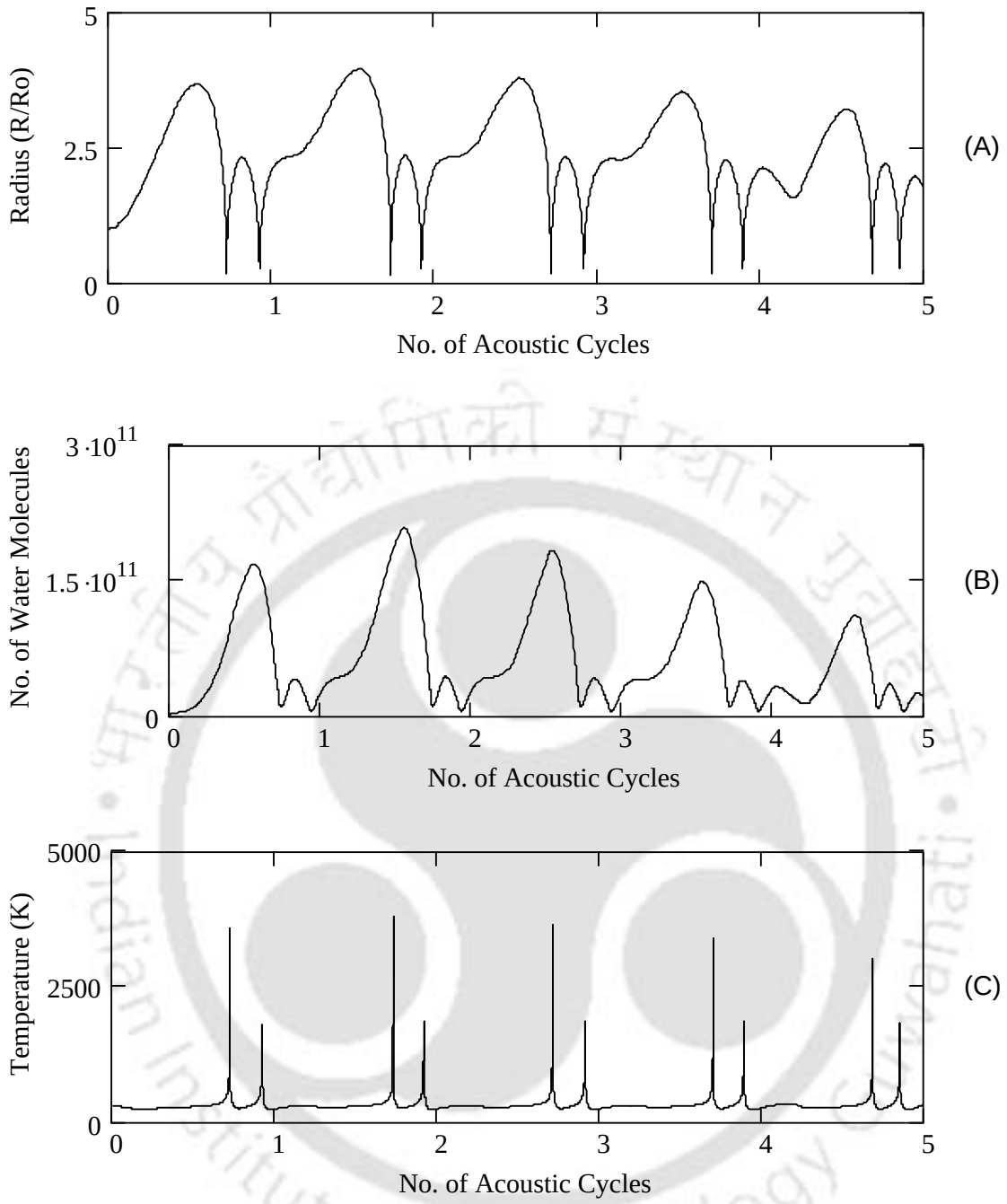

Figure 3.3. Simulation of the radial motion of 10 μm air bubble (representative of degassed medium) in 10% w/v KI solution. Time variation of (A) normalized bubble radius (R/R_o); (B) number of water molecules in the bubble; (C) temperature in the bubble.

produced by the cavitation bubbles, which in turn depends on two factors: (1) the extent of water vapor entrapped in the bubble at the time of collapse, and (2) the temperature peak attained during collapse, which decides the equilibrium composition of various species resulting out of dissociation of water vapor entrapped in the bubble. These two factors can be evaluated from

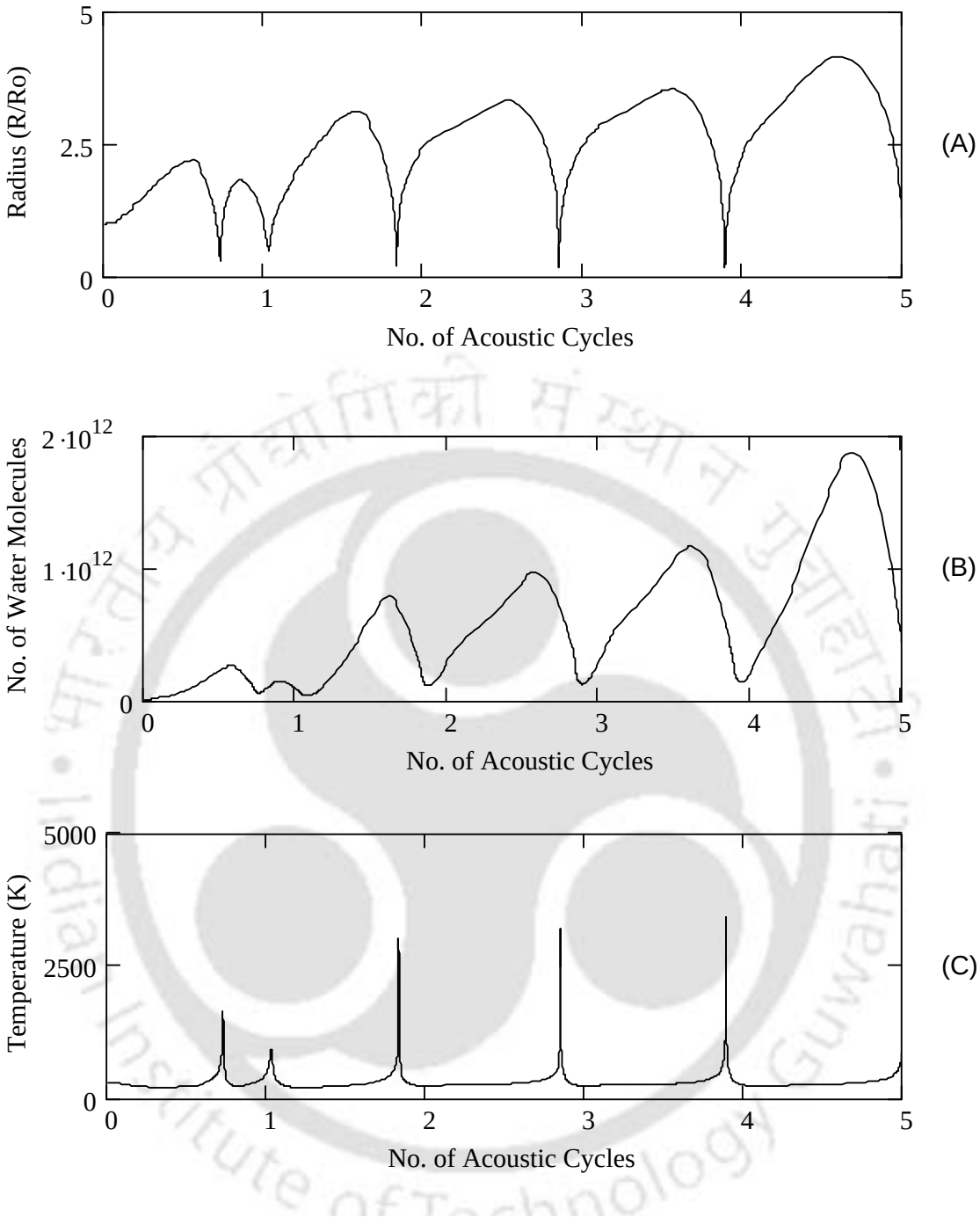

Figure 3.4. Simulation of the radial motion of 20 μm air bubble (representative of non-degassed medium) in 10% w/v KI solution. Time variation of (A) normalized bubble radius (R/R_o); (B) number of water molecules in the bubble; (C) temperature in the bubble.

solution of bubble dynamics equation. The yield of KI oxidation reaction can be defined as: number of moles of iodine liberated per unit time-per unit reaction volume-per unit mole of KI-per unit power input to system. However, the power input, sonication time and reaction volume were same for all experiments, and thus, the definition of sonochemical yield reduces to moles

of iodine liberated per unit mole of KI. With this preamble, we present the experimental and simulation results.

Trends in sonochemical yield with different experimental parameters are shown in figure 3.2. Out of all combinations of reaction conditions attempted, the highest yield is obtained for 2% w/v KI solution with degassed reaction medium, while the lowest yield is seen for 10% w/v KI concentration with non-degassed reaction medium. For either degassed or non-degassed medium, the yield decreased with increasing KI concentration. For all initial concentrations of KI (2%, 5% and 10% w/v), yield increased by about 50% with degassing of the reaction medium.

Illustrative simulations of radial motion of air bubbles with R_o = 10 μm and 20 μm in 10% w/v KI solution are shown in figure 3.3 and 3.4 respectively. The summary of entire simulation results for KI solutions of 2%, 5% and 10% w/v concentration is given in table 2. This table lists the collapse conditions (i.e. number of water molecules entrapped in the bubble and temperature peak reached in the bubble during collapse) and the equilibrium composition of the bubble contents. It is evident that OH is the dominant radical species produced in the bubble. The total number of OH radicals produced per single bubble can be calculated by the product of the number of water molecules entrapped and the equilibrium mole fraction. The OH radical contributes to the oxidation of KI to liberate iodine through reaction (Hart and Henglein, 1985): $2\ KI + 2OH^{\bullet} \rightarrow 2\ KOH + I_2$. From the simulation results presented in table 3.2, certain trends in OH radical yield per single bubble with varying gas content and initial KI concentration in the medium can be observed and explained as follows:

- The highest yield of OH radicals per single bubble is seen for 2% w/v KI solution and initial bubble size of 10 μm – representative of degassed medium. With increasing KI concentration (5% and 10% w/v) the temperature peak reached during collapse of a 10 μm bubble shows small variation; however, the extent of water vapor entrapment reduces. Consequence of this is the reduction in the yield of OH radicals per bubble. Similar trend is

Table 3.2. Simulation results for air bubble

Species	Parameters for simulations					
	R_o = 10 μm 2% w/v KI soln.	R_o = 20 μm 2% w/v KI soln.	R_o = 10 μm 5% w/v KI soln.	R_o = 20 μm 5% w/v KI soln.	R_o = 10 μm 10% w/v KI soln.	R_o = 20 μm 10% w/v KI soln.
	Conditions at the first compression of the bubble					
	T_{max} = 3607 K N_{WT} = 2.23E+010	T_{max} = 1745 K N_{WT} = 1.82E+011	T_{max} = 3620 K N_{WT} = 2.08+010	T_{max} = 1832 K N_{WT} = 1.10E+11	T_{max} = 3587 K N_{WT} = 1.89E+010	T_{max} = 1639 K N_{WT} = 9.35E+010
Equilibrium composition of different radical species in the bubble at collapse (mol fraction)						
O_2	4.9626E-01	6.2215E-01	5.1293E-01	6.2506E-01	5.3766E-01	6.6243E-01
H_2O	4.3902E-01	3.7750E-01	4.2179E-01	3.7437E-01	4.0059E-02	3.3740E-01
$OH^{\bullet}$	4.9454E-02	3.0761E-04	4.9678E-02	4.9968E-04	4.6981E-02	1.5198E-04
$O^{\bullet}$	6.2549E-03	3.2991E-06	6.5203E-03	6.9819E-06	6.294E-03	1.2329E-06
$HOO^{\bullet}$	5.8932E-03	3.3273E-05	6.0149E-03	5.2046E-05	5.7159E-03	1.7856E-05
H_2	1.8079E-03	8.3585E-07	1.7609E-03	1.7212E-06	1.5607E-03	2.6895E-07
H_2O_2	8.3459E-04	3.6320E-06	8.2776E-04	5.6382E-06	7.5433E-04	1.8173E-06
$H^{\bullet}$	4.2632E-04	1.1996E-08	4.2973E-04	3.3064E-08	3.8492E-04	2.8041E-09
O_3	5.0750E-05	1.1775E-07	5.434E-05	2.0710E-07	5.492E-05	6.0263E-08
Net amount of hydroxyl radicals produced per bubble						
N_{OH}	1.1028E+09	5.5985E+07	1.0333E+09	5.4965E+07	8.8794E+08	1.4210E+07

Note: *The number format is as follows: 4.9454E-02 should be read as 4.9454 × 10^{-2}. Species having equilibrium mole fraction less than 10^{-20} have been ignored. Species with Nitrogen as a constituent element have been ignored, as they are found in traces and have no contribution in the context of radical chemistry for oxidation of KI. An equilibrium bubble size (R_o) of 10 μm represents degassed KI solution while an equilibrium bubble size of 20 μm represents non-degassed solution. Various notations used are as follows: T_{max} – temperature peak reached in the bubble at the time of first collapse; N_{WT} – number of water molecules trapped in the bubble at the instance of first collapse.*

seen for 20 μm bubble (representing non-degassed medium) for all KI concentrations. This trend can be explained as follows: with increasing concentration of KI, the vapor pressure of water reduces. This reduces the diffusive flux of water molecules across a bubble, which is directly proportional to vapor pressure of water at bubble interface, as described by equation 3.6. Reduction in the flux of water molecules also reduces the extent of water vapor entrapment in the bubble during collapse.

- For a given initial KI concentration (either 2%, 5% or 10% w/v) the OH radical production increases with degassing of the medium. This is a combined effect of rectified diffusion and pressure amplitude of the ultrasound wave. As mentioned earlier, in a degassed medium, the process of rectified diffusion makes a bubble shrink as it oscillates under influence of ultrasound wave. A smaller bubble undergoes greater compression during collapse, giving higher peak temperatures. In addition, the attenuation of ultrasound wave is much smaller in a degassed medium, and hence, the pressure amplitude of ultrasound wave actually experienced by a bubble is high that makes the bubble collapse even more intense. This results in larger equilibrium composition of OH radicals resulting out of dissociation of entrapped water molecules in the bubble during collapse. On the contrary, in a non-degassed medium, ultrasound wave undergoes attenuation, as mentioned earlier. Moreover, rectified diffusion makes the bubble grow during oscillations. These two effects reduce the intensity of bubble collapse yielding lower peak temperatures, and hence, lesser production of OH radicals from the entrapped water molecules.

Comparison of the experimental and simulations result reveals that the trend in iodine liberation with varying gas content of the medium and initial KI concentration exactly follows the trends in OH radical production per single bubble. It is thus evident that the physical technique of degassing the medium is far more efficient in enhancing the sonochemical yield than the chemical technique of increasing initial KI concentration. In addition to the comparative evaluation of physical and chemical techniques for enhancement of sonochemical yield; this study also brings to light some interesting mechanistic features of a sonochemical reaction. The influence of various parameters on a sonochemical reaction is revealed to be highly inter-dependent. The yield of such a reaction strongly depends on the physical acoustics of the system. The major influencing parameter in this regard turns out to be the dissolved gas content of the medium, which manifests its effect through the process of rectified diffusion and attenuation that affects two other important parameters, viz. the equilibrium bubble radius and

the amplitude of the ultrasound wave, which ultimately affect the intensity of cavitation bubble collapse and the production of OH radicals from the bubble. On the other hand, initial reactant concentration turns out to be a counter-productive parameter. Due to reduction in vapor pressure of water with increasing KI concentration, the important phenomenon of water vapor trapping in the cavitation bubble during collapse – subsequently leading to radical production through dissociation – is adversely affected. The exact mechanism of influence of dissolved gas content and initial KI concentration on sonochemical yield, which can be worked out from the results and analysis presented above is shown in figure 3.5.

3.5 CONCLUSION

This chapter tries to illuminate the complex interrelations between the physics and chemistry of a sonochemical reaction system, i.e. the physical phenomena of bubble dynamics and its chemical manifestation, i.e. formation of radicals that induce chemical reaction. With experiments (using a well-known sonochemical reaction) and a mathematical model (which takes into account the essential physics of the bubble dynamics), we have shown as how the macroscopic manifestation (i.e. the sonochemical yield) of the microscopic phenomena (i.e. transient collapse of cavitation bubble) is a complicated function of several inter-dependent physical processes such as rectified diffusion, water vapor transport and entrapment in cavitation bubbles and the ultrasound wave attenuation. Degassing of the reaction medium intensifies the transient collapse of the cavitation bubble, resulting in higher production of OH and other radicals, which enhance yield of the sonochemical reaction. Quite unexpectedly, increasing the initial reactant concentration has an adverse effect on the sonochemical yield. This is a consequence of the lessening of the radical production by cavitation bubbles due to decrease in the vapor pressure of water at the bubble interface with increasing initial reactant concentration. An important conclusion of this study is that extent of water vapor entrapment in the bubble and the intensity of the transient cavitation bubble collapse are the principal physical phenomena that

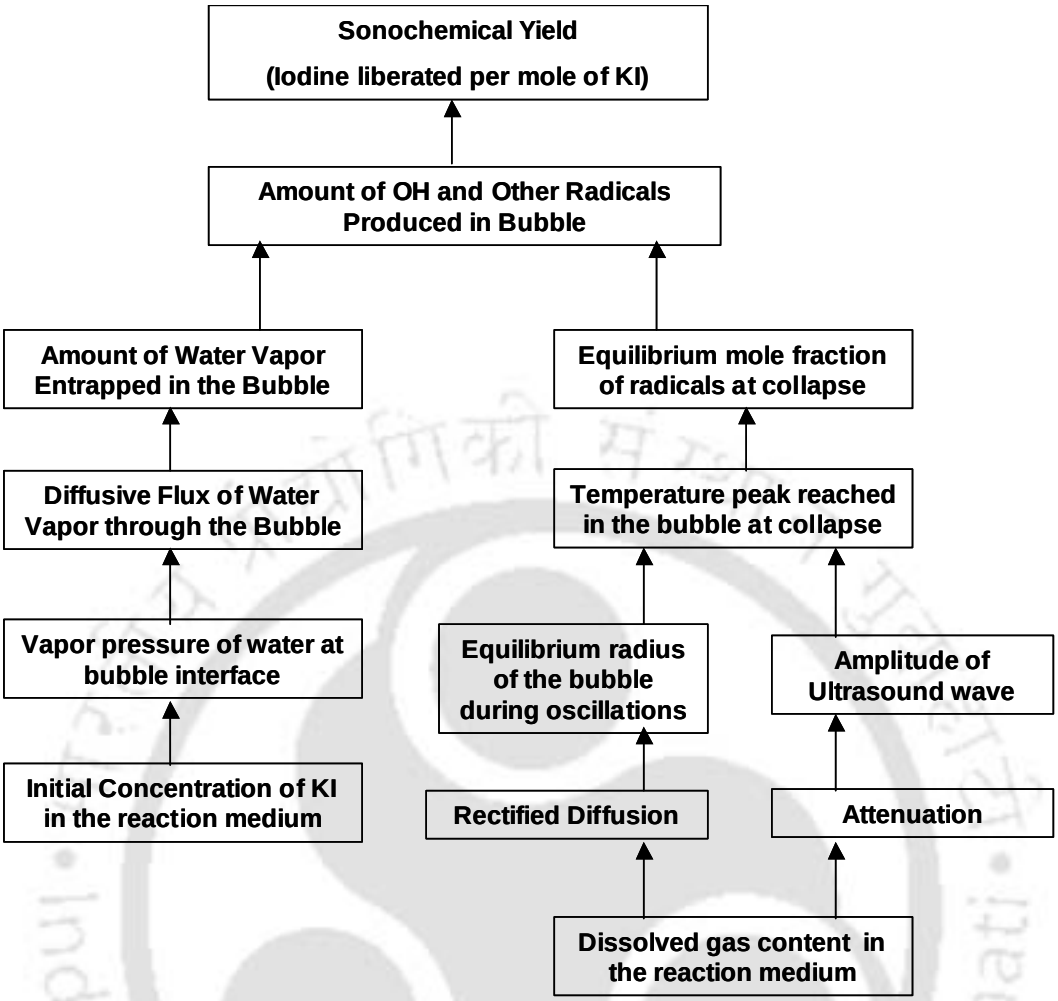

Figure 3.5. A schematic depicting the exact mechanism of influence of dissolved gas content and initial KI concentration on sonochemical yield, which can be worked out from the results and analysis presented in this study.

affect the yield of a sonochemical reaction, which is the extent of sonochemical degradation of the pollutant from the perspective of the present thesis. All reaction parameters, such as initial reactant concentration and dissolved gas content of the reaction medium, manifest their influence on the sonochemical yield through these physical phenomena. Therefore, any attempt to maximize the sonochemical yield by variation of any reaction parameter should take into account the influence of that parameter on the above-mentioned physical phenomena. The present study puts forth a framework for such an attempt, with the model reaction of oxidation of potassium iodide, which can be extended to any other sonochemical reaction system such as

sonolysis of recalcitrant organic pollutants.

ACKNOWLEDGMENT

Some work reported in this chapter was carried out jointly with Mr. Ashwin Paunikar (M.Tech. student, Roll No. 04410714, Research Supervisor: Dr. V.S. Moholkar), for which the author of this thesis would like to express gratitude. The model sonochemical reaction (oxidation of potassium iodide) and the bubble dynamics model used in this chapter have also been used in the thesis of Mr. Paunikar.

CHAPTER 4

MECHANISTIC APPROACH TO INTENSIFICATION OF SONOCHEMICAL DEGRADATION OF PHENOL

4.1 INTRODUCTION

Phenol is one of the most ubiquitous pollutants found in wastewater of chemical and process industries. Degradation of phenol with sonolysis or sonolysis coupled with other techniques such as photocatalytic oxidation, Fenton's reagent oxidation, ozonation, peroxidation has been a subject of active research with several authors addressing the problem with different perspective. A review of the literature in this area degradation has been presented in chapter 1. The main degradation intermediates of phenol have been found to be catechol and hydroquinone, which point at attack of $OH^{\bullet}$ radical (i.e. hydroxylation reaction) produced by the cavitation bubbles on the phenol molecule in the bulk liquid medium as the foremost degradation pathway. However, most of the studies in the area of sonolytic phenol degradation have experimental approach and no attempt is made to link the results to the physics of cavitation bubbles using a suitable mathematical model. As explained in greater details in the next section, such an approach forms the basis for the study on enhancement of sonochemical degradation of phenol.

This chapter addresses the matter of enhancement of the sonolytic degradation of phenol from a mechanistic perspective. With experiments under different reaction conditions coupled to a bubble dynamics model, we assess the rate of radical production from cavitation bubbles and their effective utilization for the degradation process using various scavenging

techniques. We show that the rate of radical scavenging (and not the rate of radical production) is the key factor, which influences the sonochemical degradation of phenol.

4.2 ENHANCEMENT OF DEGRADATION KINETICS OF PHENOL: A THEORETICAL CONTEMPLATION

Before proceeding to the description of experimental methodology, the mathematical model and results of this study, we would like to ponder over some fundamental aspects of the sonochemical degradation of phenol. The rate of the degradation reaction [Ph] + [$R^{\bullet}$] → [Products] can be written as: $-r_{Ph} = k_{Ph}[Ph][R^{\bullet}]$. This rate depends on the concentration of phenol molecules, [Ph], and the concentration of the radicals produced out of the cavitation bubbles, [$R^{\bullet}$]. Increasing any or both of these quantities should increase the rate of degradation reaction. However, as far as the sonochemical reactions are concerned, an additional factor that affects the rate and yield of the reaction, which is the probability of interaction between the reactant molecules (i.e. phenol) and the radicals. The radicals produced out of cavitation bubbles are extremely reactive. Thus, they react almost instantly after being released into the bulk medium with the transient collapse of the bubble – without diffusing significantly away in the bulk liquid medium from the location of the collapse of the bubble. Thus, the concentration of the radicals is rather localized (maximum at the interfacial region between cavitation bubble and the liquid medium) and not uniform throughout the total reaction volume. Thus, if the concentration of the reactant molecules in the vicinity of the bubble is low, the radicals may merely recombine without inducing any chemical change. An augmentation in the interaction probability results in the effective utilization of the radicals produced out of cavitation bubble and the consequent rise in the rate of degradation reaction. On this basis, one can postulate several methods of enhancing the degradation kinetics of phenol, as described below:

(1) ***Increasing the yield of the radicals*****:** The extent of production of radicals through cavitation bubbles depends on two factors: (1) amount of water vapor trapped in the bubble during transient collapse of the bubble and (2) the temperature peak reached in the bubble during collapse. The first factor depends on saturation (or vapor) pressure of water at the bubble–bulk interface, which in turn, decides the diffusive flux of the water molecules (Storey and Szeri, 2000; Toegel *et al.*, 2000). The second factor depends on the nature of gas itself. Monatomic gases like argon give very high temperature peaks during transient collapse than diatomic gases such as air, nitrogen and oxygen (Henglein, 1956, 1957). Therefore, bubbling of monatomic gas in the reaction mixture during sonication (in order to provide nuclei for cavitation events) can enhance the production of radicals, and hence, the rate of degradation reaction.

(2) ***Increasing the interfacial concentration of phenol*****:** Due to hydrophobic repulsive interactions with water molecules in bulk medium, the organic molecules such as phenol are driven towards the bubble-bulk interface. This results in higher concentration of these molecules near interface than in bulk. The phenol molecules can get adsorbed onto bubble interface. This phenomenon has two consequences that contribute towards intensification of degradation of phenol: first, rise in the equilibrium vapor pressure (or partial pressure) of phenol at the gas-liquid interface that results in greater evaporation of phenol in the cavitation bubble during expansion and subsequent pyrolysis during transient collapse, and secondly, greater probability of radical-phenol interaction leading to hydroxylation of phenol as the bubble-bulk interface is also a region of high concentration of radicals. This phenomenon has been studied by Seymour and Gupta (1997) and Bapat *et al*. (2007) with different approaches. The approach of Seymour and Gupta was semi-empirical. They first determined the partitioning behavior of phenol between diethyl ether and water. Proposing that the partitioning of the phenol molecules between bulk and bubble interface was proportional to

partitioning in ether-water system, they described the rate of degradation of the pollutant using first order kinetic expression. The proportionality constant between ether-water and bulk-bubble interface partition coefficients was an adjustable parameter. Next, comparing the theoretically predicted and experimentally obtained degradation rates with regression analysis, Seymour and Gupta showed that the phenol concentration at the bubble-bulk interface was ~ 3 times higher than in the bulk. On the other hand, the approach of Bapat *et al*. was theoretical. Using the Gibb's equation for the surface excess of solute as basis (Adamson and Gast, 1997; Joos and Serrien, 1989), they measured the reduction in the surface tension of the aqueous solution of phenol with concentration of phenol. Correlating the slope of the plot of surface tension vs. bulk concentration to the Gibb's equation, Bapat *et al.* determined the surface excess of phenol for bulk concentration of 1 mol/m^3. Later, with simultaneous analysis of the surface concentration of phenol and water molecules at bubble-bulk interface, Bapat *et al.* concluded that the concentration of phenol at bubble-bulk interface at equilibrium conditions would be 264 times the bulk concentration. Thus, the enrichment of phenol at bubble-bulk interface as determined by Seymour and Gupta (1997) and Bapat *et al*. (2007) differs by two orders of magnitude. However, attainment of equilibrium between bubble interface and bulk medium is difficult to achieve under transient cavitation conditions where bubble undergoes large-amplitude radial motion. The time scale of this motion is same as that of the ultrasound wave (50 μs for 20 kHz frequency). The time for the diffusion of phenol to the bubble interface through the boundary layer is expected to be several orders of magnitude higher. For representative values of boundary layer thickness as ~ 1 μm and diffusion coefficient of 10^{-10} m^2/s, the time scale of diffusion of phenol is ~ 1 ms. Due to large difference in the time scale of diffusion of phenol and the time scale of radial motion of bubble, the bubble interface is not likely to attain equilibrium (as assumed by Bapat *et al.*) under transient cavitation conditions. The enrichment factor determined

empirically by Seymour and Gupta, thus, seems to be more practical. Nonetheless, the above logic offers a useful tool for enhancing phenol degradation. The bubble-bulk interface is also a region with high concentration of radicals, as note earlier. With enrichment of phenol at bubble interface, the probability of radical-phenol interaction increases significantly giving enhanced degradation through hydroxylation route. Addition of salt to the medium increases the ionic strength of the aqueous medium, and hence, the hydrophobic repulsive interactions between organic pollutant and water. This drives the phenol molecules towards the bubble-bulk interface to a greater extent and increases the degradation rates. This technique for enhancing the degradation kinetics of pollutants has been studied earlier (Gogate *et al.*, 2004; Mahamuni and Pandit, 2006). Although simple and easy, this method has little practical utility for large-scale processes due to significantly large quantities of salt required. Moreover, addition of salt increases the total dissolved solids (TDS) content of the wastewater, which could give additional disposal problems.

(3) *Scavenging of radicals*: Another possible means of raising the probability of the radical–phenol interaction is to scavenge the radicals in the bulk medium as well as inside the bubble. The word "***scavenging***" in the present context means "***conservation***", i.e. reacting the radicals with other species (present in relatively large quantities in the bubble or in the liquid medium) to generate new radical species. This prevents the phenomenon of radical recombination, which is a loss of oxidation potential of cavitation events. Scavenging of radicals inside the bubble results in greater release of radical species in the bulk medium. Moreover, scavenging of the radicals in the bulk medium results in penetration (or diffusion) of the radicals in the bulk medium to greater distances from the location of the collapse of cavitation bubble. Consequently, the probability of interaction of the radical with phenol molecules increases giving higher degradation rates. In this work, we will assess the efficacy of the method of scavenging of radicals using a molecular (O_2) and an ionic (Fe^{2+}) species

coupled with the technique of sparging monatomic and diatomic gases through the reaction solution for the enhancement of the degradation kinetics of phenol. As noted earlier, dissociation of water molecules trapped in the cavitation bubble results in generation of radical species such as $H^{\bullet}$, $OH^{\bullet}$ and $HO_2^{\bullet}$.

Oxygen scavenging: Oxygen present in the bubble (in gaseous form) and present in the medium (in dissolved or aqueous form as well as in the form of tiny bubbles suspended in the medium) can scavenge radicals inside the bubble as well as in the bulk medium in several ways. Dissociation of molecular oxygen in the bubble influences the formation of $OH^{\bullet}$ radicals via reactions:

$$O_2 \rightleftharpoons 2O^{\bullet} \qquad \text{(R.4.1)}$$

$$O^{\bullet} + H_2O \rightleftharpoons 2OH^{\bullet} \qquad \text{(R.4.2)}$$

It should be noted that the second reaction could also occur in the bulk medium where $O^{\bullet}$ radicals released in the medium with transient collapse of the bubble can react with water molecules to generate additional $OH^{\bullet}$ radicals. The oxygen in the bubble can also react with $H^{\bullet}$ radicals formed out of water dissociation to generate $OH^{\bullet}$ and $HO_2^{\bullet}$ radicals via following reactions:

$$H_2O \rightleftharpoons H^{\bullet} + OH^{\bullet} \qquad \text{(R.4.3)}$$

$$H^{\bullet} + O_2 \rightleftharpoons O^{\bullet} + OH^{\bullet} \qquad \text{(R.4.4)}$$

$$H^{\bullet} + O_2 \rightleftharpoons HO_2^{\bullet} \qquad \text{(R.4.5)}$$

Reactions R.4.4 and R.4.5 can also occur in bulk liquid medium where dissolved oxygen can react with $H^{\bullet}$ radicals released during transient bubble collapse generating additional oxidizing species. In addition to this, the dissolved oxygen in the medium can help revert the

loss of oxidation potential due to recombination of $OH^{\bullet}$ radicals released in the medium by generating $HO_2^{\bullet}$ species as follows:

$$OH^{\cdot} + OH^{\cdot} \rightleftharpoons H_2O_2 \qquad \text{(R.4.6)}$$

$$H_2O_2 + O_2 \rightleftharpoons 2HO_2^{\cdot} \qquad \text{(R.4.7)}$$

Finally, the dissolved oxygen can also react with $OH^{\bullet}$ radicals released in the medium to generate additional oxidizing species:

$$OH^{\cdot} + O_2 \rightleftharpoons HO_2^{\cdot} + O^{\cdot} \qquad \text{(R.4.8)}$$

If any other reactive species (in addition to water vapor and oxygen) is present in the bubble (for example nitrogen in case of air bubbles), the scavenging action of oxygen is influenced as the additional species competes with oxygen. This point is discussed in greater detail later in the paper.

Fe^{2+} scavenging: Being an ionic species, the scavenging action of Fe^{2+} is restricted only in the bulk liquid medium and not inside the bubble. Fe^{2+} ions react with the hydrogen peroxide formed out of recombination of $OH^{\bullet}$ radicals released in the medium with transient collapse of cavitation bubbles. Thus, Fe^{2+} reverts the loss of oxidation potential of cavitation bubbles. In the process, Fe^{2+} is oxidized to Fe^{3+}.

$$OH^{\cdot} + OH^{\cdot} \rightleftharpoons H_2O_2 \qquad \text{(R.4.6)}$$

$$H_2O_2 + Fe^{2+} \longrightarrow Fe^{3+} + OH^{-} + OH^{\cdot} \qquad \text{(R.4.9)}$$

It must be noted that there are two sources of hydrogen peroxide in the medium. First, the H_2O_2 produced due to recombination of radicals per reaction R.4.6. Secondly, H_2O_2 is also formed in the bubble, in equilibrium proportion, due to dissociation of water molecules. However, the equilibrium fraction of H_2O_2 among various species in the bubble at the moment of collapse is usually very small. Thus, the main scavenging action of Fe^{2+} is due to

its reaction with H_2O_2 formed due to recombination of $OH^{\bullet}$ radicals. Fe^{2+} ions are regenerated in the medium by following reactions:

$$Fe^{3+} + H_2O_2 \longrightarrow Fe^{2+} + HO_2^{\bullet} + H^+ \qquad \text{(R.4.10)}$$

$$Fe^{3+} + HO_2^{\bullet} \longrightarrow Fe^{2+} + O_2 + H^+ \qquad \text{(R.4.11)}$$

Due to continuous regeneration, the average concentration of Fe^{2+} in the bulk medium stays very nearly constant. Due to this feature, Fe^{2+} can provide effective scavenging of radicals.

4.3 EXPERIMENTAL

4.3.1 Reagents

The reagents used in the present study are as follows: Phenol (Merck, Grade: Synthesis), Iron (II) sulphate heptahydrate (Merck, Grade: Purified), Acetonitrile (Merck, Grade: HPLC) and Water (Merck, Grade: HPLC). All reagents were used as received. The aqueous solution of phenol with bulk concentration of 100 ppm (typical of the concentration levels in industrial wastewater discharge) was prepared using Elix water from Millipore® purification unit (Model: Elix 3). Four gases, viz. oxygen, argon, nitrogen and air (99.99% purity) were used for bubbling the reaction solution.

4.3.2 Experimental setup

A schematic diagram of the experimental setup used in the present study is shown in figure 4.1. A microprocessor based and programmable ultrasound processor (Sonics and Materials Inc., Model VCX 500) was used for sonication of the phenol solution. The frequency of the processor was 20 kHz with maximum power output of 500W. The ultrasound probe of the processor was fabricated from high-grade titanium alloy and had a tip diameter of 13 mm. With a variable power output control, the net consumption of power during sonication was set at 100W (20% of the maximum value). The actual value of the ultrasound intensity in the medium was determined using calorimetry (Sivasankar *et al.*,

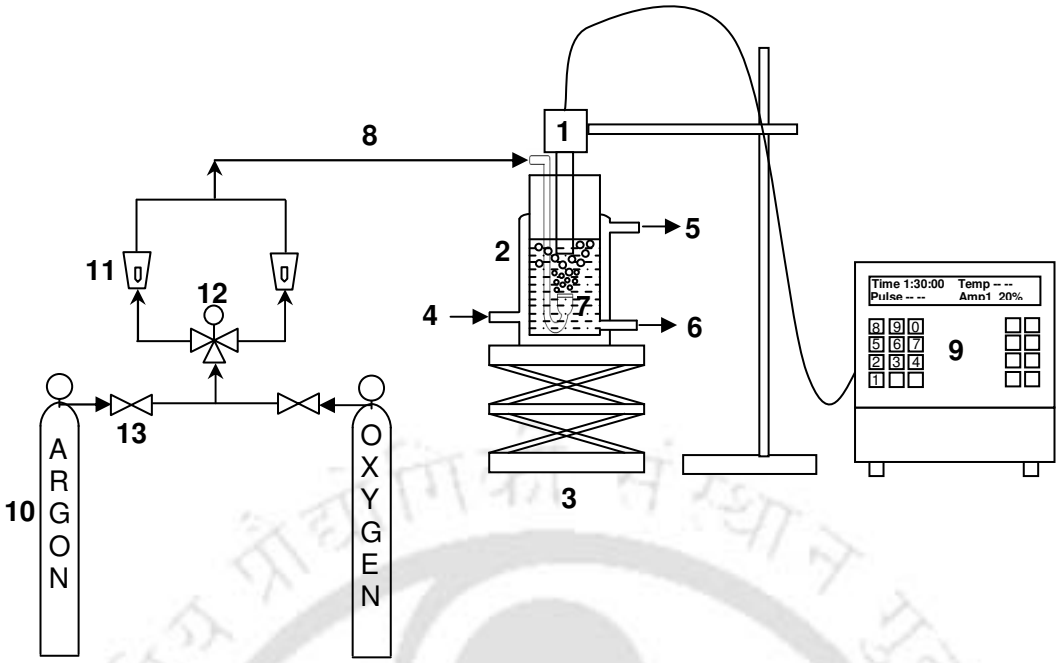

Figure 4.1. Schematic diagram of the experimental setup. Legends: 1. Ultrasound horn; 2. Jacketed glass reactor; 3. Laboratory jack; 4. Cooling water inlet; 5. Cooling water outlet; 6. Sample port; 7. Aerator; 8. Gas inlet; 9. Control unit of ultrasonic processor; 10. Gas cylinder; 11. Rotameter; 12. Three way valve; 13. Gas

2007). For a power output of 100W the ultrasound probe produced an acoustic wave with 1.5 bar amplitude. The processor had facility of automatic frequency tuning and amplitude compensation, which ensures constant power delivery to the ultrasound probe irrespective of the changes occurring in the liquid medium during degradation process. For the sonication of the phenol solution, a jacketed glass reactor (dimensions: height–120 mm, diameter–50 mm, jacket diameter–62 mm) was used. This reactor was positioned on a laboratory jack, which could be raised or lowered for exact positioning of the ultrasound probe in the solution. The tip of the ultrasound probe was placed 15 mm below liquid surface so as to ensure effective coupling between tip of the horn and the bulk liquid medium. For bubbling of the gas in the reaction solution, a glass sparger was used. This sparger had silica filter (pore size ~ 40 μm) to disperse gas in the solution in the form of fine bubbles. The sparger was so positioned that

the porous silica filter exactly faces the bottom of the ultrasound probe. This feature helps uniform distribution of gas bubbles forming cavitation nuclei in the solution. The distance between ultrasound probe tip and silica filter was fixed at 20 mm. The flow of gas to the sparger was controlled using a 3-way valve connected to two rotameters, as shown in figure 4.1.

4.3.3 Experimental procedure and analysis

Sonochemical degradation experiments: 150 ml of phenol solution with 100 ppm concentration at an initial temperature of 25°C was used for sonication. The total sonication time in all experiments was 90 minutes; however, in order to avoid significant rise in the temperature of the solution the sonication was done in pulse mode with sonication period of 15 min followed by silent period of 5 min. In addition, cooling water was circulated through the jacket during sonication in order to maintain the temperature of the reaction medium constant. The temperature of the solution was monitored continuously during sonication with a digital thermometer. The rise in the temperature of solution during experiment was ~ 2°C. The experiments were categorized as follows:

(1) Sonication of phenol solution with continuous bubbling of either of the four gases (viz. nitrogen, air, oxygen and argon) at a flow rate of 5 lit/hr.

(2) Sonication of phenol solution with bubbling of either argon or nitrogen at flow rate of 5 lit/hr during the 15 min sonication period and bubbling of oxygen during 5 min silent period at a flow rate of 10 lit/hr.

(3) Sonication of phenol solution with continuous bubbling of any of the four gases mentioned above with 0.5 mM $FeSO_4 \cdot 7H_2O$ added to the solution.

Addition of $FeSO_4 \cdot 7H_2O$ can increase the ionic strength of the medium, and hence, the repulsive hydrophobic interactions of phenol with water molecules. As a result, the partitioning of phenol between bulk and interface can rise; and the interfacial concentration

of phenol increases. This effect can enhance degradation of phenol. However, this effect is observed principally for $FeSO_4$ addition in moderate to high concentrations. In order to isolate this effect, the $FeSO_4$ addition in the present experiments has been kept quite low; i.e. at a concentration of 0.5 mM. Moreover, it needs to be mentioned that the solubility of the four gases used in this study differs. The solubilities of the gases in water at the temperature of experiment are as follows: N_2 = 0.6 mol/m^3, Ar = 1.4 mol/m^3, O_2 = 1.3 mol/m^3 and Air = 0.794 mol/m^3. It is likely that some of the gas being sparged through the solution will dissolve in water, without forming cavitation nuclei. However, the rate of sparging (or bubbling) of all four gases was 5 lit/hr (equivalent to 0.2 mol/min), which is rather high compared to the solubilities. As a result, the bulk medium gets saturated with the gas within short time. Thereafter, all of the gas entering the medium is essentially utilized for the nucleation of cavitation events. Some loss of phenol from the solution may also occur due to diffusion (or stripping) with the gas sparged through the solution. This loss may be misinterpreted as degradation. In order to assess this loss, the final phenol concentration in the solution with 100 ppm initial concentration was measured after sparging of N_2, O_2, air and argon at a rate of 5 lit/hr for 90 min; in absence of ultrasound irradiation. The final concentration of phenol was practically same as initial concentration. This result shows that no loss of phenol occurs due to diffusion (or stripping) with bubbling gas. A simple explanation for this result can be given as follows: the vapor pressure of phenol in pure form at the temperature of the experiment (25 ^oC) is mere ~ 40 Pa. The concentration of phenol in the solution is very low (~ 10^{-3} mole/lit equivalent to 100 ppm). Therefore, the equilibrium vapor pressure or partial pressure of phenol in 100 ppm solution, as determined by Raoult's law, is negligibly small ~ 0.04 Pa. Hence, practically no diffusion of phenol occurs with sparging of gas through the solution.

All experiments were done in triplicate to assess the reproducibility of the results. The mean of the percentage degradation obtained in 3 experimental runs was taken into consideration for further analysis. The final concentration of phenol in the solution after 90 min of sonication was determined using HPLC (Perkin Elmer, Model: Series 200). A C18 column (Make: Chromatopak, dimensions: 250 mm × 4.6 mm, particle size of packing: 5 μm) was used with a mixture of acetonitrile:water (80:20) as the eluent. The flow rate of eluent was maintained at 1 ml/min with sample injection volume being 20 μl. The UV detector wavelength for phenol was 275 nm. We would like to categorically state that we have not made an analysis of the intermediate products of degradation of phenol as these have been well studied and documented in the literature mentioned earlier. We have monitored the rate of disappearance of original pollutant and the analysis has been made on that basis.

Dissolved species variation: In another experiment, changes in the dissolved oxygen content of Elix water with sparging of nitrogen and argon was studied. For this puropose, the desired gas (either nitrogen or argon) was sparged through water saturated with oxygen in a 100ml beaker using the gas sparger at a flow rate of 5 lit/hr. During bubbling, the water was stirred using a magnetic stirrer. The dissolved oxygen concentration was monitored using a DO meter (Make: Consort, Model: C863). To assess the influence of sonication on the removal of dissolved oxygen with sparging of argon and nitrogen, this experiment was also conducted with simultaneous irradiation of ultrasound.

4.4 MATHEMATICAL FORMULATION

In the context of the present study, the problem of mathematical modeling comprises of simulating the radial motion of cavitation bubbles comprising of various gases (viz. nitrogen, argon, oxygen and air) with the accompanying heat transfer and evaporation/entrapment of vapor molecules, and finally determine the various chemical

species that result out of transient collapse of the bubble. For this purpose, we use the diffusion limited model of Toegel *et al.* (2000), which has been formulated on the basis of the rigorous mathematical treatment z of Storey and Szeri (2000). This model has been presented in previous chapter for the radial bubble motion of air bubbles in aqueous solutions of potassium iodide. We reproduce the model here for the convenience of the reader and highlight the changes that we need to make to adopt the model for the radial motion of bubbles of different gases (mentioned above) in aqueous phenol solution.

It should be noted that the overall degradation of phenol is a manifestation of simultaneous oscillations of millions of bubbles present in the bulk liquid medium. In such a system, numerous factors such a bubble-bubble coalescence, clustering, rectified diffusion affect the overall sonochemical yield, i.e. the extent of degradation of phenol. In addition to this, the number density of bubbles is also a crucially important parameter. No experimental method has been developed yet, which can provide an estimate of this parameter, even with an order of magnitude accuracy. No model for the radial motion of a cavitation bubble has been developed so far, which takes into account all of these facets. Research in the area of radial motion of bubble has been restricted mostly to analysis of single bubbles. The single bubble models do not address the entire physical phenomena in the system, yet they provide a qualitative physical insight into the problem, as these models address the essential physics of the problem such as heat transfer, mass transfer, vapor entrapment etc.

Attempts of modeling physical or chemical effects of multibubble systems with single bubble models have been made by earlier authors. Ilyichev *et al.* (1989) have shown that all spectral characteristics of experimental acoustic cavitation (involving multi-bubble fields) can be explained with simulations of a single bubble. Prasad Naidu *et al.* (1994) and Rajan *et al.* (1998) have successfully explained the trends in the sonochemical oxidation of water-KI and water-KI-CCl_4 system using single bubble model. More recently, Storey and Szeri (2001)

have pointed out that experimentally observed trends in sonochemistry are reflected in the trends observed in the behavior of a single representative bubble. However, the principal limitation of the single bubble models (due to the approximations in them) is that ***no quantitative*** predictions about reaction kinetics and yield can be made with them.

As far as objectives of the present study are concerned, single bubble approach for mathematical modeling is sufficient.

4.4.1 Bubble dynamics model

The bubble motion is described by Keller-Miksis equation (Prosperetti and Lezzi, 1986; Brennen, 1995) as:

$$\left(1-\frac{dR/dt}{c}\right)R\frac{d^2R}{dt^2}+\frac{3}{2}\left(1-\frac{dR/dt}{c}\right)\left(\frac{dR}{dt}\right)^2=\frac{1}{\rho}\left(1+\frac{dR/dt}{c}\right)\left(P_i-P_t\right)+\frac{R}{\rho c}\frac{dP_i}{dt}-4\nu\frac{dR/dt}{R}-\frac{2\sigma}{\rho R} \tag{4.1}$$

where P_t is the time variant pressure in the bulk liquid driving bubble motion. The pressure inside the bubble, P_i is written as:

$$P_i=\frac{N_{tot}(t)kT}{\left[\frac{4\pi}{3}\left(R^3(t)-h^3\right)\right]} \tag{4.2}$$

where h ~ R_o/8.86 is the van der Waals hard core radius determined by the excluded volume of gas molecules. Since the hard core radii of the species considered in the present work viz. nitrogen, oxygen, water and argon differ only by a small magnitude, we take a common value for the hard-core radius. Equation 4.1 can be easily transformed into two simultaneous ODEs by following substitution:

$$\frac{dR}{dt}=s \tag{4.3}$$

$$\frac{ds}{dt}=\frac{\left(1+s/c\right)}{R\rho\left(1-s/c\right)}\left(P_i-P\right)+\frac{1}{\rho c\left(1-s/c\right)}\frac{dP_i}{dt}-\frac{4\nu s}{R^2\left(1-s/c\right)}-\frac{2\sigma}{\rho R^2\left(1-s/c\right)}-\frac{3s^2\left(1-s/3c\right)}{2R\left(1-s/c\right)} \tag{4.4}$$

4.4.2 Heat and mass transfer across bubble

Both gas and vapor (of phenol and water) diffuse across the bubble wall during radial bubble motion. The time scale of gas diffusion can be given as ~ R_o^2/D where R_o is the initial radius of the bubble (~ 10 μm) and D is the diffusion coefficient (~ 10^{-9} m^2/s). Thus, the time scale of gas diffusion becomes ~ 0.1 ms, which is much higher than the time scale of radial bubble motion (which is same as time scale of ultrasound wave: 50 μsec for 20 kHz wave). Thus, the transport of gas across the bubble during radial motion can be ignored.

The equilibrium vapor pressure or partial pressure of phenol in the bulk medium (with concentration of 100 ppm) is 0.04 Pa, as note earlier. Due to hydrophobic repulsive interactions, enrichment of phenol occurs at the bubble-bulk interface, and the concentration of phenol is ~ 3 times the bulk concentration. Despite this, the partial pressure of phenol at the bubble-bulk interface is ~ 0.12 Pa, which is several orders of magnitude smaller than partial pressure of water. Due to very low partial pressure, the evaporation of phenol into the bubble during expansion is negligible and can be ignored. Diffusion of water vapor into the bubble, as a result of evaporation occurring at the bubble interface needs to be taken into account, nonetheless.

The temperature inside the bubble exceeds the surface temperature of the bubble (which is same as bulk liquid temperature) only for a very brief moment during collapse. On the basis of this condition, the bubble can be divided into two parts: (1) a “cold” boundary layer in thermal equilibrium with the liquid, and (2) a hot homogeneous core. An underlying assumption in this hypothesis is that the condensation of water molecules at the bubble wall is fast enough to maintain equilibrium phase change. By dimensional analysis, the instantaneous diffusive penetration depth is given by: $l_{diff} = \sqrt{Dt_{osc}}$, where t_{osc} is the time

scale of bubble oscillations, $R/\left|dR/dt\right|$. The rate of change of water molecules in the bubble by diffusion is given by:

$$\frac{dN_w}{dt} = 4\pi R^2 D \left.\frac{\partial C_w}{\partial r}\right|_{r=R} = 4\pi R^2 D\left(\frac{C_{wR} - C_w}{l_{diff}}\right) \tag{4.5}$$

where C_{wR} is the equilibrium concentration of water molecules at the bubble wall, and it is calculated from the equilibrium vapor pressure at the bubble wall corresponding to bulk liquid temperature. C_w is the actual concentration of water molecules in the bubble core.

With complete analogy with mass transfer, the heat transfer across bubble wall is given by:

$$\frac{dQ}{dt} = 4\pi R^2 \lambda\left(\frac{T_o - T}{l_{th}}\right) \tag{4.6}$$

where λ is the thermal conductivity of the bubble contents and l_{th} is the thermal diffusion length written as: $l_{th} = \sqrt{\kappa t_{osc}}$. The thermal diffusivity, κ of the gas-vapor mixture in the bubble is calculated as: $\kappa = \dfrac{\lambda}{\rho_{mix} C_{p,mix}}$, where $\rho_{mix} C_{p,mix} = \sum_i \rho_i C_{pi}$, ρ_is are the densities of the species present in the bubble (in molecule/m^3) and C_{pi}s are the molecular specific heats of these species. Values of C_{pi} for various species are listed in table 4.1.

Limits on the diffusion length: At the instances of maximum and minimum radius, the bubble wall velocity is zero, and thus, an alternate expression is needed for diffusion length. We set this limit as R/π after identifying that vapor transport is governed by pure diffusion equation for condition $dR/dt = 0$. The limit R/π is set on the basis of solution of the diffusion equation in spherical geometry. For greater details on this, we refer the reader to our earlier papers (Krishnan *et al.*, 2006; Kumar and Moholkar, 2007). Thus, the expressions for the mass and thermal diffusion length are given as:

$$l_{diff} = \min\left(\sqrt{\frac{RD}{|dR/dt|}}, \frac{R}{\pi}\right) \tag{4.7}$$

$$l_{th} = \min\left(\sqrt{\frac{R\kappa}{|dR/dt|}}, \frac{R}{\pi}\right) \tag{4.8}$$

We would like to mention that the bubble dynamics model of Yasui (1997) relaxes the assumption of cold boundary layer. The temperature of the bubble-bulk interface calculated with this approach exceeds 10000 K. This temperature is sufficient to cause pyrolytic degradation of phenol present in the interfacial region. However, this extreme condition lasts for very short time duration, typically 10 nanoseconds or so, at the instance of maximum compression in radial bubble motion. The kinetics of phenol pyrolysis is expected to be much slower, typically in the range of milliseconds. As a result, practically no degradation of phenol occurs through the route of pyrolysis in bubble-bulk interfacial region.

4.4.3 Overall energy balance

During radial motion, both heat and mass transfer occurs across the bubble wall, and thus the overall energy balance for the bubble contents is written as:

$$\frac{dE}{dt} = \frac{dQ}{dt} - \frac{dW}{dt} + h_w \frac{dN_w}{dt} \tag{4.9}$$

The total energy E of the bubble is a function of temperature and volume of the bubble and the number of molecules of various gas and vapor species in it. In the present study we use four gases for bubbling the reaction mixture, viz. argon, nitrogen, oxygen and air. The first three gases are single component gases while air is a two-component (nitrogen and oxygen) gas. Therefore, the energy balance for the bubbles of single component gas and air needs to be written separately:

(1) Argon/Nitrogen/Oxygen bubble:

$$\frac{dE}{dt} = \left(\frac{\partial E}{\partial N_G}\right)_{Nw,V,T} \frac{dN_G}{dt} + \left(\frac{\partial E}{\partial N_w}\right)_{N_G,V,T} \frac{dN_w}{dt} + \left(\frac{\partial E}{\partial T}\right)_{Nw,N_G,V} \frac{dT}{dt} + \left(\frac{\partial E}{\partial V}\right)_{Nw,N_G,T} \frac{dV}{dt} \tag{4.10}$$

where N_G denotes molecules of the gas (G = N_2, O_2 or Ar).

(2) Air bubble:

$$\frac{dE}{dt} = \left(\frac{\partial E}{\partial N_{N2}}\right)_{Nw,N_{O2},V,T} \frac{dN_{N2}}{dt} + \left(\frac{\partial E}{\partial N_{O2}}\right)_{N_{N2},Nw,V,T} \frac{dN_{O2}}{dt} + \left(\frac{\partial E}{\partial N_w}\right)_{N_{N2},N_{O2},V,T} \frac{dN_w}{dt} + \left(\frac{\partial E}{\partial T}\right)_{Nw,N_{N2},N_{O2},V} \frac{dT}{dt} + \left(\frac{\partial E}{\partial V}\right)_{Nw,N_{N2},N_{O2},T} \frac{dV}{dt} \tag{4.10a}$$

where N_{N2} and N_{O2} are the number of molecules of nitrogen and oxygen respectively in the bubble. As we neglect the change in the gas content of the bubble for the reasons stated earlier, $dN_G/dt = 0$ for single component gas and $dN_{N2}/dt = dN_{O2}/dt = 0$ for air. The term dN_w/dt is the rate of change of water vapor content of the bubble and is evaluated according to equation 4.5. The specific enthalpy of the water molecules entering the bubble from cold bubble interface is: $h_w = 4kT_o$. The specific energy of the water molecules in the bubble is the thermal energy, and is written in terms of vibrational temperatures as:

$$\left(\frac{\partial E}{\partial N_w}\right) = U_w = N_w kT\left(3 + \sum \frac{\theta_i / T}{\exp(\theta_i / T) - 1}\right) \tag{4.11}$$

The work done by the bubble is the expansion work: $P_i\, dV$. Moreover, $(\partial E/\partial T) = C_V$ and $(\partial E/\partial V) = 0$, as the internal energy of an ideal gas mixture is a function of its temperature and composition. With inclusion of various terms above in the overall energy balance, we obtain an equation for the change in the temperature of the bubble as:

$$C_{V,mix} \frac{dT}{dt} = \frac{dQ}{dt} - P_i dV + (h_w - U_w) \frac{dN_w}{dt} \tag{4.12}$$

The specific heat of the gas-vapor mixture ($C_{V,mix}$) present in the bubble is written as:

$$C_{V,mix} = \sum_i C_{V,i} N_i \qquad \text{where } i = N_2/O_2/\text{Ar/Air and } H_2O \tag{4.13}$$

where $C_{V,i}$ is the molecular specific heat of species i, and N_i is the number of molecules of that species present in the bubble. The C_V values for the various species considered in this work are listed in table 4.1.

Table 4.1. Thermodynamic properties of various species

Species	Degree of freedom (f)	Molecular specific heat (C_P)	Molecular specific heat (C_V)
N_2	5	$\frac{7}{2}k$	$k\left(\frac{5}{2}+\frac{\left(\theta_{N_2}/T\right)^2\exp\left(\theta_{N_2}/T\right)}{\left(\exp\left(\theta_{N_2}/T\right)-1\right)^2}\right)$
O_2	5	$\frac{7}{2}k$	$k\left(\frac{5}{2}+\frac{\left(\theta_{O_2}/T\right)^2\exp\left(\theta_{O_2}/T\right)}{\left(\exp\left(\theta_{O_2}/T\right)-1\right)^2}\right)$
H_2O	6	$4k$	$k\left(3+\sum_i^3\frac{\left(\theta_{i,H_2O}/T\right)^2\exp\left(\theta_{i,H_2O}/T\right)}{\left(\exp\left(\theta_{i,H_2O}/T\right)-1\right)^2}\right)$
Ar	3	$\frac{5}{2}k$	$\frac{3}{2}k$

Note: θ_i s are the vibrational temperatures of various species: θ_{N_2} = 3350 K, θ_{O_2} = 2273 K, θ_{1,H_2O} = 2295 K, θ_{2,H_2O} = 5255 K, θ_{3,H_2O} = 5400 K.

4.4.4 Transport parameters for the bubble of single component gas

For the bubble of single component gas (argon, nitrogen, oxygen), we encounter a binary system, viz. water vapor and the gas. For such a system, the Chapman-Enskog theory using Lennard-Jones 12-6 potential (Hirschfelder *et al.*, 1954; Reid *et al.*, 1987) can be used for the determination of diffusion coefficient (D) and the thermal conductivity (λ). Since we assume a cold boundary layer in which the effective heat and mass transport occurs, both D and λ are evaluated at the bulk liquid temperature, $T = T_o$.

Diffusion Coefficient: Diffusion coefficient of species 1 (water vapor) in the mixture of two species, viz. water vapor and the gas (species 2), to a first approximation is written as:

$$D = \frac{3}{8} \frac{\sqrt{\pi kT/\mu_{12}}}{n_{12}\pi\sigma_{12}^2\Omega_{12}^{(1,1)*}} \tag{4.14}$$

m_1 and m_2 are the molecular masses of water and gas respectively and $\mu_{12} = \frac{2m_1m_2}{m_1 + m_2}$ is the reduced molecular mass of the two species. $n_{12} = n_1 + n_2$ is the total concentration of two species at the bubble wall. $\sigma_{12} = (\sigma_1 + \sigma_2)/2$ is a parameter in the potential function characteristic of 1-2 interaction, where σ_1 and σ_2 are the molecular diameters of water and the gas, respectively. $\Omega_{12}^{(1,1)*}$ is a dimensionless correction of first order that enumerates deviation of the collisional cross-section from hard sphere cross-section. Values of this parameter are given by Hirschfelder *et al*. (1954) as a function of reduced temperature of the two species:

$$T_{12}^* = \sqrt{\left(\frac{T}{\varepsilon/k}\right)_1 \left(\frac{T}{\varepsilon/k}\right)_2} \tag{4.15}$$

Values of the potential parameter (ε/k) in K are obtained from various texts (Hirschfelder *et al*., 1954; Reid *et al*., 1987).

Thermal Conductivity: The estimation of thermal conductivity for the single component gas – water vapor mixture is rather complicated due to the fact that it is a mixture of a monatomic (argon) or diatomic (nitrogen and oxygen) and polyatomic (water) species. The coefficient of thermal conductivity for a pure monatomic gas can be obtained from rigorous kinetic theory. However, these formulae cannot be used for the polyatomic gases, as the effect of the internal degrees of freedom on the thermal conductivity is considerable. However, with Eucken correction one can apply the formulae for monatomic gases to the polyatomic gases. The coefficient of thermal conductivity for a monatomic gas is given as:

$$\lambda = \frac{15}{4} \frac{k}{m} \eta \tag{4.16}$$

where m is the molecular mass and η is the coefficient of viscosity, written as:

$$\eta = \frac{5}{16}\frac{\sqrt{\pi mkT}}{\pi\sigma^2\Omega^{(2,2)*}} \tag{4.17}$$

For a diatomic or polyatomic molecule, the corrected thermal conductivity as:

$$\lambda_{Eucken} = \frac{15}{4}\frac{k}{m}\eta\left(\frac{4}{15}\frac{C_v}{R}+\frac{3}{5}\right) \tag{4.18}$$

Using above formulae, the thermal conductivity for the mixture of single component gas (subscript 2) and water vapor (subscript 1) is calculated using a semi-empirical method (Hirschfelder *et al*., 1954). We first define a quantity λ_{12}:

$$\lambda_{12} = \frac{25}{32}\left(\frac{\sqrt{\pi kT/\mu_{12}}}{\pi\sigma_{12}^2\Omega_{12}^{(2,2)*}\ T_{12}^*}\right)\times\frac{3}{2}k \tag{4.19}$$

$\Omega_{12}^{(2,2)*}$ is again a dimensionless correction for first order, similar to quantity $\Omega_{12}^{(1,1)*}$ defined earlier. In terms of this quantity, and the thermal conductivities of pure components, viz. water (λ_1) and gas (λ_2); both being calculated using the formula for the monatomic gas stated above, a new quantity λ_{mon} is calculated as:

$$\lambda_{mon} = \frac{1 + Z}{X + Y} \tag{4.20}$$

X, Y and *Z* are defined in terms of the mole fractions of two components, x_1 and x_2 as:

$$X = \frac{x_1^2}{\lambda_1}+\frac{2\,x_1x_2}{\lambda_{12}}+\frac{x_2^2}{\lambda_2} \tag{4.21a}$$

$$Y = \frac{x_1^2}{\lambda_1}U_1+\frac{2\,x_1x_2}{\lambda_{12}}U_Y+\frac{x_2^2}{\lambda_2}U_2 \tag{4.21b}$$

$$Z = x_1^2U_1 + 2\,x_1x_2U_Z + x_2^2U_2 \tag{4.21c}$$

The quantities U_1, U_2, U_Y and U_Z are given as:

$$U_1 = \frac{4}{15}A_{12}^* - \frac{1}{12}\left(\frac{12}{5}B_{12}^*+1\right)\frac{m_1}{m_2}+\frac{1}{2}\frac{(m_1-m_2)^2}{m_1m_2} \tag{4.22a}$$

$$U_2 = \frac{4}{15}A_{12}^* - \frac{1}{12}\left(\frac{12}{5}B_{12}^* + 1\right)\frac{m_2}{m_1} + \frac{1}{2}\frac{\left(m_2 - m_1\right)^2}{m_1 m_2} \qquad (4.22b)$$

$$U_Y = \frac{4}{15}A_{12}^*\left[\frac{\left(m_1 + m_2\right)^2}{4m_1 m_2}\right]\frac{\lambda_{12}^2}{\lambda_1\lambda_2} - \frac{1}{12}\left(\frac{12}{5}B_{12}^* + 1\right) - \frac{5}{32A_{12}^*}\left(\frac{12}{5}B_{12}^* - 5\right)\frac{\left(m_1 - m_2\right)^2}{m_1 m_2} \qquad (4.22c)$$

$$U_Z = \frac{4}{15}A_{12}^*\left\{\left[\frac{\left(m_1 + m_2\right)^2}{4m_1 m_2}\right]\left(\frac{\lambda_{12}}{\lambda_1} + \frac{\lambda_{12}}{\lambda_2}\right) - 1\right\} - \frac{1}{12}\left(\frac{12}{5}B_{12}^* + 1\right) \qquad (4.22d)$$

The quantities A_{12}^* and B_{12}^* are functions of the quantities Ω defined earlier and are written as: $A_{12}^* = \frac{\Omega^{(2,2)*}}{\Omega^{(1,1)*}}$ and $B_{12}^* = \frac{5\,\Omega^{(1,2)*} - 4\Omega^{(1,3)*}}{\Omega^{(1,1)*}}$. Values of A_{12}^* and B_{12}^* are tabulated in Hirschfelder *et al*. (1954) as a function of the reduced temperature $T^* = T/(\varepsilon/k)$. After determining λ_{mon}, the coefficient of the thermal conductivity for the mixture is determined using the correlation:

$$\lambda = \lambda_{mon}\left(x_1 E_1 + x_2 E_2\right) \qquad (4.23)$$

where E_1 and E_2 are the ratios of the experimental value and the theoretical value of thermal conductivity, determined by the formula for monatomic gas. For argon, E_2 ~ 1, as it is a monatomic gas and the experimental value of its thermal conductivity is almost equal to the value determined with the formula. For nitrogen and oxygen, E_2 is calculated as $\frac{\lambda_{exptl}}{\lambda_2}$. For the experimental value of thermal conductivity of nitrogen and oxygen, we use the following correlation given by Reid *et al*. (1987):

Nitrogen: $\lambda_{exptl} = 3.919\times10^{-4} + 9.816\times10^{-5}T - 5.067\times10^{-8}T^2 + 1.504\times10^{-11}T^3$

Oxygen: $\lambda_{exptl} = -3.273\times10^{-4} + 9.966\times10^{-5}T - 3.743\times10^{-8}T^2 + 0.9732\times10^{-11}T^3$

For water vapor, E_1 is calculated as $\frac{\lambda_{exptl}}{\lambda_1}$. For the experimental value of thermal conductivity of water, we use the following correlation given by Reid *et al.* (1987):

Water vapor: $\lambda_{\exp tl} = 7.341\times10^{-3} - 1.013\times10^{-5}T + 1.801\times10^{-7}T^2 - 9.1\times10^{-11}T^3$

where T is in K and λ in W/m K.

4.4.5 Transport parameters for the air bubble

In case of air bubble we encounter a ternary system: N_2–O_2–H_2O. Again, we use the Chapman-Enskog theory for the estimation of transport parameters, however, with a slightly different approach. After determination of binary diffusion coefficient for N_2–H_2O and O_2–H_2O binary mixtures using equation 4.14, the overall diffusion coefficient is determined as (Hirschfelder *et al*., 1954):

$$\frac{1}{D} = \frac{\varepsilon_{N2}}{(1-\varepsilon_{H2O})D_{N2-H2O}} + \frac{\varepsilon_{O2}}{(1-\varepsilon_{H2O})D_{O2-H2O}} \tag{4.24}$$

where ε is the mole fraction of the respective species at the bubble wall.

For the determination of conductivity of the ternary mixture, the viscosity of individual species is evaluated first using equation 4.17. Thereafter, the conductivity of species is related to its viscosity using the following formula that accounts for contribution of internal degree of freedom to the heat conduction:

$$\lambda = \frac{15k}{m}\eta\left(\frac{4f}{30} + \frac{3}{5}\right) \tag{4.25}$$

where f is the number of degree of freedom of the species at bubble wall. Values of f for various species are listed in table 4.1. The effective heat conduction is now written using the following formula (Wilke, 1950; Condon and Odishaw, 1958):

$$\lambda_{mix} = \sum_i \frac{\varepsilon_i \lambda_i}{\sum_j \varepsilon_i \phi_{i,j}} \tag{4.26}$$

The parameter ϕ is given as:

$$\phi_{i,j} = \frac{1}{\sqrt{8}}\left(1+\frac{m_i}{m_j}\right)^{-1/2}\left[1+\left(\frac{n_i}{n_j}\right)^{-1/2}\left(\frac{m_i}{m_j}\right)^{1/4}\right]^2 \tag{4.27}$$

where *i, j* = N_2, O_2 *and* H_2O.

4.4.6 Numerical solution

The equations 4.1, 4.5, 4.6 and 4.12 constitute complete formulation for the radial motion of cavitation bubble with associated heat and mass transfer effects. This set of simultaneous ODEs can be solved using Runge-Kutta 4^{th} order – 5^{th} order adaptive step size method (Press *et al.*, 1992). The cavitation bubble may collapse at the instance of maximum compression during radial motion. The word "collapse" essentially means fragmentation of the cavitation bubble. This factor depends on many factors such as shape (or surface) instability of bubbles, the local flow conditions and the bubble population density in the vicinity of the bubble. For conditions of maximum shape and flow instability, the cavitation bubble fragmentation can occur at the first compression after an initial expansion. In view of this, the condition for the bubble collapse is taken to be first compression during radial motion. Four important parameters required for the simulation of the radial motion of the cavitation bubble are: (1) frequency and (2) pressure amplitude of ultrasound, (3) vapor pressure of water and (4) initial (or equilibrium) bubble radius. Numerical values for these parameters have been determined as follows:

(1) *Frequency*: The frequency of the ultrasound wave was taken as 20 kHz, which is the frequency of the sonicator used in the experiments.

(2) *Pressure amplitude*: A calorimetric method was used to determine the amplitude of the ultrasound wave emitted by the sonicator probe (Sivasankar *et al.*, 2007). The amplitude of the ultrasound wave generated by the sonicator probe was 1.5 bar. However, the actual pressure amplitude sensed by the cavitation bubble located away from the probe tip is lesser than 1.5 bar, as the ultrasound wave attenuates during propagation through the medium. This attenuation varies directly with the viscosity of the medium and the size and population density of bubbles in the medium (Mason and Lorimer, 1989; Prosperetti and Commander,

1989). A direct measurement of the local pressure amplitude in the vicinity of the cavitation bubble is beyond the capabilities of the instrumentation used in the present study. Therefore, we assume about 15% attenuation and use a value of 1.3 bar for acoustic pressure amplitude in the numerical simulations.

(3) *Vapor pressure of water*: The vapor pressure of the bulk medium (i.e. water) was calculated with Antoine's equation using initial temperature of the solution (25 ^{o}C). The temperature rise during sonication was ~ 2 ^{o}C, as noted earlier. The difference between vapor pressure of water at 25 ^{o}C and 27 ^{o}C is quite small (< 10%). Therefore, we have ignored the temperature rise during simulations, assuming the liquid medium at constant temperature. An alternate approach would be to calculate the vapor pressure of water using average of initial and final temperatures. However, this would make trivial quantitative changes to the simulation results; and the trends in the simulation results remain essentially unchanged.

(4) *Initial (or equilibrium) bubble radius*: This parameter is difficult to estimate. Moreover, the equilibrium size of the bubble keeps on changing due to phenomena such as rectified diffusion, fragmentation of the bubble etc. The minimum radius of the cavitation nuclei which would grow into a bubble for particular amplitude of acoustic wave can be determined by the analysis given by Young (1989). For the acoustic pressure amplitude in the present experiments, this value is ~ 2 μm. As mentioned earlier, a gas sparger distributing the desired gas through a glass frit with pore size of ~ 40 μm was used to provide cavitation nuclei. The gas bubbles generated out of the glass frit would of size same as that of pore. However, these bubbles get shattered into multiple fragments with wide size distribution due to ultrasound. We have chosen a representative value of 10 μm for the initial or equilibrium bubble radius.

Moreover, the initial water vapor content of the bubble (of all four gases) is taken to be zero during simulations. In other words, initially (at t = 0) the cavitation bubble is assumed

to be comprised of gas alone. Thus, the cavitation bubbles of a single component gas, e.g. oxygen, nitrogen and argon, initially contain oxygen, nitrogen and argon respectively. The cavitation bubble of air, however, contains two components, viz. nitrogen and oxygen in proportion of 80%-20% by mole.

Equilibrium composition of the various species formed in the bubble with dissociation of entrapped water molecules (i.e. H_2O, H_2, O_2, $H^{\bullet}$, $OH^{\bullet}$, $O^{\bullet}$, H_2O_2, $HO_2^{\bullet}$, O_3) at the conditions of temperature and pressure at first the compression was calculated using software FACTSAGE, which uses the free-energy minimization algorithm proposed by Eriksson (1975). This software has an in-built database of C_p vs. temperature relationship, entropy and heat of formation of all the above species. A more rigorous approach in this regard would be to include various radical reactions in the mass balance equations along with heats of these reactions included in the energy balance (Toegel, 2002; Toegel and Lohse, 2003; Storey and Szeri, 2000). Endothermicity of some of the radical reactions (for example $H_2O \rightleftharpoons H^{\bullet} + OH^{\bullet}$) works towards lowering of the peak temperature reached during transient bubble collapse. However, addition of this feature in the present model would change only the final quantitative answers, with trends remaining essentially unaltered.

4.5 RESULTS AND DISCUSSION

The concentration of phenol in the aqueous solutions used in the present study is 100 ppm, which is rather dilute. Therefore, the probability of interaction between phenol molecules and radicals becomes a crucial parameter influencing the kinetics of degradation. For such a situation, significant fraction of the radicals generated out of cavitation bubbles may undergo recombination without reacting with the phenol molecules. Therefore, merely increasing the rate of production of radicals may not give required enhancement in degradation rates. The radicals generated out of cavitation bubbles need to be scavenged in

order to raise the probability of their interaction with phenol molecules. As noted previously, the word "***scavenging***" in the present context means "***conservation***", i.e. reacting the radicals with other species (such as dissolved oxygen in the medium) to generate new radical species. The extent of radical scavenging in the medium depends on the concentration of the scavenging species in the bulk liquid medium. This concentration needs to be maintained uniform throughout the sonication period (nearly to the saturation level) in order to achieve effective scavenging leading to faster degradation kinetics. With this preface, we present the results of the experiments and simulation of radial bubble motion.

Trends in degradation of phenol obtained in three categories of experiments are shown in figure 4.2. The variation in the dissolved oxygen content of Millipore water with bubbling of nitrogen and argon is shown in figure 4.3. Simultaneous irradiation of ultrasound, in addition to bubbling of nitrogen and argon, did not make any noticeable change to the rate of reduction in the dissolved oxygen in the solution. An explanation for this result can be given in terms of difference in the time scale of bubbling of gases and the time scale of ultrasound irradiation. The time scale of sparging of the gas (nitrogen and argon) is in seconds, while the time scale of ultrasound in microseconds, which 6 orders of magnitude smaller. Due to such large difference in the time scale of two processes, the removal of dissolved oxygen in the medium is principally influenced by the sparging of gas. The highest degradation of phenol is obtained with bubbling of oxygen through reaction mixture as well as 0.5 mM $FeSO_4 \cdot 7H_2O$ added to the solution; while the lowest degradation is seen for nitrogen as the bubbling gas. Some other salient features of the experimental results are as follows:

(1) The degradation obtained with bubbling of air and argon through reaction mixture is almost similar.

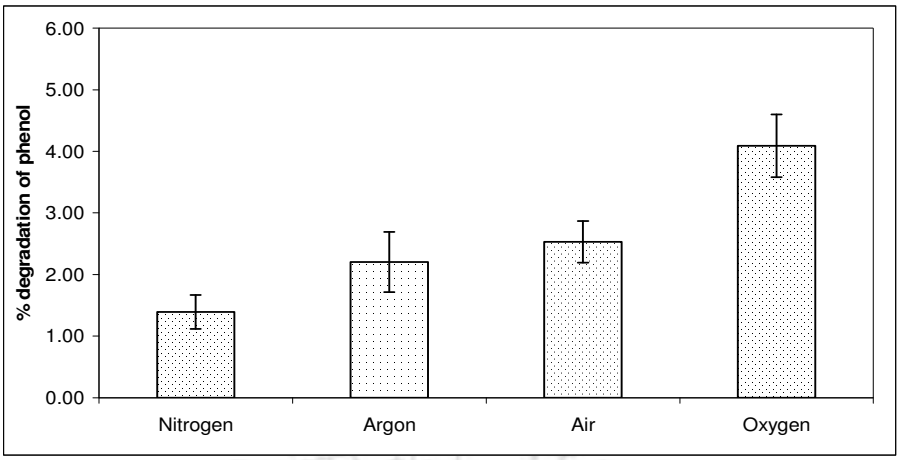

(A)

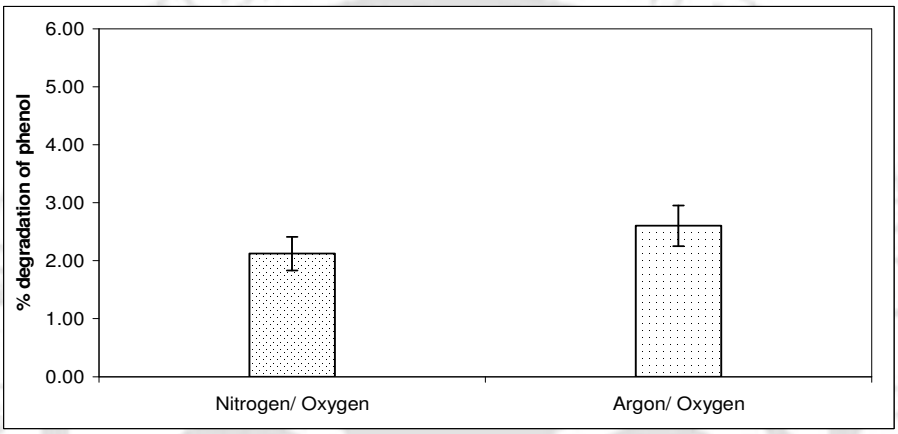

(B)

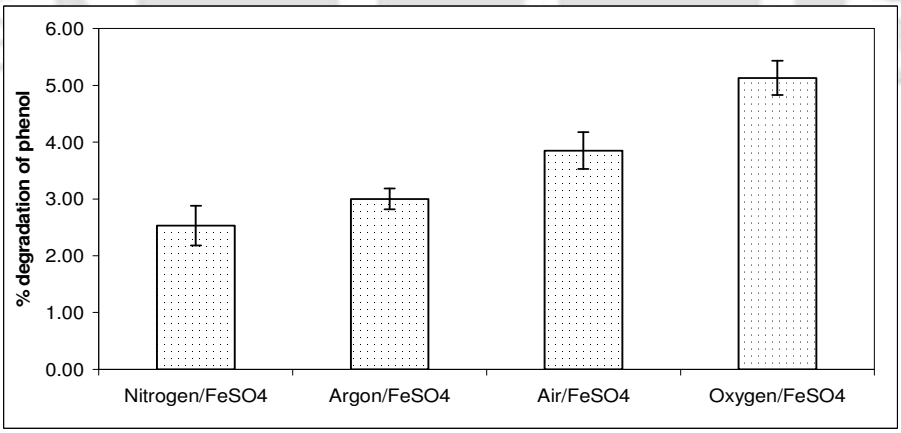

(C)

Figure 4.2. Experimental results on degradation of phenol in various categories of experiments. (A) Sonication of phenol solution with continuous bubbling of either of the four gases (viz. nitrogen, air, oxygen and argon). (B) Sonication of phenol solution with bubbling of either argon or nitrogen during sonication period and bubbling of oxygen during silent period. (C) Sonication of phenol solution with continuous bubbling of either of the four gases with $FeSO_4 \cdot 7H_2O$ added to the solution.

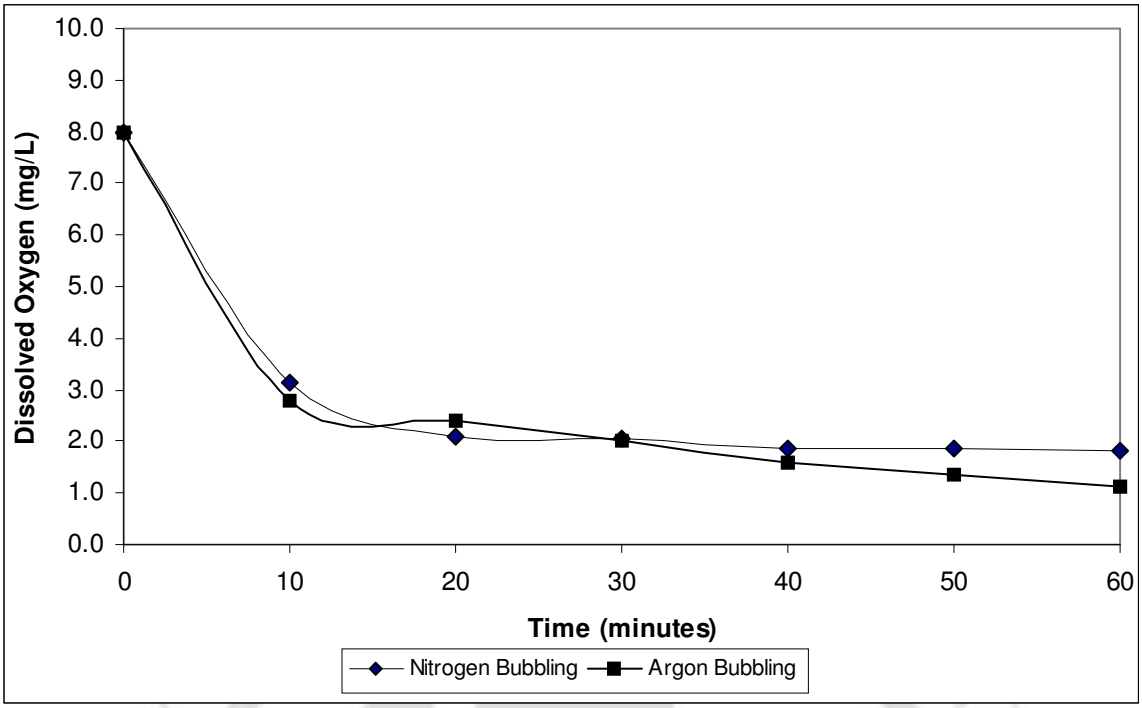

Figure 4.3. Reduction in the dissolved oxygen content of Millipore water with continuous bubbling of nitrogen and argon.

(2) With alternate bubbling of argon/nitrogen and oxygen, the degradation of phenol rises. However, the extent of this rise is different for argon and nitrogen. For nitrogen the rise is ~ 50% while for argon the rise is rather marginal ~ 25%.

(3) The degradation obtained for all four gases shows a marked rise (> 50% or so) with addition of $FeSO_4 \cdot 7H_2O$ to the medium.

Illustrative simulations of radial motion of argon and oxygen bubble are shown in figure 4.4 and 4.5 respectively. The summary of entire simulation results (viz. temperature and pressure peak attained during transient collapse and the number of water molecules entrapped in the bubble) is given in table 4.2A along with equilibrium compositions of various species generated out of dissociation of molecules present in the bubble. It can be seen that argon bubble gives much higher temperature peak during transient collapse than oxygen, nitrogen and air bubble. This is attributed to the nature of gas: argon being a monatomic gas has lower

heat capacity than the other gases, which are diatomic, due to which the bubble heats up to a greater extent, resulting in higher collapse temperature. On the other hand, the collapse temperatures of oxygen, nitrogen and air bubbles are almost similar (with a difference of ~ 5% or so). Conversely, the pressure peak reached at the collapse of argon bubble is lower than oxygen, nitrogen and air. It can be perceived, however, that the collapse conditions for cavitation bubbles of all four gases are beyond the critical temperature and pressure of water (647.096 K and 217.7 bar respectively). Therefore, the equilibrium distribution of the chemical species in the bubble is predominantly a function of temperature inside the bubble and the pressure inside the bubble has practically no influence on this distribution. The net production of four major radicals, viz. $H^{\bullet}$, $OH^{\bullet}$, $O^{\bullet}$ and $HO_2^{\bullet}$, per bubble is given in table 4.2B. The trends in the yield of these radicals are as follows:

$OH^{\bullet}$: Ar > Air > O_2 > N_2

$H^{\bullet}$: Ar > Air > O_2 > N_2

$O^{\bullet}$: Ar > Air > O_2 > N_2

$HO_2^{\bullet}$: Ar > O_2 > Air > N_2

An explanation to the above trends can be given as follows:

Argon bubble: Due to highest temperature peak attained during transient collapse, the extent of production of all four radicals is highest for argon bubble. For $H^{\bullet}$, $O^{\bullet}$ and $OH^{\bullet}$ radicals, the production rate is 2 – 4 orders of magnitude higher than other gases, while for $HO_2^{\bullet}$ radical the yield is ~ 2 times that of oxygen bubble, which has second highest production of these radicals among all gases used. Due to absence of any scavenging species in argon bubble (such as oxygen and nitrogen), the population of $H^{\bullet}$ and $O^{\bullet}$ radicals is also quite high.

Air bubble: The extent of production of all four radicals from air bubble is rather moderate. Presence of two radical scavenging species, viz. nitrogen and oxygen, in the bubble affects

the distribution of radical species. The scavenging action of oxygen through reactions R.4.1 to R.4.7 has been explained earlier. The predominant nitrogen species produced is NO followed N_2O, NO_2, HNO and HNO_2. Nitrogen present in the air bubble scavenges $H^{\bullet}$, $OH^{\bullet}$ and $O^{\bullet}$ radicals produced by dissociation of entrapped water vapor through various reactions. A few representative reactions are (Toegel, 2002):

$$N_2 + O^{\bullet} \rightleftharpoons N^{\bullet} + NO \quad \text{(R.4.12)}$$

$$N_2 + OH^{\bullet} \rightleftharpoons N_2H + O^{\bullet} \quad \text{(R.4.13)}$$

$$N_2 + OH^{\bullet} \rightleftharpoons N_2O + H^{\bullet} \quad \text{(R.4.14)}$$

$$N_2 + OH^{\bullet} \rightleftharpoons NH + NO \quad \text{(R.4.15)}$$

$$N_2 + H^{\bullet} \rightleftharpoons N_2H \quad \text{(R.4.16)}$$

$$N_2 + H^{\bullet} \rightleftharpoons NH + N^{\bullet} \quad \text{(R.4.17)}$$

The nitrogen species produced in the above reactions also scavenge the radicals through various reactions. Some representative reactions are (Toegel, 2002):

$$N + OH^{\bullet} \rightleftharpoons NO + H^{\bullet} \quad \text{(R.4.18)}$$

$$N_2O + O^{\bullet} \rightleftharpoons 2NO \quad \text{(R.4.19)}$$

$$NO + O^{\bullet} \rightleftharpoons NO_2 \quad \text{(R.4.20)}$$

$$NH + OH^{\bullet} \rightleftharpoons NH_2 + O^{\bullet} \quad \text{(R.4.21)}$$

$$NH_2 + O^{\bullet} \rightleftharpoons H^{\bullet} + HNO \quad \text{(R.4.22)}$$

$$HNO + O^{\bullet} \rightleftharpoons NH + O_2 \quad \text{(R.4.23)}$$

$$HNO + O^{\bullet} \rightleftharpoons NO + OH^{\bullet} \quad \text{(R.4.24)}$$

$$HNO + OH^{\bullet} \rightleftharpoons NO + H_2O \quad \text{(R.4.25)}$$

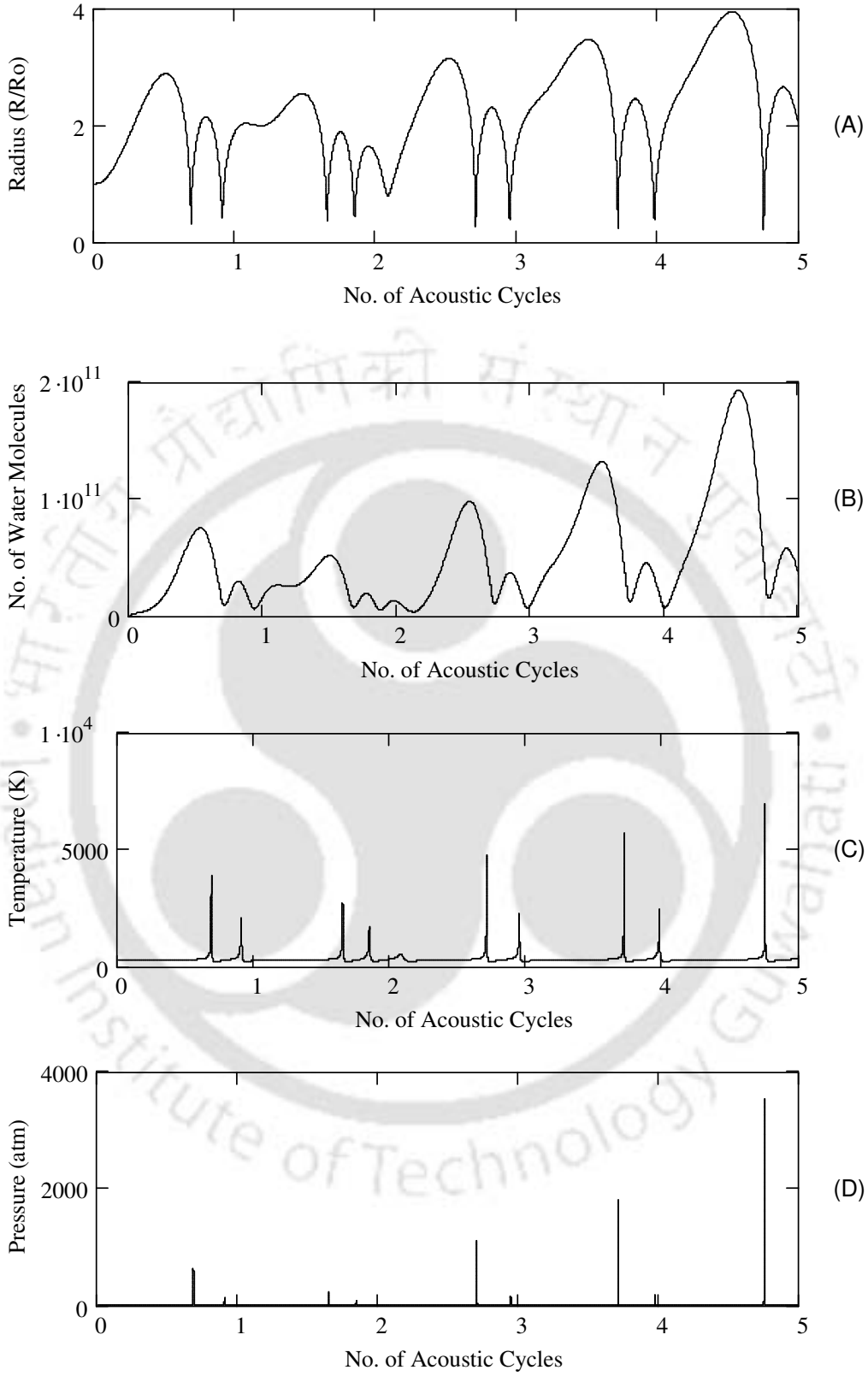

Figure 4.4. Simulation of the radial motion of 10 μm argon bubble in the 100-ppm aqueous solution of phenol. Time variation of (A) normalized bubble radius (R/R_o); (B) number of water molecules in the bubble; (C) temperature in the bubble; (D) pressure inside the bubble.

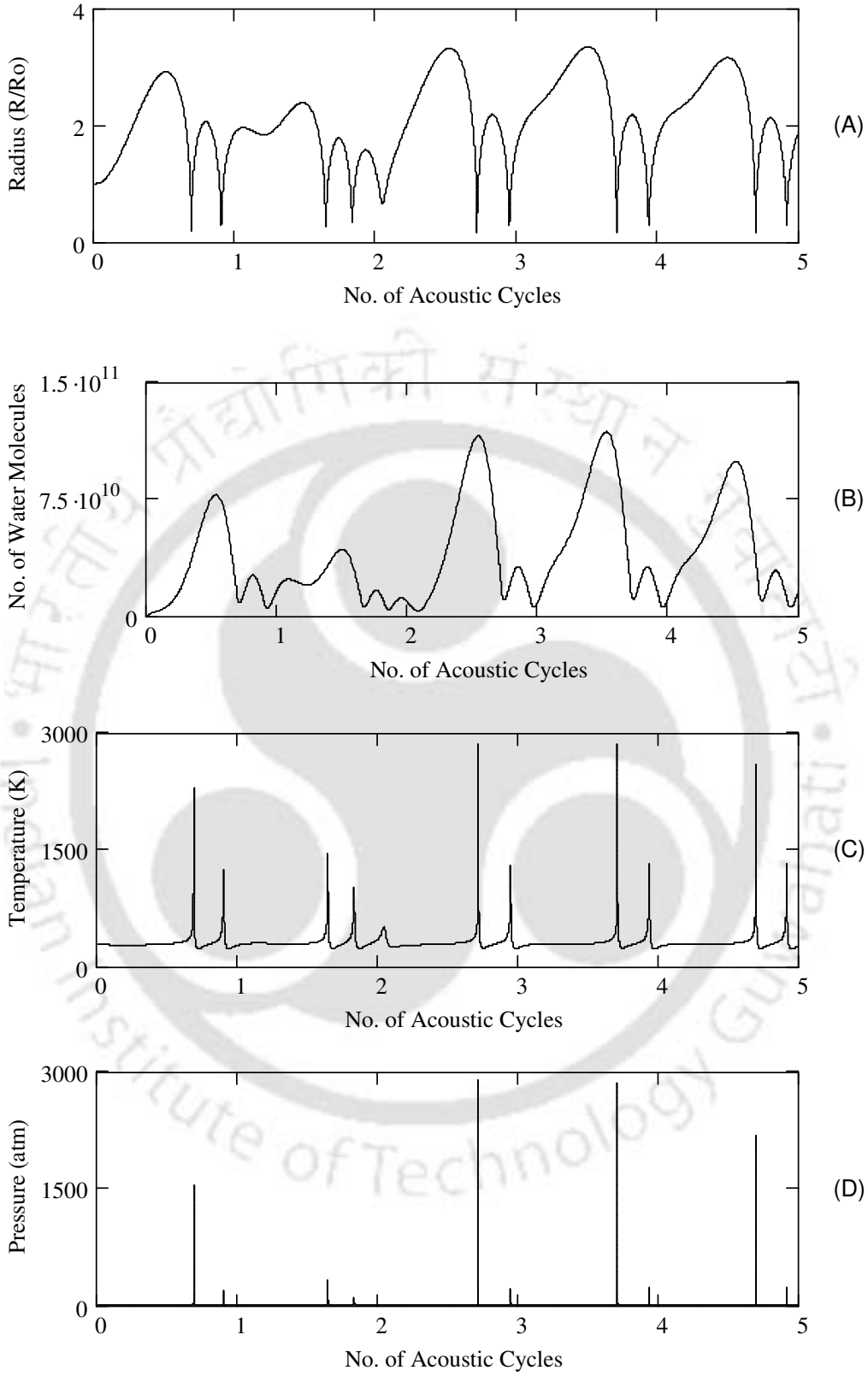

Figure 4.5. Simulation of the radial motion of 10 μm oxygen bubble in the 100-ppm aqueous solution of phenol. Time variation of (A) normalized bubble radius (R/R_o); (B) number of water molecules in the bubble; (C) temperature in the bubble; (D) pressure inside the bubble.

Table 4.2 (A) Summary of the simulation results

Species	Parameters for simulation			
	Argon Bubble	**Air Bubble**	**Oxygen Bubble**	**Nitrogen Bubble**
	Conditions at the first compression of the bubble			
	T_{max} = 3937 K	T_{max} = 2478 K	T_{max} = 2303 K	T_{max} = 2397 K
	P_{max} = 628.6 bar	P_{max} = 1044 bar	P_{max} = 1539 bar	P_{max} = 1407 bar
	N_{Ar} = 1.1789E+011 N_{WT} = 1.51E+010	N_{N2} = 9.3053E+010 N_{O2} = 2.4736E+010 N_{WT} = 1.09E+010	N_{O2} = 1.1789E+011 N_{WT} = 1.4768E+10	N_{N2} = 1.1789E+011 N_{WT} = 1.4895E+010
Equilibrium composition of various species in the bubble at collapse (mole fraction)				
H_2O	6.5869E-01	8.3792E-02	1.0988E-01	1.1087E-01
H_2	1.3142E-01	3.2542E-05	6.2505E-06	9.2108E-04
$OH^{\bullet}$	1.1454E-01	2.1262E-03	1.8089E-03	2.8384E-04
O_2	3.6855E-02	1.8047E-01	8.8788E-01	1.2790E-04
$H^{\bullet}$	3.8884E-02	4.0055E-06	6.2320E-07	1.2623E-05
$O^{\bullet}$	1.8991E-02	1.6967E-04	1.2059E-04	2.5566E-06
$HOO^{\bullet}$	5.4629E-04	1.0538E-04	2.7775E-04	4.6263E-07
H_2O_2	7.1496E-05	7.6294E-06	1.8075E-05	2.6132E-07
O_3	3.6545E-07	6.9832E-07	5.3947E-06	1.2032E-11
N_2	--	7.1224E-01	--	8.8726E-01
NO	--	2.0465E-02	--	5.2435E-04
N_2O	--	3.1507E-05	--	1.0453E-06
NH_3	--	1.8232E-09	--	4.5055E-07
NO_2	--	5.0932E-04	--	4.4288E-07
HNO	--	1.6511E-06	--	2.5843E-07
HNO_2	--	4.6585E-05	--	2.9780E-07
HNO_3	--	1.7913E-07	--	3.8363E-11
N	--	6.1669E-09	--	2.6931E-09
NH	--	6.1642E-10	--	1.9732E-09
NH_2	--	7.3593E-10	--	1.9954E-08
NO_3	--	3.9991E-08	--	9.8969E-13
N_3	--	4.5001E-11	--	3.6032E-11
N_2H_2	--	8.6303E-13	--	2.8980E-11
N_2O_3	--	6.3221E-09	--	1.9798E-13
N_2O_4	--	1.6757E-11	--	--
N_2H_4	--	--	--	1.8212E-14
N_2O_5	--	3.4491E-13	--	--

Note: *The number format is as follows: 6.5869E-01 should be read as* 6.5869×10^{-1}. *Various notations used are as follows:* T_{max} *– temperature peak reached in the bubble at the time of first collapse;* P_{max} *– pressure peak reached in the bubble at the time of first collapse;* N_{WT} *– number of water molecules trapped in the bubble at the instance of first collapse;* N_{O2} *– number of oxygen molecules in the bubble (for air and oxygen bubbles).*

Table 4.2(B) Net production of various radicals per bubble

Parameter	Argon bubble	Air bubble	Oxygen bubble	Nitrogen bubble
N_T	1.3299E+011	1.2879E+011	1.3266E+011	1.3279E+011
N_{OH}	1.5233E+09	2.7383E+08	2.3997E+08	3.7683E+07
N_H	5.1711E+09	5.1587E+05	8.2672E+04	1.6761E+06
N_O	2.5256E+09	2.1852E+07	1.5997E+07	3.3948E+05
N_{HO2}	7.2651E+09	1.3572E+07	3.6846E+07	6.1430E+04

Nomenclature: N_T – total number of molecules present in the bubble at transient collapse; N_{OH} – number of OH radicals present in the bubble at transient collapse; N_H – number of H radicals present in the bubble at transient collapse; N_O – number of O radicals present in the bubble at transient collapse; N_{HO2} – number of HO_2 radicals present in the bubble at transient collapse.

It needs to be specifically mentioned that reactions R.4.12 to R.4.25 also occur in the bulk liquid medium due to reaction of dissolved nitrogen with various radicals released into the bulk medium with collapse of cavitation bubble.

However, the oxygen present in the bubble reacts concurrently with nitrogen species to regenerate $O^{\bullet}$ and $OH^{\bullet}$ radicals through following reactions:

$$N + O_2 \rightleftharpoons NO + O^{\bullet} \quad \text{(R.4.26)}$$

$$NO + O_2 \rightleftharpoons NO_2 + O^{\bullet} \quad \text{(R.4.27)}$$

$$NH + O_2 \rightleftharpoons HNO + O^{\bullet} \quad \text{(R.4.28)}$$

$$NH + O_2 \rightleftharpoons NO + OH^{\bullet} \quad \text{(R.4.29)}$$

$$N_2 + O_2 \rightleftharpoons N_2O + O^{\bullet} \quad \text{(R.4.30)}$$

Reactions R.4.26 to R.4.30 are also possible in the bulk liquid medium due to dissolved oxygen.

In addition, oxygen also reacts with the $H^{\bullet}$ and $OH^{\bullet}$ radicals to yield $HO_2^{\bullet}$ radicals through following reactions:

$$H^{\bullet} + O_2 \rightleftharpoons HO_2^{\bullet} \qquad \text{(R.4.5)}$$

$$OH^{\bullet} + O_2 \rightleftharpoons HO_2^{\bullet} + O^{\bullet} \qquad \text{(R.4.8)}$$

Reaction of $O^{\bullet}$ radicals with oxygen molecules, however, results in loss of oxidation potential due to formation of ozone:

$$O^{\bullet} + O_2 \longrightarrow O_3 \qquad \text{(R.4.31)}$$

As a result of all of above simultaneous reactions, the predominant radical species produced by air bubble is $OH^{\bullet}$ followed by $O^{\bullet}$, $HO_2^{\bullet}$ and $H^{\bullet}$ – in that order.

Oxygen bubble: Although the temperature peak reached during transient collapse of oxygen bubble is not much different than that for air bubble, large presence of oxygen in the bubble significantly alters the equilibrium distribution of various radical species. Scavenging of $H^{\bullet}$ radicals by oxygen molecules reduces the mole fraction of $H^{\bullet}$ significantly (reactions R.4.4 and R.4.5), with concurrent rise in quantity of $HO_2^{\bullet}$ radicals (reaction R.4.5). $O^{\bullet}$ radicals formed out of dissociation of oxygen molecules react with oxygen to form ozone (reaction R.4.31). Moreover, $HO_2^{\bullet}$ radicals can combine to form H_2O_2 through reaction:

$$2HO_2^{\bullet} \rightleftharpoons H_2O_2 + O_2 \qquad \text{(R.4.32)}$$

It can be seen from table 4.2A that the mole fraction of H_2O_2 and O_3 for oxygen bubble is one order of magnitude higher than air bubble. Both reactions R.4.31 and R.4.32 result in loss of oxidation potential. The overall result of all simultaneous reactions is production of $OH^{\bullet}$ and $HO_2^{\bullet}$ as the predominant radical species.

Nitrogen bubble: Although the temperature peak attained during collapse of nitrogen bubble is higher than the oxygen bubble, the radical production from it is significantly less. Except for $H^{\bullet}$ radical, the yield of other radicals (viz. $O^{\bullet}$, $OH^{\bullet}$ and $HO_2^{\bullet}$) is 1–3 order(s) of magnitude smaller. This effect is attributed to extensive scavenging of radicals by nitrogen

molecules (through reactions R.4.12 to R.4.25). The absence of oxygen in the bubble has two effects on the equilibrium composition: first, low yield of $HO_2^{\bullet}$ radicals which form out of scavenging of $H^{\bullet}$ radicals by oxygen (reaction R.4.4), and secondly, larger population of $H^{\bullet}$ radicals in the bubble during transient collapse as a consequence of first effect.

Simultaneous assessment of the simulation results and experimental results in different categories as stated earlier reveals some interesting mechanistic features of the sonochemical degradation of phenol, as described below:

Category I (Continuous bubbling of Ar / N_2 / O_2 / Air):

- The extent of degradation obtained for air and argon as bubbling gas is almost equal, although the extent of radical production differs by an order of magnitude. This effect is explained in terms of variation in the dissolved oxygen content, and hence, the extent of radical scavenging in the liquid medium with bubbling of the gas through reactions R.4.1 to R.4.8. In case of bubbling of air, the oxygen in air dissolves in the liquid medium, and thus, the concentration of the dissolved oxygen is maintained nearly to the saturation level that helps in effective scavenging of radicals. On the other hand, bubbling of argon strips out dissolved oxygen present in the medium (refer to figure 4.3), which annihilates the scavenging of radicals. Therefore, the radical recombination phenomenon dominates causing loss in oxidation potential, resulting in lower degradation in 90 min of sonication than expected.
- Least degradation with nitrogen as the bubbling gas is a combined result of lower rate of production of radicals coupled with the stripping away of dissolved oxygen in the medium due to which radical scavenging is hampered. The probability of phenol-radical interaction is, thus, very sparse and most of the radicals undergo recombination.
- Although the net production of radicals per cavitation bubble for air and oxygen does not differ much, the degradation with oxygen is much higher than air. Higher degradation for

oxygen as bubbling gas is a result of effective scavenging of radicals outside the bubble by oxygen molecules dissolved in the medium, as well as tiny bubbles of oxygen that remain suspended in the medium during bubbling of oxygen through reactions R.1 to R.8 discussed earlier. Moreover, the dissolved oxygen content of the bulk medium stays at saturation level all along sonication, which gives maximum scavenging effect resulting in highest degradation in 90 min of sonication.

Category II (Alternate bubbling of Ar / N_2 and oxygen):

With alternate bubbling of oxygen and nitrogen or argon, the extent of degradation shows marginal enhancement. One can easily perceive that intermittent bubbling of O_2 at a relatively high rate of 10 lit/hr for 5 minutes during silent period of the reaction will increase the dissolved oxygen content of the medium, close to the saturation level of 8 ppm. With this, the radical scavenging action is restored temporarily. However, the dissolved oxygen content of the medium drops rapidly with bubbling of N_2 or Ar in the ensuing sonication period of 15 minutes. As seen in figure 4.3, the dissolved oxygen content reduces from saturation value of 8 ppm to ~ 2 ppm in 15 min. Accordingly, the rise in degradation of phenol is only marginal in second category of experiments.

Category III (Continuous bubbling of Ar / N_2/ O_2 / Air with $FeSO_4 \cdot 7H_2O$ added to the liquid medium):

Addition of $FeSO_4 \cdot 7H_2O$ to the aqueous solution of pollutant results in a marked rise in the degradation obtained. Although the trend in the degradation with different gases remains same as category I, the absolute values of the degradation are higher. Several factors contribute to this effect: (1) the scavenging action of $FeSO_4 \cdot 7H_2O$ is due to reaction of Fe^{2+} ions with H_2O_2 generated in the medium as a result of recombination of $OH^{\bullet}$ radicals (reaction R.6). In the process Fe^{2+} ions are oxidized to Fe^{3+}. Being an ionic species the reactivity of Fe^{2+} is far higher than oxygen, which exists as molecular species; (2) bubbling of

gas (in case of nitrogen and argon) does not reduce the concentration of this species, as it is not stripped out of the medium; (3) Fe^{2+} is continuously regenerated in the medium due to reaction of Fe^{3+} ion with hydrogen peroxide and $HO_2^{\bullet}$ radicals (per reaction R.10 and R.11). It should be noted that the H_2O_2 generated by the cavitation bubble in equilibrium proportion among various species generated out of dissociation of water vapor is negligible (with mole fraction $< 10^{-6}$ for bubbles of all four gases). Thus, the H_2O_2 that reacts with Fe^{2+} is mainly generated due to recombination of $OH^{\bullet}$ radicals. The overall result is far more effective scavenging of radical scavenging in the medium giving high degradation in 90 min of sonication. It is interesting to note that in the third category of experiments, the degradation with air and oxygen is still higher than with argon, although the radical production by an argon bubble is one order of magnitude higher than air and oxygen bubbles, as mentioned earlier. We attribute this anomaly to the additive effect of Fe^{2+} and oxygen for radical scavenging for air and oxygen as bubbling gases.

4.6 CONCLUSION

In this chapter, we have tried to reveal interesting facets of the overall physics and mechanism of the sonochemical degradation of phenol, which have vital involvement in the enhancement of the degradation rates. With experiments under different reaction conditions and a mathematical model for the radial motion of cavitation bubbles, we have shown the relative influence of two physical processes, viz. radical generation (using monatomic and diatomic gases, viz. argon, nitrogen, oxygen and air) and radical scavenging or conservation (using molecular and ionic species, viz. oxygen and Fe^{2+}), on the sonochemical degradation of phenol. As stated earlier, the degradation of phenol occurs in the bulk liquid medium due to hydroxylation reaction induced by OH radicals generated from cavitation bubble. This is a

consequence of low vapor pressure of phenol (due to which it does not evaporate into the cavitation bubble) and the hydrophilic nature of the phenol molecule.

Unlike conventional chemical reactions where the rate is determined by the concentration of reactants, the rate of sonochemical degradation of phenol (with phenol and OH radical as the reactants) seems to be governed by the rate of scavenging of the radicals. This effect originates from low concentration of phenol in the liquid medium due to which the probability of interaction between radicals and phenol molecules becomes an important factor influencing overall degradation. The scavenging phenomenon increases this probability and gives higher degradation. Moreover, the concentration of the radical scavenging species is another important factor affecting the degradation. Atypically, monatomic gas such as argon, which is generally used for increasing the yield of the sonochemical reactions, is found to give low degradation. This is an outcome of the counterproductive effect of bubbling of argon on scavenging phenomena due to stripping out of dissolved oxygen from the liquid medium. On the other hand, the ionic species Fe^{2+} is found to be far more efficient for radical scavenging even at very low concentration levels. This is attributed to faster reactivity of Fe^{2+} ions and uniform concentration of the Fe^{2+} ions during sonication.

On a whole, the results of this study give a mechanistic assessment of various techniques that can enhance the sonochemical degradation of phenol. It will be shown in subsequent chapters that the approach presented in this chapter could also form a framework for study in intensification of sonochemical degradation of any other non-volatile organic pollutant, which has similar degradation chemistry (i.e. hydroxylation route) as phenol.

CHAPTER 5

MECHANISTIC FEATURES OF SONOCHEMICAL DEGRADATION OF VOLATILE AND NON-VOLATILE POLLUTANTS

5.1 INTRODUCTION

Harnessing cavitation and sonochemistry as an advanced oxidation technology is being increasingly attempted in recent years. The possible chemical mechanisms for the degradation of an organic pollutant under influence of ultrasound irradiation have been discussed in chapter 2. The first possible mechanism is hydroxylation, which is reaction with OH radicals generated out of cavitation bubbles. The extreme conditions (~ 5000 K and ~ 500 bars) created during transient collapse of a cavitation bubble (Suslick, 1990; Flint and Suslick, 1991) result in the generation of highly reactive species such as hydroxyl ($OH^{\bullet}$), hydrogen ($H^{\bullet}$) and hydroperoxyl ($HO_2^{\bullet}$) radicals due to dissociation of water vapor trapped in the bubble at the moment of collapse (Hart and Henglein, 1985, 1987). As the bubble fragments during collapse, these radicals get mixed with the bulk liquid, where they can initiate and promote the hydroxylation reactions leading to degradation of pollutants. Another possible mechanism for the degradation of pollutants is the thermal pyrolysis in the cavitation bubble. During the expansion phase of radial bubble motion, evaporation of the pollutant molecules occurs at the bubble wall and these molecules diffuse towards the center of the bubble. In the subsequent compression phase, the pollutant molecules diffuse outward, i.e. towards bubble wall, and condense at bubble wall. During the final moments of compression

phase, the bubble motion becomes extremely rapid and not all of the pollutant molecules that have entered the bubble can condense. The entrapped molecules are subjected to extreme conditions generated during transient collapse and undergo thermal pyrolysis (Weavers and Hoffmann, 1998; Lesko, 2004; Storey and Szeri, 2000). The third possible mechanism for the hydrolysis of the organic pollutants is the formation of transient supercritical water packets in the close vicinity of cavitation bubble as proposed by Hua *et al.* (1995). Out of these pathways, the major pathway contributing to the overall degradation depends on the nature and properties of the organic compound.

In this study we have investigated the mechanistic aspects of the sonochemical degradation of the volatile and non-volatile organic pollutants. Phenol and chlorobenzene have been selected as the model compounds in non-volatile and volatile categories, respectively. These are very common pollutants found in industrial wastewater and several authors have studied their sonochemical degradation (a review of the literature has been presented in chapter 1). The primary degradation products of phenol have been hydroquinone and catechol, which hint at attack of $OH^{\bullet}$ radical on phenol as the degradation pathway (or the principal chemical mechanism), which results in hydroxylated products. The degradation kinetics of chlorobenzene is found to be first order with major degradation products such as methane, acetylene, butenyne, butadiene, HCl, HOCl and $Cl^{\bullet}$ etc. These products hint at thermal pyrolysis as the principal chemical mechanism for the degradation. However, the approach in these studies for both compounds was mainly experimental and no confirmation of the degradation mechanism was made on the basis of a model for the radial motion of cavitation bubbles.

In this chapter, we try to provide a physical insight into the sonochemical degradation of the organic pollutants. As noted earlier, any attempt to elucidate the physical mechanism of the process should basically mean establishing relationship between the sonochemical

degradation through two pathways (viz. pyrolysis and hydroxylation) and the cavitation bubble dynamics. Therefore, in this study we try to correlate the extent of degradation of the two pollutants under similar conditions to the physical properties of the pollutants and the fundamental phenomena of transport of vapor of water and organic pollutant across cavitation bubble using a bubble dynamics model. Moreover, the influence of parameters such as initial concentration of pollutants and salt addition to the pollutant solution on the extent of degradation is also explored from a mechanistic perspective. The results of this study not only establish the predominant physical mechanism for the sonochemical degradation of volatile and non-volatile organic pollutants but also give an interesting account of the interlinks between cavitation physics and the chemistry of the sonochemical degradation of these pollutants.

5.2 EXPERIMENTAL

5.2.1 Reagents

Phenol (Merck, Grade: Synthesis), Chlorobenzene (Merck, Grade: GR), Sodium Chloride (Merck, Grade: Pure), Acetonitrile (Merck, Grade: HPLC) and Water (Merck, Grade: HPLC) were used as received. Elix water from Millipore (Model: Elix 3) was used for preparing the solutions of the pollutants. Bulk concentration of phenol and chlorobenzene in the solution was varied as 50 ppm and 100 ppm.

5.2.2 Experimental setup

A schematic diagram of the experimental setup used in the present study is shown in figure 5.1. For the sonication of the aqueous solutions of pollutants, a microprocessor based and programmable ultrasound processor was used (Sonics & Materials Inc., Model VCX 500). This processor had a frequency of 20 kHz with maximum power output of 500W. The ultrasound probe of the processor was fabricated from high-grade titanium alloy and had a tip

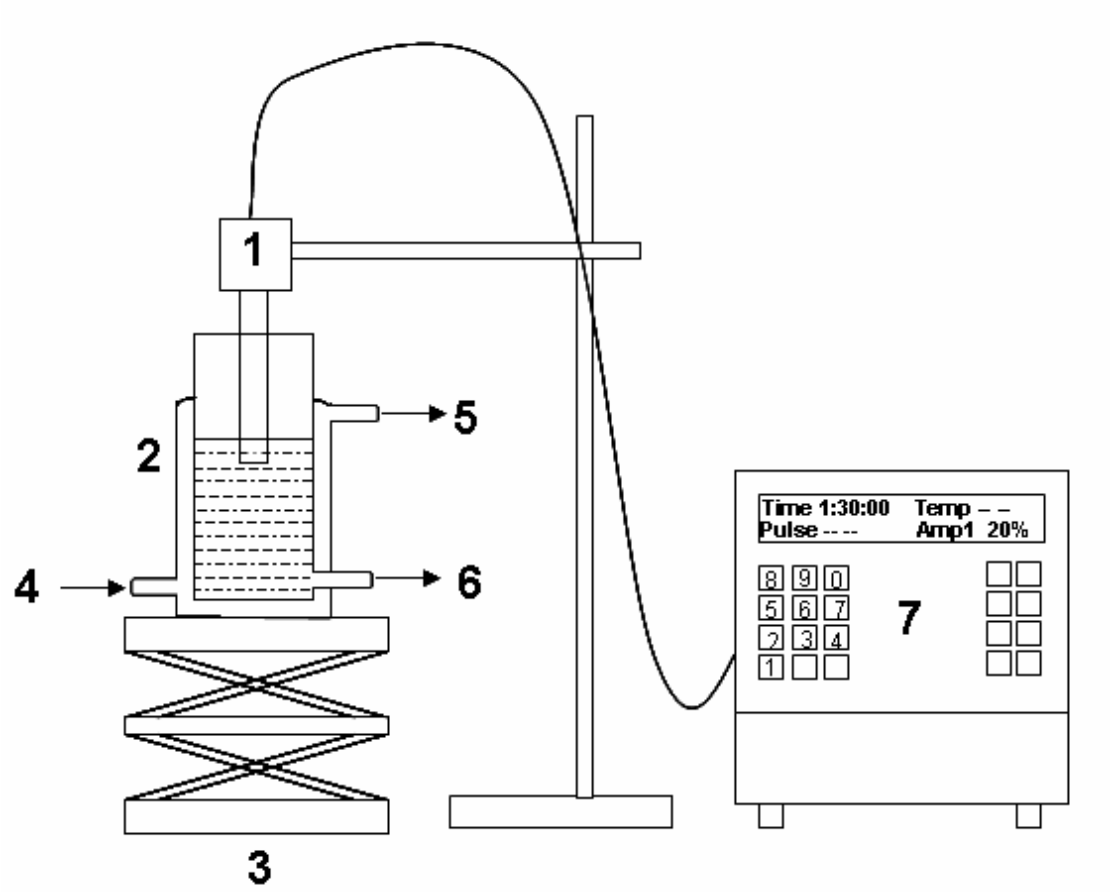

Figure 5.1. Experimental set-up [Legends: 1. Ultrasound probe; 2. Reactor with cooling jacket; 3. Laboratory jack; 4. Cooling water inlet; 5. Cooling water outlet; 6. Sample withdrawl port; 7. Control unit of the ultrasound processor].

diameter of 13 mm. The processor had variable power output control, which was set at 20% during experiments, resulting in net consumption of 100W power during sonication. It needs to be mentioned that this value corresponds to the theoretical maximum ultrasound intensity. The actual value of ultrasound intensity in the medium was measured using calorimetry (Sivasankar *et al.*, 2007). In addition, the processor had facility of automatic frequency tuning and amplitude compensation, which ensures constant power delivery to ultrasound probe irrespective of the changes occurring in liquid medium. Sonication of the pollutant solution was done in a jacketed glass reactor (dimensions: height – 120 mm, diameter – 50 mm and jacket diameter – 62 mm) placed on a laboratory jack, which could be raised or lowered for

exact positioning of the ultrasound probe tip in the solution.

5.2.3 Experimental procedure and method of analysis

The volume of the solution of pollutant used for sonication was 150 ml at an initial temperature of 25^{o}C. The total reaction time was 90 min; however, in order to avoid significant rise in the temperature of the solution, the sonication was done in cycles of 15 min sonication – 5 min silent period. In addition, cooling water was circulated through the jacket during sonication in order to maintain the temperature of the reaction medium constant. The temperature of the solution was monitored continuously during sonication with a digital thermometer. The rise in temperature of solution during the experiment was ~ 2°C. Due to small reaction volume (150 ml) and single source of ultrasound in the medium (in the form of sonicator probe), the equilibration of reaction system (or steady state) after onset of sonication is expected to be quite rapid. Therefore, the procedure of intermittent sonication adopted in this study is not expected to cause reduction in overall (or gross) degradation of pollutant obtained during total 90 min of sonication.

Experiments were done for two concentrations of phenol and chlorobenzene, viz. 50 ppm and 100 ppm. These values are typical of the concentration levels of the pollutants in industrial effluents (Gogate and Pandit, 2004). For each of these concentrations, experiments were done for the pure solution and for the solution with 4% w/v (or 0.67 mol/l) salt addition. All experiments were done in triplicate to assess the reproducibity of the results. The mean of the degradation obtained in three experimental runs was taken into consideration for further analysis. We would like to mention that no gas was sparged through the reaction mixture during sonication. Therefore, the sonochemical reaction was left to the radicals generated out of cavitation bubbles already present in the medium – in the form of air pockets trapped in the solid boundaries such as tip of the ultrasound probe or the tiny air bubbles already suspended in the medium.

The final concentration of phenol and chlorobenzene in the solution after 90 minutes of sonication was determined using High Performance Liquid Chromatography (Perkin Elmer, Model: Series 200). A C18 column (Make: Chromatopak, dimensions: 250 mm × 4.6 mm, particle size of packing: 5 µm) was used and a mixture of acetonitrile:water (80:20) as the eluent. The flow rate of the eluent was maintained at 1 ml/min with the sample injection volume being 20 µl. The UV detector wavelengths for phenol and chlorobenzene were 275 nm and 205 nm respectively. We would like to categorically state that we have not made an analysis of the intermediate products of degradation of phenol and chlorobenzene, as these have been well studied and documented in previous literature (referred to in previous section). We have monitored the overall or gross degradation of the original pollutant in 90 min of sonication only and the analysis has been made on that basis.

5.3 THE MATHEMATICAL MODEL

In the context of the present study, the problem of mathematical modeling comprises of simulating the radial motion of cavitation bubbles with the accompanying heat transfer and evaporation/entrapment of water and pollutant molecules, and finally determine the various chemical species that result out of transient collapse of the bubble. The model used in this chapter is essentially same as in chapter 3 and 4 (the diffusion limited model developed by Toegel *et al.*, 2000), however, we make several changes to it so as to adopt it for the present situation. This model makes two approximations as follows:

(1) *Analysis on single bubble basis*: We simulate the radial motion of the cavitation bubble in the bulk liquid medium using mathematical model for a single cavitation bubble. In other words, we ignore the influence of the bubble population in the neighborhood of a single bubble on its radial motion, and also the collective oscillations of bubble clouds in the medium. A justification for such an approach was given in previous chapter. This

approximation is based on the findings of Ilyichev *et al*. (1989) who proved that all characteristic features of the cavitation bubble fields in the liquid medium can be explained on the basis of dynamic behavior of a single bubble. Moreover, other studies (Prasad Naidu *et al.*, 1994; Sivasankar *et al.*, 2007) using a model reaction (oxidation of KI to liberate iodine) have also proven that the trends in the yield of a sonochemical reaction can be explained on the basis of simulations of radial motion of a single cavitation bubble.

(2) *Thermodynamic equilibrium of the bubble contents*: While calculating the composition of the bubble contents at the moment of transient collapse, we assume that equilibrium is attained among various chemical species present in the bubble. Moreover, in the energy balance for the bubble we do not incorporate various radical reactions along with their heats of reactions. It needs to be mentioned that the endothermicity of some of the reactions (for example $H_2O \rightleftharpoons H^{\bullet} + OH^{\bullet}$) works towards reduction in the temperature peak attained during transient bubble collapse. The assumption of attainment of thermodynamic equilibrium at the bubble collapse is based on the relative magnitudes of the bubble collapse time scale and the time scales of various radical reactions. The time scale of bubble collapse, as determined by Storey and Szeri (2000) is of the order of few tens of nanoseconds (~ 10^{-8}). The specific rate constants for the various radical reactions calculated from the Arrhenius equation at temperatures 2500-3000K (typical of the temperature peaks attained during transient bubble collapse) are of the order of 10^{12} cm^3 mol^{-1} s^{-1}. Moreover, the concentrations of various species in the bubble at the moment of collapse are very high. An order of magnitude calculation done with representative numbers [~ 10^{10} molecules or 10^{-13} moles in a 10 μm bubble (or ~ 10^{-4} cm) compressed to $1/10^{th}$ of its original size, i.e. ~ 10^{-5} cm] puts concentrations as high as ~ 100 mol/cm^3 (Krishnan *et al.*, 2006). As a collective result of these two features, rates of various reactions among various species present in the bubble are expected to be extremely fast. Even with a conservative estimate of concentration, the time-

scale for the reaction (t_{react}) can be taken as ~ 1/specific reaction rate. Comparison of the time scale of bubble collapse with the time scale of reactions reveals that the latter is at least two orders of magnitude smaller. Thus, thermodynamic equilibrium should prevail till the point of minimum radius during collapse. This justifies our assumption of thermodynamic equilibrium. Brenner *et al*. (2002) have also supported the attainment of thermal equilibrium in a sonoluminescing bubble.

We emphasize that our approach with the above approximations addresses the basic physics of the problem, which is sufficient for the present case. A more rigorous approach relaxing approximations in this study would only modify quantitative answers. We have reproduced some components the model again here for the convenience of the reader.

5.3.1 Radial motion of bubble

The radial motion of the bubble is described by the Keller-Miksis equation (Brennen, 1995; Prosperetti and Lezzi, 1986):

$$\left(1-\frac{dR/dt}{c}\right)R\frac{d^2R}{dt^2}+\frac{3}{2}\left(1-\frac{dR/dt}{3c}\right)\left(\frac{dR}{dt}\right)^2 = \frac{1}{\rho_L}\left(1+\frac{dR/dt}{c}\right)(P_i-P_t)+\frac{R}{\rho_L c}\frac{dP_i}{dt}-4\nu\frac{dR/dt}{R}-\frac{2\sigma}{\rho_L R} \quad (5.1)$$

This is a modification of the Rayleigh-Plesset equation, which takes into account liquid compressibility. R denotes the radius of the bubble at time t and ρ_L, σ, ν denote the physical properties of the liquid medium, viz. the density, surface tension and kinematic viscosity respectively. c is the speed of sound in the medium and the pressure inside the bubble (P_i) is written using van der Waals type equation of state (Hilgenfeldt *et al.*, 1996):

$$P_i = \frac{N_{tot}(t)\,kT}{\left[\frac{4\pi}{3}\left(R^3(t)-h^3\right)\right]} \quad (5.2)$$

k is the Boltzmann constant, N_{tot} denotes the total number of molecules in the bubble that vary according to condensation/vaporization of the bulk medium (i.e. the solution containing the pollutant, in present case) and T is the temperature inside the bubble. h is the van der

Waal's hard core radius of various species in the bubble viz. nitrogen, oxygen, water and chlorobenzene or phenol. As an approximation we take a common value $h \approx R_0/8.86$ for all species, where R_0 is the equilibrium radius of bubble. A simple expression for P_t (the bulk pressure during ultrasound irradiation) is written as (Hilgenfeldt *et al.*, 1996):

$$P_t = P_0 - P_A \sin(2\pi f t) \tag{5.3}$$

here P_0 is the ambient pressure and P_A and f denote the pressure amplitude and frequency of acoustic wave.

5.3.2 Mass transfer across bubble

During the radial motion of bubble, both gas and water vapor diffuse across the bubble wall. The time scale for the diffusion of gas is ~ R_0^2/D where D is the diffusion coefficient (Toegel and Lohse, 2003). For representative values as R_0 ~ 10 µm, D ~ 10^{-9} m^2/s, the time scale for the gas diffusion is 0.1s, which is far higher than time scale of bubble dynamics (Brenner *et al.*, 2002) (~ 50 µsec for 20 kHz ultrasound wave). Thus, the transport of gas across bubble can be ignored. Diffusion of vapor across the bubble wall, however, needs to be accounted for. In the present situation, the bulk liquid medium contains two components (either chlorobenzene–water or phenol–water) that evaporate into the bubble. The surface temperature of bubble exceeds the bulk water temperature only for a very brief moment during collapse (Kamath *et al.*, 1993). On this basis, the present model divides the bubble into two parts: (1) a cold boundary layer in thermal equilibrium with liquid and (2) a hot homogeneous core. The rate of change of vapor molecules in the bubble is given by:

Water vapor:
$$\frac{dN_w}{dt} = 4\pi R^2 D_w \left.\frac{\partial C_w}{\partial r}\right|_{r=R} \approx 4\pi R^2 D_w \left(\frac{C_{wR} - C_w}{l_{diff}}\right) \tag{5.4}$$

Pollutant (either chlorobenzene or phenol) vapor:
$$\frac{dN_p}{dt} = 4\pi R^2 D_p \left.\frac{\partial C_p}{\partial r}\right|_{r=R} \approx 4\pi R^2 D_p \left(\frac{C_{pR} - C_p}{l_{diff}}\right) \tag{5.5}$$

where l_{diff} is the instantaneous diffusive penetration depth and D_w and D_p are the effective diffusion coefficients for water vapor and pollutant respectively. Using dimensional analysis (Toegel *et al.*, 2000; Toegel and Lohse, 2003) it is taken to be $l_{diff} = \sqrt{D_w t_{osc}}$ for water molecules and $l_{diff} = \sqrt{D_p t_{osc}}$ for pollutant molecules. t_{osc} is the time scale of bubble dynamics estimated as $R/|dR/dt|$, again using dimensional analysis. C_{wR} and C_{pR} is the equilibrium concentration of the water and pollutant molecules at bubble wall. C_w and C_p are the concentrations of water and the pollutant in the core of the bubble. Since the concentrations of phenol and chlorobenzene are rather dilute, the behavior of solution is close to ideal and the activity coefficients of solvent and solute can be assumed to ~ 1. Thus, we assume the Raoult's law to hold good. The total vapor pressure of the pollutant-water mixture in this situation is:

$$P_v = x_{wR}P_w + x_{pR}P_p \tag{5.6}$$

where x_{wR} and x_{pR} are the mole fractions of water and pollutant components in liquid. The concentrations of water and pollutant molecules at bubble-bulk interface are written in terms of their partial pressures:

$$C_{wR} = \left(x_{wR}P_w\right)/kT_0 \text{ and } C_{pR} = \left(x_{pR}P_p\right)/kT_0 \tag{5.7}$$

The mole fraction (or in other words, concentration) of the pollutant molecule at the bubble-water interfacial region is not the same as the bulk concentration of the pollutant in the medium (50 or 100 ppm). This is due to the fact that hydrophobic repulsive interactions of the pollutant molecules with aqueous phase drive the pollutant molecules towards the bubble-bulk interface (Joos and Serrien, 1989; Price *et al.*, 2004). As a result, the concentration of the pollutant molecules in the thin liquid shell surrounding the bubble increases. A direct measurement of the pollutant concentration in the interfacial region is beyond the capabilities of the instrumentation used in the present study. However, an indirect estimation of the

interfacial concentration has been done by Bapat *et al.* (2007) and Seymour and Gupta (1997).

The approach of Bapat *et al*. (2007) was theoretical. Using the Gibb's equation for the surface excess of solute as basis (Adamson and Gast, 1997), they measured the reduction in the surface tension of the aqueous solution of phenol with concentration of phenol. Correlating the slope of the plot of surface tension vs. bulk concentration to the Gibb's equation, Bapat *et al.* (2007) determined the surface excess of phenol for bulk concentration of 1 mol/m^3. Later, with simultaneous analysis of the surface concentration of phenol and water molecules at bubble-bulk interface, Bapat *et al.* (2007) concluded that the concentration of phenol at bubble-bulk interface at equilibrium conditions would be 264 times the bulk concentration.

Seymour and Gupta (1997) measured the partitioning behavior of chlorobenzene and phenol between an organic phase (diethyl ether) and water. A partition coefficient $K_{ether\text{-}water}$ was defined as c_{org}/c_{aq} where c_{org} is the concentration of pollutant in the organic phase and c_{aq} is the concentration in the aqueous phase. This partition coefficient was related to the interface-bulk liquid partition coefficient as:

$$K_{interface\text{-}bulk} = c_1 K_{ether\text{-}water} \qquad (5.8)$$

where c_1 is constant of proportionality. With the best fit of experimental data, Seymour and Gupta (1997) found c_1 = 4 for chlorobenzene and c_1 = 0.67 for phenol. Additional of salt (NaCl) to the aqueous phase raises the ionic strength of the solution, and hence, the hydrophobic repulsive interactions. Due to this, the pollutant molecules are driven to the organic phase to a greater extent, which results in a rise in c_{org} and $K_{interface\text{-}bulk}$. The values of partition coefficients for chlorobenzene and phenol are listed in table 5.1A.

The enrichment of phenol at bubble-bulk interface as determined by Seymour and Gupta (1997) and Bapat *et al*. (2007) differs by two orders of magnitude. However,

Table 5.1

(A) Partitioning behavior of the pollutants*

Phenol			Chlorobenzene		
Salt concentration	**$K_{ether\text{-}water}$**	**$K_{interface\text{-}bulk}$**	**Salt concentration**	**$K_{ether\text{-}water}$**	**$K_{interface\text{-}bulk}$**
0% w/v	4.9	3.283	0% w/v	7.3	29.2
4% w/v	17.5	11.725	4% w/v	12.0	48.0

(B) Mole fractions of the pollutants

Concentration of solution	**Phenol**	**Chlorobenzene**
	overall or bulk mole fraction (x_p)	
50 ppm solution	9.574×10^{-6}	7.995×10^{-6}
100 ppm solution	1.915×10^{-5}	1.6×10^{-6}
	saturation mole fraction (x_s)	
	1.53×10^{-3}	8×10^{-5}

* - data taken from Seymour and Gupta (1997)

attainment of equilibrium between bubble interface and bulk medium is difficult to achieve under transient cavitation conditions where bubble undergoes large-amplitude radial motion. The time scale of this motion is same as that of the ultrasound wave (50 μs for 20 kHz frequency). The time for the diffusion of phenol to the bubble interface through the boundary layer is expected to be several orders of magnitude higher. For representative values of boundary layer thickness around bubble as ~ 1 μm and diffusion coefficient of pollutant in water as 10^{-10} m^2/s, the time scale of diffusion of phenol is ~ 1 ms. Due to large difference in the time scale of diffusion of phenol and the time scale of radial motion of bubble, the bubble interface is not likely to attain equilibrium (as assumed by Bapat *et al.*, 2007) under transient cavitation conditions. The enrichment factor determined empirically (under non-equilibrium conditions) by Seymour and Gupta (1997), thus, seems to be more practical. Therefore we have used the data of Seymour and Gupta (1997) for our analysis.

Using the partition coefficients in table 5.1A, we estimate the mole fraction of the pollutant molecules in the interfacial region as:

$$x_{pR} = K_{interface\text{-}bulk}\, x_p \tag{5.9}$$

where x_p is the overall or bulk mole fraction of the pollutant in the medium. It must be mentioned that x_{pR} cannot rise indefinitely with addition of salt. The upper limit to x_{pR} is decided by the solubility of the pollutant, which is 0.5 *g/l* for chlorobenzene and 8 *g/l* for phenol. Table 5.1B lists the values of bulk (x_p) and saturation (x_s) mole fraction of phenol and chlorobenzene. If ($x_p\, K_{interface\text{-}bulk}$) > x_s, the interface remains saturated with pollutant, i.e. $x_{pR} = x_s$.

P_w and P_p are the vapor pressures of water and pollutant in pure form at the bulk temperature (T_0). We use the following Antoine's equations for calculation of P_w and P_p (in Pa)[73]:

$$P_p(for\ phenol) = 10^5 \times 10^{\left(4.24688-1509.677/(T-98.949)\right)} \tag{5.10}$$

$$P_p(for\ chlorobenzene) = 10^5 \times 10^{\left(4.11083-1435.675/(T-55.124)\right)} \tag{5.11}$$

$$P_w = \frac{10^5}{760}\exp\left(18.3036-\frac{3816.44}{T-46.13}\right). \tag{5.12}$$

The influence of salt addition to the solution on the vapor pressure of water is accounted for by the following equation (Al-shayji, 1998):

$$P_w' = P_w\left(1-0.537C_B\right) \tag{5.13}$$

5.3.3 Limits on diffusion length

At the instances of maximum and minimum radius, the bubble wall velocity is zero, and thus, an alternate expression is needed for diffusion length. We set this limit as R/π after identifying that vapor transport is governed by pure diffusion equation for condition $dR/dt = 0$. The limit R/π is set on the basis of solution of the diffusion equation in spherical geometry. For greater details on this, we refer the reader to our earlier papers (Krishnan *et al.*, 2006; Kumar and Moholkar, 2007). Thus, the diffusion length for water molecules is:

$l_{diff} = \min\left(\sqrt{\frac{RD_w}{|dR/dt|}}, \frac{R}{\pi}\right)$ while the diffusion length for the pollutant molecules is:

$l_{diff} = \min\left(\sqrt{\frac{RD_p}{|dR/dt|}}, \frac{R}{\pi}\right)$.

5.3.4 Determination of diffusion coefficient

In the present situation (air bubbles oscillating in the aqueous solution of pollutants) we encounter a quaternary system: nitrogen-oxygen-water-pollutant. The diffusion of nitrogen and oxygen across bubble wall is ignored for the reasons stated earlier. For water and the pollutant (either phenol or chlorobenzene) we first calculate the binary diffusion coefficients using kinetic theory of gases (Hirschfelder, 1954) with properties of boundary layer evaluated at bulk temperature (for greater details we refer the reader to our earlier papers, Krishnan *et al.*, 2006; Kumar and Moholkar, 2007). From these binary coefficients, the overall (or effective) diffusion coefficient for water (D_w) and the pollutant (D_p) is calculated as (Bird *et al.*, 2001):

$$\frac{1}{D_w} = \frac{\varepsilon_{N_2}}{(1-\varepsilon_w) D_{w\text{-}N_2}} + \frac{\varepsilon_{O_2}}{(1-\varepsilon_w) D_{w\text{-}O_2}} + \frac{\varepsilon_p}{(1-\varepsilon_w) D_{w\text{-}p}} \tag{5.14}$$

$$\frac{1}{D_p} = \frac{\varepsilon_{N_2}}{(1-\varepsilon_p) D_{p\text{-}N_2}} + \frac{\varepsilon_{O_2}}{(1-\varepsilon_p) D_{p\text{-}O_2}} + \frac{\varepsilon_w}{(1-\varepsilon_p) D_{p\text{-}w}} \tag{5.15}$$

Here ε denotes the mole fraction of the individual component. Subscripts p, O_2 and N_2, w represent pollutant, oxygen, nitrogen and water respectively.

5.3.5 Heat transfer across bubble

In analogy with mass transfer, the rate of heat transfer (Q) across bubble wall is:

$$\frac{dQ}{dt} = 4\pi R^2 \lambda \left.\frac{\partial T}{\partial r}\right|_{r=R} \approx 4\pi R^2 \lambda \left(\frac{T_0 - T}{l_{th}}\right) \tag{5.16}$$

where λ is the effective thermal conductivity of bubble contents and l_{th} is the thermal

diffusion length: $\min\left(\sqrt{\frac{R\kappa}{|dR/dt|}}, \frac{R}{\pi}\right)$. Thermal diffusivity ($\kappa$) is calculated as: $\kappa = \lambda/\rho_{mix}C_{p,mix}$, where ρ_{mix} and $C_{p,mix}$ represent the overall density and specific heat capacity of the mixture of various species in the bubble. The molecular specific heats (C_p) for various components are as follows:

$N_2 = 7k/2$, $O_2 = 7k/2$ *and* $H_2O = 4k$. As the concentration of pollutant in the solution is quite small, so will be the equilibrium pressure at the bubble-bulk interface and the diffusive flux of the pollutant. The bubble contents will be dominated by air and water vapor. In view of this, we have not included the pollutant as a component in the determination of the thermal conductivity and thermal diffusivity. The thermal conductivity of the bubble contents has been calculated considering only three components, viz. oxygen, nitrogen and water vapor. To calculate the effective thermal conductivity, we first determine the thermal conductivity (λ) and viscosity (η_i) of the individual species using the kinetic theory of gases (again we refer readers to our earlier papers (Krishnan *et al.*, 2006; Kumar and Moholkar, 2007) for greater details). The effective thermal conductivity of the mixture of species is given by following relation (Condon and Odishaw, 1958):

$$\lambda_{mix} = \sum \frac{\varepsilon_i \lambda_i}{\sum \varepsilon_j \phi_{ij}} \tag{5.17}$$

where *i, j* = O_2, N_2 *and* H_2O, and

$$\phi_{ij} = \frac{1}{\sqrt{8}}\left(1+\frac{m_i}{m_j}\right)^{-1/2}\left[1+\left(\frac{\eta_i}{\eta_j}\right)^{-1/2}\left(\frac{m_i}{m_j}\right)^{1/4}\right]^2 \tag{5.18}$$

where m_i and m_j are the molecular masses of various species.

5.3.6 Overall energy balance

During the radial motion, the bubble is an open system through which water and

pollutant molecules diffuse. However, in a very dilute solution (such as 50 ppm and 100 ppm of organic pollutant), the transaction of water molecules through bubble wall will be several orders of magnitude larger than the solute or pollutant molecules. Thus, we write the energy balance for the bubble on the basis of ternary system: O_2-N_2-H_2O. The total energy balance for the bubble content is:

$$\frac{dE}{dt} = \frac{dQ}{dt} - \frac{dW}{dt} + h_W \frac{dN_W}{dt} \tag{5.20}$$

The total energy E is a function of temperature and volume of the bubble and the number of molecules of various species in it. The rate of change of E is:

$$\frac{dE}{dt} = \left(\frac{\partial E}{\partial N_W}\right)_{N_{N_2},N_{O_2},V,T}\left(\frac{dN_W}{dt}\right) + \left(\frac{\partial E}{\partial N_{N_2}}\right)_{N_W,N_{O_2},V,T}\left(\frac{dN_{N_2}}{dt}\right) + \left(\frac{\partial E}{\partial N_{O_2}}\right)_{N_{N_2},N_W,V,T}\left(\frac{dN_{O_2}}{dt}\right) + \left(\frac{\partial E}{\partial T}\right)_{N_W,N_{N_2},N_{O_2},V}\left(\frac{dT}{dt}\right) + \left(\frac{\partial E}{\partial V}\right)_{N_W,N_{N_2},N_{O_2},T}\left(\frac{dV}{dt}\right) \tag{5.21}$$

where V is the volume of the bubble and N_{N_2}, N_{O_2} and N_W are the number of nitrogen, oxygen and water molecules in the bubble. For the reasons stated earlier, we ignore the transport of oxygen and nitrogen molecules across bubble, and hence: $dN_{N_2}/dt = dN_{O_2}/dt = 0$. dN_W/dt is the rate of change of water vapor content of the bubble and is evaluated using equation 5.4. Moreover we identify thermodynamic relations:

$$\left(\frac{\partial E}{\partial T}\right)_{N_w,N_{N_2},N_{O_2},V} = C_{V,\,mix} \;\; and \;\; \left(\frac{\partial E}{\partial V}\right)_{N_w,N_{N_2},N_{O_2},T} = 0 \tag{5.22}$$

as the internal energy of an ideal gas is a principal function of composition and temperature. The specific enthalpy of the water molecules entering the bubble from cold bubble interface is: $h_w = 4kT_o$. $\left(\partial E/\partial N_w\right)$ is the specific internal energy of water molecule (U_w) and is written as

$$\left(\frac{\partial E}{\partial N_w}\right) = U_w = N_w kT\left(3 + \sum_{i=1}^{3}\frac{\theta_i/T}{\exp(\theta_i/T)-1}\right) \tag{5.23}$$

with characteristics vibration temperatures (θ_i) for water molecule are listed below. Equating the RHS of equations 5.14 and 5.15 above we get:

$$C_{V,\,mix}\frac{dT}{dt} = \frac{dQ}{dt} - P_i dV + (h_w - U_w)\frac{dN_w}{dt} \tag{5.24}$$

The specific heat of mixture $C_{V,\,mix}$ is written in terms of the molecular specific heat of individual components ($C_{V,i}$) and the number of molecules of individual components (N_i) as:

$$C_{V,\,mix} = \sum C_{V,\,i}N_i \qquad i = \mathrm{N_2},\ \mathrm{O_2},\ \mathrm{H_2O} \tag{5.25}$$

The molecular specific heats C_V for various components are written as:

$$C_{V,N_2} = k\left[\frac{5}{2} + \frac{(\theta_{N2}/T)^2\exp(\theta_{N2}/T)}{(\exp(\theta_{N2}/T)-1)^2}\right] \qquad \theta_{\mathrm{N_2}} = 3350\ \mathrm{K} \tag{5.26}$$

$$C_{V,O_2} = k\left[\frac{5}{2} + \frac{(\theta_{O2}/T)^2\exp(\theta_{O2}/T)}{(\exp(\theta_{O2}/T)-1)^2}\right] \qquad \theta_{\mathrm{O_2}} = 2273\ \mathrm{K} \tag{5.27}$$

$$C_{V,W} = k\left[3 + \sum_{i=1}^{3}\frac{(\theta_i/T)^2\exp(\theta_i/T)}{(\exp(\theta_i/T)-1)^2}\right] \qquad \theta_{i,W} = 2295,\ 5255,\ 5400\ \mathrm{K} \tag{5.28}$$

5.3.7 Numerical solution

Equations 5.1, 5.4, 5.5, 5.16 and 5.24 give the formulation of radial motion of bubble with accompanying heat and mass transfer. For the convenience of the reader, we have summarized the complete bubble dynamics formulation in table 5.2 along with boundary conditions. We use the Runge-Kutta 4th order-5th order method with adaptive step size (Press *et al.*, 1992) (also known as Cash-Karp method) for the numerical solution of these simultaneous ordinary differential equations. The collapse of the cavitation bubble depends on several factors such as surface instability, local flow conditions and bubble population in

Table 5.2. Summarization of the Bubble Dynamics Formulation

Variable	Equation	Boundary Condition
1. Radius of the bubble (R) 2. Bubble wall velocity (dR/dt)	$\left(1-\frac{dR/dt}{c}\right)R\frac{d^2R}{dt^2}+\frac{3}{2}\left(1-\frac{dR/dt}{3c}\right)\left(\frac{dR}{dt}\right)^2=\frac{1}{\rho_L}\left(1+\frac{dR/dt}{c}\right)(P_i-P_t)+\frac{R}{\rho_L c}\frac{dP_i}{dt}-4\nu\frac{dR/dt}{R}-\frac{2\sigma}{\rho_L R}$ Internal pressure in the bubble: $P_i=\frac{N_{tot}(t)\,kT}{\left[4\pi\left(R^3(t)-h^3\right)/3\right]}$ Pressure in bulk liquid medium: $P_t=P_0-P_A\sin(2\pi ft)$	At $t=0$, $R=R_o$ and $dR/dt=0$.
3. Number of water molecules in the bubble (N_w) 4. Number of pollutant molecules in the bubble (N_p)	$\frac{dN_w}{dt}=4\pi R^2 D_w\left.\frac{\partial C_w}{\partial r}\right\|_{r=R}\approx 4\pi R^2 D_w\left(\frac{C_{wR}-C_w}{l_{diff}}\right)$ $\frac{dN_p}{dt}=4\pi R^2 D_p\left.\frac{\partial C_p}{\partial r}\right\|_{r=R}\approx 4\pi R^2 D_p\left(\frac{C_{pR}-C_p}{l_{diff}}\right)$ Instantaneous diffusive penetration depths: $l_{diff}=\min\left(\sqrt{\frac{RD_w}{\lvert dR/dt\rvert}},\frac{R}{\pi}\right)$; $l_{diff}=\min\left(\sqrt{\frac{RD_p}{\lvert dR/dt\rvert}},\frac{R}{\pi}\right)$ Diffusion coefficients: $\frac{1}{D_w}=\frac{\varepsilon_{N_2}}{(1-\varepsilon_w)D_{w\text{-}N_2}}+\frac{\varepsilon_{O_2}}{(1-\varepsilon_w)D_{w\text{-}O_2}}+\frac{\varepsilon_p}{(1-\varepsilon_w)D_{p\text{-}O_2}}$ $\frac{1}{D_p}=\frac{\varepsilon_{N_2}}{(1-\varepsilon_p)D_{p\text{-}N_2}}+\frac{\varepsilon_{O_2}}{(1-\varepsilon_p)D_{p\text{-}O_2}}+\frac{\varepsilon_w}{(1-\varepsilon_p)D_{p\text{-}H_2O}}$	At $t=0$, $N_w=0$ and $N_p=0$
5. Heat transfer through bubble (Q)	$\frac{dQ}{dt}=4\pi R^2\lambda\left.\frac{\partial T}{\partial r}\right\|_{r=R}\approx 4\pi R^2\lambda\left(\frac{T_0-T}{l_{th}}\right)$ Thermal diffusion length: $l_{th}=\min\left(\sqrt{\frac{R\kappa}{\lvert dR/dt\rvert}},\frac{R}{\pi}\right)$ Thermal conductivity: $\lambda_{mix}=\sum\frac{\varepsilon_i\lambda_i}{\sum\varepsilon_j\phi_{ij}}$ $\phi_{ij}=\left(1/\sqrt{8}\right)\left(1+m_i/m_j\right)^{-1/2}\left[1+\left(\eta_i/\eta_j\right)^{-1/2}\left(m_i/m_j\right)^{1/4}\right]^2$	At $t=0$, $Q=0$
6. Temperature of the bubble (T)	$C_{V,mix}dT/dt=dQ/dt-P_i dV+\left(h_w-U_w\right)dN_w/dt$ Mixture heat capacity: $C_{V,mix}=\sum C_{V,i}N_i$ Molecular properties of water: Enthalpy: $h_w=4kT_o$ Internal energy: $U_w=N_w kT\left(3+\sum_{i=1}^{3}\frac{\theta_i/T}{\exp(\theta_i/T)-1}\right)$	At $t=0$, $T=T_0$

the vicinity of the cavitation bubble. As a conservative estimate, the condition for the bubble collapse is taken to be first compression after an initial expansion. Four important parameters required for the simulation of the radial motion of the cavitation bubble are: (1) frequency and (2) pressure amplitude of ultrasound, (3) vapor pressure of water and pollutant and (4) initial (or equilibrium) bubble radius. Numerical values for these parameters have been determined as follows: The frequency of the wave (f) is taken as 20 kHz (i.e., the frequency of the ultrasound processor). The pressure amplitude of the acoustic wave (P_A) was determined as 1.5 bar using calorimetric techniques. However, the ultrasound wave undergoes attenuation during its passage through the medium. Therefore, the actual acoustic wave amplitude sensed by the bubble is lesser than that at the ultrasound probe tip. A direct measurement of this value is beyond the capabilities of instrumentation used in this study, and hence, we take a representative value as 1.25 bar, assuming ~ 15% attenuation. We would like to specifically mention that the attenuation of 15% is merely a representative number. Use of any other value (10% or 20%) makes only quantitative changes to the simulation results with the trends remaining essentially unchanged. The equilibrium radius of the bubble (R_0) is difficult to estimate. Moreover, the equilibrium size of the bubble keeps on changing due to phenomena such as rectified diffusion, fragmentation of the bubble etc. We have chosen a representative value of R_0 as 10μm for simulations. Once again we would like to mention that choice of any other value for this parameter (for example 5 μm or 15 μm) makes only quantitative changes to the simulation results with trends essentially remaining unchanged. The vapor pressure of water and pollutant has been calculated at the initial temperature of the bulk medium (i.e., 25^{o}C) using Antoine equations (equations 5.10-5.12). For the simulation of bubble motion in salt-added solution, we take into account the reduction in vapor pressure of water, as explained earlier (eqn. 5.13). However, changes in other physical properties of water such as density, viscosity, surface tension and heat capacity have

been neglected as the salt concentrations used in the experiment (4% w/v or 0.67 *g/l*) is too small to make any appreciable changes to the physical properties (Al-Shayji, 1998).

The composition of the bubble at the time of collapse is calculated assuming that thermodynamic equilibrium is reached in the bubble. The equilibrium mole fraction of various species in bubble at the conditions of temperature and pressure at the first compression of the bubble was calculated using software FACTSAGE, which uses the free energy minimization algorithm proposed by Eriksson (1975). It should be noted that FACTSAGE gives an equilibrium distribution of the species resulting from transient collapse of the cavitation bubble. These species are formed out of dissociation of various molecules (gas, water vapor and pollutant vapor) entrapped in the bubble at the moment of transient collapse. These are *different* than the degradation intermediates obtained with GC-MS or HPLC analysis of the samples withdrawn from the bulk medium. Some of the species resulting from the cavitation bubble are radicals, which can further react with pollutant molecules in the bulk giving variety of products (mentioned in the Introduction section) – which are detected as degradation intermediates. The water vapor and pollutant molecules entrapped in the bubble are subjected to extreme conditions generated at the transient bubble collapse, which results in dissociation of water vapor into radical species and pyrolysis of the pollutant creating mineralization products. Therefore, the species obtained with FACTSAGE are expected to mainly comprise of radicals and mineralization products.

5.4 RESULTS AND DISCUSSION

The sonochemical degradation of pollutant occurs by two mechanisms, viz. pyrolysis in the cavitation bubble and hydroxylation (i.e. reaction with $OH^{\bullet}$ radicals generated by cavitation bubbles) in the bulk liquid medium. The principal factor that decides the contribution of the pyrolysis pathway is the diffusive flux of the pollutant molecules across

bubble-bulk interface. The higher this flux, the higher the evaporation and the subsequent entrapment of the pollutant molecules in the bubble, which undergo thermal decomposition (pyrolysis) at the extreme conditions generated at the transient bubble collapse. The diffusive flux, as given by equation 5.5, depends on the partial pressure of the pollutant at the bubble-bulk interface, which in turn depends on the concentration of the pollutant in the interfacial region.

The principal factors that decide the contribution of the hydroxylation pathway are the rate of radical generation by the cavitation bubbles and the probability of interaction between the radicals and pollutant molecules. The extent of radical generation by the cavitation bubbles depends on amount of vapor (both water and pollutant) molecules trapped in the bubble at the collapse and the temperature reached during collapse. The radicals generated in the bubble mix with the bulk liquid medium with the fragmentation of the bubble during transient collapse. As the radical species are extremely reactive and unstable, they do not diffuse away significantly from the location of collapse of the bubble. Thus, significant fraction of the radical induced degradation (or hydroxylation) reaction occurs in a thin shell of liquid surrounding the cavitation bubble (Suslick, 1990; Seymour and Gupta, 1997; Suslick, 1989; Riesz *et al.*, 1985; Hoffmann *et al.*, 1996). Obviously, the higher the concentration of pollutant molecules in this shell, the higher the probability of interaction between pollutant molecule and radical species and the higher the degradation. It needs to be mentioned that some hydroxylation reaction leading to degradation of the pollutant also occurs in the bulk medium. Rise in the bulk concentration of the pollutant increases the probability of the interaction between radical and pollutant in the bulk medium. Briefly, concentration of pollutant in the bubble-bulk interfacial region influences contribution of both pyrolysis and hydroxylation pathway to the degradation of pollutants. With this prelude,

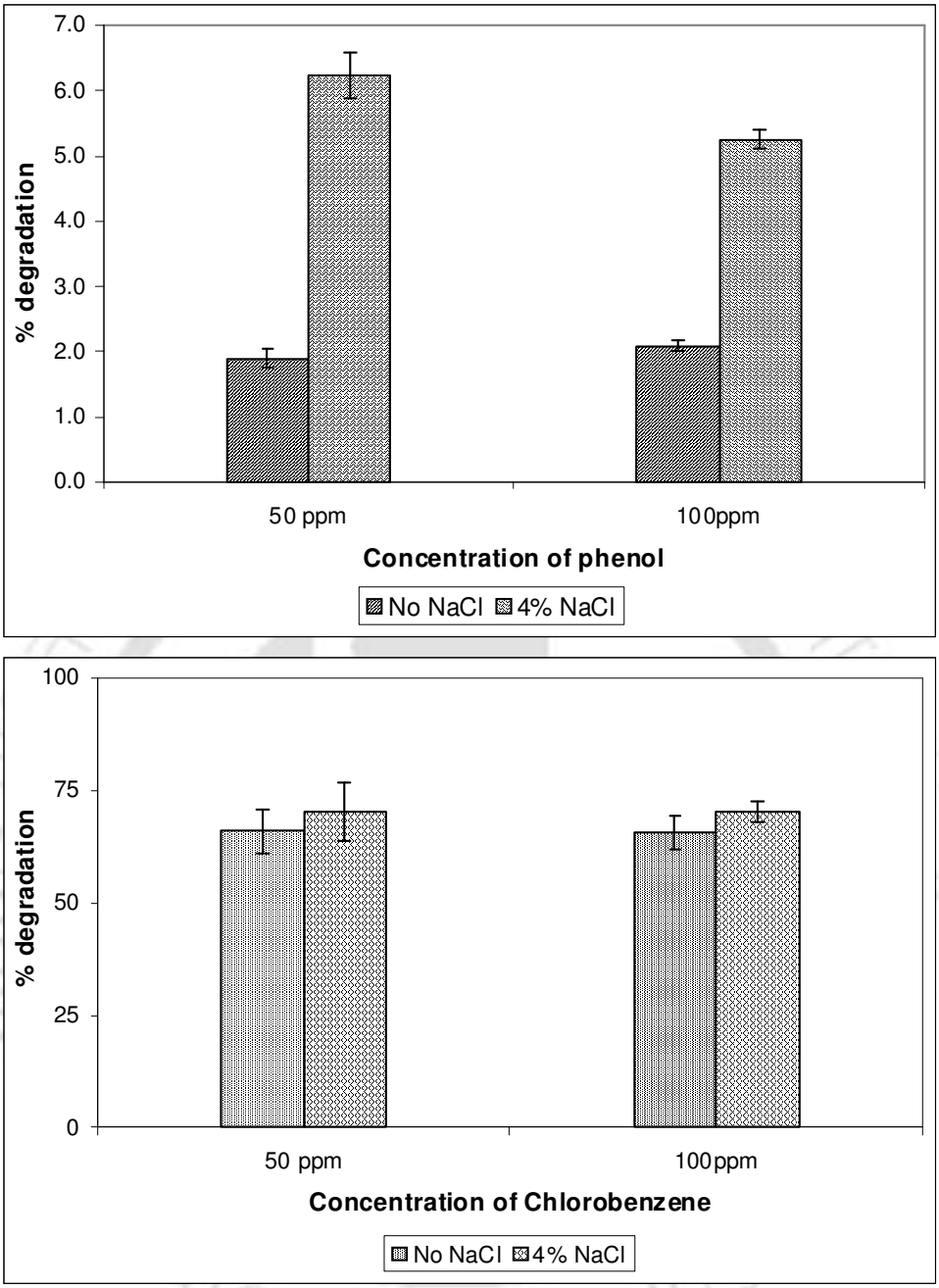

Figure 5.2. Experimental results on degradation of phenol and chlorobenzene under various reaction conditions (the mean value of the degradation obtained in 3 experimental runs has been shown along with standard deviation).

we present the results of experiments and simulations and try to establish the link between them.

Results for the degradation of phenol and chlorobenzene with different experimental conditions are shown in figure 5.2. Certain trends in the experimental results are observed as

follows: (1) the absolute amount of pollutant degraded in 90 min of sonication, in case of both phenol and chlorobenzene, increases with initial concentration of the pollutant – with all other conditions remaining the same; (2) with addition of 4% w/v NaCl, the extent of degradation for phenol rises ~ 3-fold, while salt addition has negligible enhancement effect on the degradation of chlorobenzene; (3) other experimental conditions remaining the same, the degradation of chlorobenzene is one order of magnitude higher than the degradation of phenol.

Illustrative simulations of the radial motion of air bubbles in 50 ppm solution of phenol (with 4% w/v salt) and 100 ppm solution of chlorobenzene are shown in figure 5.3 and 4 respectively. The summary of the entire simulation results is given in table 5.3. This table lists the collapse conditions (i.e. the number of water and pollutant molecules trapped and the temperature peak reached in the bubble at transient collapse) along with equilibrium composition of various species that result out of dissociation of water and pollutant molecules trapped in the bubble. Some distinct trends observed in the simulation results are as follows: (1) the extent of entrapment of phenol molecules in the cavitation bubble is at least two orders of magnitude smaller than the chlorobenzene molecules; (2) with initial concentration increased from 50 ppm to 100 ppm, the entrapment of phenol molecules in the bubble rises 3-fold, while the entrapment of chlorobenzene molecules remains practically unchanged. Moreover, with addition of 4% w/v salt to the solution, the entrapment of phenol in the bubble again rises by ~ 3 fold while entrapment of chlorobenzene molecule shows a slight (~ 10%) increase. These trends can be explained as follows:

(1) Vapor pressure of phenol at the temperature of experiment (25 ^{o}C) is 46 Pa while that of chlorobenzene is 1598 Pa. Due to the difference of two orders of magnitude in

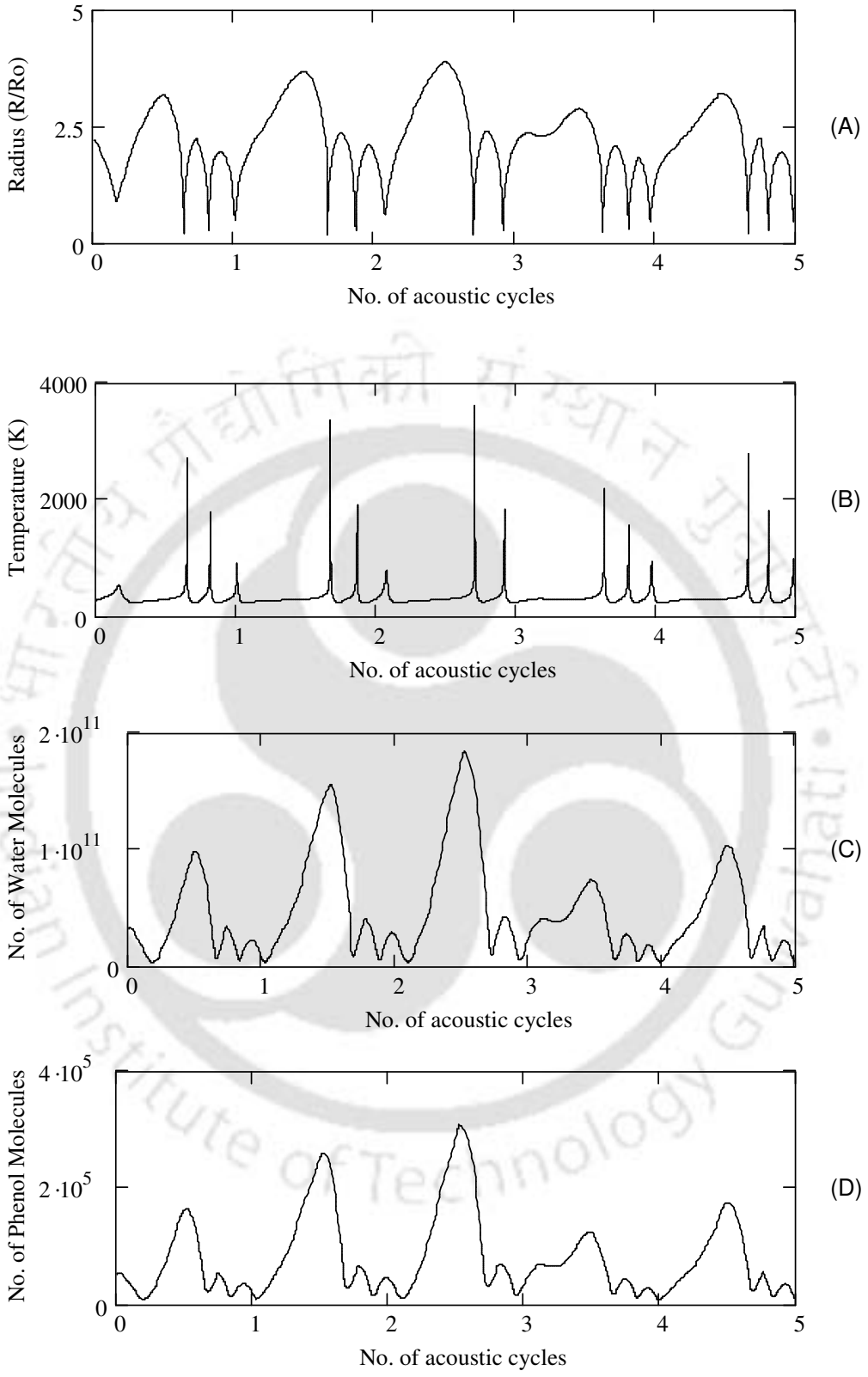

Figure 5.3. Simulation of the radial motion of 10 μm air bubble in 50 ppm phenol solution with 4% w/v NaCl. Time variation of (A) Normalized bubble radius (R/R_0); (B) Temperature in the bubble; (C) Number of water molecules in the bubble; (D) Number of phenol molecules in the bubble.

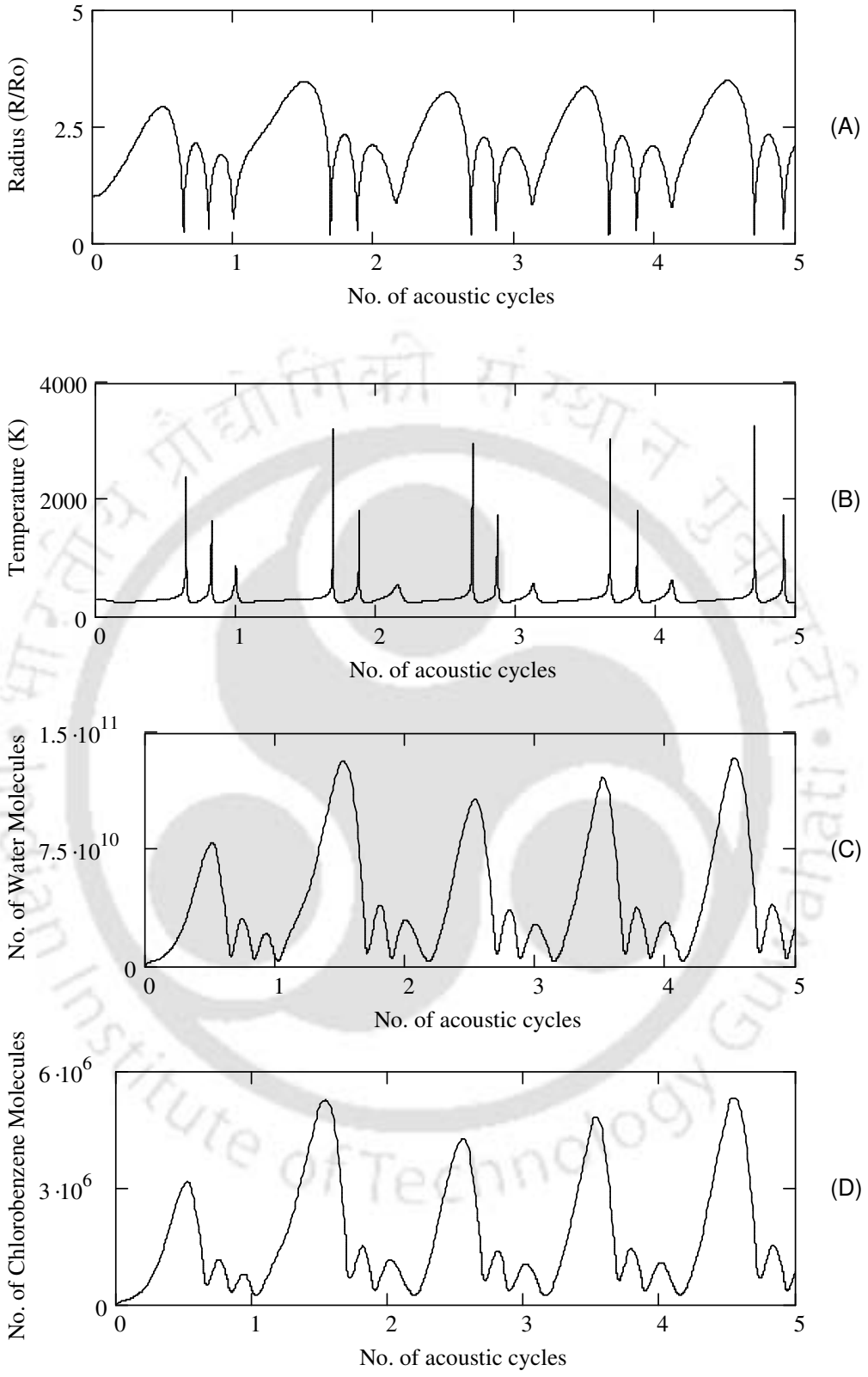

Figure 5.4. Simulation of the radial motion of 10 μm air bubble in 100 ppm chlorobenzene solution. Time variation of (A) Normalized bubble radius (R/R_0); (B) Temperature in the bubble; (C) Number of water molecules in the bubble; (D) Number of chlorobenzene molecules in the bubble.

vapor pressure, the diffusive flux and entrapment of chlorobenzene molecules is far higher than phenol.

(2) The diffusive flux of pollutant molecules depends on the partial pressure of pollutant at bubble-bulk interface, which in turn depends on the concentration or mole fraction of the pollutant in the bulk liquid at the interface. As mentioned earlier, this mole fraction is given as: $x_{pR} = x_p K_{\text{interface-bulk}}$. Thus, a rise in either x_p (overall mole fraction of pollutant) or $K_{\text{interface-bulk}}$ (interfacial partition coefficient, which increases with salt addition) would raise the partial pressure of pollutant. However, the maximum limit to x_{pR} is decided by the solubility of pollutant. As seen from table 5.1, in case of chlorobenzene, the partition coefficients are high while solubility is quite small (0.5 g/l), due to its hydrophobic nature. As a result, the interfacial region always remains saturated with chlorobenzene for all experimental conditions. Thus, the diffusive flux and entrapment of chlorobenzene remains practically unchanged irrespective of initial concentration and salt addition. In case of phenol, however, partition coefficients are relatively small due to its hydrophilic nature and the solubility is much higher (8 g/l). Therefore, the liquid in the interfacial region is considerably unsaturated. Increasing the bulk concentration or salt addition to the solution causes a net rise in the interfacial concentration of phenol, which raises its partial pressure. This results in an augmentation in the diffusive flux and the entrapment of phenol.

An immediate conclusion, which can be drawn from the results presented above, is that principal contribution to the sonochemical degradation of chlorobenzene is through pyrolysis route, while the principal contribution to the sonochemical degradation of phenol is through the hydroxylation route. This conclusion is further corroborated by the composition of various species generated in the bubble during transient collapse. As mentioned earlier,

Table 5.3. (A) Simulation Results for the Phenol Solution

Species	Parameters for simulation			
	50 ppm solution	**50 ppm solution with 4% w/v NaCl**	**100 ppm solution**	**100 ppm solution with 4% w/v NaCl**
	Conditions at the first compression of the bubble			
	T_{max} = 2926 K	T_{max} = 2716 K	T_{max} = 2991 K	T_{max} = 2578 K
	N_{ph} = 8907	N_{ph} = 26300	N_{ph} = 20150	N_{ph} = 49500
	N_w = 9.25E+09	N_w = 7.41E+09	N_w = 1.06E+10	N_w = 7.13E+09
Equilibrium composition of different radical species in the bubble at collapse (mole fraction)				
O_2	8.644E-01	8.030E-01	8.784E-01	7.727E-01
H_2O	1.214E-01	1.866E-01	1.062E-01	2.194E-01
OH	1.090E-02	8.492E-03	1.158E-02	6.512E-03
O	1.862E-03	9.104E-04	2.261E-03	6.619E-04
HOO	1.202E-03	8.849E-04	1.300E-03	5.345E-04
H_2	1.051E-04	8.600E-05	1.095E-04	6.226E-05
H_2O_2	7.164E-05	6.611E-05	7.245E-05	5.387E-05
H	2.945E-05	1.474E-05	3.551E-05	9.292E-06
O_3	2.913E-05	1.428E-05	3.535E-05	8.672E-06
CO_2	1.863E-06	5.117E-06	4.278E-06	8.007E-06
CO	1.136E-08	1.555E-08	3.161E-08	1.650E-08

some of the intermediate species observed during sonochemical degradation of chlorobenzene comprise of HCl, HOCl and $Cl^{\bullet}$. The simulation results for the radial bubble motion in chlorobenzene solution indeed show formation of these species during transient collapse of the bubble. On the other hand, the amount of phenol molecule entrapment in the bubble is quite small, and hence, the composition of the bubble contents at the transient collapse is dominated by radical species generated out of dissociation of water molecules such as $OH^{\bullet}$, $H^{\bullet}$ and $HO_2^{\bullet}$. These species react with the phenol molecules present in the bubble-bulk interfacial region forming hydroxylated products such as hydroquinone and catechol, which have been observed as degradation intermediates, as noted earlier.

Table 5.3. (B) Simulation Results for the Chlorobenzene Solution

Species	Parameters for simulation			
	50 ppm solution	**50 ppm solution with 4% w/v NaCl**	**100 ppm solution**	**100 ppm solution with 4% w/v NaCl**
	Conditions at the first compression of the bubble			
	T_{max} = 2383 K	T_{max} = 2753 K	T_{max} = 2383 K	T_{max} = 2753 K
	N_{cb} = 8.1E+05	N_{cb} = 9.412E+05	N_{cb} = 8.1E+05	N_{cb} = 9.412E+05
	N_w = 1.0502E+10	N_w = 1.18E+10	N_w = 1.0502E+10	N_w = 1.18E+10
Equilibrium composition of different radical species in the bubble at collapse (mole fraction)				
O_2	6.994E-01	8.188E-01	6.994E-01	8.188E-01
H_2O	2.955E-01	1.700E-01	2.955E-01	1.700E-01
OH	4.262E-03	8.826E-03	4.262E-03	8.826E-03
O	2.207E-04	1.037E-03	2.207E-04	1.037E-03
HOO	4.127E-04	9.384E-04	4.127E-04	9.384E-04
CO_2	1.375E-04	1.817E-04	1.375E-04	1.817E-04
H_2	3.879E-05	8.732E-05	3.879E-05	8.732E-05
H_2O_2	3.963E-05	6.695E-05	3.963E-05	6.695E-05
HCl	2.113E-05	2.540E-05	2.113E-05	2.540E-05
O_3	3.702E-06	1.658E-05	3.702E-06	1.658E-05
H	3.049E-06	1.647E-05	3.049E-06	1.647E-05
Cl	1.182E-06	3.306E-06	1.182E-06	3.306E-06
ClO	3.504E-07	1.163E-06	3.504E-07	1.163E-06
CO	1.035E-07	6.230E-07	1.035E-07	6.230E-07
HOCl	2.675E-07	5.066E-07	2.675E-07	5.066E-07
ClO_2	1.233E-09	6.043E-09	1.233E-09	6.043E-09
Cl_2	1.972E-10	4.655E-10	1.972E-10	4.655E-10

Note for Table 5.3A & B: *In the equilibrium composition, the number format is as follows: 2.075E-07 should be read as: 2.075 $\times 10^{-7}$. Species having equilibrium mole fraction less than 10^{-10} have been ignored. Species with Nitrogen as a constituent element have been ignored, as they are found in traces and contribute little in the degradation reaction. Notations: T_{max} = Temperature in the bubble at the instance of first compression; N_W = water molecules trapped in the bubble at the instance of first compression; N_{ph} = phenol molecules trapped in the bubble during transient collapse; N_{cb} = chlorobenzene molecules trapped in the bubble during transient collapse.*

The overall degradation of both phenol and chlorobenzene increases with bulk concentration. Rise in bulk concentration influences both the pathways of degradation, i.e. pyrolysis and hydroxylation, to certain extent. Simulation results help us determine this

extent for the two pollutants. As far as chlorobenzene is concerned the bubble-bulk interface is always saturated and increasing bulk concentration does not make any change. Hence, the diffusive flux and entrapment of chlorobenzene molecules remains practically unaltered with changes in bulk concentration. Moreover, the degree of hydroxylation reaction occurring in the interfacial region also does not change, as the pollutant concentration in this region is already at its maximum. With this, the rise in the extent of degradation is clearly attributed to larger degradation (mostly by hydroxylation) occurring in the bulk liquid, due to higher probability of interaction between radicals and pollutant molecules. For phenol, the mechanism is different. In this case, the liquid at the interfacial region is considerably unsaturated. With rise in bulk concentration, the concentration in the interfacial region also increases. This has two evident consequences: rise in the diffusive flux and entrapment of phenol molecules in the bubble, and secondly, increase in the probability of radical-pollutant interaction, which increases the degree of hydroxylation region occurring in the interfacial region.

The difference in the extent of degradation of phenol and chlorobenzene under similar conditions can be explained on the basis of simulation results. The entrapment of chlorobenzene molecules in the bubble is quite high. These molecules undergo complete degradation (or mineralization) at the extremes of temperature and pressure generated during transient bubble collapse. As a result, the degradation of chlorobenzene is rapid, with more than 60% of pollutant degraded in 90 minutes. Degradation of phenol occurs outside the bubble. Due to rather dilute solution used in the experiments, the probability of interaction of phenol molecules with radical species is relatively low. Hence, not all of the radical species generated by the bubble undergo reaction with phenol. Most of the species mere recombine to yield O_2, H_2O_2 and H_2O without inducing any degradation reaction. Accordingly, the extent of degradation is slow.

Assessment of the experimental and simulation results also explains the effect of salt addition on the degradation rate of the two pollutants. As stated earlier, the addition of salt increases the ionic strength of the solution that enhances the hydrophobic repulsive interactions between aqueous phase and pollutant, which drives the pollutant molecules towards bubble-bulk interface. Therefore, the concentration of the pollutant in the bubble-bulk interfacial region increases. This phenomenon has two consequences that contribute towards the enhancement of degradation. Firstly, the partial pressure of the pollutant at the interface increases. This results in rise of the diffusive flux and entrapment of pollutant molecules in the bubble. Thus, the contribution of the pyrolysis pathway to the degradation increases. Secondly, the probability of interaction between radical and pollutant molecule in the interfacial region also increases, which increases the extent of hydroxylation reaction occurring in this region. However, the magnitude of salt induced enhancement is different for the two pollutants. For chlorobenzene, as the interfacial region is always saturated, neither the entrapment of molecules nor the interactions with radicals change with salt addition. As a result, the extent of degradation practically remains constant. On the other hand, entrapment of phenol molecules rises by ~ 3 fold with salt addition. Therefore, contribution of the pyrolysis route to phenol degradation boosts drastically. Secondly, the net production of the $OH^{\bullet}$ radicals per bubble remains practically constant with salt addition to the solution but the net utility of these radicals for the degradation of pollutant increases. Higher concentration of phenol molecules near bubble-bulk interface also raises the probability of interaction with radical species, which further adds to the degradation via hydroxylation route. On the whole, salt addition causes a sharp rise in the overall degradation of phenol in 90 min of sonication.

5.5 CONCLUSION

In this chapter, we have tried to explain the physical or mechanistic features of the sonochemical degradation of volatile and non-volatile organic pollutants. With experiments using chlorobenzene and phenol as model pollutants and a mathematical model for radial motion of cavitation bubbles, we have explored some remarkable mechanistic features of the sonochemical degradation of these pollutants. Our results reveal that thermal decomposition or pyrolysis in the cavitation bubble is the predominant mechanism of degradation of volatile pollutants while hydroxylation in the bulk medium is the principal pathway for the degradation of non-volatile pollutants. These results are in accordance with the previous literature in which intermediates and products of the degradation reaction have been used to determine the mechanism of sonochemical degradation. We have also investigated changes in the extent of degradation with variation of some experimental parameters such as bulk concentration of pollutant and salt addition to the solution of pollutant. Concurrent evaluation of experimental and simulation results reveals that these parameters influence both the pathways of degradation. However, the magnitude of this influence is different for phenol and chlorobenzene, which is attributed to the different nature (hydrophobic and hydrophilic) of the pollutant. To conclude, this study provides a framework for deducing the mechanistic features of the sonochemical degradation of organic pollutants, knowledge of which is of paramount importance in designing large-scale processes for ultrasound-aided wastewater treatment.

CHAPTER 6

PHYSICAL FEATURES OF SONOCHEMICAL DEGRADATION OF NITROAROMATIC POLLUTANTS

6.1 INTRODUCTION

This chapter addresses the matter of mechanistic or physical features of the sonochemical degradation of nitroaromatic compounds. Nitroaromatics are omnipresent pollutants in industrial wastewater. Some common pollutants in this category are nitrobenzene, p-nitrophenol, p-nitrophenyl acetate, nitrotoluene, aniline, dinitrobenzene etc. We select two model nitroaromatic compounds for our study, viz. nitrobenzene and p-nitrophenol. Nitrobenzene is primarily a synthetic compound used in production of aniline, which is a major intermediate in chemical industry for polyurethane production. In the pharmaceutical industry nitrobenzene is used in the production of the analgesic acetaminophen, or paracetamol. Nitrobenzene is also used in shoe and floor polishes, leather dressings, paint solvents to mask unpleasant odors, and solvent for cellulose ethers and acetate. p-nitrophenol is an intermediate in synthesis of azodyes and a number of pesticides, mainly insecticides such as parathion, parathion-methyl, and to a lesser extent herbicides such as nitrofen and bifenox.

The review of the literature in the area of sonochemical degradation of nitrobenzene and p-nitrophenol has been given in chapter 1. The chemical mechanisms of the degradation of p-nitrophenol and nitrobenzene have been well established on the basis of intermediate and products of the degradation process. The principal degradation products for sonochemical

degradation of nitrobenzene at low frequency (20 kHz) are 4-nitrophenol, 3-nitrophenol and 4-nitrocatechol (Weavers *et al.*, 1998). These products hint at hydroxylation (or reaction with OH radicals generated from cavitation bubbles) as the major chemical pathway for degradation. Cropek and Kemme (1998) have also reported formation of phenol and benzoquinone as degradation products of nitrobenzene. Kotronarou *et al.* (1991) have reported degradation products of p-nitrophenol (for 20 kHz frequency) as NO_2^-, NO_3^-, benzoquinone, hydroquinone, 4-nitrocatechol, formate and oxalate. On the basis of these products, Kotronarou *et al.* (1991) have proposed that the major chemical mechanism for degradation of p-nitrophenol was carbon-nitrogen bond cleavage in the interfacial region of cavitation bubbles with hydroxylation in bulk medium providing secondary reaction channel.

This study attempts to discern the physical mechanism of the sonochemical degradation of nitrobenzene and p-nitrophenol using similar approach as earlier chapters, i.e. correlating the extent of degradation of the two pollutants under similar conditions to the physical properties of the pollutants and the fundamental phenomena of transport of vapor of water and organic pollutant across cavitation bubble using a bubble dynamics model that takes into account essential physics and chemistry of cavitation bubbles. Apart from establishing the predominant physical mechanism for the sonochemical degradation of nitroaromatic pollutants, this study also gives hints for the intensification of the process.

6.2 SONOCHEMICAL DEGRADATION OF ORGANIC POLLUTANTS: SOME THEORETICAL CONSIDERATIONS

Prior to describing the main components (experimental, bubble dynamics modeling and results) of the paper, we would like to depict the objectives and approach of our study. The rate of sonochemical degradation of a pollutant through hydroxylation route [Pollutant] + [$OH^\bullet$] $\rightarrow$ [Products] is written as: $-r_d = k_d[\text{Pollutant}][\text{OH}]$. This rate depends

on the concentration of pollutant molecules and the concentration of radicals produced from cavitation bubbles. Increasing either or both of the quantities increases the rate of degradation of pollutant. We have demonstrated in a previous work that extent of radical production by the cavitation bubbles, and hence, the concentration of the radicals in the liquid medium can be increased by reducing the dissolved gas content of the medium (Sivasankar *et al.*, 2007). For the sonochemical reactions an additional factor that influences the rate is the probability of interaction between radicals and the pollutant molecules. The phenomenon of production of radicals from cavitation bubbles in the liquid medium is rather local (maximum at the interfacial region between bubble and bulk medium) and not uniform throughout the medium. The radicals are extremely reactive and they react almost instantly after being released into the medium with transient collapse of the bubble. If the concentration of the pollutant molecules in the bubble-bulk interfacial region is low, the radicals may merely recombine, which is loss in the oxidation potential. The lower the concentration of the pollutant in the bulk medium, the greater is the impact of the probability factor on overall degradation of the pollutant. An obvious technique for the effective utilization of the radicals produced from cavitation bubbles would be to increase the concentration of pollutant molecules in the interfacial region. An alternate technique for the same purpose would be to scavenge the radicals released from the cavitation bubble. The word scavenging means reacting the radicals with other species in the medium (present in sufficiently large quantities) to generate new radical species. Scavenging of radicals has two consequences that contribute towards enhancing the degradation of pollutant: (1) prevention of the recombination of radicals and (2) penetration or diffusion of radicals in the bulk medium to greater distances from location of the collapse of the bubble, which increases the probability of radical-pollutant interaction.

Another important aspect is the nature of the pollutant itself. If the pollutant is hydrophobic in nature, characterized by low solubility in water, it tends to partition between

bulk medium and bubble interface (Seymour and Gupta, 1997; Bapat *et al.*, 2007). The bubble-bulk interface also has hydrophobic character, and hence, the concentration of the hydrophobic pollutant molecules in this region is much higher than the bulk. On the other hand, the hydrophilic pollutant (characterized by relatively large solubility in water) has more-or-less uniform concentration throughout the medium. A consequence of this in the context of sonochemical degradation of pollutants (through hydroxylation route) is in terms of effective interception of the radicals produced from the bubble in the interfacial region of the bubble and bulk medium. For a hydrophobic pollutant, the probability of interaction between pollutant molecules and radicals is high as the interfacial region between bubble and bulk is also rich in radical concentration, as noted earlier. For the degradation of hydrophilic pollutant, the interfacial concentration is low, and hence, the probability of interaction with radical in the interfacial region is small. In such a situation, phenomenon of radical scavenging in the medium can favorably affect the rate of degradation.

An easy technique to raise the interfacial concentration of a pollutant would be addition of an electrolyte (i.e. NaCl) to the medium (Seymour and Gupta, 1997; Bapat *et al.*, 2007). With addition of salt, the ionic strength of the medium increases, and hence, the hydrophobic repulsive interactions between the pollutant and water molecules increase. The pollutant molecules are driven towards the bubble-bulk interface.

Prominent species that contribute to radical scavenging in the medium is the dissolved oxygen. The dissolved oxygen present in the medium can react with H radicals generated from cavitation bubbles (via dissociation of entrapped water molecules) as follows:

$$H_2O \rightleftharpoons H^{\bullet} + OH^{\bullet} \qquad \text{(R.6.1)}$$

$$H^{\bullet} + O_2 \rightleftharpoons O^{\bullet} + OH^{\bullet} \qquad \text{(R.6.2)}$$

$$H^{\bullet} + O_2 \rightleftharpoons HO_2^{\bullet} \qquad \text{(R.6.3)}$$

Dissolved oxygen can also revert, to some extent, the loss of oxidation potential through

recombination of OH radicals as follows:

$$OH^{\bullet} + OH^{\bullet} \rightleftharpoons H_2O_2 \qquad \text{(R.6.4)}$$

$$H_2O_2 + O_2 \rightleftharpoons 2HO_2^{\bullet} \qquad \text{(R.6.5)}$$

Finally, the dissolved oxygen can also react with $OH^{\bullet}$ radicals released in the medium to generate additional oxidizing species:

$$OH^{\bullet} + O_2 \rightleftharpoons HO_2^{\bullet} + O^{\bullet} \qquad \text{(R.6.6)}$$

Scavenging of the radicals can also be achieved using ionic species such as Fe^{2+} (added in the form of $FeSO_4 \cdot 7H_2O$). The scavenging action of Fe^{2+} is described by following equations:

$$OH^{\bullet} + OH^{\bullet} \rightleftharpoons H_2O_2 \qquad \text{(R.6.4)}$$

$$H_2O_2 + Fe^{2+} \longrightarrow Fe^{3+} + OH^- + OH^{\bullet} \qquad \text{(R.6.7)}$$

It can be seen that Fe^{2+} ions are oxidized to Fe^{3+} in the process of scavenging of OH radicals. However, Fe^{2+} ions are regenerated in the medium by following reactions:

$$Fe^{3+} + H_2O_2 \longrightarrow Fe^{2+} + HO_2^{\bullet} + H^+ \qquad \text{(R.6.8)}$$

$$Fe^{3+} + HO_2^{\bullet} \longrightarrow Fe^{2+} + O_2 + H^+ \qquad \text{(R.6.9)}$$

Due to continuous regeneration, the average concentration of Fe^{2+} in the bulk medium stays very nearly constant. Due to this feature, Fe^{2+} can provide effective scavenging of radicals in the bulk medium; outcome of which is an effective degradation of the pollutant through hydroxylation route.

Experiments in this work have been planned on the basis of above contemplations.

6.3 EXPERIMENTAL

6.3.1 Reagents

Nitrobenzene (Merck, Grade: Synthesis), *p*-nitrophenol (Loba Chemicals, Grade: Pure), Sodium hydroxide (Merck, Grade: Purified pellets), Ferrous sulphate heptahydrate

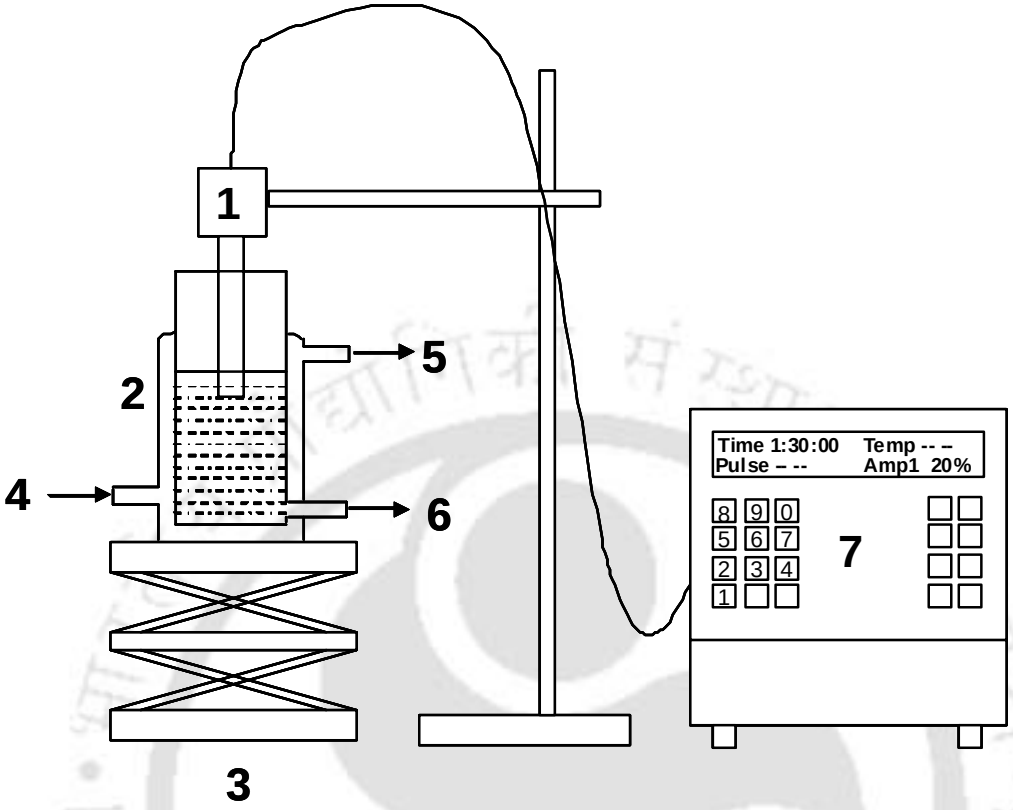

Figure 6.1. Schematic of the experimental set-up [Legends: 1. Ultrasound horn; 2. Jacketed glass reactor; 3. Laboratory jack; 4. Cooling water inlet; 5. Cooling water outlet; 6. Sample port; 7. Microprocessor based control unit of ultrasonic processor].

($FeSO_4 \cdot 7H_2O$, Merck, Grade: Purified crystals), Acetonitrile (Merck, Grade: HPLC) and Water (Merck, Grade: HPLC) were used as procured without any further purification. The solution of the two pollutants was prepared using water from Millipore (Model: Elix 3).

6.3.2 Experimental setup

A schematic diagram of the experimental setup used in the present study is shown in Fig. 6.1. A microprocessor based and programmable ultrasound processor (Sonics and Materials Inc., Model VCX 500) was used for sonication of the aqueous solution of the pollutant. The frequency of the processor was 20 kHz with maximum power output of 500W. The ultrasound probe of the processor was fabricated from high-grade titanium alloy and had

a tip diameter of 13 mm. With a variable power output control, the net consumption of power during sonication was set at 100W (20% of the maximum value). The actual value of the ultrasound intensity in the medium was determined using calorimetry (Sivasankar *et al.*, 2007). For a power output of 100W the ultrasound probe produced an acoustic wave with 1.5 bar amplitude. The processor had facility of automatic frequency tuning and amplitude compensation, which ensures constant power delivery to the ultrasound probe irrespective of the changes occurring in the liquid medium during degradation process. For the sonication of the pollutant solution, a jacketed glass reactor (dimensions: height–120 mm, diameter–50 mm, jacket diameter–62 mm) was used. This reactor was positioned on a laboratory jack, which could be raised or lowered for exact positioning of the ultrasound probe in the solution. The tip of the ultrasound probe was placed 15 mm below liquid surface so as to ensure effective coupling between tip of the horn and the bulk liquid medium.

6.3.3 Experimental procedure

The volume of the reaction medium used for sonication was 150 ml. The initial concentration of the nitrobenzene solution was 100 ppm, while the concentration of *p*-nitrophenol solution was 10 ppm. The total sonication time was 90 min. Sonication was done intermittently with cycles of 15 min on and 5 min off period. Cooling water was circulated through the jacket of the reactor throughout the experiment in order to remove the heat generated during sonication. A combination of these two procedures maintains the temperature of the reaction medium almost constant. The temperature of the reaction medium was monitored using a digital thermometer. The rise in the temperature during the total reaction period was ~ 2ºC. The experiments were done in two categories:

Category I: Sonication with saturated liquid medium

In this category, experiments were done with three techniques:

(1) Sonication of the pollutant solution in pure form (without any additives).

(2) Sonication of the pollutant solution with 0.5mM $FeSO_4 \cdot 7H_2O$ (which is a radical scavenging species) added to the solution.

(3) Sonication of the pollutant solution with addition of 4% w/v NaCl.

All of the above techniques were adopted for degradation of both *p*-nitrophenol and nitrobenzene. However, as noted earlier, the initial concentrations of the two pollutants were different. To assess the reproducibility of results, all experiments were performed in triplicate and average of the degradation obtained in these experiments been considered for analysis.

Category II: Sonication with unsaturated medium

In this category of experiments, the dissolved oxygen content of the aqueous solution of the pollutant was reduced prior to sonication by means of applying vacuum for about 40 minutes. The vacuum pump used for this purpose (Riviera, Model: TID-25-S) produced a vacuum of 700 mm Hg. During vaccumization, the solution of the pollutant was stirred intermittently, which helped in the effective removal of gas bubbles attached to solid boundaries such as wall of the reactor or the surface of the magnetic needle. With this procedure, the solution of the pollutant becomes highly unsaturated with dissolved oxygen content reduced to 2.7 ppm. Using this unsaturated solution, experiments were conducted applying the three techniques mentioned earlier. Once again, all experiments were done in triplicate and the average percentage degradation is considered for analysis.

The saturation level of the medium rises slowly during experiments due to dissolution of air in it. In order to maintain the unsaturation of the liquid medium, the dissolved oxygen content of the medium was monitored during the silent period of reaction using a DO meter. The reaction mixture was degassed again once the dissolved oxygen content increased beyond 4 ppm.

6.3.4 Method of analysis

Nitrobenzene: The extent of sonochemical degradation of nitrobenzene was monitored with

HPLC (Perkin Elmer, Model: Series 200). A C18 column (Make: Chromatopak) with dimension of 250 mm (length) × 4.5 mm (inner diameter) with the packing of 5 µm size silica particles was used. The mobile phase was a mixture of acetonitrile and water (80: 20). The sample injection volume is 20 µl and the eluent flow rate was maintained at 1ml/min. The UV detector wavelength for nitrobenzene was 254 nm. We would like to categorically state that we have not made an analysis of the intermediate products of degradation of nitrobenzene as these have been well studied and documented in the literature mentioned earlier. We have monitored the rate of disappearance of original pollutant and the analysis has been made on that basis.

***p*-Nitrophenol:** Sonochemical degradation of p-nitrophenol was analyzed using UV-Vis spectrophotometer (Perkin Elmer, Model: Lamda 35). Before analysis, the sample is made alkaline (with pH of the solution raised to 11) by adding few drops of 0.5 N sodium hydroxide solution. The peak absorbance spectrum occurred at 355 nm. With addition of $FeSO_4 \cdot 7H_2O$ to the medium, the peak of the absorbance spectrum shifts from 355 nm to 395 nm. Hence, a separate calibration charts were prepared for measuring the concentration of p-nitrophenol in pure solution and $FeSO_4$-added solution. Like analysis of nitrobenzene, only the reduction in concentration of original pollutant is considered for analysis and no attempt is made to quantify the degradation intermediates as these have been well studied and documented in previous literature.

6.3.5 Surface tension measurement

Surface tension of water is likely to alter with addition of pollutant to it. This is an important physical property of the liquid medium, which influences the radial motion and the intensity of the transient collapse of the cavitation bubble in the solution. Therefore, surface tension of the aqueous solutions of both pollutants (with concentration of 100 ppm for nitrobenzene and concentration of 10 ppm for p-nitrophenol) was measured using a

tensiometer (Make: Krűss, Model: K9). The Wilhemy plate method was used to measure surface tension of the solutions of pollutants. All the surface tension measurements were done at room temperature (i.e. 25ºC). For a 10 ppm p-nitrophenol solution and 100 ppm nitrobenzene solution, the surface tensions were found to be 63.4 mN/m and 70.1 mN/m, respectively. These values have been used in simulation of radial motion of cavitation bubble.

6.4 MATHEMATICAL FORMULATION

The model used in this chapter is essentially same as in earlier chapters. The approximations made (single bubble analysis and assumption of attainment of thermodynamic equilibrium in the bubble) are also same as earlier chapters. However, in this chapter we also try to account for the heating up of the thin liquid shell surrounding the bubble. This feature is incorporated for the analysis of the sonochemical degradation of p-nitrophenol. For the convenience of the reader we reproduce here major components of the model. For other details, we refer the reader to earlier chapters. As no particular gas (such as argon or oxygen) was sparged through the reaction mixture, we have considered an air bubble for the analysis.

6.4.1 Radial motion of the bubble

The bubble motion is described by Keller-Miksis equation (Prosperetti and Lezzi, 1986; Brennen, 1995) as:

$$\left(1-\frac{dR/dt}{c}\right)R\frac{d^2R}{dt^2}+\frac{3}{2}\left(1-\frac{dR/dt}{c}\right)\left(\frac{dR}{dt}\right)^2=\frac{1}{\rho}\left(1+\frac{dR/dt}{c}\right)\left(P_i-P_t\right)+\frac{R}{\rho c}\frac{dP_i}{dt}-4\nu\frac{dR/dt}{R}-\frac{2\sigma}{\rho R} \tag{6.1}$$

where P_t is the time variant pressure in the bulk liquid driving bubble motion. The pressure inside the bubble, P_i is written as:

$$P_i=\frac{N_{tot}(t)kT}{\left[\frac{4\pi}{3}\left(R^3(t)-h^3\right)\right]} \tag{6.2}$$

where h ~ $R_o/8.86$ is the van der Waals hard core radius determined by the excluded volume of gas molecules. Since the hard core radii of the species considered in the present work viz. nitrogen, oxygen and water differ only by a small magnitude, we take a common value for the hard-core radius.

6.4.2 Heat and mass transfer across bubble

Both gas (basically air dissolved in the liquid) and vapor (of water as well as pollutant) diffuse across the bubble wall during radial bubble motion. The time scale of gas diffusion can be given as ~ R_o^2/D where R_o is the initial radius of the bubble (~ 10 μm) and D is the diffusion coefficient (~ 10^{-9} m^2/s). Thus, the time scale of gas diffusion becomes ~ 0.1 ms, which is much higher than the time scale of radial bubble motion (which is same as time scale of ultrasound wave: 50 μsec for 20 kHz wave). Thus, the transport of gas across the bubble during radial motion can be ignored. Diffusion of water and pollutant vapor into the bubble, as a result of evaporation occurring at the bubble interface needs to be taken into account, nonetheless.

Among the two pollutants considered in this work, p-nitrophenol has very small vapor pressure at ambient conditions: 0.003 Pa (Boehncke *et al.*, 2000). In addition, the concentration of p-nitrophenol in solution was also quite dilute (10 ppm). As a result, the equilibrium vapor pressure or partial pressure of p-nitrophenol in the bulk medium is negligibly small. Due to hydrophobic repulsive interactions with water molecules, enrichment of p-nitrophenol occurs at the bubble-bulk interface. Despite this, the partial pressure of p-nitrophenol at the bubble-bulk interface is not likely to rise significantly. Due to very low partial pressure at the bubble-bulk interface, the evaporation of p-nitrophenol into the bubble during expansion is negligible and can be ignored.

The temperature inside the bubble exceeds the surface temperature of the bubble (which is same as bulk liquid temperature) only for a very brief moment during collapse. On

the basis of this condition, the bubble can be divided into two parts: (1) a "cold" boundary layer in thermal equilibrium with the liquid, and (2) a hot homogeneous core. An underlying assumption in this hypothesis is that the condensation of water molecules at the bubble wall is fast enough to maintain equilibrium phase change. By dimensional analysis, the instantaneous diffusive penetration depth for water vapor and pollutant vapor are given by: $l_{diff} = \sqrt{D_w t_{osc}}$ and $l_{diff} = \sqrt{D_p t_{osc}}$ respectively, where t_{osc} is the time scale of bubble oscillations given as $R/|dR/dt|$ and D_p and D_w are the diffusion coefficients of pollutant and water molecules. The rate of change of water molecules in the bubble by diffusion is given by:

$$\frac{dN_w}{dt} = 4\pi R^2 D \left.\frac{\partial C_w}{\partial r}\right|_{r=R} = 4\pi R^2 D \left(\frac{C_{wR} - C_w}{l_{diff}}\right) \qquad (6.3a)$$

$$\frac{dN_p}{dt} = 4\pi R^2 D \left.\frac{\partial C_p}{\partial r}\right|_{r=R} = 4\pi R^2 D_p \left(\frac{C_{pR} - C_p}{l_{diff}}\right) \qquad (6.3b)$$

where C_{wR} and C_{pR} is the equilibrium concentrations of water and pollutant molecules at the bubble wall. These are calculated using the partial pressures (or equilibrium vapor pressures) of water and pollutant at the bubble wall corresponding to bulk liquid temperature. C_w and C_p are the concentrations of water and pollutant molecules in the bubble core. It should be noted that the initial water and pollutant vapor content of the bubble is zero, i.e. at $t = 0$, the bubble initially comprises of air only.

With complete analogy with mass transfer, the heat transfer across bubble wall is given by:

$$\frac{dQ}{dt} = 4\pi R^2 \lambda \left(\frac{T_o - T}{l_{th}}\right) \qquad (6.4)$$

where λ is the thermal conductivity of the bubble contents and l_{th} is the thermal diffusion length written as: $l_{th} = \sqrt{\kappa t_{osc}}$. The thermal diffusivity, κ of the gas-vapor mixture in the

Table 6.1. Thermodynamic properties of various species

Species	Degree of freedom (*f*)	Molecular specific heat (C_P)	Molecular specific heat (C_V)
N_2	5	$\frac{7}{2}k$	$k\left(\frac{5}{2}+\frac{\left(\theta_{N_2}/T\right)^2\exp\left(\theta_{N_2}/T\right)}{\left(\exp\left(\theta_{N_2}/T\right)-1\right)^2}\right)$
O_2	5	$\frac{7}{2}k$	$k\left(\frac{5}{2}+\frac{\left(\theta_{O_2}/T\right)^2\exp\left(\theta_{O_2}/T\right)}{\left(\exp\left(\theta_{O_2}/T\right)-1\right)^2}\right)$
H_2O	6	$4k$	$k\left(3+\sum_i^3\frac{\left(\theta_{i,H_2O}/T\right)^2\exp\left(\theta_{i,H_2O}/T\right)}{\left(\exp\left(\theta_{i,H_2O}/T\right)-1\right)^2}\right)$

Note: θ_i s are the vibrational temperatures of various species: θ_{N_2} = 3350 K, θ_{O_2} = 2273 K, θ_{1,H_2O} = 2295 K, θ_{2,H_2O} = 5255 K, θ_{3,H_2O} = 5400 K.

bubble is calculated as: $\kappa=\frac{\lambda}{\rho_{mix}C_{p,mix}}$, where $\rho_{mix}C_{p,mix}=\sum_i\rho_iC_{pi}$, ρ_is are the densities of the species present in the bubble (in molecule/m^3) and C_{pi}s are the molecular specific heats of these species. Values of C_{pi} for various species are listed in Table 6.1.

Limits on the diffusion length: At the instances of maximum and minimum radius, the bubble wall velocity is zero, and thus, an alternate expression is needed for diffusion length. We set this limit as R/π after identifying that vapor transport is governed by pure diffusion equation for condition $dR/dt=0$. The limit R/π is set on the basis of solution of the diffusion equation in spherical geometry. For greater details on this, we refer the reader to our earlier papers (Krishnan *et al.*, 2006; Kumar and Moholkar, 2007). Thus, the expressions for the mass and thermal diffusion length are given as:

$$l_{diff}=\min\left(\sqrt{\frac{RD_w}{|dR/dt|}},\frac{R}{\pi}\right)\text{ and }\min\left(\sqrt{\frac{RD_p}{|dR/dt|}},\frac{R}{\pi}\right) \quad (6.5a)$$

$$l_{th}=\min\left(\sqrt{\frac{R\kappa}{|dR/dt|}},\frac{R}{\pi}\right) \quad (6.5b)$$

It needs to be mentioned that a thin shell of liquid surrounding the bubble also gets heated up during transient collapse due to heat transfer out of the bubble. The present model assumes a cold bubble-bulk interface, and hence, the temperature attained by the liquid in this shell cannot be estimated with this model. Nonetheless, the thickness of this liquid shell ($l_{th\text{-}L}$) can be estimated with the simulation results using dimensional analysis. The thermal diffusion length in the liquid medium is: $\sqrt{\frac{R\kappa_L}{|dR/dt|}}$, where κ_L is the thermal diffusivity of the liquid medium, i.e. water. Once again, we set the limit for the diffusion length at the instances of minimum and maximum radius during bubble collapse as R/π, and hence, $l_{th-L} = \min\left(\sqrt{\frac{R\kappa_L}{|dR/dt|}}, \frac{R}{\pi}\right)$.

6.4.3 Transport parameters for the bubble

Diffusion coefficient: The diffusion coefficient for the transport of water vapor and pollutant vapor across the bubble has been determined using the Chapman-Enskog theory using Lennard-Jones 12-6 potential. For greater details on calculation of diffusion coefficient, we refer the readers to our earlier chapters.

Thermal conductivity: As noted earlier, water vapor as well as pollutant vapor evaporates into the bubble during expansion phase. The extent of evaporation, however, depends on the partial pressure at the bubble interface. The partial pressure of a species is given as the product of mole fraction of the species in the solution and the vapor pressure at given temperature. The concentration of nitrobenzene in the solution is quite dilute (100 ppm). Moreover, the vapor pressure of nitrobenzene is two orders of magnitude small (~ 30 Pa) than that of water (~ 2500 Pa) at ambient conditions. Therefore, evaporation of water in the bubble is expected to be far higher than that of pollutant, and at any moment during radial motion the bubble contents primarily comprise of air and water vapor. In view of this, we

estimate the effective thermal conductivity of the bubble contents on the basis of two species, viz. water and air, ignoring the pollutant vapor present in the bubble. A semi-empirical method has been used for calculation of the thermal conductivity, described in Hirschfelder *et al.* (1954). This method uses thermal conductivity of the individual components, viz. oxygen, nitrogen and water. These have been calculated using Chapman-Enskog theory using Lennard-Jones 12-6 potential. For the polyatomic species, Eucken correction has been applied. For greater details on this, we refer the readers to earlier chapters.

6.4.4 Overall energy balance

During radial motion, both heat and mass transfer occurs across the bubble wall, and thus the overall energy balance for the bubble contents is written as:

$$\frac{dE}{dt} = \frac{dQ}{dt} - \frac{dW}{dt} + h_w \frac{dN_w}{dt} \tag{6.6}$$

The total energy E of the bubble is a function of temperature and volume of the bubble and the number of molecules of various gas and vapor species in it. Therefore, the energy balance for the air bubble is written as:

$$\frac{dE}{dt} = \left(\frac{\partial E}{\partial N_{N2}}\right)_{Nw,N_{O2},V,T} \frac{dN_{N2}}{dt} + \left(\frac{\partial E}{\partial N_{O2}}\right)_{N_{N2},Nw,V,T} \frac{dN_{O2}}{dt} + \left(\frac{\partial E}{\partial N_w}\right)_{N_{N2},N_{O2},V,T} \frac{dN_w}{dt} + \left(\frac{\partial E}{\partial T}\right)_{Nw,N_{N2},N_{O2},V} \frac{dT}{dt} + \left(\frac{\partial E}{\partial V}\right)_{Nw,N_{N2},N_{O2},T} \frac{dV}{dt} \tag{6.7}$$

where N_{N2} and N_{O2} are the number of molecules of nitrogen and oxygen respectively in the bubble. As we neglect the change in the gas content of the bubble for the reasons stated earlier, and thus, $dN_{N2}/dt = dN_{O2}/dt = 0$ for air. The term dN_w/dt is the rate of change of water vapor content of the bubble and is evaluated according to equation 6.3. The specific enthalpy of the water molecules entering the bubble from cold bubble interface is: $h_w = 4kT_o$. The specific energy of the water molecules in the bubble is the thermal energy, and is written in

terms of vibrational temperatures as:

$$\left(\frac{\partial E}{\partial N_w}\right) = U_w = N_w kT\left(3 + \sum \frac{\theta_i / T}{\exp(\theta_i / T) - 1}\right) \qquad (6.8)$$

The work done by the bubble is the expansion work: $P_i\, dV$. Moreover, $(\partial E/\partial T) = C_V$ and $(\partial E/\partial V) = 0$, as the internal energy of an ideal gas mixture is a function of its temperature and composition. With inclusion of various terms above in the overall energy balance, we obtain an equation for the change in the temperature of the bubble as:

$$C_{V,mix}\frac{dT}{dt} = \frac{dQ}{dt} - P_i dV + (h_w - U_w)\frac{dN_w}{dt} \qquad (6.9)$$

The specific heat of the gas-vapor mixture ($C_{V,mix}$) present in the bubble is written as:

$$C_{V,mix} = \sum_i C_{V,i} N_i \qquad \text{where } i = N_2, O_2 \text{ and } H_2O \qquad (6.10)$$

where $C_{V,i}$ is the molecular specific heat of species i, and N_i is the number of molecules of that species present in the bubble. The C_V values for the various species considered in this work are listed in Table 6.1.

6.4.5 Numerical solution

The equations 6.1, 6.3 and 6.9 constitute complete formulation for the radial motion of cavitation bubble with associated heat and mass transfer effects. This set of simultaneous ODEs can be solved using Runge-Kutta 4th order – 5th order adaptive step size method (Press *et al.*, 1992). The cavitation bubble may collapse at the instance of maximum compression during radial motion. The word "collapse" essentially means fragmentation of the cavitation bubble. This factor depends on many factors such as shape (or surface) instability of bubbles, the local flow conditions and the bubble population density in the vicinity of the bubble. For conditions of maximum shape and flow instability, the cavitation bubble fragmentation can occur at the first compression after an initial expansion. In view of this, the condition for the bubble collapse is taken to be first compression during radial motion. Four important

parameters required for the simulation of the radial motion of the cavitation bubble are: (1) frequency and (2) pressure amplitude of ultrasound, (3) vapor pressure of water and (4) initial (or equilibrium) bubble radius. Numerical values for these parameters have been determined as follows:

(1) *Frequency*: The frequency of the ultrasound wave was taken as 20 kHz, which is the frequency of the sonicator used in the experiments.

(2) *Pressure amplitude*: A calorimetric method was used to determine the amplitude of the ultrasound wave emitted by the sonicator probe (Sivasankar *et al.*, 2007). The amplitude of the ultrasound wave generated by the sonicator probe was 1.5 bar. However, due to the attenuation in the medium, the actual pressure amplitude sensed by the cavitation bubble located away from the probe tip is lesser than 1.5 bar. Principal physical factors affecting the attenuation are viscosity of the medium and the size and population density of bubbles in the medium (Mason and Lorimer, 1989; Prosperetti and Commander, 1989). A direct measurement of the local pressure amplitude in the vicinity of the cavitation bubble is beyond the capabilities of the instrumentation used in the present study. Therefore, we assume about 15% attenuation and use a value of 1.3 bar for acoustic pressure amplitude in the numerical simulations.

(3) *Vapor pressure of bulk medium and pollutant*: The vapor pressure of the bulk medium (i.e. water) and pollutant (nitrobenzene) was calculated with Antoine's equations using initial temperature of the solution (25 ^{o}C) as given below:

$$P_w = \frac{10^5}{760}\exp\left(18.3036 - \frac{3816.44}{T - 46.13}\right) \tag{6.11}$$

$$P_{NB} = 10^5 \times 10^{\left(4.21553 - 1727.592/(T - 73.438)\right)} \tag{6.12}$$

The temperature rise during sonication was ~ 2 ^{o}C, as noted earlier. The difference between vapor pressures of water and nitrobenzene at 25 ^{o}C and 27 ^{o}C is quite small (< 10%). Therefore, we have ignored the temperature rise during simulations, assuming the liquid

medium at constant temperature. An alternate approach would be to calculate the vapor pressure of water using average of initial and final temperatures. However, this would make trivial quantitative changes to the simulation results; and the trends in the simulation results remain essentially unchanged. Vapor pressure of water reduces with addition of salt. This reduction is accounted for using formulae given by Al-Shayji (1998).

(4) *Initial (or equilibrium) bubble radius*: This parameter is difficult to estimate. Moreover, the equilibrium size of the bubble keeps on changing due to phenomena such as rectified diffusion, fragmentation of the bubble etc. The minimum radius of the cavitation nuclei which would grow into a bubble for particular amplitude of acoustic wave can be determined by the analysis given by Young (1989). For the acoustic pressure amplitude in the present experiments, this value is ~ 2 μm. We have chosen a representative value of 10 μm for the initial or equilibrium bubble radius for a degassed (or unsaturated) medium and a value of 20 μm for the non-degassed (or saturated) medium.

Equilibrium composition of the various species formed in the bubble with dissociation of entrapped water and pollutant molecules at the conditions of temperature and pressure at first the compression was calculated using software FACTSAGE, which uses the free-energy minimization algorithm proposed by Eriksson (1975). This software has an in-built database of C_p vs. temperature relationship, entropy and heat of formation of all the above species. A more rigorous approach in this regard would be to include various radical reactions in the mass balance equations along with heats of these reactions included in the energy balance (Toegel and Lohse, 2003; Storey and Szeri, 2000). Endothermicity of some of the radical reactions (for example $H_2O \rightleftharpoons H^{\cdot} + OH^{\cdot}$) works towards lowering of the peak temperature reached during transient bubble collapse. However, addition of this feature in the present model would change only the final quantitative answers, with trends remaining essentially unaltered.

6.5 RESULTS

The principal pathways for sonochemical degradation of an organic pollutant are: (1) hydroxylation reaction at bubble interface as well as in bulk liquid medium; (2) thermal decomposition in the thin liquid shell surrounding the bubble and (3) pyrolysis inside the cavitation bubble. The extent of degradation through hydroxylation pathway depends on two factors: (1) amount of OH radicals produced from cavitation bubbles and (2) probability of interaction between pollutant and OH radicals, which in turn depends on extent of radical scavenging in the bulk liquid medium. The contribution of the pyrolytic pathway, on the other hand, depends on amount of evaporation and subsequent entrapment of the pollutant vapor in the cavitation bubble. Finally, the extent of pyrolysis in the thin liquid shell depends on the thickness of this shell and concentration of the pollutant molecules in it. As noted earlier, on the intermediates and products of degradation, hydroxylation is the major chemical mechanism of nitrobenzene degradation while pyrolysis in the thin liquid shell followed by hydroxylation in the bulk medium is the chemical mechanism of p-nitrophenol degradation. Solubility of p-nitrophenol in water is high (16 g/l) indicative of the hydrophilic nature, while the solubility of nitrobenzene is low (1.9 g/l) indicative of hydrophobic nature. This means that the concentration of the p-nitrophenol is expected to be uniform in the medium while the nitrobenzene molecules tend to concentrate at the bubble-bulk interface, which also has a hydrophobic character. With this preamble we present the results of experiments and simulations.

6.5.1 Experimental results

The trends in the degradation of nitrobenzene and p-nitrophenol in the two categories of experiments using different techniques are shown in Fig. 6.2. The salient features of experimental results are as follows:

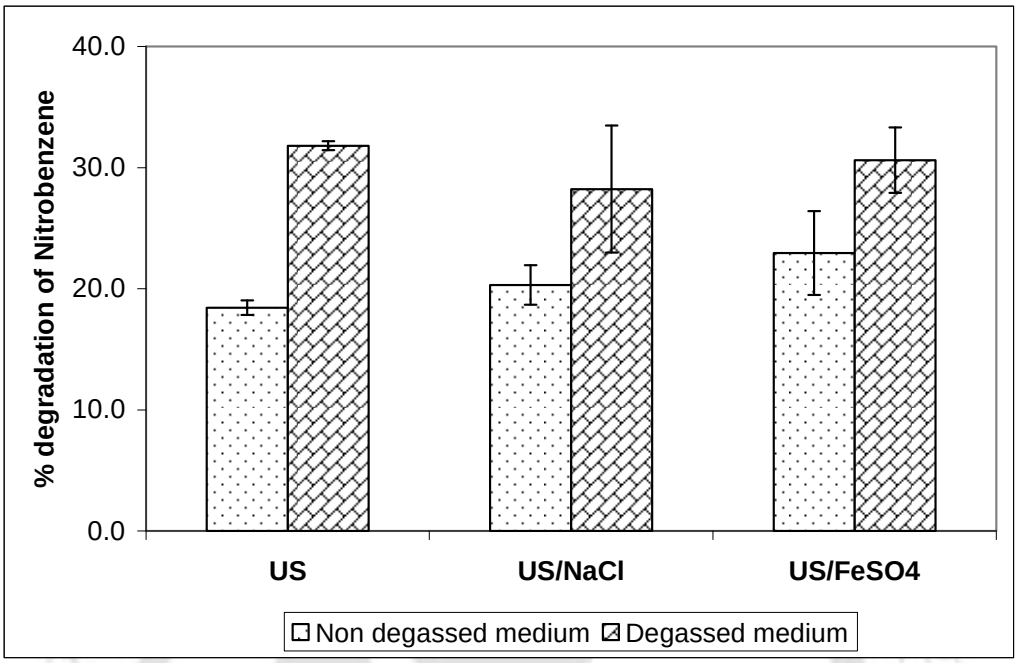

(A)

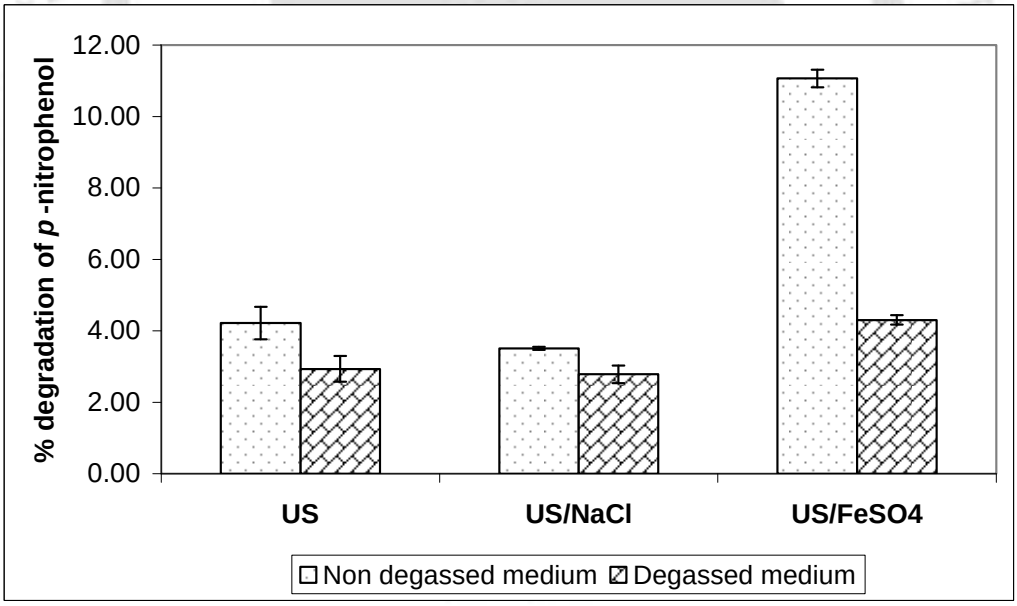

(B)

Figure 6.2. Experimental results on degradation of pollutant with various experimental conditions. (A) Nitrobenzene degradation. (B) p-Nitrophenol degradation.

Nitrobenzene degradation: (1) The extent of sonochemical degradation of nitrobenzene in 90 minutes of sonication is significant (~ 30%). (2) The extent of degradation in an unsaturated medium is more than in a saturated medium. (3) Addition of NaCl as well as $FeSO_4 \cdot 7H_2O$ to the liquid medium does not make any appreciable change to the extent of degradation.

p-Nitrophenol degradation: (1) Overall degradation of p-nitrophenol in 90 minutes of sonication is quite small (~ 3-10%). (2) With unsaturation of the medium, the extent of degradation decreases. This trend is seen with all three techniques adopted: sonication of medium alone, sonication with addition of NaCl or Fe^{2+} to the medium. (3) Addition of NaCl in either saturated or unsaturated medium reduces extent of degradation. (4) Addition of Fe^{2+} in both saturated and unsaturated medium results in rise in degradation; the rise in the unsaturated medium is much higher than saturated medium.

6.5.2 Simulations Results

Illustrative simulations of radial motion of 10 μm bubble in 10 ppm p-nitrophenol solution and 100 ppm nitrobenzene salt-added (4% w/v) solution are shown in Fig. 6.3 and 6.4 respectively. A summary of the simulation results is given in Tables 6.2 and 6.3 respectively for p-nitrophenol and nitrobenzene solutions respectively. These tables list the temperature and pressure peaks reached during transient collapse of a cavitation bubble, number of pollutant as well water molecules trapped in the bubble at the moment of collapse, the thickness of the liquid shell in which temperature is likely to rise above ambient and the equilibrium composition of chemical species resulting from dissociation of entrapped molecules in the bubble. It can be seen from Table 6.2 and 6.3 that among several radical species generated at the transient collapse of cavitation bubble, OH is the dominant species. The total number of OH radical species produced per bubble can be calculated by the product of total number of oxygen, water and pollutant (in case of nitrobenzene only) molecules in the bubble and the mole fraction of the OH radicals. Some other salient features of the

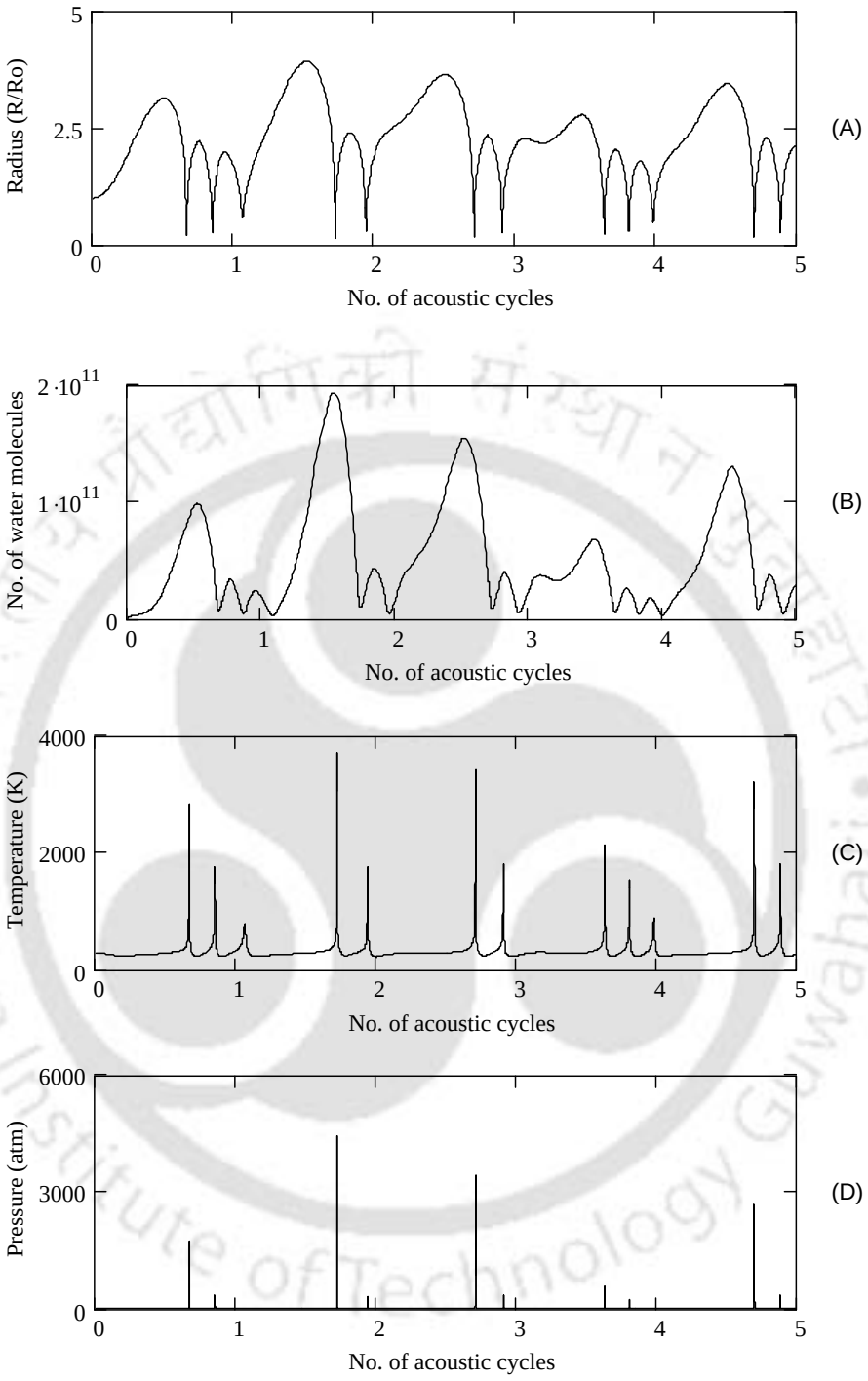

Figure 6.3. Simulation of the radial motion of 10 μm air bubble in 10 ppm aqueous solution of p-nitrophenol. Time variation of (A) normalized bubble radius (R/R_o); (B) number of water molecules in the bubble; (C) temperature in the bubble; (D) pressure in the bubble.

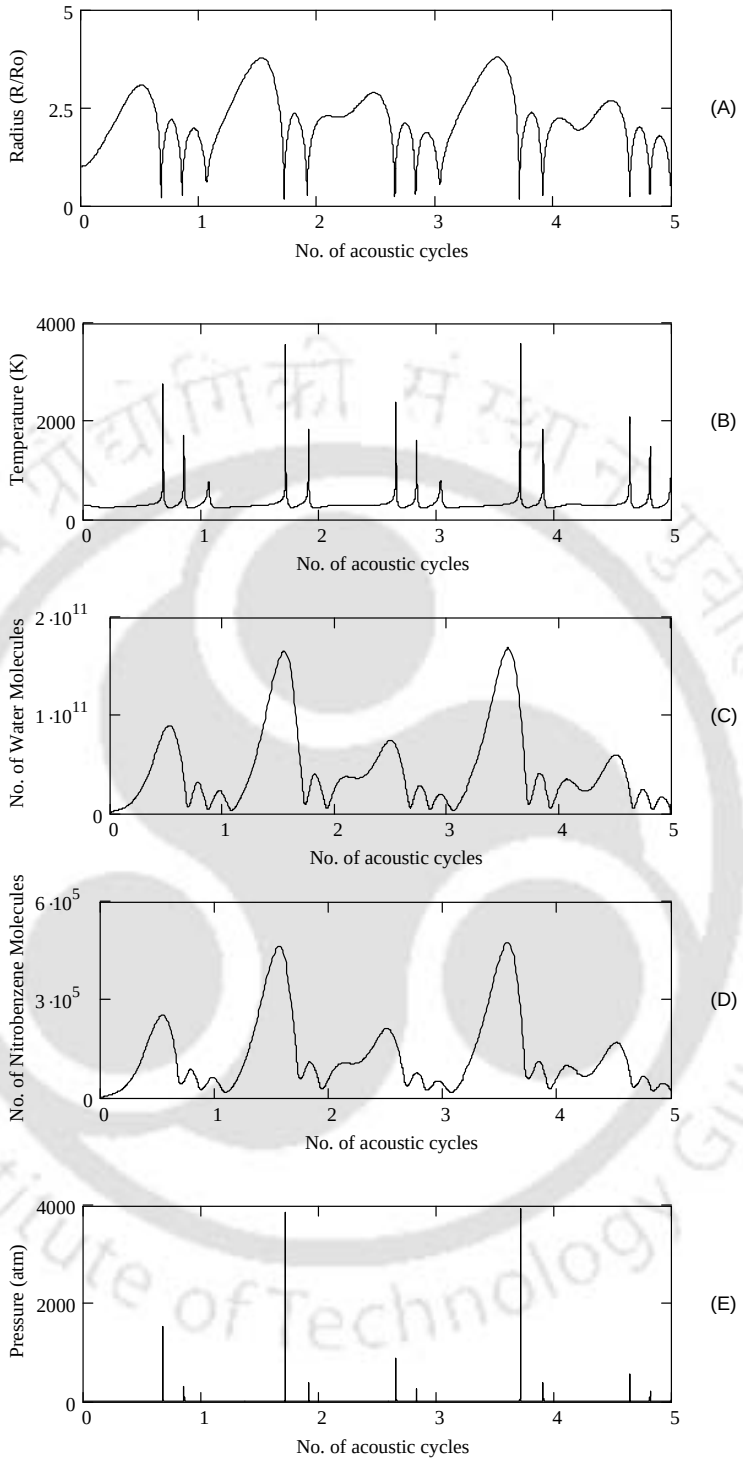

Figure 6.4. Simulation of the radial motion of 10 μm air bubble in 100 ppm aqueous solution (with 4% w/v NaCl added) of nitrobenzene. Time variation of (A) normalized bubble radius (R/R_o); (B) temperature in the bubble; (C) number of water molecules in the bubble; (D) number of nitrobenzene molecules in the bubble; (E) pressure in the bubble.

Table 6.2. Simulation results for cavitation bubble dynamics in solution of p-Nitrophenol

Species	**Parameters for simulation**			
	R_o = 10 μm 10 ppm solution	R_o = 10 μm 10 ppm solution with 4% w/v NaCl	R_o = 20 μm 10 ppm solution	R_o = 20 μm 10 ppm solution with 4% w/v NaCl
	Conditions at the first compression of the bubble			
	T_{max} = 2846 K	T_{max} = 2846 K	T_{max} = 1992 K	T_{max} = 1992 K
	P_{max} = 1731 bar	P_{max} = 1731 bar	P_{max} = 447.8 bar	P_{max} = 447.8 bar
	l_{th} = 0.7653 μm	l_{th} = 0.7653 μm	l_{th} = 2.137 μm	l_{th} = 2.137 μm
	N_{WT} = 1.24E+010 N_{N2} = 9.1512E+010 N_{O2} = 2.4326E+010	N_{WT} = 1.24E+010 N_{N2} = 9.1512E+010 N_{O2} = 2.4326E+010	N_{WT} = 1.05E+011 N_{N2} = 6.9138E+011 N_{O2} = 1.8379E+011	N_{WT} = 1.05E+011 N_{N2} = 6.9138E+011 N_{O2} = 1.8379E+011
Equilibrium composition of different radical species in the bubble at collapse (mole fraction)				
O_2	8.4788E-01	8.4788E-01	6.3676E-01	6.3676E-01
H_2O	1.3956E-01	1.3956E-01	3.6200E-01	3.6200E-01
OH	9.8441E-03	9.8441E-03	1.0943E-03	1.0943E-03
O	1.4270E-03	1.4270E-03	2.3566E-05	2.3566E-05
HOO	1.0771E-03	1.0771E-03	1.0505E-04	1.0505E-04
H_2	9.4777E-05	9.4777E-05	5.7838E-06	5.7838E-06
H_2O_2	6.9369E-05	6.9369E-05	1.1175E-05	1.1175E-05
H	2.2334E-05	2.2334E-05	1.7406E-07	1.7406E-07
O_3	2.2950E-05	2.2950E-05	5.3748E-07	5.3748E-07
Total amount of OH radicals produced per bubble				
N_{OH}	3.6153E+08	3.6153E+08	3.1602E+08	3.1602E+08

simulation results can be observed and explained as follows:

(1) The yield of OH radicals per cavitation bubble reduces with addition of salt in the medium. The number of OH radicals produced per cavitation bubble depends on two factors: first, the number of water molecules entrapped in the bubble, and secondly, the equilibrium mole fraction of the OH radicals at the conditions of temperature and pressure reached in the bubble. As far as the second factor is concerned, the temperature and pressure reached in the bubble do not change significantly with salt addition to the medium; however, the extent of water vapor entrapment reduces. This is attributed to decrease in vapor pressure of the liquid medium due to which the diffusive flux of water vapor and the entrapment of water vapor lessens.

Table 6.3. Simulation results for cavitation bubble dynamics in solution of nitrobenzene

Species	Parameters for simulation			
	R_o = 10 μm 100 ppm solution	R_o = 10 μm 100 ppm solution with 4% w/v NaCl	R_o = 20 μm 100 ppm solution	R_o = 20 μm 100 ppm solution with 4% w/v NaCl
	Conditions at the first compression of the bubble			
	T_{max} = 2787 K	T_{max} = 2757 K	T_{max} = 1946 K	T_{max} = 1992 K
	P_{max} = 1599 bar	P_{max} = 1543 bar	P_{max} = 422.4 bar	P_{max} = 447.8 bar
	N_{NB} = 7.09E+04	N_{NB} = 6.89E+04	N_{NB} = 4.29E+05	N_{NB} = 4.30E+05
	N_{WT} = 1.22E+010 N_{N2} = 9.1512E+010 N_{O2} = 2.4326E+010	N_{WT} = 1.18E+010 N_{N2} = 9.1512E+010 N_{O2} = 2.4326E+010	N_{WT} = 1.03E+011 N_{N2} = 6.9138E+011 N_{O2} = 1.8379E+011	N_{WT} = 1.01E+011 N_{N2} = 6.9138E+011 N_{O2} = 1.8379E+011
Equilibrium composition of different radical species in the bubble at collapse (mole fraction)				
O_2	8.3057E-01	8.2167E-01	6.4120E-01	6.4557E-01
H_2O	1.5787E-01	1.6731E-01	3.5780E-01	3.5334E-01
OH	9.1919E-03	8.8246E-03	8.7697E-04	9.5293E-04
O	1.1682E-03	1.0486E-03	1.6915E-05	1.9398E-05
HOO	9.8886E-04	9.4386E-04	8.6723E-05	9.4152E-05
H_2	8.9889E-05	8.6593E-05	4.0965E-06	4.5977E-06
H_2O_2	6.7894E-05	6.6885E-05	9.2071E-06	9.9265E-06
H	1.8433E-05	1.6537E-05	1.0912E-07	1.2989E-07
O_3	1.8760E-05	1.6928E-05	4.2843E-07	4.8122E-07
CO_2	1.4379E-05	1.3796E-05	8.9281E-06	9.0243E-06
NO	2.2809E-06	2.1871E-06	1.3730E-06	1.3906E-06
NO_2	1.1091E-07	1.0673E-07	8.7561E-08	8.7625E-08
CO	5.5291E-08	4.7745E-08	4.4009E-10	5.1367E-10
HNO_2	1.1822E-09	1.2742E-11	7.4929E-09	7.5892E-09
N_2	7.2812E-10	7.3648E-10	9.9460E-09	9.0942E-09
HNO	3.9258E-10	3.6178E-10	0	0
Total amount of OH radicals produced per bubble				
N_{OH}	3.3574E+08	3.1879E+08	2.5151E+08	2.7138E+08

Note for table 6.2 and 6.3: *The number format is as follows: 8.3057E-01 should be read as 8.3057 × 10^{-1}. Species with mole fractions less than 10^{-12} have been ignored in equilibrium calculations. Various notations used are as follows: T_{max} – temperature peak reached in the bubble at the time of first collapse; P_{max} – pressure peak reached in the bubble at the time of first collapse; N_{WT} – number of water molecules trapped in the bubble at the instance of first collapse; N_{O2} – number of oxygen molecules present in the air bubble; N_{N2} – number of nitrogen molecules present in the air bubble; N_{NB} – number of nitrobenzene molecules trapped in the air bubble at the instance of transient collapse; N_{OH} – number of hydroxyl radicals produced per cavitation bubble.*

(2) Higher yield of OH radicals per cavitation bubble is seen for 10 μm bubble – representative of an unsaturated medium. This is attributed to two effects: first, smaller bubbles undergo greater compression during radial motion resulting in higher temperature peak reached, and secondly, lesser attenuation of ultrasound wave due to smaller bubble population (or number density) in the medium, as a result of which the actual acoustic amplitude sensed by the bubble is high. This causes further augmentation in the intensity of the collapse of the cavitation bubble and also in the equilibrium mole fraction of the OH radicals generated from collapse of transient cavitation bubble.

(3) The thickness of the liquid shell surrounding the bubble, in which temperature rises above ambient, is higher for 20 μm bubble – representative of saturated medium. This shell is, in principle, the thermal penetration depth in the bulk medium. As seen from equations given in section 6.4.2, it varies directly with the radius of the bubble and inversely with the bubble wall velocity. Bubbles present in a saturated medium are of higher size. Moreover, the intensity of the collapse of larger bubbles is small, which means that the bubble wall velocity attained at the instance of transient collapse is also less. As a combined result of these factors, the thickness of liquid layer around the bubble that gets heated up is larger for an unsaturated medium. Thus, larger amount of pollutant molecules are subjected to high temperature pyrolysis.

6.6 DISCUSSION

Correlating the experimental and simulations results helps reveal some interesting physical features of the sonochemical degradation of nitrobenzene and p-nitrophenol.

6.6.1 Degradation of nitrobenzene

As noted earlier, the principal degradation route of nitrobenzene is through hydroxylation reaction. Degassing of the medium shows a marked rise in the extent of

nitrobenzene degradation. However, addition of salt as well as $FeSO_4$ to either saturated or unsaturated medium made only trivial changes to the extent of degradation. These results are explained in terms of high hydrophobicity of nitrobenzene and greater radical production by smaller bubbles present in the degassed medium, as revealed by the simulation results. Due to high hydrophobicity the nitrobenzene molecules tend to accumulate at the bubble-bulk interfacial region, as noted earlier. This interfacial region is also region of high concentration of radicals. Various radicals generated in the bubble at the moment of transient collapse get released into the medium with fragmentation of the bubble. As these radicals are highly reactive species, they do not diffuse far away from the location of bubble collapse. Most of the radicals react either among themselves or with pollutant molecules in the interfacial region. Since the concentration of nitrobenzene molecules is quite high in this region, the radicals are quite effectively intercepted by the pollutants resulting in large degradation. The extent of radicals production, and hence, the degradation rises with degassing of the medium.

Addition of NaCl increases the ionic strength of the medium. Consequently, the hydrophobic repulsive interactions between water and pollutant molecules increase and the pollutant molecules are driven towards bubble-bulk interface, as noted earlier. This effect is observed for both saturated and unsaturated liquid medium. Concentration of the pollutant molecules at bubble-bulk interface results in higher interaction between radicals and the pollutant molecules, which can raise the extent of degradation. However, in case of nitrobenzene, which is hydrophobic in nature, the bubble-bulk interface is already saturated. Addition of NaCl, therefore, does not augment the concentration of nitrobenzene in bubble-bulk interfacial region. The extent of degradation essentially stays the same with addition of NaCl.

$FeSO_4$ addition in the medium gives rise to scavenging of the radicals in the bulk liquid medium (both saturated and unsaturated), as noted earlier. However, this causes

insignificant changes to the extent of degradation. This is again attributed to low solubility of nitrobenzene and large presence of nitrobenzene molecules in the bubble-bulk interfacial region. As a result of these two features, the hydroxylation reaction of nitrobenzene occurs in the interfacial region and scavenging of the radicals in the bulk medium has little relevance towards overall degradation of nitrobenzene.

6.6.2 Degradation of p-nitrophenol

As stated previously, the degradation route of p-nitrophenol has two contributions: thermal pyrolysis in the thin liquid shell surrounding the bubble, which is the primary mechanism; and secondly, hydroxylation in the bulk medium, which is the secondary pathway (Kotronarou *et al.*, 1991). With unsaturation of the medium, the extent of degradation of p-nitrophenol reduces marginally. Addition of NaCl makes insignificant changes to the extent of degradation while addition of $FeSO_4$ raises the degradation by about 30%. These results are attributed to hydrophilic nature, low initial concentration and the basic route of degradation (i.e. thermal pyrolysis in the bubble-bulk interfacial region as well as hydroxylation) of p-nitrophenol. Due to hydrophilic nature, the concentration of p-nitrophenol molecules at bubble interface is low, and hence, the efficiency of interception of radicals by the pollutant molecules in the bubble-bulk interfacial region is small. Reduction in the dissolved gas content of the medium has two contrary effects on degradation of p-nitrophenol. Although the extent of radical generation increases with unsaturation of the medium, it does not make significant positive alterations to hydroxylation of p-nitrophenol due to its low interfacial concentration. Secondly, the thickness of the liquid shell surrounding the bubble, in which temperature can rise, is small for smaller bubbles present in an unsaturated medium. Accordingly, the amount of p-nitrophenol molecules undergoing thermal pyrolysis in the bubble-bulk interfacial region reduces. The net effect of these effects is lessening of the extent of degradation.

Addition of NaCl to the medium (both saturated and unsaturated) also reduces the extent of degradation marginally. This is attributed to simultaneous and conflicting effects of NaCl addition. Partitioning of the p-nitrophenol molecules between interfacial and bulk region increases with addition of NaCl. However, this effect is not marked as the bulk concentration of p-nitrophenol is quite small (10 ppm). Besides, addition of salt in the liquid medium reduces the dissolved oxygen concentration (Hall, 1975), and hence, the scavenging of the radicals. As a result, the probability of interaction between p-nitrophenol molecules and radicals decreases. The overall effect is reduction in the extent of degradation.

Addition of $FeSO_4$ in a saturated medium increases the degradation rate almost 3 fold. This is clearly attributed to extensive scavenging of radicals by the Fe^{2+} ions. On the other hand, addition of $FeSO_4$ in an unsaturated medium does not have an equally marked effect – although the extent of degradation is about ~ 30% higher than other experimental conditions. This effect can be explained on the basis of adverse effect of unsaturation of the medium on extent of degradation, as described earlier. The amount of p-nitrophenol molecules undergoing thermal pyrolysis in the thin liquid shell decreases with reduction in the saturation level of medium. Thus, contribution of the pyrolysis pathway to the overall degradation decreases with degassing of the medium. The extent of OH radical production from bubble increases with unsaturation of the medium. However, this effect is not able to compensate for the reduction in degradation. This is a corroboration of the conclusions of Kotronarou *et al.* (1991) that hydroxylation is the secondary pathway for degradation of p-nitrophenol.

6.7 CONCLUSION

This chapter attempts to provide a physical (or mechanistic) insight into the sonochemical degradation of two nitroaromatic compounds, viz. nitrobenzene and p-

nitrophenol. The basic chemical mechanism of the sonochemical degradation of these pollutants is hydroxylation, which is reaction of the pollutant molecules with OH radicals generated from cavitation bubbles. An alternate pathway is the thermal pyrolysis of the pollutant molecules in the thin liquid shell surrounding the bubble that gets heated up during transient collapse of the bubbles. The experimental conditions employed in this study (variation of the saturation level of the medium and addition of NaCl and Fe^{2+} to the medium) influence important physical parameters related to cavitation bubbles such as extent of radical production from the bubble, thickness of the liquid shell surrounding the bubble, the concentration of the pollutant in the interfacial region and extent of radical scavenging in the medium. Concurrent analysis of the experimental and simulation results reveals that overall degradation of the pollutant achieved for a given combination of experimental conditions is a function of competing (and sometimes conflicting) effect of these parameters. On a whole, this chapter gives a semi-quantitative account of the relative influences of these parameters and the interrelations between them.

CHAPTER 7

MECHANISTIC ASPECTS OF THE SONOCHEMICAL DEGRADATION OF 2,4-DICHLOROPHENOL

7.1 INTRODUCTION

This paper attempts to discern the physical or mechanistic features of sonochemical degradation of chlorophenols. As the model compound, we choose a principal member of chlorophenol family, viz. 2,4 dichlorophenol (abbreviated hereafter as 2,4 DCP). Chlorophenols have been used as mothproofing agents, miticides, germicides, algicides, fungicides, and wood preservatives and to manufacture of other chemicals. All the chlorophenols have been used as biocides. Chlorophenols with at least two chlorines either have been used directly as pesticides or have been converted into pesticides. 2,4,6-Trichlorophenol was previously used as an antiseptic, a pesticide for wood, leather, and glue preservation and as an anti-mildew treatment. 2,4-DCP is a chemical intermediate used principally in the manufacture of the herbicide 2,4-dichlorophenoxyacetic acid. Several authors have addressed the matter of degradation of 2,4-DCP. However, most of these studies have employed biological techniques for the purpose. A review of the literature in this area is given in chapter 1. The intermediates and product of sonochemical degradation of 2,4 DCP reported by Goskonda *et al.* (2002), Wu *et al.* (2007) and Yasman *et al.* (2004) hint at hydroxylation as the dominant chemical mechanism.

This study tries to discern the mechanistic (or physical) features of the sonochemical degradation of 2,4 DCP. The approach that we adopt for this aim is same as in previous

chapters: simultaneous analysis of the experimental results under different conditions and the simulations of a bubble dynamics model that takes into account physics and chemistry of the cavitation bubbles.

7.2 OBJECTIVES AND APPROACH

To begin with, we describe the objectives and approach of this study. According to basic principles of chemical kinetics, the rate of sonochemical degradation of a pollutant depends on the concentration of radicals and the concentration of the pollutants. The kinetics of degradation can be enhanced by increasing either or both of these quantities. However, the sonochemical reaction systems are different than the conventional ones due to a distinctive feature that the concentration of radicals produced by cavitation bubbles is not uniform throughout the volume, but rather confined to a small area at the location of the bubble. Being extremely unstable and energetic, the radicals react almost instantly in the bubble-bulk interfacial region (after being released at the instance of bubble collapse) and do not diffuse deeper into the medium. Therefore, a supplementary factor that affects the kinetics and yield of a sonochemical process is the probability of interaction between reactant and the radical. Correspondingly, if the concentration of pollutant molecules in the bubble-bulk interfacial region is low, the probability of interaction between a pollutant molecules and radical is low, and the radicals generated from the cavitation bubbles undergo recombination. This is clearly the loss of oxidation potential. On the other hand, an effective utilization of radicals in the bulk medium through scavenging action would result in enhanced degradation of the pollutant through hydroxylation, i.e. reaction with OH radicals. The word scavenging means reaction of the radicals with other species in the medium (present in relatively large concentration) to generate additional radical species. This helps in greater infiltration of the radicals into the bulk medium from the location of collapse of the bubble, and thus, an

enhancement in the probability of radical – pollutant interaction and extent of degradation. It should be noted that although major part of the hydroxylation reaction occurs in the bubble-bulk interfacial region (which has rich concentration of radicals), some hydroxylation can also occur in bulk medium.

The main objective of this study was to discern the mechanistic or physical features of the sonochemical degradation of chlorophenols. On the basis of forethoughts given above, we take an experimental approach as described below to meet this objective. Variation in the extent of degradation with the experimental techniques employed reveals different facets of the physics of the sonochemical degradation of the pollutants.

(1) *Addition of salt (NaCl) into the medium*: Addition of NaCl increases the ionic strength of the medium. As a result, the hydrophobic repulsive interactions between water and pollutant molecules increase and the pollutant molecules are driven towards the bubble-bulk interface and the concentration of the pollutant in the interfacial region becomes higher than bulk concentration (Seymour and Gupta, 1997; Bapat *et al.*, 2007). This phenomenon raises the probability of interaction between radicals and pollutant molecules, and hence, the extent of degradation.

(2) *Addition of Fe^{2+} (in the form of $FeSO_4 \cdot 7H_2O$) to the medium*: Fe^{2+} ions can effectively scavenge OH radicals in the bulk medium through following reactions (Kavitha and Palanivelu, 2005; Zhang *et al.*, 2007):

$$OH^{\cdot} + OH^{\cdot} \rightleftharpoons H_2O_2$$

$$H_2O_2 + Fe^{2+} \longrightarrow Fe^{3+} + OH^{-} + OH^{\cdot}$$

$$Fe^{3+} + H_2O_2 \longrightarrow Fe^{2+} + HO_2^{\cdot} + H^{+}$$

$$Fe^{3+} + HO_2^{\cdot} \longrightarrow Fe^{2+} + O_2 + H^{+}$$

This scavenging action results in extent of degradation of the pollutant molecules in the bulk medium, as a result of greater probability of interaction between radical and pollutant.

(3) *Variation in the saturation level (dissolved gas content) of the medium*: The saturation level or dissolved gas content of the medium influences extent of radical production in the medium through process of rectified diffusion. The process of rectified diffusion makes a cavitation bubble grow or shrink during radial motion. Reduction in the dissolved gas content or unsaturated medium makes a cavitation bubble shrink in size (Fyrillas and Szeri, 1994; Lofstedt *et al.*, 1995). Smaller bubbles undergo more intense collapse, which increases radical production from the bubble (Sivasankar *et al.*, 2007), and hence, the degradation of the pollutant.

(4) *Bubbling of monatomic and diatomic gases (such as Ar, Air, O_2, N_2) through the medium*: The intensity of the collapse of the cavitation bubble depends on the gas of which it is made up of. Bubbles made of monatomic gas such as argon by virtue of smaller heat capacity give much higher collapse temperature, while bubbles of diatomic gases (such as air, oxygen and nitrogen) have relative lower collapse temperature. Quite obviously, the extent of radical production from bubbles of monatomic gases is higher. However, as far as pollutant degradation is concerned, radical production from bubbles as well as scavenging of these radicals is important. In case of air and oxygen, the oxygen molecules present in the bulk medium as well as inside the bubble act as dominant radical scavengers and give effective utilization of radicals towards pollutant degradation. In case of argon, the extent of degradation could be lower as argon strips out the oxygen dissolved in the medium which hampers the scavenging of radicals, lowering probability of radical-pollutant interaction. An absence of scavenging, the recombination of radicals could prevail resulting in loss of oxidation potential. Variation of the extent of degradation with different bubbling gases

shows the contribution of the scavenging phenomena to the overall degradation of the pollutants.

7.3 EXPERIMENTAL

7.3.1 Materials

2,4-DCP (Grade: Synthesis) was procured from Loba Chemie, India. Additional chemicals such as sodium chloride (Grade: GR), iron (II) sulphate heptahydrate (Grade: Purified), acetonitrile (Grade: HPLC) and water (Grade: HPLC) were procured from Merck and used as received. All solutions were prepared using Elix water from Millipore® purification unit (Model: Elix 3). Four gases, viz. oxygen, argon, nitrogen and air (99.99% purity) were used for bubbling (or sparging) through the reaction medium.

7.3.2 Experimental setup

Schematic of the experimental setup is shown in figure 7.1. The experiments were performed in a jacketed glass reactor (volume 250 ml). A probe type ultrasonic processor operating at a frequency of 20 kHz was used (Sonics & Materials Inc., Model VCX 500) for sonication of the reaction medium. The processor had a sonicator probe with a tip diameter of 13 mm. The processor had variable power output control, which was set at 20% during experiments, resulting in net consumption of 100W power during sonication. In addition, the processor had facility of automatic frequency tuning and amplitude compensation, which ensured constant power delivery to ultrasound probe irrespective of the changes in condition of the reaction medium. The temperature of the reaction medium during sonication was controlled by circulating cooling water through the jacket of the reactor. The actual value of the ultrasound intensity in the medium was determined using calorimetry (Sivasankar *et al.*, 2007). For a power output of 100W, the ultrasound probe produced an acoustic wave with 1.5 bar amplitude. For bubbling of different gases through the reaction medium during

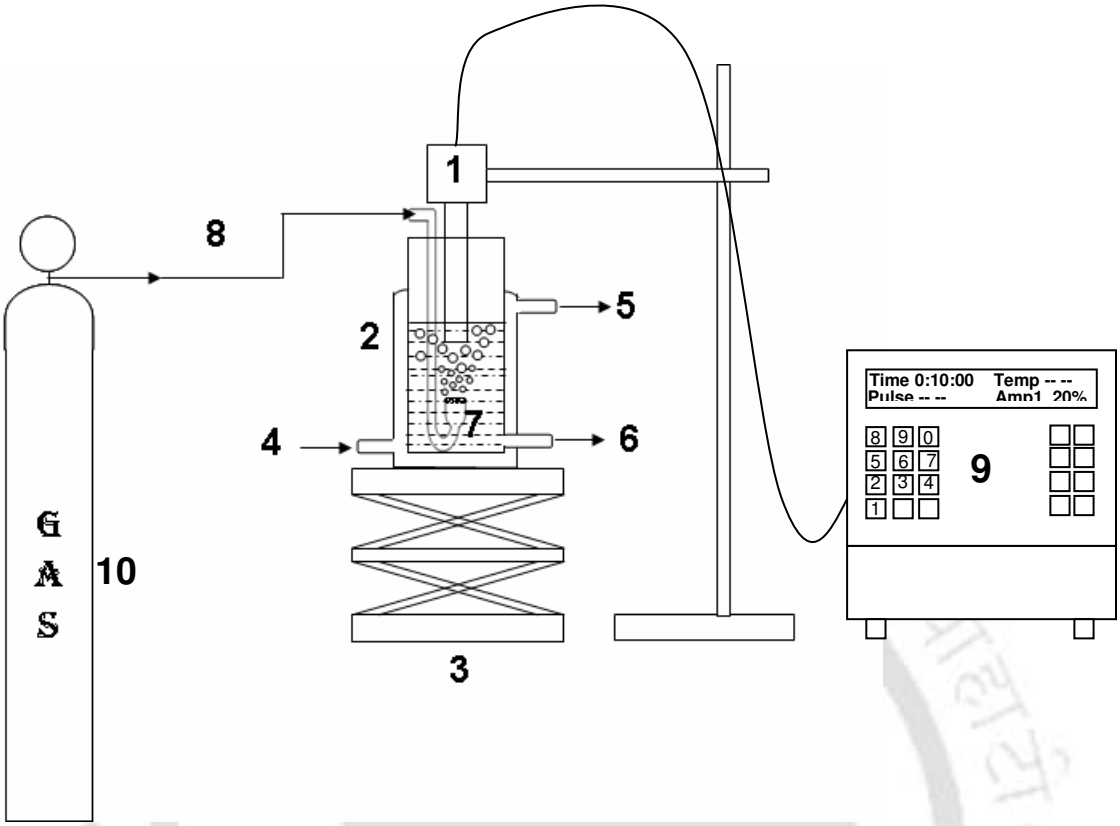

Figure 7.1. Schematic of experimental set-up [Legends: 1. Ultrasound horn; 2. Jacketed glass reactor; 3. Laboratory jack; 4. Cooling water inlet; 5. Cooling water outlet; 6. Sample port; 7. Aerator; 8. Gas inlet; 9. Control unit of ultrasonic processor; 10. Gas cylinder]

sonication, a glass sparger was used. This sparger distributed the gas entering into the reaction medium through a porous silica filter of pore size ~ 40µm. The flow rates of the bubbling gases were maintained at 5 lph.

7.3.3 Experimental procedure

Synthetically prepared solutions of 2,4-DCP (concentration: 100 ppm; volume: 150 ml) were sonicated for a total reaction time of 90 min. Sonication was done with 15 minutes on and 5 minutes off cycle in order to reduce the significant temperature rise in the reaction medium. The temperature of the reaction medium was monitored continuously using a digital

thermometer. The rise in temperature of the medium during 90 minutes of sonication was only 2˚C. The set of experiments were categorized as follows:

1. *Sonication of the saturated liquid medium*: In this category, experiments were done with sonication alone, sonication with the addition of 4 % NaCl to the reaction medium and sonication with the addition of 0.5 mM $FeSO_4 \cdot 7H_2O$ to the medium.

2. *Sonication with unsaturated liquid medium without sparging of any particular gas during sonication.*

3. *Sonication of the pollutant solution with bubbling or sparging of various gases (viz. air, argon, nitrogen and oxygen) through the medium.*

The dissolved gas content of the liquid medium was reduced by subjecting the medium to reduced pressure by means of a vacuum pump (Make: Riviera). A vacuum of 650 mm of Hg was applied for a time period of 30 min with intermittent stirring. This procedure reduced the dissolved oxygen content of the medium to 2.7 ppm. The dissolved gas content, however, rises during sonication. In order to maintain the unsaturation of the medium, the dissolved oxygen content of the medium was continuously monitored. When the dissolved oxygen content increased above 4 ppm, the reaction solution was removed from the glass reactor and vaccumized once again. With this procedure, the average dissolved oxygen content of the solution in the experiments with degassed medium was ~ 3 ppm.

7.3.4 Analytical procedure

The concentration of 2,4-DCP in aqueous solution after 90 min of sonication was quantitatively monitored using High Performance Liquid Chromatography (Perkin Elmer, Model: Series 200). A C18 column (250mm x 4.6 mm, 5µm particle size, Make: Chromatopack) was used with mixture of acetonitrile (70%) and water (30%) as mobile phase. The eluent mixture was passed at a constant flow rate of 0.75 ml/min and the sample injection volume was 20 µl, with UV detector wavelength being 275 nm. The extent of

degradation was assessed using a calibration chart prepared with known concentrations of 2,4-DCP. We would like to categorically state that we have not made an analysis of the intermediate products of degradation, as these have been extensively studied and documented in previous literature (Goskonda *et al.*, 2002; Yasman *et al.*, 2004; Wu *et al.*, 2007). We have only monitored the rate of disappearance of original pollutant and the analysis has been made on that basis.

7.4 MATHEMATICAL FORMULATION

The model used in this chapter is essentially same as used in chapter 2 (sonochemical degradation of phenol). The assumptions and approximations made in the model as also identical. Therefore, we describe here only the essential equations and thermodynamic data of this model (table 7.1A and B). For greater details on other aspects of the model, we refer the reader to our earlier papers mentioned earlier.

The main components of the model are:

(1) Keller-Miksis equation for the radial motion of the bubble (Prosperetti and Lezzi, 1986; Brennen, 1995).

(2) Equation for the diffusive flux of water vapor and heat conduction through bubble wall. The transport parameters for the heat and mass transfer (thermal conductivity and diffusion coefficient) are determined using Chapman-Enskog theory using Lennard-Jones 12-6 potential at the bulk temperature of the liquid medium (Hirschfelder *et al.*, 1954; Condon and Odishaw, 1958; Bird *et al.*, 2001). Thermal and diffusive penetration depths are estimated using dimensional analysis.

(3) Overall energy balance treating the cavitation bubble as an open system.

The model ignores diffusion of gases across bubble wall as the time scale for the diffusion of gases is much higher than the time scale for the radial motion of bubble. Moreover, the

Table 7.1 (A) Model for the radial motion of cavitation bubble**

Model Component	Equation	Boundary Condition
1. Radial motion of the cavitation bubble	$\left(1-\frac{dR/dt}{c}\right)R\frac{d^2R}{dt^2}+\frac{3}{2}\left(1-\frac{dR/dt}{3c}\right)\left(\frac{dR}{dt}\right)^2 = \frac{1}{\rho_L}\left(1+\frac{dR/dt}{c}\right)(P_i-P_t)+\frac{R}{\rho_L c}\frac{dP_i}{dt}-4\nu\frac{dR/dt}{R}-\frac{2\sigma}{\rho_L R}$ Internal pressure in the bubble: $P_i = \frac{N_{tot}(t)\,kT}{\left[4\pi\left(R^3(t)-h^3\right)/3\right]}$ Pressure in bulk liquid medium: $P_t = P_0 - P_A\sin(2\pi ft)$	At $t = 0$, $R = R_o$ and $dR/dt = 0$.
2. Diffusive flux of water molecules across bubble wall	$\frac{dN_w}{dt} = 4\pi R^2 D_w \left.\frac{\partial C_w}{\partial r}\right\|_{r=R} \approx 4\pi R^2 D_w \left(\frac{C_{wR}-C_w}{l_{diff}}\right)$ Instantaneous diffusive penetration depth: $l_{diff} = \min\left(\sqrt{\frac{RD_w}{\lvert dR/dt\rvert}}, \frac{R}{\pi}\right)$	At $t = 0$, $N_w = 0$
3. Heat conduction across bubble wall	$\frac{dQ}{dt} = 4\pi R^2\lambda\left.\frac{\partial T}{\partial r}\right\|_{r=R} \approx 4\pi R^2\lambda\left(\frac{T_0-T}{l_{th}}\right)$ Thermal diffusion length: $l_{th} = \min\left(\sqrt{\frac{R\kappa}{\lvert dR/dt\rvert}}, \frac{R}{\pi}\right)$	At $t = 0$, $Q = 0$
4. Overall energy balance treating bubble as an open system	$C_{V,mix}dT/dt = dQ/dt - P_i dV + (h_w - U_w)dN_w/dt$ Mixture heat capacity: $C_{V,mix} = \sum C_{V,i}N_i$ Molecular properties of water: Enthalpy: $h_w = 4kT_o$ Internal energy: $U_w = N_w kT\left(3+\sum_{i=1}^{3}\frac{\theta_i/T}{\exp(\theta_i/T)-1}\right)$ Heat capacity (argon): $C_V = 3kN_{Ar}/2$ Heat capacity of other species (i = N_2/O_2/H_2O): $C_{V,i} = N_i k\left(f_i/2+\sum\left((\theta_i/T)^2\exp(\theta_i/T)/\left(\exp(\theta_i/T)-1\right)^2\right)\right)$	At $t = 0$, $T = T_0$

evaporation of the pollutant molecules in the bubble is also ignored as the partial pressure of the pollutant at the bubble-bulk interface is very small (0.0128 Pa, calculated assuming bubble-bulk interfacial region at saturation concentration due to partitioning of the 2,4 DCP molecules between bulk medium and bubble-bulk interface).

Table 7.1 (B) Thermodynamic properties of various species*

Species	Degrees of freedom (translational + rotational) (f_i)	Lennard-Jones force constants		Characteristic vibrational temperatures θ (K)
		σ (10^{-10} m)	ε/k (K)	
N_2	5	3.68	92	3350
O_2	5	3.43	113	2273
H_2O	6	2.65	380	2295, 5255, 5400
Ar	3	3.42	124	--

** - Data taken from Toegel (2002); Hirschfelder et al. (1954); Reid et al. (1987).*

***** Notation for Table 7.1(A):*** *R – radius of the bubble; dR/dt – bubble wall velocity; c – velocity of sound in bulk liquid medium; ρ_L – density of the liquid; ν - kinematic viscosity of liquid; σ - surface tension of liquid; λ - thermal conductivity of bubble contents; κ - thermal diffusivity of bubble contents; θ - characteristic vibrational temperature(s) of the species; N_w – number of water molecules in the bubble; t – time, D_w – diffusion coefficient of water vapor; C_w – concentration of water molecules in the bubble; C_{wR} – concentration of water molecules at the bubble wall or gas-liquid interface; Q – heat conducted across bubble wall; T – temperature of the bubble contents; T_o – ambient (or bulk liquid medium) temperature; k – Bolzmann constant; N_{Ar} – number of argon molecules in the bubble; f_i – translational and rotational degrees of freedom; $C_{V,i}$ – heat capacity at constant volume; N_{tot} – total number of molecules (gas + vapor) in the bubble; h – van der Waal's hard core radius; P_o – ambient (bulk) pressure in liquid; P_A – pressure amplitude of ultrasound wave; f – frequency of ultrasound wave.*

7.4.1 Numerical solution

The equations given in table 7.1A constitute complete formulation for the radial motion of cavitation bubble with associated heat and mass transfer effects. This set of simultaneous ODEs can be solved using Runge-Kutta 4th order – 5th order adaptive step size method (Press *et al.*, 1992). The cavitation bubble may collapse at the instance of maximum compression during radial motion. The word "collapse" essentially means fragmentation of the cavitation bubble. This factor depends on many factors such as shape (or surface) instability of bubbles, the local flow conditions and the bubble population density in the vicinity of the bubble. For conditions of maximum shape and flow instability, the cavitation bubble fragmentation can occur at the first compression after an initial expansion. In view of this, the condition for the bubble collapse is taken to be first compression during radial

motion. Four important parameters required for the simulation of the radial motion of the cavitation bubble are: (1) frequency and (2) pressure amplitude of ultrasound, (3) vapor pressure of water and (4) initial (or equilibrium) bubble radius. Numerical values for these parameters have been determined as follows:

(1) *Frequency*: The frequency of the ultrasound wave was taken as 20 kHz, which is the frequency of the sonicator used in the experiments.

(2) *Pressure amplitude*: A calorimetric method was used to determine the amplitude of the ultrasound wave emitted by the sonicator probe (Sivasankar *et al.*, 2007). The amplitude of the ultrasound wave generated by the sonicator probe was 1.5 bar. However, due to the attenuation in the medium, the actual pressure amplitude sensed by the cavitation bubble located away from the probe tip is lesser than 1.5 bar. Principal physical factor affecting the attenuation is size and population density of bubbles in the medium (Mason and Lorimer, 1989; Prosperetti and Commander, 1989). A direct measurement of the local pressure amplitude in the vicinity of the cavitation bubble is beyond the capabilities of the instrumentation used in the present study. Therefore, we assume about 15% attenuation of the ultrasound wave in a saturated or non-degassed medium and use a value of P_A = 1.3 bar in the numerical simulations for saturated medium. For the degassed or unsaturated medium, the bubble population density is relatively much less, and hence, attenuation effect is negligible. Therefore, we assume a value of P_A = 1.5 bar in simulations for the unsaturated or degassed medium.

(3) *Vapor pressure of bulk medium and pollutant*: The vapor pressure of the bulk medium (i.e. water) was calculated with Antoine's equations using initial temperature of the solution (25 ^{o}C) as given below:

$$P_w = \frac{10^5}{760}\exp\left(18.3036 - \frac{3816.44}{T - 46.13}\right)$$

The temperature rise during sonication was ~ 2 ^{o}C, as noted earlier. The difference between

vapor pressures of water and nitrobenzene at 25 ^{o}C and 27 ^{o}C is quite small (< 10%). Therefore, we have ignored the temperature rise during simulations, assuming the liquid medium at constant temperature. An alternate approach would be to calculate the vapor pressure of water using average of initial and final temperatures. However, this would make trivial quantitative changes to the simulation results; and the trends in the simulation results remain essentially unchanged. Vapor pressure of water reduces with addition of salt. This reduction is accounted for using formulae given by Al-Shayji (1998).

(4) *Initial (or equilibrium) bubble radius*: This parameter is difficult to estimate. Moreover, the equilibrium size of the bubble keeps on changing due to phenomena such as rectified diffusion, fragmentation of the bubble etc. The minimum radius of the cavitation nuclei, which would grow into a bubble for particular amplitude of acoustic wave, can be determined by the analysis given by Young (1989). For the acoustic pressure amplitude in the present experiments, this value is ~ 2 μm. We have chosen a representative value of 5 μm for the initial or equilibrium bubble radius for a degassed (or unsaturated) medium and a value of 10 μm for the non-degassed (or saturated) medium.

Equilibrium composition of the various species formed in the bubble with dissociation of entrapped water and pollutant molecules at the conditions of temperature and pressure at the first compression was calculated using software FACTSAGE, which uses the free-energy minimization algorithm proposed by Eriksson (1975). This software has an in-built database of C_p vs. temperature relationship, entropy and heat of formation of all the above species.

7.5 RESULTS

The concentration of 2,4 DCP used in this study is quite dilute. Therefore, the phenomenon of radical scavenging becomes a major parameter influencing extent of degradation. For the experimental conditions used in this study, there are two possible means

of scavenging of radicals in the liquid medium, as describe below:

(1) Radical scavenging due to dissolved oxygen present in the medium. Oxygen present in the medium can react with $H^{\bullet}$ and $OH^{\bullet}$ radicals generated from cavitation bubble to generate additional radicals:

$$H^{\cdot} + O_2 \rightleftharpoons O^{\cdot} + OH^{\cdot}$$

$$H^{\cdot} + O_2 \rightleftharpoons HO_2^{\cdot}$$

$$OH^{\cdot} + O_2 \rightleftharpoons HO_2^{\cdot} + O^{\cdot}$$

Moreover, dissolved oxygen in the medium can also react with H_2O_2 formed out of combination of $OH^{\bullet}$ radicals to generate hydroperoxy radicals:

$$OH^{\cdot} + OH^{\cdot} \rightleftharpoons H_2O_2$$

$$H_2O_2 + O_2 \rightleftharpoons 2HO_2^{\cdot}$$

(2) Radical scavenging due to Fe^{2+} ions (in the experiments with $FeSO_4 \cdot 7H_2O$ added to the medium). The reactions describing scavenging of radicals by Fe^{2+} have been described before. However, there exists difference between locations of the two scavenging actions by oxygen and Fe^{2+}. The scavenging action of oxygen, which is a molecular species, is uniform in the reaction volume; in the bulk medium as well as in the bubble-bulk interfacial region. On the other hand, scavenging action of Fe^{2+} is expected to be restricted in the bulk medium. This is attributed to the ionic nature of Fe^{2+} due to which it prefers to stay in the bulk medium – rather than in the bubble-bulk interfacial region, which has a hydrophobic character.

Another important feature that influences the sonochemical degradation of the pollutant is the chemical nature of pollutant itself. If the pollutant is hydrophobic (as characterized by low solubility or high octanol-water partition coefficient), it preferentially stays in the bubble-bulk interfacial region. Thus, the concentration of pollutant in the interfacial region is much higher than the bulk concentration (Seymour and Gupta, 1997;

Bapat *et al.*, 2007). In such a situation, the probability of radical-pollutant interaction increases significantly, as the interfacial region has high concentration of radicals, as stated earlier. In addition, presence of a radical scavenging species in the interfacial region can further assist in effective utilization of radicals giving high degradation of pollutant. With this preamble we present the results of experiments and simulations.

7.5.1 Experimental results

The experiments were performed in three different categories, as stated earlier. The extent of degradation of 2,4 DCP for different categories of experiments is shown in figure 7.2A and B respectively. Some distinctive features of the degradation of 2,4 DCP evident from figures 7.2A and B are as follows:

(1) As compared to the degradation with sonication of saturated liquid medium, addition of NaCl (4% w/w) as well as Fe^{2+} to the medium (in the form of $FeSO_4 \cdot 7H_2O$ at concentration of 0.5 mM) makes practically no change to the extent of degradation.

(2) Unsaturation or degassing of the medium results in a marked rise (~ 40%) in the degradation.

(3) Sparging of different gases during sonication shows interesting features. Highest degradation is obtained with sparging of air and the least degradation is seen for nitrogen sparging. On the other hand, oxygen and argon give an intermediate and almost similar degradation.

7.5.2 Simulation results

Representative simulations of 5 and 10 μm air bubble and 10 μm nitrogen bubble are shown in figures 7.3, 7.4 and 7.5 respectively. The summary of entire simulation results along with equilibrium composition of various radical species resulting out of dissociation of molecules present in the bubble is shown in tables 7.2A and B. Table 7.2C depicts the net production of four key radicals per cavitation bubble (obtained by product of total number of

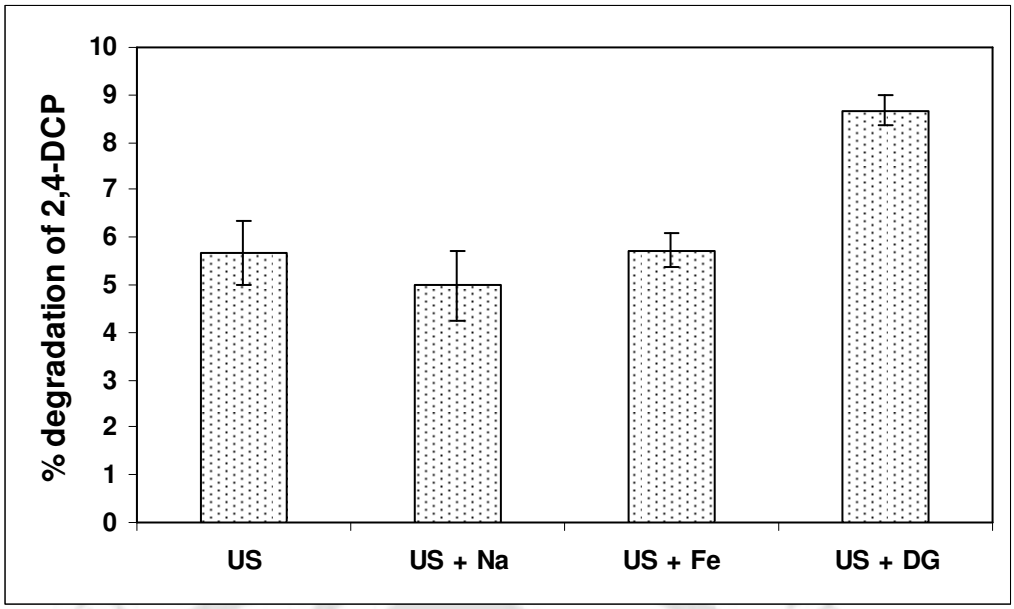

Figure 7.2(A). Experimental results on degradation of 2,4 DCP with different conditions. **US:** Degradation with sonication alone (saturated liquid medium); **US + Na**: Degradation with sonication of NaCl added medium (saturated liquid medium); **US+Fe**: Degradation with sonication of $FeSO_4 \cdot 7H_2O$ added medium (saturated liquid medium); **US+DG**: Degradation with sonication of unsaturated (or degassed) liquid medium.

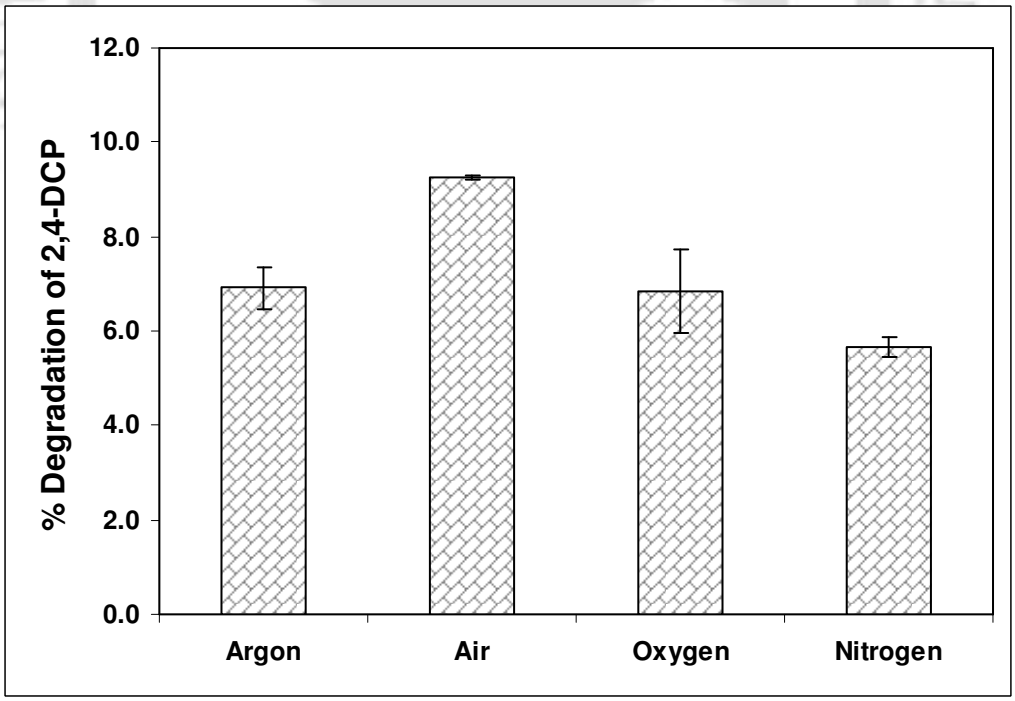

Figure 7.2(B). Experimental results on degradation of 2,4 DCP with sparging (or bubbling) of different gases during sonication (saturated liquid medium).

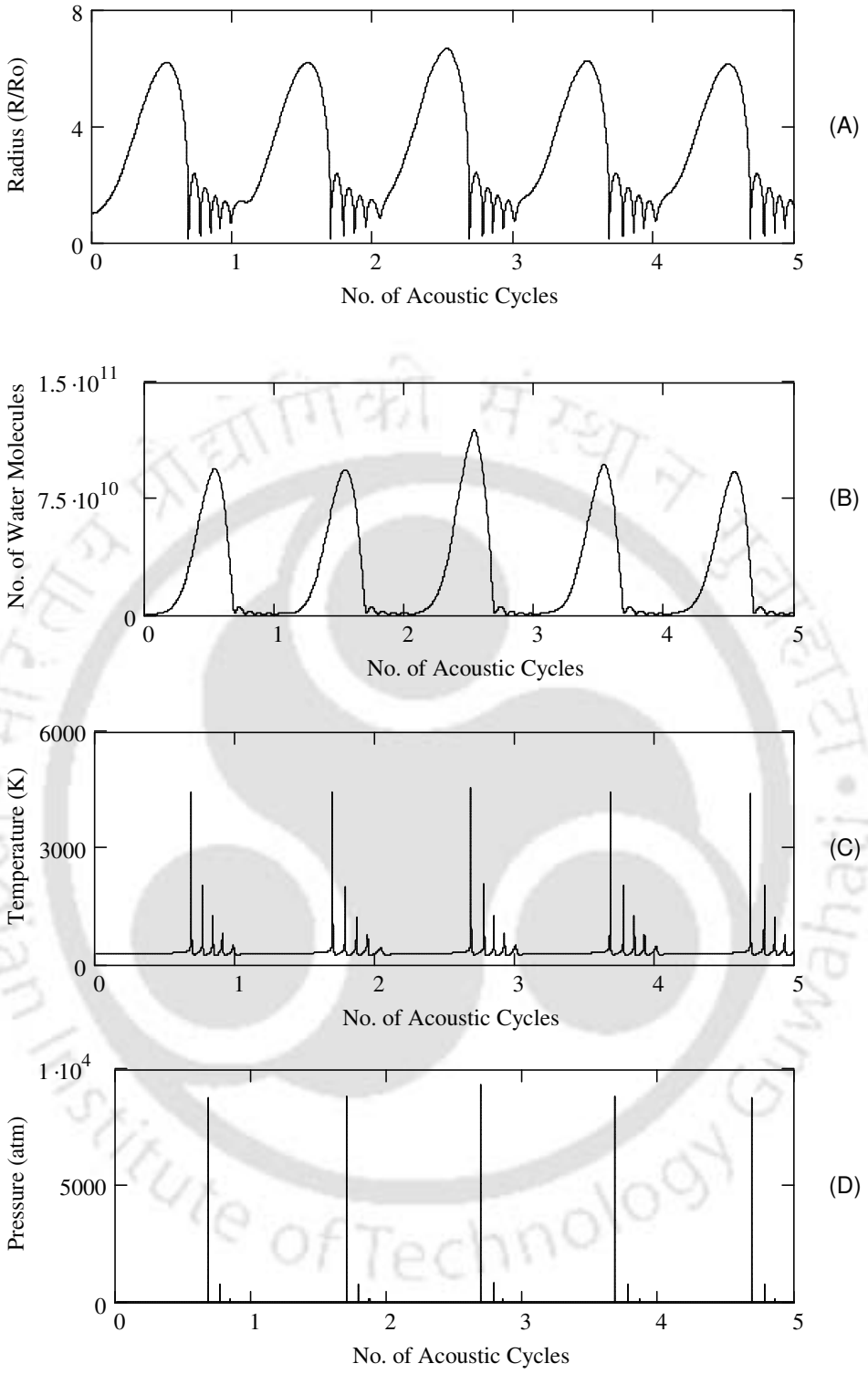

Figure 7.3. Simulation of radial motion of 5 μm air bubble in 100 ppm aqueous solution of 2,4 DCP. Time variation of (A) normalized bubble radius (R/R_o); (B) number of water molecules in the bubble; (C) temperature of the bubble; (D) pressure inside the bubble.

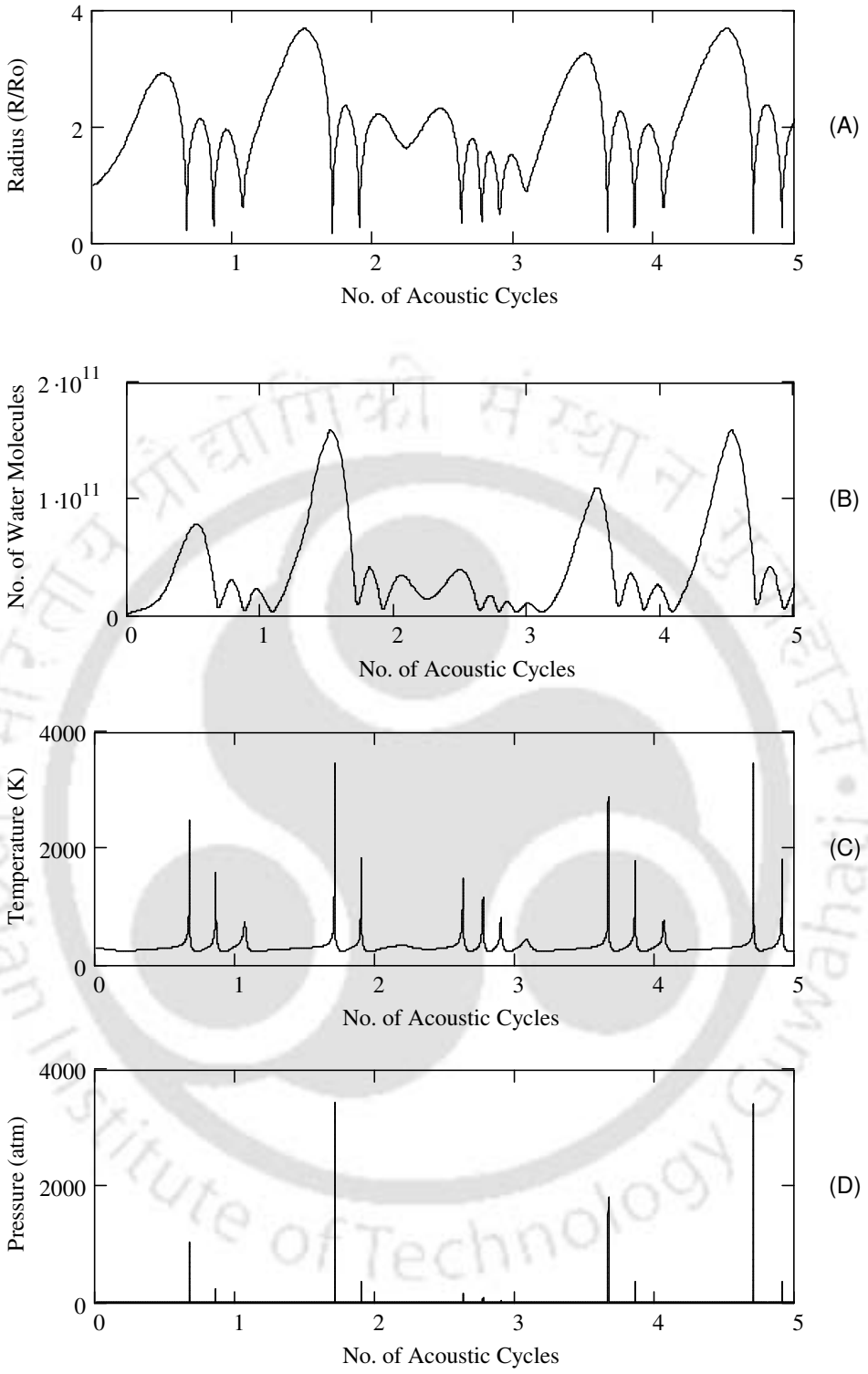

Figure 7.4. Simulation of radial motion of 10 μm air bubble in 100 ppm solution of 2,4 DCP. Time variation of (A) normalized bubble radius (R/R_o); (B) number of water molecules in the bubble; (C) temperature of the bubble; (D) pressure inside the bubble.

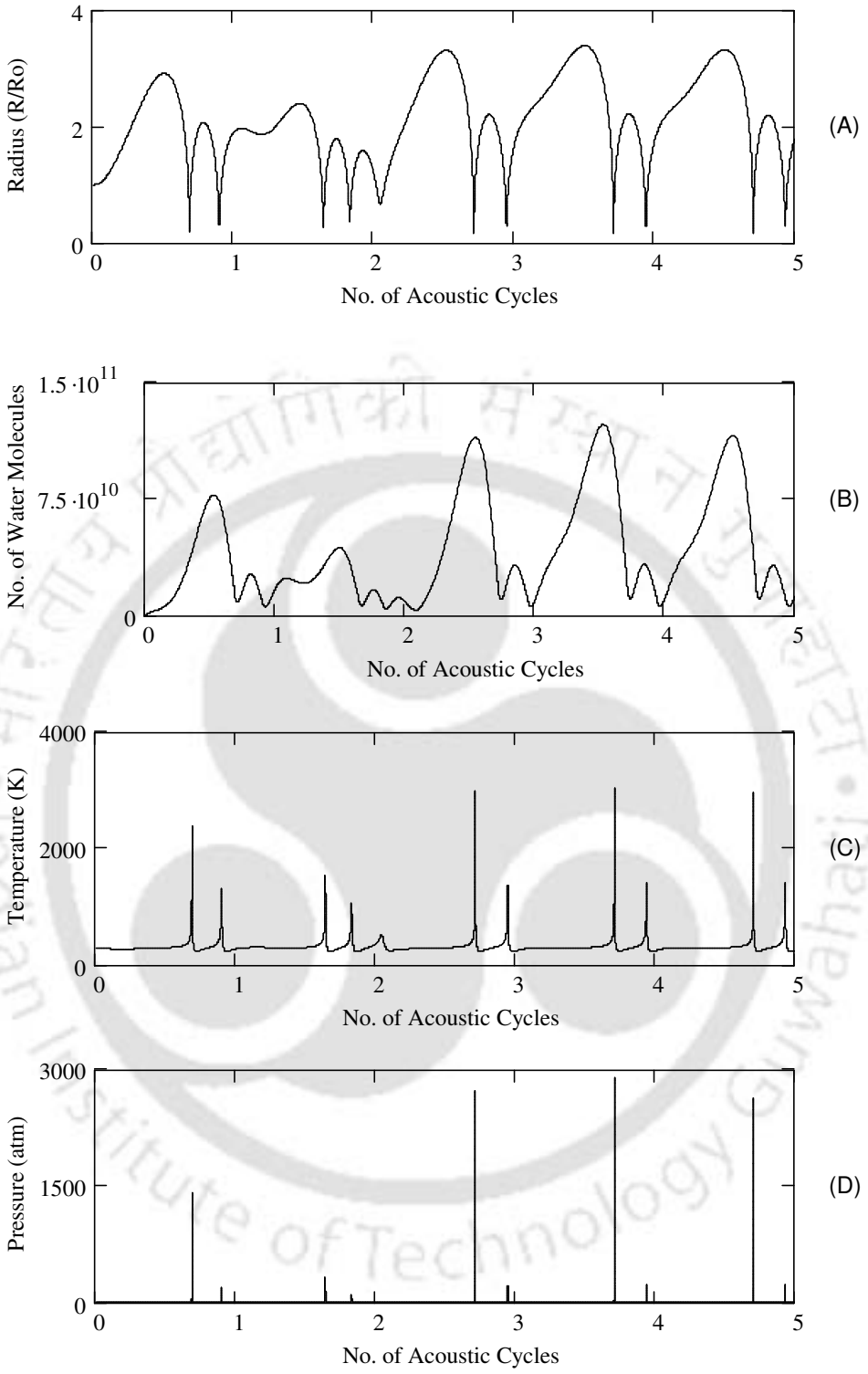

Figure 7.5. Simulation of radial motion of 10 μm nitrogen bubble in 100 ppm solution of 2,4 DCP. Time variation of (A) normalized bubble radius (R/R_o); (B) number of water molecules in the bubble; (C) temperature of the bubble; (D) pressure inside the bubble.

Table 7.2 (A) Summary of the simulation results (Argon, Nitrogen and Oxygen Bubbles)

Species	Parameters for simulations		
	Argon bubble R_o = 10 μm	Nitrogen bubble R_o = 10 μm	Oxygen bubble R_o = 10 μm
	Conditions at the first collapse of the bubble		
	T_{max} = 3937 K P_{max} = 628.7 bar	T_{max} = 2397 K P_{max} = 1407 bar	T_{max} = 2303 K P_{max} = 1539 bar
	N_{Ar} = 1.1779E+011 N_{WT} = 1.51E+010	N_{N2} = 1.1779E+011 N_{WT} = 1.48E+010	N_{O2} = 1.1779E+011 N_{WT} = 1.47E+010
	Equilibrium composition of bubble contents at transient collapse		
H_2O	6.5869E-01	1.1087E-01	1.0988E-01
H_2	1.3142E-01	9.2108E-04	6.2505E-06
OH	1.1454E-01	2.8384E-04	1.8089E-03
H	3.8884E-02	1.2623E-05	6.2320E-07
O_2	3.6855E-02	1.2790E-04	8.8788E-01
O	1.8991E-02	2.5566E-06	1.2059E-04
HO_2	5.4629E-04	4.6263E-07	2.7775E-04
H_2O_2	7.1496E-05	2.6132E-07	1.8075E-05
O_3	3.6545E-07	0	5.3947E-06
N_2	0	8.8726E-01	0
NO	0	5.2435E-04	0
N_2O	0	1.0453E-06	0
NH_3	0	4.5055E-07	0
NO_2	0	4.4288E-07	0
HNO	0	2.5843E-07	0
HNO_2	0	2.9780E-07	0
NH_2	0	1.9954E-08	0

Note: *The number format is as follows: 6.5869E-01 should be read as* 6.5869×10^{-1}. *Various notations used are as follows:* T_{max} *– temperature peak reached in the bubble at the time of first collapse;* P_{max} *– pressure peak reached in the bubble at the time of first collapse;* N_{WT} *– number of water molecules trapped in the bubble at the instance of first collapse;* N_{O2} *– number of oxygen molecules in the bubble (for air and oxygen bubbles).*

molecules in the bubble and equilibrium mole fraction of radicals) contributing to degradation, viz. H, OH, O and HO_2. It can be seen that OH radical is the dominant species among the radical species formed out of transient collapse of cavitation bubbles. Some distinct features of the simulation results are as follows:

(1) The extent of entrapment of water molecules in a 10 μm bubble (representative of saturated liquid medium) shows little variation for bubbles of different gases. However, argon bubble produces the highest temperature peak, and hence, largest number of radicals. This is clearly attributed to the monatomic nature and lower heat capacity of argon.

Table 7.2 (B) Summary of the simulation results (Air Bubbles)

Species	Parameters for simulations	
	Air bubble R_o = 5 μm	Air bubble R_o = 10 μm
	Conditions at first compression of the bubble	
	T_{max} = 4426 K P_{max} = 8812 bar	T_{max} = 2478 K P_{max} = 1044 bar
	N_{N2} = 1.2711E+010 N_{O2} =3.3789E+09 N_{WT} = 2.701E+09	N_{N2} = 9.3053E+010 N_{O2} = 2.4735E+010 N_{WT} = 1.09E+010
	Equilibrium composition of bubble contents at transient collapse	
N_2	7.0850E-01	7.1224E-01
O_2	1.3347E-01	1.8047E-01
NO	1.1880E-01	2.0465E-02
H_2O	9.7968E-03	8.3792E-02
OH	1.2415E-02	2.1262E-03
O	1.2143E-02	1.6967E-04
NO_2	2.1824E-03	5.0932E-04
HO_2	7.1353E-04	1.0538E-04
H_2	3.4189E-04	3.2542E-05
N_2O	5.8624E-04	3.1507E-05
H	6.1056E-04	4.0055E-06
HNO_2	2.0532E-04	4.6585E-05
HNO	1.0478E-04	1.6511E-06
H_2O_2	1.9723E-05	7.6294E-06
O_3	2.9139E-05	6.9832E-07
N	6.4438E-05	0
HNO_3	7.6620E-07	1.7913E-07
NO_3	1.3681E-06	3.9991E-08
NH	6.3207E-06	0
N_2O_3	8.7895E-07	0
NH_2	1.1976E-06	0
NH_3	1.8221E-07	0
N_3	1.3325E-06	0

Table 7.2 (C) Net production of various radicals per bubble

Parameter	Ar bubble	Air bubble (5 μm)	Air bubble (10 μm)	O_2 bubble	N_2 bubble
N_{OH}	1.7295E+09	2.3328E+08	2.7361E+08	2.3966E+08	3.7634E+07
N_H	5.8714E+08	1.1472E+07	5.1545E+05	8.2567E+04	1.6736E+06
N_O	2.8676E+08	2.2817E+08	2.1834E+07	1.5976E+07	3.3897E+05
N_{HO2}	8.2489E+06	1.3407E+07	1.3561E+07	3.6799E+07	6.1340E+04

***Nomenclature**: N_{OH} – number of OH radicals present in the bubble at transient collapse; N_H – number of H radicals present in the bubble at transient collapse; N_O – number of O radicals present in the bubble at transient collapse; N_{HO2} – number of HO_2 radicals present in the bubble at transient collapse.*

(2) As illustrated by the simulation of 5 μm bubble, degassing of the medium (as a result of which the bubble size shrinks) shows a marked rise in both water vapor entrapment and the temperature peak attained during transient collapse. Higher water vapor entrapment is attributed to greater expansion of the bubble (~ 6 times its original size), due to which large amount of water evaporates into the bubble. The greater temperature peak attained at transient collapse is a result of greater compression of the bubble during collapse (or at the instance of minimum radius during bubble motion). The cause leading to this effect is the presence of lesser amount of non-condensable gas inside the bubble, which would "cushion" (or oppose) the collapse of the bubble. As a result of these effects, the net production of radicals from the bubble increases sharply, as seen from results given in table 7.2C.

(3) Extent of radical production in a 10 μm air bubble is relatively lower as compared with argon bubble of same size. This is a consequence of lesser temperature peak attained during transient collapse (due to diatomic nature of nitrogen and oxygen), and secondly, the scavenging of the radicals by nitrogen molecules present in the bubble to generate species such as NO, NO_2, N_2O etc. Oxygen molecules present in the bubble compete in radical scavenging and compensate the loss of radicals due to nitrogen scavenging (to some extent) by regenerating oxidizing species such as $O^{\bullet}$, $OH^{\bullet}$ and $HO_2^{\bullet}$.

(4) The radical production from a nitrogen bubble is the least. In addition to lower temperature peak attained during collapse, another factor that contributes to this effect is extensive scavenging of radicals by nitrogen molecules present in the bubble. Due to absence of oxygen in the bubble (unlike air bubble), there is no regeneration of oxidizing species.

7.6 DISCUSSION

Simultaneous analysis of the simulations and experimental results helps discern the physical features of the sonochemical degradation of 2,4 DCP. Addition of NaCl and Fe^{2+}

makes no changes to the degradation of 2,4 DCP. These results can be explained on the basis of hydrophobic nature of 2,4 DCP. Due to high hydrophobicity, the molecules of 2,4 DCP partition between the bulk medium and bubble interface. The concentration of 2,4 DCP in the interfacial region is, thus, likely to be near or at saturation. Addition of NaCl increases the ionic strength of the medium, as a result of which the hydrophobic repulsive interaction between an organic pollutant and water molecules increase. These interactions drive the pollutant molecules towards bubble interface. This phenomenon results in greater interaction between radicals generated out of cavitation bubble and the pollutant molecules, which enhances the degradation of the pollutant through hydroxylation route. However, in the present case, the bubble interface is already near or at saturation, and hence, salt addition makes no difference to the extent of degradation. Addition of Fe^{2+} enhances radical scavenging in the bulk medium and contributes to greater interaction between radical and the pollutant in the bulk medium. No change in the extent of degradation with Fe^{2+} addition reveals that majority of the degradation of 2,4 DCP occurs in the interfacial region and the contribution of degradation in bulk medium is trivial. High concentration of 2,4 DCP in the interfacial region helps effective interception of radicals in the interfacial region. Thus, a very small fraction of the radicals are expected to diffuse into the bulk medium where they can induce degradation (hydroxylation) reaction. The above result clearly show that the location of the degradation of 2,4 DCP is bubble-bulk interfacial region. Degassing of the medium makes a bubble shrink, as stated earlier. As revealed by the simulation results, smaller bubbles produce more radicals. Therefore, unsaturation of the medium is expected to enhance the degradation of 2,4 DCP, as confirmed by the experimental results.

Contrasting the experimental results with bubbling of different gases through the medium with simulation results reveals interesting physical facets of the sonochemical degradation of 2,4 DCP. If we assume that the extent of degradation is a direct function of

extent of radical production, we see three anomalies. The first anomaly is lower degradation for argon bubbling than air bubbling (in a saturated medium); although extent of radical production by argon bubbles is one order of magnitude larger than air bubbles. Second anomaly is lesser degradation with bubbling of oxygen than air. Third anomaly is higher degradation in the degassed medium (in absence of sparging of any gas during sonication) than in the saturated medium with bubbling of argon; although the radical production by 10 μm argon bubble is greater than 5 μm air bubble. All of these anomalies can be explained on the basis of scavenging of radicals in the bulk medium as well as inside the bubble as follows:

(1) Sparging of argon as well as nitrogen during sonication strips off the dissolved oxygen in the medium. To quantify this effect, we monitored the level of dissolved oxygen in the (initially saturated) liquid medium with sparging of both of these gases. The dissolved oxygen content falls sharply within 10 min of sparging of nitrogen or argon and stays at ~ 1 ppm. A major consequence of this concerning degradation of 2,4 DCP is the reduction in extent of radical scavenging in the bulk medium as well as interfacial region. In absence of scavenging, the radicals undergo recombination, which is loss of oxidation potential. Accordingly, the effective utilization of radicals and the extent of degradation of the pollutant reduces. Conversely, sparging of air through the medium maintains the dissolved oxygen level at saturation (in bulk liquid as well as interfacial region), as oxygen in air dissolves in the medium. Therefore, the radicals produced from an air bubble, although less in number, are effectively utilized towards pollutant degradation. Similarly, for the unsaturated medium, the average dissolved oxygen level in the medium during sonication is ~ 3 ppm, which is higher than argon sparged medium. Correspondingly, the extent of radical scavenging is higher resulting in greater degradation of pollutant.

(2) For the oxygen bubble, the net production of radicals is lesser than air bubble. This is

attributed to extensive scavenging of $OH^{\bullet}$, $H^{\bullet}$ and $O^{\bullet}$ radicals by oxygen molecules in the bubble leading to formation of O_3 and H_2O_2. This is a loss in oxidation potential, which reflects in lesser degradation of the pollutant.

These observations clearly reveal an important physical feature of the sonochemical degradation of 2,4 DCP that it is governed mainly by scavenging of the radicals in the interfacial region – and not by the extent of generation of radicals by the cavitation bubbles.

7.7 CONCLUSION

This study attempts to elucidate the physical or mechanistic features of the sonochemical degradation of 2,4 DCP – which is a common and ubiquitous pollutant in industrial wastewater. With the dual approach of coupling experimental results to a mathematical model for radial motion of bubbles (which is the fundamental physical phenomenon underlying sonochemical effect), we have established two important facets of the degradation of 2,4 DCP: First, the location of the degradation is predominantly the interfacial region between bubble and bulk medium, and secondly, the extent of degradation is controlled by scavenging – and not the production – of oxidizing radicals. The first feature is a manifestation of the hydrophobic nature of the 2,4 DCP. As a result of the second feature, sparging of monatomic gas such as argon results in lesser degradation than the diatomic gas such as air. Presence of a radical scavenging species such as dissolved oxygen in the bubble-bulk interface is of key importance for effective utilization of radicals produced by the bubbles for the degradation of the pollutant. Contrary to our expectations, oxygen bubbles give lesser degradation than air or argon. This is attributed to loss of oxidation potential due to excessive scavenging of radicals inside the bubble by oxygen molecules to form ozone and hydrogen peroxide.

CHAPTER 8

OVERVIEW AND RECOMMENDATIONS FOR FUTURE WORK

This thesis tries to illuminate the physical (or mechanistic) features of sonochemical degradation of five most common organic pollutants present in industrial wastewater. These pollutants are biorefractory and not easily degraded by conventional biological techniques. In broader sense, this work tries to bridge the physics and chemistry of the sonochemical route of degradation of recalcitrant aromatic pollutants. The physical properties of these pollutants differed widely, which affected their response to the ultrasound irradiation and the sonochemistry induced by it. In this chapter, we summarize the major findings of this thesis and try to devise a general logic and methodology on the basis of which one can predict the physical features of sonochemical degradation of any other organic pollutant:

- The principal pathways for sonochemical degradation of an organic pollutant are: (a) hydroxylation reaction (or reaction with OH radicals) at the bubble interface or bulk liquid medium, (b) pyrolysis inside cavitation bubble at transient collapse of the bubble and (c) pyrolysis outside cavitation bubble in the thin liquid shell surrounding the bubble.
- Water vapor transport and entrapment in the cavitation bubble is the principal physical phenomenon behind generation of OH radicals from cavitation bubbles. These radicals induce hydroxylation reaction leading to degradation of pollutants. However, being extremely reactive and unstable, these radicals do not diffuse in the

medium to larger distances from the location of bubble collapse. Thus, the reaction zone of these radicals is restricted in a thin liquid shell surrounding the bubble.

- Scavenging or conservation of the radicals can broaden the reaction zone of the radicals. The word scavenging essentially means reacting the radicals with other species present in the medium (in relatively large quantities) to generate additional radicals. Such species are dissolved oxygen in the medium or ions such as Fe^{2+} added to the medium externally.
- Nature of gas (monatomic or diatomic) and saturation level of the medium are other factors that influence radical generation from the cavitation bubbles, and hence, the extent of production of radicals from the bubbles. Monatomic gases such as produce far more radicals than the diatomic gases such as oxygen and nitrogen. Presence of a radical scavenging species such as oxygen in the bubble can influence the production of radicals from the bubble.
- Principal physical properties that decide the pathway for the sonochemical degradation of pollutants are vapor pressure, solubility and partition coefficient.
- For pollutants with high vapor pressure (or volatile pollutants), significant evaporation occurs in the cavitation bubble. Some of the pollutant molecules evaporated into the bubble get trapped at the instance of transient collapse and are subjected to extremes of temperature and pressure generated in the bubble. These conditions are enough to cause pyrolysis of the pollutant molecules. Thus, pyrolytic decomposition inside the bubble is the predominant degradation mechanism for volatile organic pollutants.
- For non-volatile pollutants hydroxylation (i.e. the reaction with OH radicals generated by cavitation bubbles) is the principal degradation mechanism. The scavenging of radicals in the bulk medium by either ionic (Fe^{2+}) or molecular species (O_2), which

decides the probability of radical-pollutant interaction (and not the extent of radical generation in the medium), governs the degradation process for non-volatile pollutants present in dilute concentrations.

- Other important factor influencing degradation of non-volatile pollutant is the hydrophobicity of the pollutant (indicated octanol-water partitioning behavior). Hydrophobic pollutants concentrate near bubble-bulk interface and undergo faster degradation due to greater interaction with radicals generated from the bubble.
- On the other hand, hydrophilic pollutants stay in the bulk medium (away from the bubble interface). For effective degradation of such pollutants, scavenging of the radicals becomes crucially important. Simple techniques such as salt addition, which enhance the hydrophobic interactions between pollutant and water molecules driving the pollutant molecules towards bubble-bulk interface, can be effectively used for enhancing degradation.

The inferences of the present thesis give several clues for future work in this area of sonochemical wastewater treatment:

1. Comprehensive kinetic study of influence of various techniques on the intermediates and products of sonochemical degradation.
2. Assessment of applicability of techniques described in this thesis for other pollutants such as herbicides, pesticides, azo dyes etc.
3. Techno-economic study on pilot scale set-up.
4. Feasibility with a hybrid wastewater treatment system in combination with biological techniques.

References

Adamson, A.W., Gast, A.P., 1997. *Physical chemistry of surfaces*. John Wiley and Sons, New York.

Adewuyi, Y.G., 2001. Sonochemistry: Environmental science and engineering application. *Ind. Eng. Chem. Res.* **40**, 4681–4715.

Akulichev, V.A., 1967. Pulsations of cavitation bubbles in the field of an ultrasonic wave. *Sov. Phys. Acoust.* **13**, 149–154.

Al-Shayji, K.A., 1998. *Modeling, simulation and optimization of large scale commercial desalination plants*. Ph.D. Thesis, Virginia Polytechnique Institute and State University, Blacksburg.

Andreozzi, R., Caprio, V., D'Amore, M.G., Insola, A., 1995. Manganese catalysis in water pollutants abatement by ozone, *Environ. Technol.* **16**, 885–891.

Andreozzi, R., Caprio, V., Insola, A., D'Amore, M.G., 1992. The kinetic of Mn(II) catalysed ozonation of oxalic acid in aqueous solution. *Water Res.* **26(7)**, 917–921.

Andreozzi, R., Caprio, V., Insola, A., Marotta, R., 1999. Advanced oxidation processes (AOP) for water purification and recovery. *Catalysis Today* **53**, 51–59.

Apfel, R.E., 1981. Methods in experimental physics, Vol. 19 (Ed. P.D. Edmonds), Academic Press, New York, pp. 355–413.

Apfel, R.E., 1986. Possibility of microcavitation from diagnostic ultrasound. *IEEE Trans. Ultrasonics Ferroelectrics Freq. Control UFFC* **33**, 139–142.

Atchley, A.A., Prosperetti, A., 1989. The crevice model of bubble nucleation. *J. Acoust. Soc. Am.* **86**, 1065–1084.

Bapat, P.S., Gogate, P.R., Pandit, A.B., 2007. Theoretical analysis of sonochemical

degradation of phenol and its chloro-derivatives. *Ultrason. Sonochem.* **14(1)**, 564–570.

Barber, B.P., Hiller, R.A., Lofstedt, R., Putterman, S.J., Weninger, K.R., 1997. Defining the unknowns of sonoluminescence. *Phys. Rep.* **281**, 65–143.

Barbier, P., Petrier, C., 1996. Study at 20 kHz and 500 kHz of ultrasound-ozone advanced oxidation system: 4-nitrophenol degradation. *J. Adv. Oxid. Technol.* **1**, 154–159.

Bauer, R., Fallmann, H., 1997. The photo-Fenton oxidation – a cheap and efficient wastewater treatment method. *Res. Chem. Intermediates* **23**, 341–354.

Baxendale, J.H., Wilson, J.A., 1957. The photolysis of hydrogen peroxide at high light intensities. *Trans. Faraday Soc.* **53**, 344–356.

Beckett, M., Hua, I., 2000. Elucidation of the 1,4-Dioxane Decomposition Pathway at Discrete Ultrasonic Frequencies. *Environ. Sci. Technol.* **34**, 3944–3953.

Berlan, J., Trabelsi, F., Delmas, H., Wilhelm, A.M., Petrignani, J.F., 1994. Oxidative degradation of phenol in aqueous media using ultrasound. *Ultrason. Sonochem.* **1(2)**, S97–S102.

Besant, W., 1889. *Hydrostatics and hydrodynamics*. Deighton-Bell, Cambridge.

Bhatkhande, D.S., Pangarkar, V.G., Beenackers, A.A.C.M., 2003. Photocatalytic degradation of nitrobenzene using titanium dioxide and concentrated solar radiation: chemical effects and scale up. *Water Res.* **37**, 1223–1230.

Bhatnagar, A., Cheung, H., 1994. Sonochemical Destruction of Chlorinated C_1 and C_2 Volatile Organic Compounds in Dilute Aqueous Solution. *Environ. Sci. Technol.* **28**, 1481–1486.

Bhatti, Z.I., Toda, H., Furukawa, K., 2002. p-Nitrophenol degradation by activated sludge attached to non-wovens. *Water Res.* **36**, 1135–1142.

Bird, R.B., Stewart, W.E., Lightfoot, E.N., 2001. *Transport phenomena (2nd Ed.)*. Wiley, New York.

Boehncke, A., Koennecker, G., Mangelsdorf, I., Wibbertmann, A., 2000. Mononitrophenols. *Int. Chem. Assess. Doc.* **20**, World Health Organization, Geneva.

Brennen, C.E., 1995. *Cavitation and bubble dynamics*. Oxford University Press, Oxford.

Brenner, M., Hilgenfeldt, S., Lohse, D., 2002. Single-bubble sonoluminescence. *Rev. Mod. Phys.* **74**, 425–484.

Chen, J., Chang, J., Smith, G., 1971. Sonocatalytic Oxidation in Aqueous Solutions. *Chemical Engineering Progress Symposium Series*, **67(109)**, 18–26.

Chen, Y., Smirniotis, P., 2002. Enhancement of photocatalytic degradation of phenol and chlorophenols with ultrasound. *Ind. Eng. Chem. Res.* **41(24)**, 5958–5965.

Colussi, A.J., Hoffmann, M.R., 1999. Vapor supersaturation in collapsing bubbles: relevance to mechanisms of sonochemistry and sonoluminescence. *J. Phys. Chem. A* **103**, 11336–11339.

Colussi, A.J., Hung, H., Hoffmann, M.R., 1999. Sonochemical degradation rates of volatile solutes. *J. Phys. Chem. A* **103**, 2696–2699.

Colussi, A.J., Weavers, L.K., Hoffmann, M.R., 1998. Chemical bubble dynamics and quantitative sonochemistry. *J. Phys. Chem. A* **102(35)**, 6927–6934.

Compton, R.G., Akkermans, R.P., Coles, B.A., Marken. F., 1997. Ultrasound in Photoelectrochemistry: A New Approach to the Enhancement of the Efficiency of Semiconductor Electrode Processes. *Ultrason. Sonochem,* **4**, 223–228.

Condon, E.U., Odishaw, H., 1958. *Handbook of physics*. McGraw Hill, New York.

Cost, M., Mills, G., Glisson, P., Lakin, J., 1993. Sonochemical degradation of p-nitrophenol in the presence of chemical contaminants of natural waters. *Chemosphere* **27**, 1737–1743.

Crank, J., 1975. *The mathematics of diffusion*. Clarendon Press, Oxford.

Cropek, D.M., Kemme, P.A., 1998. Sonolysis of nitroaromatic compounds: 1,3 Dinitrobenzene and nitrobenzene. USACERL Tech. Rep. 99/13.

Crum, L.A., 1980. Measurements of the growth of air bubbles by rectified diffusion. *J. Acoust. Soc. Am.* **68(1)**, 203–211.

Daneshvar, N., Behnajady, M.A., Asghar, Y.Z., 2007. Photooxidative degradation of 4-nitrophenol (4-NP) in UV/H_2O_2 process: Influence of operational parameters and reaction mechanism. *J. Haz. Mater.* **B139**, 275–279.

Davydov, L., Reddy, E.P., France, P., Smirniotis, P.G., 2001. Sonophotocatalytic Destruction of Organic Contaminants in Aqueous Systems Using TiO_2 Powder. *Appl. Catal. B: Environ.*, **32(1-2)**, 95–105.

Dewulf, J., Langenhove, H.V., Visscher, A.D., Sabbe, S., 2001. Ultrasonic degradation of trichloroethylene and chlorobenzene at micromolar concentration: kinetics and modeling. *Ultrason. Sonochem.* **8**, 143–150.

Drijvers, D., Langenhove, H.V., Beckers, M., 1999. Decomposition of phenol and trichloroethylene by the US/H2O2/CuO process. *Water Res.* **33(5)**, 1187–1194.

Drijvers, D., Langenhove, H.V., Herrygers, V., 2000. Sonolysis of fluoro-, chloro-, bromo- and iodobenzene: A comparative study. *Ultrason. Sonochem.* **7**, 87–95.

Drijvers, D., Langenhove, H.V., Vervaet, K., 1998. Sonolysis of chlorobenzene in aqueous solution: organic intermediates. *Ultrason. Sonochem.* **5**, 13–19.

Eller, A.I., Flynn, H.G., 1965. Rectified diffusion through non-linear pulsations of cavitation bubbles. *J. Acoust. Soc. Am.* **37**, 493–503.

Ensminger, D., 1988. *Ultrasonics: Fundamentals, Technology, Applications*, Marcel Dekker: New York.

Entezari, M.H., Kruus, P., 1994. Effect of frequency on sonochemical reactions. I. Absolute rates. *Ultrason. Sonochem.* **1**, 75–79.

Entezari, M.H., Kruus, P., 1996. Effect of frequency on sonochemical reactions. II: Temperature and intensity effects. *Ultrason. Sonochem.* **3**, 19–24.

Entezari, M.H., Petrier, C., 2003. A combination of ultrasound and oxidative enzyme: Sono-biodegradation of substituted phenols. *Ultrason. Sonochem.* **10**, 241–246.

Entezari, M.H., Petrier, C., 2004. A Combination of Ultrasound and Oxidative Enzyme: Sono-biodegradation of Phenol. *Appl. Catal. B: Environ.* **53(4)**, 257–263.

Entezari, M.H., Petrier, C., 2005. A Combination of ultrasound and oxidative enzyme: sonoenzyme degradation of phenols in a mixture. *Ultrason. Sonochem.* **12(4)**, 283–288.

Entezari, M.H., Petrier, C., Devidal, P., 2003. Sonochemical degradation of phenol: A comparison of classical equipment with a new cylindrical reactor. *Ultrason. Sonochem.* **10(2)**, 103–108.

Eriksson, G., 1975. Thermodynamic studies of high temperature equilibria—XII: SOLGAMIX, a computer program for calculation of equilibrium composition in multiphase systems. *Chem. Scr.* **8**, 100–103.

Essam, T., Aly Amin, M., El Tayeb, O., Mattiasson, B., Guieysse, B., 2007. Solar based detoxification of phenol and p-nitrophenol by sequential TiO_2 photocatalysis and photosynthetically aerated biological treatment. *Water Res.* **41**, 1697–1704.

Feigelson, L., Muszkat, L., Bir, L., Muszkat, K.A., 2000. Dye photo-enhancement of TiO_2 – photocatalyzed degradation of organic pollutants: the organobromine herbicide bromacil. *Water Sci. Technol.* **42(1-2)**, 275–279.

Fenton, H.J.H., 1894. Oxidation of tartaric acid in the presence of iron. *J. Chem. Soc.* **65,** 899–910.

Flint, E.B., Suslick, K.S., 1991. The temperature of cavitation. *Science* **253**, 1397–1399.

Flynn, H.G., 1964. Physics of acoustic cavitation in liquids: in *Physical Acoustics* (Ed. W.P. Mason), Academic Press, New York, pp. 57–172.

Flynn, H.G., 1975. Cavitation dynamics I. A mathematical formulation. *J. Acoust. Soc. Am.* **57**, 1379–1396.

Fujikawa, S., Akamatsu, T., 1980. Effects of the non-equilibrium condensation of vapor on the pressure wave produced by the collapse of a bubble in a liquid. *J. Fluid Mech.* **97**, 481–512.

Fyrillas, M. M., Szeri, A.J., 1996. Surfactant dynamics and rectified diffusion of microbubbles. *J. Fluid Mech.* **311**, 361–378.

Fyrillas, M., Szeri, A.J., 1994. Dissolution and growth of soluble spherical oscillating bubbles. *J. Fluid Mech.* **277**, 381–407.

Gilmore, F.R., 1954. Hydrodynamic Laboratory Report. California Institute of Technology, 26–4.

Glaze, W.H., Kang, J.W., 1989. Advanced oxidation processes. Description of a kinetic model for the oxidation of hazardous materials in aqueous media with ozone and hydrogen peroxide in a semibatch reactor. *Ind. Eng. Chem. Res.* **28**, 1573–1580.

Gogate, P.R., Mujumdar, S., Pandit, A.B., 2003. Large scale sonochemical reactors for process intensification: design and experimental validation. *J. Chem. Technol. Biotechnol.* **78(6)**, 685–693.

Gogate, P.R., Mujumdar, S., Thampi, J., Wilhelm, A.M., Pandit, A.B., 2004. Destruction of phenol using sonochemical reactors: Scale-up aspects and comparison of novel configuration with conventional reactors. *Sep. Purif. Technol.* **34**, 25–34.

Gogate, P.R., Pandit, A.B., 2004. A review of imperative technologies for wastewater treatment I: Oxidation technologies at ambient conditions. *Adv. Environ. Res.* **8**, 501–551.

Gogate, P.R., Pandit, A.B., 2004a. A Review of Imperative Technologies for Wastewater Treatment II: Hybrid Methods. *Adv. Environ. Res.* **8,** 553–597.

Gogate, P.R., Shirgaonkar, I.Z., Sivakumar, M., Senthil kumar, P., Vichare, N.P., Pandit, A.B., 2001. Cavitation reactors: efficiency assessment using a model reaction. *AIChE J.* **47(11)**, 2526–2538.

Gong, C., Hart, D.P., 1998. Ultrasound induced cavitation and sonochemical yields. *J. Acoust. Soc. Am.* **104**, 2675–2682.

Goskonda, S., Catallo, W.J., Junk, T., 2002. Sonochemical degradation of aromatic organic pollutants. *Waste Manage.* **22**, 351–356.

Gutierrez, M., Henglein, A., Ibanez, F., 1991. Radical scavenging in the sonolysis of aqueous solutions of iodide, bromide and azide. *J. Phys. Chem.* **95(15)**, 6044–6047.

Haber, F., Weiss, J., 1934. The catalytic decomposition of hydrogen peroxide by iron salts. *Proc. R. Soc. Series A* **147**, 332–351.

Hall, B.A., 1975. Materials problems associated with the development of geothermal energy resources. US Dept of the Interior Bureau of Mines, Washinton DC.

Hart, E.J., Henglein, A., 1985. Free radical and free atom reactions in the sonolysis of aqueous iodide and formate solutions. *J. Phys. Chem.* **89(20)**, 4342–4347.

Hart, E.J., Henglein, A., 1987. Sonochemistry of aqueous solutions: hydrogen-oxygen combustion in cavitation bubbles. *J. Phys. Chem.* **91(13)**, 3654–3656.

Henglein, A., 1956. The acceleration of chemical reaction induced by ultrasound in solutions of oxygen noble gas mixtures. *Naturwissenschaften* **43**, 277.

Henglein, A., 1957. Hydrogen peroxide formation by ultrasound in aqueous solutions of mixtures of hydrogen, argon and oxygen. *Naturwissenschaften* **44**, 179.

Henglein, A., Gutierrez, M., 1990. Chemical effects of continuous and pulsed ultrasound: a comparative study of polymer degradation and iodide oxidation. *J. Phys. Chem.* **94(12)**, 5169–5172.

Hilgenfeldt, S., Lohse, D., Brenner, M.P., 1996. Phase diagrams for sonoluminescing bubbles. *Phys. Fluids* **8(11)**, 2808–2826.

Hirschfelder, J.O., Curtiss, C.F., Bird, R.B., 1954. *Molecular Theory of Gases and Liquids.* Wiley, New York.

Hoffmann, M.R., Hua, I., Hochemer, R., 1996. Application of ultrasonic irradiation for degradation of chemical contaminants in water. *Ultrason. Sonochem.* **3**, S163–S172.

Hoigné, J., 1998. Chemistry of aqueous ozone and transformation of pollutants by ozone and advanced oxidation processes, in: J. Hrubec (Ed.), *The Handbook of Environmental Chemistry*, vol. 5, part C, Quality and Treatment of Drinking Water, Part II, Springer, Berlin Heidelberg.

Holland, C.K., Apfel, R.E., 1989. An improved theory for prediction of microcavitation thresholds. *IEEE Trans. Ultrasonics Ferroelectrics Freq. Control* **36**, 204–208.

Horvath, A.L., 1985. *A handbook of aqueous electrolyte solutions*. Ellis Horwood, Chichester.

Hsieh, D.-Y., Plesset, M.S., 1961. Theory of rectified diffusion of mass into gas bubbles. *J. Acoust. Soc. Am.* **33**, 206–215.

Hua, I., Hochemer, R.H., Hoffmann, M.R., 1995. Sonochemical degradation of p-Nitrophenol in a parallel plate near field acoustic processor. *Environ. Sci. Technol.* **29**, 2790–2796.

Hua, I., Hoffmann, M.R., 1996. Kinetics and mechanism of sonolytic degradation of CCl_4: Intermediates and byproducts. *Environ. Sci. Tech.* **30**, 864–871.

Hung, H., Hoffmann, M.R., 1999. Kinetics and mechanism of sonolytic degradation of chlorinated hydrocarbons: frequency effects. *J Phys. Chem. A* **103**, 2734–2739.

Hung, H.-M., Ling, F.H., Hoffmann, M.R., 2000. Kinetics and mechanism of the enhanced reductive degradation of nitrobenzene by elemental iron in the presence of ultrasound. *Environ. Sci. Technol.* **34**, 1758–1763.

Ilyichev, V.I., Koretz, V.L., Melnokov, N.P., 1989. Spectral characteristics of acoustic cavitation. *Ultrasonics* **27**, 357–361.

Jiang, Y., Chen, Y., Li, L., Petrier, C., 1999. Effects of ultrasonic frequency on reaction rates during sonochemical degradation of organic pollutants in aqueous solution. *Proceedings*

of Global Conference on Environmental Control in Mining and Metallurgy 319–323.

Jiang, Y., Petrier, C., David Waite, T., 2002. Effect of pH on the ultrasonic degradation of ionic aromatic compounds in aqueous solutions. *Ultrason. Sonochem.* **9(3)**, 163–168.

Jiang, Y., Waite, T.D., 2003. Degradation of trace contaminants using coupled. sonochemistry and Fenton's reagent. *Water Sci. Technol.* **47(10)**, 85–92.

Joos, P., Serrien, G., 1989. Adsorption kinetics of lower alkanols at the air/water interface: effect of structure makes and structure breakers. *J. Colloid Interfacial Sci.* **127(1)**, 97–103.

Joseph, J., Destaillats, H., Hung, H., Hoffmann, M.R., 2000. The sonochemical degradation of azobenzene and related azo dyes: rate enhancements via Fenton's reactions. *J. Phys. Chem. A* **104**, 301–307.

Kalumuck, K.M., Chahine, G.L., 2000. The use of cavitation jets to oxidize organic compounds in water. *J. Fluids Eng.* **122**, 465–470.

Kamath, V., Prosperetti, A., Egolfopoulos, F.N., 1993. A theoretical study of sonoluminescence. *J. Acoust. Soc. Am.* **94**, 248–260.

Kang, J., Hung, H., Lin, A., Hoffmann, M.R., 1999. Sonolytic destruction of methyl tert-butyl ether by ultrasonic irradiation: The role of O_3, H_2O_2, frequency, and power density. *Environ. Sci. Tech.* **33**, 3199–3205.

Kavitha, V., Palanivelu, K., 2005. Degradation of nitrophenols by Fenton and photo-Fenton processes. *J. Photochem. Photobiol. A: Chemistry* **170**, 83–95.

Keller, J.B., Kolodner, I.I., 1956. Damping of underwater explosion bubble oscillations. *J. Appl. Phys.* **27**, 1152–1161.

Keller, J.B., Miksis, M.J., 1980. Bubble oscillations of large amplitude. *J. Acoust. Soc. Am.* **68**, 628.

Kidak, R. Ince, N.H., 2007. Catalysis of advanced oxidation reactions by ultrasound: a case

study with phenol. *J. Haz. Mater.* **146(3)**, 630–635.

Kirchoff, G., 1868. Uber den Einfluss der Warmteleitung in einem Gase auf die Schallbewegung. *Ann. Phys. (Leipzig)* **134(6)**, 177–193.

Kirkwood, J.G., Bethe, H.A., 1942. The pressure wave produced by an under water explosion. Office of Science Research and Development, Rep. 558.

Kirpalani, D.M., McQuinn, K.J., 2006. Experimental quantification of cavitation yield revisited: focus on high frequency ultrasound reactors. *Ultrason. Sonochem.* **13(1)**, 1–5.

Kiwi, J., Pulgarin, C., Peringer, P., Gratzel, M., 1993. Beneficial effect of homogeneous photo-Fenton pretreatment upon the biodegradation of anthraquinone sulfonate in wastewater treatment. *Appl. Catal. B: Environ.* **3**, 85–99.

Kotronarou, A., Mills, G., Hoffmann, M.R., 1991. Ultrasonic irradiation of p-nitrophenol in aqueous solution. *J. Phys. Chem.* **95(9)**, 3630–3638.

Kotronarou, A., Mills, G., Hoffmann, M.R., 1992. Decomposition of parathion in aqueous solution by ultrasonic irradiation. *Environ. Sci. Technol.* **26**, 1460–1462.

Krishnan, S.J., Dwivedi, P., Moholkar, V.S., 2006. Numerical investigation into the chemistry induced by hydrodynamic cavitation. *Ind. Eng. Chem. Res.* **45**, 1493–1504.

Kruus, P., Burk, R.C., Entezari, M.H., Otson, R., 1997. Sonication of aqueous solutions of chlorobenzene. *Ultrason. Sonochem.* **4**, 229–233.

Kubo, M., Hiroto, F., Juan, C.X., Toshikuni, Y., 2005a. Ultrasonic degradation of phenol in the presence of composite particles of TiO_2 and activated carbon. *Proc. 2005 AIChE Annual Meeting,* Cincinnati, Ohio.

Kubo, M., Matsuoka, K., Takahashi, A., Shibasaki-Kitakawa, N., Yonemoto, T., 2005. Kinetics of ultrasonic degradation of phenol in presence of TiO_2 particles. *Ultrason. Sonochem.* **12(4)**, 263–269.

Kumar, A., Kumar, S., Kumar, S., Gupta, D.V., 2007. Adsorption of phenol and 4-

nitrophenol on granular activated carbon in basal salt medium: Equilibrium and kinetics. *J. Haz. Mater.* **127(1-2)**, 155–166.

Kumar, K.S., Moholkar, V.S., 2007. Conceptual design of a novel hydrodynamic cavitation reactor. *Chem. Eng. Sci.* **62**, 2698–2711.

Kwak, H.-Y., Na, J.-H., 1996. Hydrodynamic solutions for sonoluminescing gas bubble. *Phys. Rev. Lett.* **77**, 4454–4457.

Kwak, H.Y., Na, J.-H., 1997. Physical processes for single bubble sonoluminescence. *J. Phys. Soc. Jpn.* **66**, 3074–3083.

Kwak, H.Y., Yang, H., 1995. An aspect of sonoluminescence from hydrodynamic theory. *J. Phys. Soc. Jpn.* **64**, 1980–1992.

Latifoglu, A., Gurol, M.D., 2003. The effect of humic acids on nitrobenzene oxidation by ozonation and O_3/UV process. *Water Res.* **37**, 1879–1889.

Leighton, T.G., 1994. *The Acoustic Bubble*, San Diego: Academic Press.

Lesko, T.M., 2004. *Chemical effects of acoustic cavitation*. Ph.D. Thesis, California Institute of Technology, Pasadena.

Lin, J., Ma, Y., 1999. Magnitude of effect of reaction parameters on 2-chlorophenol decomposition by ultrasonic process. *J. Haz. Mat. B* **66**, 291–305.

Lofstedt, R., Weninger, K., Puttermann, S.J., Barber, B.P., 1995. Sonoluminescing bubbles and mass diffusion. *Phys. Rev. E* **51**, 4400–4410.

Lure', Y., Kandzas, P.F., Mokina, A.A., 1962. Oxidation of Phenol in an Ultrasound Field. *Russ. J. Phys. Chem.* **36**, 2616–2620.

Ma, J., Sui, M., Zhang, T., Guan, C., 2005. Effect of pH on MnO_x/GAC catalyzed ozonation for degradation of nitrobenzene. *Water Res.* **39**, 779–786.

Mahamuni, N.N., Pandit, A.B., 2006. Effect of additives on ultrasonic degradation of phenol. *Ultrason. Sonochem.* **13**, 165–174.

Majumder, P.S., Gupta, S.K., 2003. Hybrid reactor for priority pollutant nitrobenzene removal. *Water Res.* **37**, 4331–4336.

Mantzavinos, D., Hellenbrand, R., Livingston, A.G., Metcalf, I.S., 1997. Reaction mechanisms and kinetics of chemical pretreatment of bioresistant organic molecules by wet air oxidation. *Water Sci. Technol.* **35**, 119–127.

Mason, T.J., Lorimer, J.P., 1989. *Sonochemistry: Theory, application and uses of ultrasound in chemistry*. Ellis Horwood, New York.

Mason, T.J., Lorimer, J.P., 2002. *Applied sonochemistry: The uses of power ultrasound in chemistry and processing*. Wiley-VCH, Coventry.

Mishra, V.S., Mahajani, V.V., Joshi, J.B., 1995. Wet air oxidation. *Ind. Eng Chem. Res.* **34(1)**, 2–48.

Moholkar, V.S., 2002. *Intensification of textile treatments: Sonoprocess engineering*. Ph.D. Thesis, Twente University Press, Enschede.

Moholkar, V.S., Warmoeskerken, M.M.C.G., 2003. An integrated approach to optimization of an ultrasonic processor. *AIChE J.* **49**, 2918–2932.

Moholkar, V.S., Warmoeskerken, M.M.C.G., Ohl, C.D., Prosperetti, A., 2004. The mechanism of mass transfer enhancement in textile with ultrasound. *AIChE J.* **50**, 58–64.

Moss, W.C., Young, D.A., Harte, J.A., Levalin, J.L., Rozsnyai, B.F., Zimmerman, G.B., Zimmerman, I.H., 1999. Computed optical emissions from sonoluminescing bubbles. *Phys. Rev. E* **59**, 2986–2992.

Nakui, H., Okitsu, K., Maeda, Y., Nishimura, R., 2007. Effect of coal ash on sonochemical degradation of phenol in water. *Ultrason. Sonochem.* **14(2)**, 191–196

Neppiras, E.A., 1980. Acoustic cavitation. *Phys. Rep.* **61**, 159–251.

Nikolopoulos, A.N., Markopoulou, O.I., Papayannakos, N., 2006. Ultrasound assisted catalytic wet peroxide of phenol: Kinetics and intraparticle diffusion effects. *Ultrason.*

Sonochem. **13(1)**, 92–97.

NIST Data Gateway, *Chemistry Webbook,* 2001 (http://webbook.nist.gov/chemistry).

Noltingk, B.E., Neppiras, E.A., 1950. Cavitation produced by ultrasonics. *Proc. Phys. Soc.* **B63**, 674–685.

Okouchi, S., Nojima, O., Arai, T., 1992. Cavitation induced degradation of phenol by ultrasound. *Water Sci. Technol.* **26(9-11)**, 2053–2056.

Okuno, H., Yim, B., Mizukoshi, Y., Nagata, Y., Maeda, Y., 2000. Sonolytic degradation of hazardous organic compounds in aqueous solutions. *Ultrason. Sonochem.* **7**, 261–264.

Ollis, D., Al-Ekabi, H., 1993. *Photocatalytic purification of water and air*. Elsevier, New York.

Ondruschka, B., Hofmann, J., 1999. Aquasonolysis of halogenated pollutants. Enhancement of sonochemical effectivity by variation of system parameters. *Hamburger Berichte zur Siedlungswasserwirtschaft* **25** (*Ultrasound in Environmental Engineering*)**,** 139–151.

Papadaki, M., Emery, R.J., Abu-Hassan, M.A., Diaz-Bustos, A., Metcalfe, I.S., Mantzarinos, D., 2004. Sonocatalytic oxidation process for the removal of contaminants containing aromatic ring from aqueous effluents. *Sep. Purif. Technol.* **34(1-3)**, 35–42.

Peller, J., Wiest, O., Kamat, P., 2001. Sonolysis of 2,4-dichlorophenoxyacetic acid in aqueous solution. Evidence for OH radical mediated degradation. *J. Phys. Chem. A* **105**, 3176–3181.

Petrier, C., Combet, E., Mason, T., 2007. Oxygen induced concurrent ultrasonic degradation of volatile and non-volatile aromatic compounds. *Ultrason. Sonochem.* **14**, 117–121.

Petrier, C., Francony, A., 1997. Ultrasonic waste-water treatment: incidence of ultrasonic frequency on the rate of phenol and carbon tetrachloride degradation. *Ultrason. Sonochem.* **4(4)**, 295–300.

Petrier, C., Francony, A., 1997a. Incidence of wave frequency on the reaction rates during

wastewater treatment. *Water Sci. Tech.* **35(4)**, 175–180.

Petrier, C., Jiang, Y., Francony, A., Lamy, M.-F., 1999. Aromatics and chloroaromatics sonochemical degradation. Yields and byproducts. *Hamburger Berichte zur Siedlungswasserwirtschaft* **25** (*Ultrasound in Environmental Engineering*)**,** 23–27.

Petrier, C., Jiang, Y., Lamy, M.-F., 1998. Ultrasound and Environment: Sonochemical Destruction of Chloroaromatic Derivatives. *Environ. Sci. Tech.* **32**, 1316–1318.

Petrier, C., Lamy, M.F., Francony, A., Benahcene, A., David, B., Renaudin, V., Gondrexon, N., 1994. Sonochemical degradation of phenol in dilute aqueous solutions: Comparison of the reaction rates at 20 and 487 kHz. *J. Phys. Chem.* **98**, 10514–10520.

Peyton, G.R., Glaze, W.H., 1988. Destruction of pollutants in water with ozone in combination with ultraviolet radiation. Part 3. Photolysis of aqueous ozone. Mechanism of photolytic ozonation. *Environ. Sci. Technol.* **22**, 761–767.

Pierce, A.D. 1989. *Acoustics: An introduction to its physical principles and applications*. Acoustical Society of America, New York.

Plesset, M.S., 1949. Dynamics of cavitation bubbles. *J. Appl. Mech. (Trans. ASME)* **16**, 277–282.

Plesset, M.S., Prosperetti, A., 1977. Bubble dynamics and cavitation. *Ann. Rev. Fluid Mech.* **9**, 145–185.

Poritsky, H., 1952. The collapse or growth of a spherical bubble or cavity in a viscous fluid. *Proc. 1st US National Cong. Appl. Mech. (Ed. E. Sternberg)* 813–821.

Prado, J., Arantegui, J., Chamarro, E., Esplugas, S., 1994. Degradation of 2,4-dichlorophenoxyacetic acid by ozone and light. *Ozone Sci. Eng.* **16,** 235–245.

Prasad Naidu, D.V., Rajan, R., Kumar, R., Gandhi, K.S., Arakeri, V.H., Chandrasekaran, S., 1994. Modeling of a batch sonochemical reactor. *Chem. Eng. Sci.* **49(6)**, 877–888.

Press, W.H., Teukolsky, S.A., Flannery, B.P., Vetterling, W.T., 1992. *Numerical Recipes (2nd*

Ed.). Cambridge University Press, New York.

Price, G.J., Ashokkumar, M., Grieser, F., 2004. Sonoluminescence quenching of organic compounds in aqueous solution: frequency effects and implications for sonochemistry. *J. Am. Chem. Soc.* **126**, 2755–2762.

Price, G.J., Matthias, P., Lenz, E.J., 1994. The use of high power ultrasound for the destruction of aromatic compounds in aqueous solutions. *Trans. Inst. Chem. Engrs.* **72(B1)**, 27–31.

Prosperetti, A., Commander, K.W., 1989. Linear pressure waves in bubbly liquids: Comparison between theory and experiments. *J. Acoust. Soc. Am.* **85**, 732–746.

Prosperetti, A., Lezzi, A., 1986. Bubble dynamics in a compressible liquid. Part 1. First order theory. *J. Fluid Mech.* **168**, 457–477.

Pulgarin, C., Kiwi, J., 1996. Overview on photocatalytic and electrocatalytic pretreatment of industrial non-biodegradable pollutants and pesticides, *Chimia* **50**, 50–53.

Rajan, R., Kumar, R., Gandhi, K.S., 1998. Modeling of sonochemical oxidation of the water-KI-CCl_4 system. *Chem. Eng. Sci.* **53**, 255–271.

Rajeshwar, K., 1995. Photoelectrochemistry and the environment**.** *J. Appl. Electrochem.* **25(12)**, 1067–1082.

Rayleigh, Lord, 1917. On the pressure developed in a liquid during the collapse of spherical cavity. *Phil. Mag.* **34**, 94–98.

Reid, R.C., Prausnitz, J.M., Poling, B.E., 1987. *Properties of gases and liquids*. McGraw Hill, New York.

Riesz, P., Berdahl, D., Christman, C.L., 1985. Free radical generation by ultrasound in aqueous and non-aqueous solutions. *Environ. Health Perspect.* **64**, 233–252.

Rodriguez, M.L., Timokhin, V.I., Contreras, S., Chamarro, E., Esplugas, S., 2003. Rate equation for the degradation of nitrobenzene by 'Fenton – like' reagent. *Adv. Environ.*

Res. **7**, 583–595.

Rong, L., Koda, S., Nomura, H., 2001. Study on degradation rate constant of chlorobenzene in aqueous solution using a recycle ultrasonic reactor. *J. Chem. Eng. Jpn.* **34(8)**, 1040–1044.

Rosenberg, L.D., 1971. High intensity ultrasonic field (Part IV – VI), Plenum Press, New York, pp. 203–419.

Safar, M.H., 1968. Comments on the paper concerning rectified diffusion of cavitation bubbles. *J. Acoust. Soc. Am.* **43**, 1188–1189.

Safarzadehet-Amiri, A., Bolton, J.R., Cater, S.R., 1996. Ferrioxalatemediated solar degradation of organic contaminants in water. *Solar Energy* **56(5)**, 439–443.

Safarzadehet-Amiri, A., Bolton, J.R., Cater, S.R., 1997. Ferrioxalatemediated photo degradation of organic pollutants in contaminated water. *Water Res.* **31(4)**, 787–798.

Sekiguchi, H., Saita, Y., 2001. Effect of alumina particles on sonolysis degradation of chlorobenzene in aqueous solution. *J. Chem. Eng. Jpn.* **34(8)** 1045–1048.

Serpone, N., Terzian, R., Colarusso, P., 1992. Sonochemical oxidation of phenol and three of its intermediates in aqueous media: catechol, hydroquinone and benzoquinone: kinetics and mechanistic aspects. *Res. Chem. Intermediates* **18(2-3)**, 183–202.

Seymour, J., Gupta, R.B., 1997. Oxidation of aqueous pollutants using ultrasound: salt induced enhancement. *Ind. Eng. Chem. Res.* **36(9)**, 3453–3457.

Seymour, J.D., Wallace, H.C., Gupta, R.B., 1994. Sonochemical reaction at 640 kHz using an efficient reactor. Oxidation of potassium iodide. *Ultrason. Sonochem.* **1(2)**, S75–S79.

Shah, Y.T., Pandit, A.B., Moholkar, V.S., 1999. *Cavitation reaction engineering*. Plenum Press, New York.

Shirgaonkar, I.Z., Pandit, A.B., 1997. Degradation of aqueous solution of potassium iodide and sodium cyanide in the presence of carbon tetrachloride. *Ultrason. Sonochem.* **4**, 245–

253.

Sivakumar, M., Tatake, P.A., Pandit, A.B., 2002. Kinetics of p-nitrophenol degradation: Effect of reaction conditions and cavitational parameters for a multiple frequency system. *Chem. Eng. J.* **85**, 327–338.

Sivasankar, T., Paunikar, A.W., Moholkar, V.S., 2007. Mechanistic approach to enhancement of the yield of a sonochemical reaction. *AIChE J.* **53(5)**, 1132–1143.

Sochard, S., Wilhelm, A.M., Delmas, H., 1997. Modeling of free radicals production in a collapsing gas-vapor bubble. *Ultrason. Sonochem.* **4**, 77–84.

Sponza, D.T., Cigal, C., 2008. Relationships between anaerobic consortia and removal efficiencies in an USAB reactor degrading 2,4 dichlorophenol. *J. Environ. Manage.* **87(1)**, 177–192.

Stavarache, C., Vinatoru, M., Nishimura, R., Maeda, Y., 2004. Short time Sonolysis of chlorobenzene in presence of Pd(II) salts and Pd(0). *Ultrason. Sonochem.* **11**, 429–434.

Stavarache, C., Yim, B., Vinatoru, M., Maeda, Y., 2002. Sonolysis of chlorobenzene in Fenton type aqueous systems. *Ultrason. Sonochem.* **9**, 291–296.

Stokes, G.G., 1849. On the theories of the internal friction of fluids in motion, and of the equilibrium and motion of elastic solids. *Trans. Camb. Phil. Soc.* **8**, 287–319.

Storey, B.D., Szeri, A.J., 2000. Water vapor, sonoluminescence and sonochemistry. *Proc. R. Soc. Lond. Ser. A* **456**, 1685–1709.

Storey, B.D., Szeri, A.J., 2001. A reduced model of cavitation physics for use in sonochemistry. *Proc. R. Soc. Lond. Ser. A* **457**, 1685–1700.

Suslick, K.S., 1988. *Ultrasound: Its physical, chemical and biological effects*. VCH, New York.

Suslick, K.S., 1989. The chemical effects of ultrasound. *Sci. Am.* **260**, 80–86.

Suslick, K.S., 1990. Sonochemistry. *Science* **247**, 1439–1445.

Takizawa, Y., Akama, M., Yoshihara, N., Nojima, O., Arai, K., Okouchi, S., 1996. Hydroxylation of phenolic compounds under conditions of ultrasound in aqueous solutions. *Ultrason. Sonochem.* **3**, S201–S204.

Tauber, A., Schuchmann, H.-P., von Sonntag, C., 2000. Sonolysis of aqueous 4-nitrophenol at low and high pH. *Ultrason. Sonochem.* **7**, 45–52.

Toegel, R., 2002. *Reaction–diffusion kinetics of a single sonoluminescing bubble*. Ph.D. Dissertation, Twente University Press, Enschede.

Toegel, R., Gompf, B., Pecha, R., Lohse, D., 2000. Does water vapor prevent upscaling sonoluminescence? *Phys. Rev. Lett.* **85**, 3165–3168.

Toegel, R., Lohse, D., 2003. Phase diagrams for sonoluminescing bubbles: A comparison between experiment and theory. *J. Chem. Phys.* **118(4)**, 1863–1875.

Trabelsi, F., Ait-Lyazidi, H., Ratsimba, B., Wilhelm, A.M., Delmas, H., Fabre, P.L., Berlan, J., 1996. Oxidation of phenol in wastewater by sonochemistry. *Chem. Eng. Sci.* **51(10)**, 1857–1865.

Tuziuti, T., Yasui, K., Iida, Y., Taoda, H., Koda, S., 2004. Effect of particle addition on sonochemical reaction. *Ultrasonics* **42**, 597–601.

Tuziuti, T., Yasui. K., Sivakumar, M., Iida, Y., Miyoshi, N., 2005. Correlation between acoustic cavitation noise and yield enhancement of sonochemical reaction by particle addition. *J. Phys. Chem. A* **109(21)**, 4869–4872.

Vinodgopal, K., Peller, J., 2003. Hydroxyl radical-mediated advanced oxidation processes for textile dyes: A comparison of the radiolytic and sonolytic degradation of the monoazo dye acid orange 7. *Res. Chem. Intermediates* **29**, 307–316.

Wang, J.-P., Feng, H.-N., Yu, H.-Q., 2007. Analysis of adsorption charateristics of 2,4 dichlorophenol from aqueous solutions by activated carbon fiber. *J. Haz. Mater.* **144**, 200–207.

Wang, S.-G., Liu, X.-W., Zhang, H.-Y., Gong, W.-X., Sun, X.-F., Gao, B.-J., 2007a. Aerobic granulation for 2,4 dichlorophenol biodegradation in a sequencing batch reactor. *Chemosphere* **69**, 769–775.

Weavers, L.K., Hoffmann, M.R., 1998. Sonolytic decomposition of ozone in aqueous solutions: mass transfer effects. *Environ. Sci. Technol.* **32**, 3941–3947.

Weavers, L.K., Ling, F.H., Hoffmann, M.R., 1998. Aromatic compound degradation in water by combination of sonolysis and ozonolysis. *Environ. Sci. Tech.* **32**, 2727–2733.

Weavers, L.K., Malmstadt, N., Hoffmann, M.R., 2000. Kinetics and mechanism of pentachlorophenol degradation by sonication, ozonation and sonolytic ozonation. *Environ. Sci. Tech.* **34**, 1280–1285.

Wilke, C.R., 1950. A viscosity equation for gas mixtures. *J Chem. Phys.* **18**, 517–519.

Wu, C., Liu, X., Wei, D., Fan, J., Wang, L., 2001. Photosonochemical degradation of phenol in water. *Water Res.* **35(16)**, 3927–3933.

Wu, J., Yu, H.-Q., 2008. Biosorption of 2,4 dichlorophenol from aqueous solutions by immobilized Phanerochaete chrysosporium biomass in a fixed bed column. *Chem. Eng. J.* **138(1-3)**, 128–135.

Wu, L., Li, A., Gao, G., Fei, Z., Xu, S., Zhang, Q., 2007. Efficient photodegradation of 2,4 di- chlorophenol in aqueous solution catalyzed by polydivinyl benzene supported zinc phthalocyanine. *J. Mol. Catal. A: Chemical* **269**, 183–189.

Yasman, Y., Bulatov, V., Gridin, V.V., Agur, S., Galil, N., Armon, R., Schechter, I., 2004. A new sono-electrochemical method for enhanced detoxification of hydrophilic chloroorganic pollutants in water. *Ultrason. Sonochem.* **11**, 365–372.

Yasman, Y., Bulatov, V., Rabin, I., Binetti, M., Schechter, I., 2006. Enhanced Electro-catalytic Degradation of Chloroorganic Compounds in the Presence of Ultrasound. *Ultrason. Sonochem,* **13**, 271–277.

Yasui, K., 1997. Alternative model for single-bubble sonoluminescence. *Phys. Rev. E* **56**, 6750–6760.

Yasui, K., 1997a. Chemical reactions in a sonoluminescing bubble. *J. Phys. Soc. Jpn*. **66**, 2911–2920.

Yi, J., Petrier, C., David Waite, T., 2002. Effect of pH on the ultrasonic degradation of ionic aromatic compounds in aqueous solutions. *Ultrason. Sonochem.* **9**, 163–168.

Yi, J., Petrier, C., Waite, D., 2002. Kinetics and mechanism of ultrasonic degradation of volatile chlorinated aromatics in aqueous solutions. *Ultrason. Sonochem.* **9**, 317–323.

Young, F.R., 1989. *Cavitation*. McGraw Hill, London.

Zhang, H., Fei, C., Zhang, D., Tang, F., 2007. Degradation of 4-nitrophenol in aqueous medium by electro-fenton method. *J. Haz. Mater.* **145(1-2)**, 227–232.

Zhang, Y., Crittenden, J.C., Hand, D.W., 1994. The Solar Photocatalytic Decontamination of Water. *Chem. Ind.* **18**, 714–717.

Zhao, C., Lu, X., 2003. Degradation of nitrobenzene in wastewater by ultrasound/ozone. *Proc. 226th ACS National Meeting*, New York.

Zhao, C., Zhao, D., 2001. Degradation of nitrobenzene in wastewater by ultrasound/Fenton's reagent. *Proc. 222nd ACS National Meeting*, Chicago.

Zhao, C., Zhao, D., 2003. Experimental study on degradation of wastewater containing phenol by ultrasound/ozone. *Proc. 226th ACS National Meeting*, New York.

Zheng, W., Michelle, M., Tarr, M.A., 2005. Enhancement of degradation of phenol using hydrogen atom scavengers. *Ultrason. Sonochem.* **12(4)**, 313–317.

Zhou, M., Lei, L., 2006. An improved UV/Fe^{3+} process by combination with electrocatalysis for p-nitrophenol degradation. *Chemosphere* **63**, 1032–1040.

Zhou, T., Li, Y., Wong, F.-S., Lu, X., 2008. Enhanced degradation of 2,4-dichlorophenol by ultrasound in a new Fenton like system (Fe/EDTA) at ambient circumstance. *Ultrason.*

Sonochem., DOI: 10.1016/j.ultsonch.2008. 01.005.

Ziagova, M., Liakopoulou-Kyriakides, M., 2007. Kinetics of 2,4 dichlorophenol and 4-Cl-m-Cresol degradation by Pseudomonas sp. cultures in the presence of glucose. *Chemosphere* **68**, 921–927.

ACKNOWLEDGEMENTS

I express my sincere thanks to my research supervisor **Dr. Vijay S. Moholkar** for his valuable guidance throughout my research work. I am indeed indebted to him for giving me an opportunity to work in a very interesting area of research "**cavitation**" whose wonder would have remained unknown to me otherwise. His continuous encouragement, patience towards research and support gave me lot of spirit in regard to research. I would like to thank him for spending his precious time for discussion by which I have gained immense skills of knowledge in terms of research. I am fortunate to have him as a guide whose immense thinking and knowledge made my work fruitful without him this dissertation would not have been possible. I would like to express my deepest appreciation for his persistent guidance throughout my research work.

I would like to thank my doctoral committee members, **Dr. Mohammed Jawed,** Department of Civil Engineering, **Dr. Anugrah Singh and Dr. Bishnupada Mandal,** Department of Chemical Engineering, for their valuable suggestion and effort which made my thesis successful.

This thesis attempted to bring together the physics and chemistry of the sonochemical degradation of organic pollutants. During the research work, Dr. Moholkar and I got valuable suggestions and help from eminent scientists in the area of cavitation physics and sonochemistry. They help us in modeling of bubble dynamics with associated transport phenomena, understanding the complicated physics of bubble-bulk interface and the radical chemistry in the bubble. Their assistance has played a major role in meaningful contributions made by this thesis. I deem myself very fortunate in that I have privilege to thank the following people for their invaluable help: **Professor Andrea Prosperetti (John Hopkins University, Baltimore, USA), Dr. Brian Storey (Olin College, Boston, USA), Dr. Rudiger Toegel (University of Twente, Enschede, Netherlands), Professor Franz Grieser and Dr. M. Ashokkumar (University of Melbourne, Australia) and Professor A.B. Pandit and Dr. P.S. Bapat (UICT, Mumbai)**.

My special thanks to **Dr. Prabirkumar Saha,** Secretary, Department Postgraduate Programme Committee, for his constant encouragement and friendly help in various ways. I should thank **Dr. Aloke Kumar Ghoshal,** Head, Department of Chemical Engineering, for providing me the necessary support throughout my work. I have been grateful to **Dr. G. Pugazhenthi** for sharing his experience, suggestions and caring which guided me in right path.

I must thank **Dr. Ramgopal Uppaluri** in providing the required facilities during my work. I must thank **Dr. Sasidhar Gumma** for his help in accessing various analytical facilities for my research work. I thank all the faculty members of the Department of Chemical Engineering for their help in various means.

In addition I thank **Dr. Pallab Ghosh** for his help in accessing Tensiometer for surface tension measurement. I extent my thanks to his student **B. Praveen** for his assistance in surface tension measurement.

I am thankful to **Dr. P.C. Sabumon,** Civil Engineering, School of Mechanical and Building Sciences, Vellore Institute of Technology, who has been instrumental throughout in extending my research carrier.

I am very much grateful and infact lucky to get full support from all the non-teaching staffs. Their timely help both technical and personal, without any hesitation have been invaluable. I thank **Balenji**, **Luku, Subodh, Sumedha, Kaustav, Bipul, Bhagya, Pankaj, Prasun and Deepak** for their contribution**.**

Helps done my fellow research scholars, **Dr. J. Williams, Biswaranjan, Murugadoss,** Department of Chemistry in providing chemicals and their assistance in analysis have to be greatly acknowledged.

My sincere thanks to **Ashwin Paunikar,** M.Tech student of our research group, for his co-operative assistance in performing experiments on oxidation of potassium iodide. I also extend my thanks to our research group members **Abhishek, Narendra, Venkat, Bhaskar, Ramesh, Buljit and Mrs. Amrita Ranjan** for their kindness and support during my research work.

I am thankful to my fellow research scholars **Saravanan, Debasis, Barun, Mehabub and Subham,** for their help, useful discussions and exchanging their feelings.

I would like to thank my friends and well-wishers, **Nagaraju, Sureshpandian, Pandithevan, Wilfred Godfrey, Senthil, Anandkumar, Reddy Suresh, Sampathkumar, Hariharanath, Lakshminarayana Reddy, Gandhi, Srinivasulu, Y. Praveen** and all others friends for making my stay in IITG memorable. I also thank my friends, **Arunkumar, Sankar, Neelamegam, senthil, udaykumar, Aravind and Ashraf.**

My special thanks to **Harsha** and his father and mother for their sweet love and affection showed towards me.

Finally, I express my gratitude to my beloved father, mother, sister, uncle, brother and his family, saran and especially, my sister's daughter **Devinivethitha**, for showering their love throughout my life which eased me whenever I was in trouble. I extend my gratefulness to my father, who has been the motivation behind my hardwork, patience and character.

T. Sivasankar
April, 2008

LIST OF PUBLICATIONS

Journal Papers

- Sivasankar T, Paunikar AW, Moholkar VS., Mechanistic approach to enhancement of the yield of a sonochemical reaction. *A.I.Ch.E. Journal* 2007;53(5):1132–1143.
- Sivasankar, T., Moholkar, V.S., Mechanistic Features of the Sonochemical Degradation of Organic Pollutants. *A.I.Ch.E. Journal* (Accepted for publication).
- Sivasankar, T., Moholkar, V.S., Mechanistic Approach to Intensification of Sonochemical Degradation of Phenol, under review.
- Sivasankar, T., Moholkar, V.S., Physical Features of Sonochemical Degradation of Nitroaromatics, under review.
- Sivasankar, T., Moholkar, V.S., Physical Features of Sonochemical Degradation of Chlorophenols – manuscript under preparation.

Conference Presentations

- Sivasankar, T., Moholkar**,** V.S.**,** A mechanistic approach to enhancement of phenol degradation with ultrasound, *Proceedings of The International Conference on Cleaner Technologies and Environmental Management*, PEC, Pondicherry, pp. 298-302, 2007.
- Sivasankar, T., Moholkar V.S., Enhancement of Sonochemical Degradation of Hydrophillic and Hydrophobic organics pollutants, *Proceedings and Abstracts of the 8th IWA Specialized Conference on Small Water and Wastewater Systems and 2nd IWA Specialized Conference on Decentralised Water and Wastewater International Network*, KCT, Coimbatore, pp. 104, 2008.